SIALON CERAMIC MATRIX COMPOSITES

BY

HAMZA J. EDREES

B.Sc. (Basrah) & M.Sc. (Strathclyde)

A THESIS SUBMITTED FOR THE DEGREE OF DOCTOR OF PHILOSOPHY OF THE METALLURGY & ENGINEERING MATERIALS, FACULTY OF ENGINEERING, UNIVERSITY OF STRATHCLYDE.

DECEMBER 1990

CONTENTS

CHAPTER THREE EXPERIMENTAL TECHNIQUE.

CHAPTER FOUR CARBON FIBER/CERAMIC COMPOSITES.

PREFACE

This thesis discribes original work which has not been submitted for a degree at any other university.

The work was carried out in the Department of Metallurgy & Engineering Materials, Faculty of Engineering, Strathclyde University during the period April 1988 to November 1990 under the supervision of Prof. Alan Hendry.

This thesis describes the preparation of β'–sialon matrix composites and reports on the effect of the reinforced phases on the sintering behaviour and also describes their mechanical and electrical properties.

ACKNOWLEDGEMENTS

I would like to thank **Prof. Alan Hendry** for his remarkable help, marvellous advice and continuous encouragement during the supervision of this work

I also wish to thank:

Mr Jim Doherty for his help during the preparation of this work, **Mrs Mary Aird** for her kindness and care during the last five years, **Miss Wendy Hanson** for her advice and help with the English language and the technical staff for their help.

I also wish to thank **Osaka Gas Company of Japan** for supply of materials and sponsorship of the work on carbon composites.

Also I would like to thank **Mr Asaad M. A. Kenbar** for the good time we have had together.

Finally my thanks and regards to my family for their encouragement and specially my brother **Edrees J. Edrees** for his continuous contact during the last five years.

ABSTRACT

The present study has been performed on β'-sialon matrix reinforced with either carbon fiber, metals or TiN components. The study describes the optimum methods of fabrication of these composites and also investigates their mechanical and electrical properties.

In carbon fiber/sialon system, reaction between the fiber and the matrix has been identified and overcomed by applying **high densification rate** and low temperature sintering. Samples containing 10-20V% fiber was hot pressed to **almost theoretical** density at temperatures 1500–1550°C.

In metal reinforced sialon matrix composites there is always a reaction between the metal and the sialon to form metal silicide liquid at relatively low temperatures, which is found to be helpfull in decreasing the maximum densification temperature. Sialon reinforced by 15V% Ni powder is pressureless sintered to over 95% of the theoretical density at temperature of **1450°C**. Reaction in such composites can be controlled by increasing the sintering heating rate and the amount of silicon metal dissolveed into the metal particles (which strongly influences the composites mechanical properties) can be controlled by a two stage heat treatment sintering particularly in the stainless steel/sialon system.

The addition of TiN to sialon matrix resulted in processing with no troubles of chemical incompatibility and composites with attractive mechanical properties . Density of **almost theoretical** was achieved in the addition of 10-30V%TiN to sialon.

The crack type investigations on sialon and sialon matrix composites shows that the cracks are of **Palmqvist type.** The indentation fracture toughness of the composites mentioned above is dependant on the reinforced phase type, volume fraction and sintering temperature. In fiber/sialon composites fracture toughness of

7.9 $MNm^{-3/2}$ was achived by hot pressing 15V% carbon fiber/sialon composites. In metal/sialon composites, however, fracture toughness of **13 $MNm^{-3/2}$**is achieved, whilst the indentation fracture toughness of 30V%TiN reinforced sialon composites is **8.9 $MNm^{-3/2}$.**

The electrical conductivity of these composites is strongly dependant on the reinforced phase volume fraction and most importantly on the **particles size** of the conductive phase. However, resistivity of **0.5 Ω.cm** is achieved in the addition of 20V% carbon to the sialon matrix. In metal/sialon systems resistivity of **3.37 Ω.cm** is achieved in 20V% Ni/sialon composite whilst 30V%TiN is required to create a resistivity of **443 Ω.cm** in such composites.

CHAPTER ONE

INTRODUCTION

During recent years significant progress has been made in the development of engineering ceramic materials. A new generation of non-oxide ceramics has been developed, which are expected to find a wide range of applications at high temperature and a good combination of mechanical, thermal, electrical and chemical properties is obtained from silicon nitride (Si_3N_4), one of the most promising materials in this class. It has good strength at high temperature in addition to a good oxidation resistance compared with other materials and this combination of properties can be used to increase operating temperatures. Moreover, the low density of silicon nitride (3.2 $g.cm^{-3}$ - approximately 40% of high temperature superalloys) may offer components of reduced weight providing an important advantage over other high temperature materials. Potential application of silicon nitride ceramics are in the ceramic gas turbine or replacement of metallic components in internal combustion engines. Moreover other engineering applications are also under consideration such as energy conversion systems, industrial heat exchangers, wear resistant materials for metals processing and ball bearings. During the last fifteen years technological knowledge in the area of silicon nitride ceramics processing has been greatly developed particularly because of its planned application in the vehicle gas turbine.

Investigations have mainly been concentrated during this time on Si_3N_4 and Si_3N_4 based ceramics ; the sialons.

CHAPTER TWO

SILICON NITRIDE BASED MATERIALS

2.1 Crystal structure.

Silicon nitride crystals exist in two hexagonal forms, designated as α and β phase [Turkdogan et al 1958]. It was believed that α is a low temperature form and β is the high temperature form [Hardie and Jack 1957]. In both forms, however, the basic building unit is the silicon–nitrogen tetrahedron joined such that each nitrogen is shared by three tetrahedra. In 1968, however, Grieveson et al reported that the α and β forms were respectively high and low oxygen potential and later they [Wild et al 1972] described α-Si_3N_4 as a defect structure with oxygen replacing nitrogen on some sites having compositional range from $Si_{11.4}N_{15}O_{0.3}$ to $Si_{11.5}N_{15}O_{0.5}$. With increasing temperature the α phase becomes increasingly unstable with respect to β phase. The transformation, however, is reconstructive and can only occur with solution-precipitation by means of liquid phase [Drew & Lewis 1974 and Messier et al 1978] .It was also shown that α-β transformation in silicon nitride can also be completed without liquid phase at 1.5 GPa and 1500°C within 60 mins [Shimada et al 1983].

According to the Si_6N_8 and $Si_{12}N_{16}$ unit cell of β and α phases and the lattice parameters [a = 0.7606 ± 0.0005 nm, c = 0.2907 ± 0.0003 nm for β and a

=0.7755 ± 0.0005 nm, c = 0.5616 ± 0.0005 nm for α phase], the theoretical densities are 3.196 g.cm^{-3} and 3.185 g.cm^{-3} for β and α phases respectively. In addition to the pure α and β phases, there exists some solid solutions of silicon nitride with certain compounds having structures identical to the α and β structures [Jack 1977]. As far as is known today, solid solutions based on the β structure are formed with alumina by limited substitution of Si^{4+} and N^{3-} by Al^{3+} and O^{2-} in which the cation /anion ratio of 3/4 remains constant. This may be represented by $Si_{6-Z}Al_ZO_ZN_{8-Z}$ with a limit for Z < 4.2 (β'–sialon) [Lumby et al 1975], where Z is the amount of Si and N substituted by Al and O. The stability region of this solution is shown in figure (2.1). As can be seen from this phase diagram, β'–sialon is actually a solid solution between Si_3N_4 and Al_2O_3-AlN. The formation of this solution results in a linear change in the lattice parameter, a and c, as can be given by the following equations [Liddell 1984],

$$Z = (a-7.6023)/0.03$$

$$Z = (c-2.906)/0.027$$

Changing the starting compositions from the solid solution stoichiometric ratio leads to the additional formation of amorphous or crystalline phases such as O', X or several AlN–based polytypes as can be seen in figure (2.1). All these polytypes however, show certain regions of solid solution with a compositional metal:non-metal ratio of the type M_mX_{m+1} ($4 < m < 11$) [Thompson et al 1983].

In addition to the β–Si_3N_4 solid solution, α–Si_3N_4 based structures have been detected with certain additives such as Li, Ca or Y [Hampshire et al 1978] in a smaller range of solid solution than β'-sialon. These α- solid solutions are formed by partial replacement of Si^{4+} by Al^{3+}. Valence compensation occurs by incorporation of additional cations (such as Ca, Li, or Y) which occupy the interstices in the (Si, Al)–N

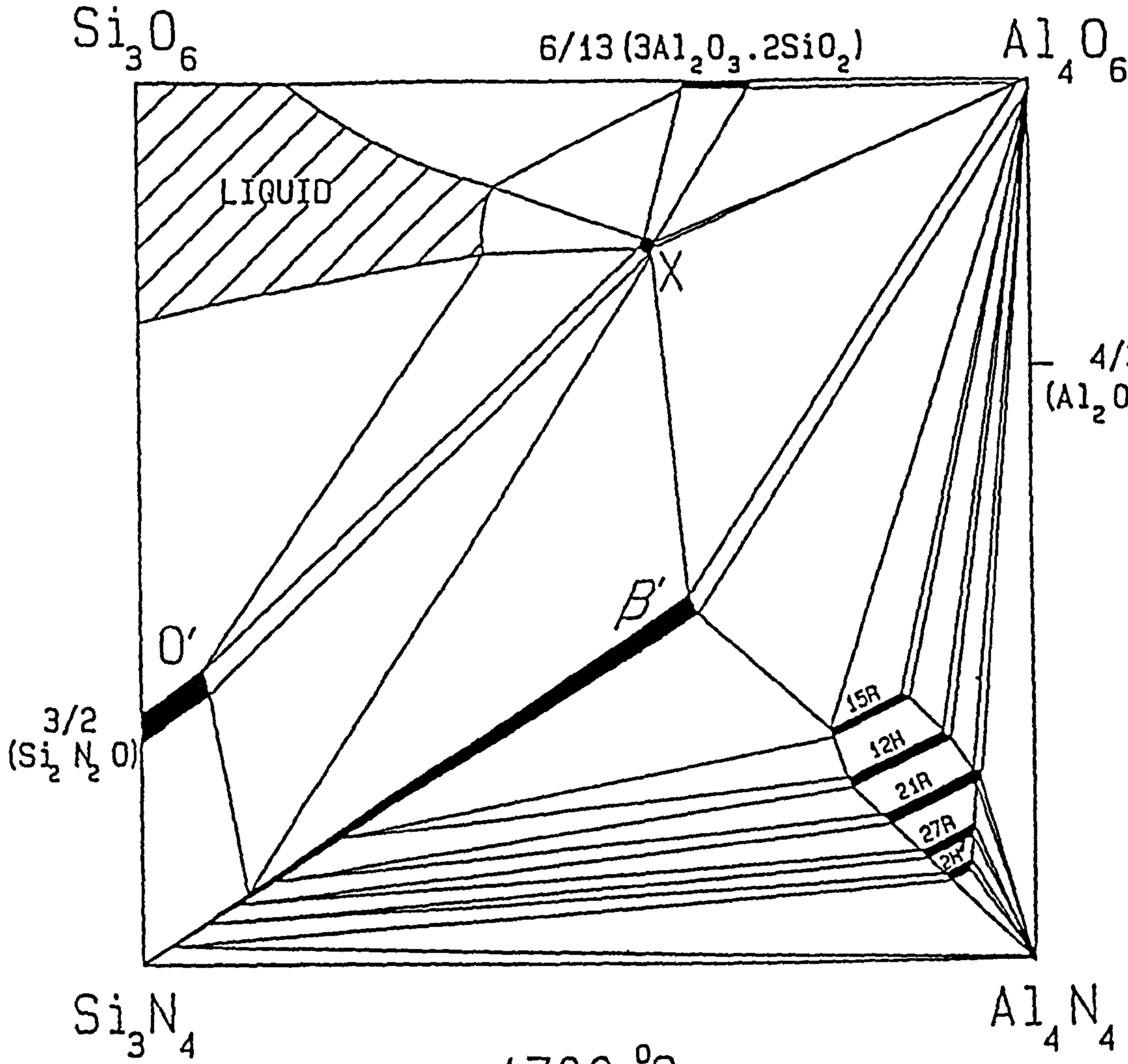

figure 2.1

Isothermal section on Si–Al–O–N phase diagram at 1700°C

structure. These sialons can be described by $M_xSi_{12-(m+n)}Al_{(m+n)}O_nN_{16-n}$ which means a replacement of m(Si–N) units by n(Al–O) units. The M incorporation seems to be limited X<2. With increasing substitution the lattice constants increase.

2.2 Processing Technique.

In fabrication of nitrogen ceramics the objective is to produce near net shape components with high strength resulting from a high density material, at relatively low temperature by an economic process. The development of improved production techniques is a complex process beginning with the powder characterisation and ending with the firing method. Sintering conditions, however, represent an important factor among those which play a part in the fabrication process. Dense engineering ceramics are manufactured by different densification methods.

2.2.1 Reaction-bonded sintering.

Because pure silicon nitride powder appears not to be sinterable without the use of additives, the reaction bonded process is an alternative route for fabrication of dense materials of Si_3N_4 ceramic. This material is formed by heating silicon powder compacts (consolidated by techniques such as uniaxial and isostatic pressing, injection moulding, or slip casting) in a nitrogen atmosphere at temperature in excess of 1300°C for several hours. The aim of such processing being to produce high conversion of silicon to silicon nitride. RBSN materials can be fabricated with a variety of mass production techniques and very complex shapes are obtainable with these methods. It has been shown, however, that reaction kinetics for such nitriding processes are extremely difficult to control even in high quality laboratory experiments[Moulson

1979]. These difficulties are due to the differences in nitriding kinetics which in some way can be attributed to variable low levels of cationic impurities such as iron and iron compounds [Messier & Wong 1973] and to impurities in the nitriding atmosphere such as oxygen, [Moulson 1979]. As a result this method is suitable(for RBSN production), reliable, easy to follow, and cheap. By contrast, it is difficult to understand, the nitriding is time consuming and product density is not high enough for most engineering applications.

2.2.2 Hot pressing.

Hot pressing as a fabrication process has found increased use in ceramics processing and is extremely effective in the preparation of materials with improved properties (composition, microstructure and density). In hot pressing the pressure can be applied uniaxially, biaxially or isostatically. Uniaxial hot pressing, however, is the technique most frequently used. The process in general, consists of applying pressure to the ceramic powder or cold compact form, in a refractory mould (usually graphite) which is heated to a specific temperature for densification. For compounds which are covalently bonded, such as silicon nitride, silicon carbide and sialon, it was found that additives are required to promote densification even at high pressure. Various oxide additives have been used as densification agents in both hot pressing and pressureless sintering of silicon nitride based materials.

In spite of the ease of fabrication of dense samples by hot pressing, it has limited effectiveness in production of complex shapes and is generally uneconomical because of the prohibitive cost of the processing technique and the difficulties in machining the product.

2.2.3 Pressureless sintering.

Pressureless sintering is a process in which compacted ceramic powder is sintered at atmospheric pressure in a controlled environment . Attempts to sinter covalently bonded ceramics, however, require higher sintering temperature, where problems with compositional instability exist. Controlling boundary mobility and chemistry by sintering additives (metal oxides) where a sufficiently high diffusion coefficient could be obtained at temperature where materials are stable, represent the key to applying this technique to materials such as silicon nitride or sialon. Also understanding the thermodynamics and kinetics of decomposition in addition to reactions that might occur during the course of sintering (particularly of ceramic matrix composites) is required to control the process. Moreover particular care with green sample preparation is required to promote optimum densification

2.3 Influence Of Densification Additives.

The type and amount of sintering additives has a major influence on the sintering temperature and hence on the rate of densification during both pressureless and hot press sintering. Moreover they have an effect on the morphology of the grains and the behaviour of the grain boundary phases, which control the high temperature properties. It is well known, however, that the sintering additives react with the surface silica which is always present on the particles of silicon nitride based ceramic materials, to form a liquid phase. If the amount of the liquid phase is high enough and the viscosity at sintering temperature is sufficiently low, rearrangement processes (according to Kingery's model) will occur, followed by solution in the liquid and reprecipitation. So the characteristics of the liquid phase are important, these include

the solidus temperature of the additives + SiO_2 composition, the amount and viscosity of the resulting liquid phase at the sintering temperature and the solubility of nitrogen in the liquid phase. It was thought, however, that the liquid phase in the MO-SiO_2 system,(M is Mg , Ca, Y.....etc) for example in the MgO–SiO_2 case, is near to the $MgSiO_3$–SiO_2 eutectic [Wild et al 1972]. Later it was established that the liquid is an oxynitride in the form of M–Si–O–N or M–Si–Al–O–N where M is Mg , Ca, Y etc. [Jack 1977].

The temperature of the initial liquid observed with addition of different metal oxides to silicon nitride is found to be affected by nitrogen as can be seen in table (2.1).[Hampshire & Jack 1981]. This suggests that nitrogen as an additional component lowers the eutectic temperature .It was also noticed that substitution of oxygen by nitrogen

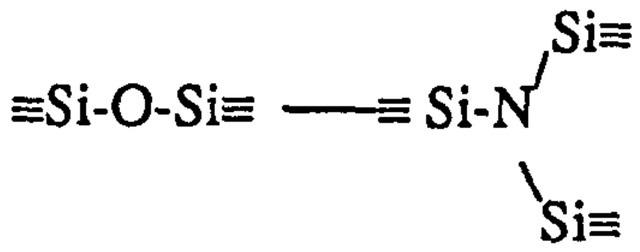

leads to higher liquid viscosity [Mulfinger 1966] as can be seen in figure (2.2 a & b). [Drew et al 1981]. From figure (2.2 a & b), for a given amount of nitrogen in the liquid phase, increasing the temperature reduces the viscosity. Also at these temperatures, nitrogen solubility and viscosity relations change with the type of additive. In general temperature always decreases viscosity and therefore enhances the densification rate. A schematic plot of the influence of various oxide additives on densification behaviour, compared to silicon nitride densified without sintering aid, is shown in figure (2.3).[Jack 1977]. The upper curve in the figure shows that the shrinkage of silicon nitride is limited without additive even at high temperature. The other curves are determined by the softening temperature and viscosity of the secondary phase, which mainly controls the rearrangement and solution-precipitation processes. The data given in table(2.1) show that the eutectic temperature of oxide–

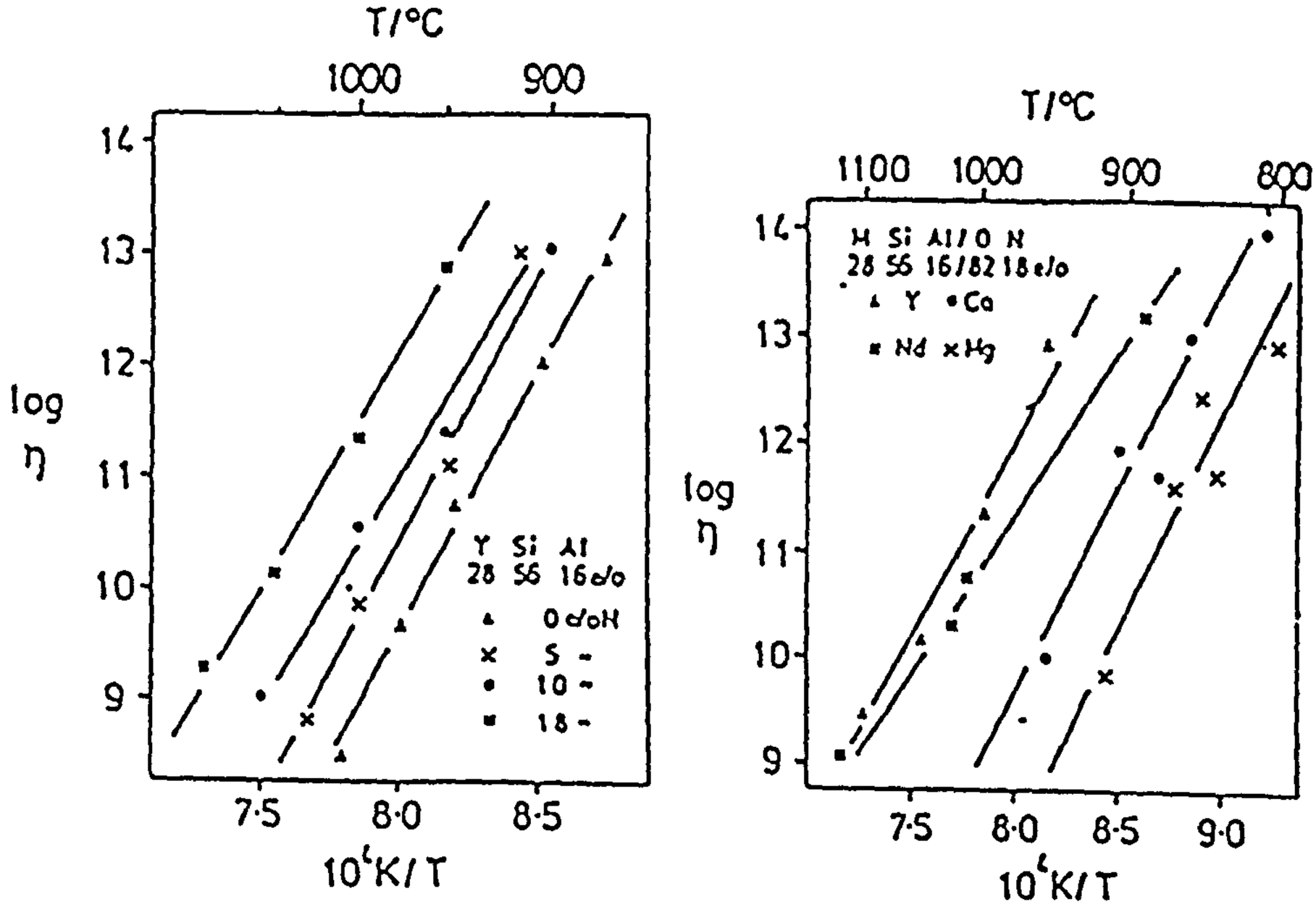

figure 2.2

a- Variation of viscosity with temperature for Si–Al–O–N glasses of different nitrogen concentration.

b- Viscosity of glass with 18e% N and the same M:Si: Al cation ratio [Drew et al 1981]

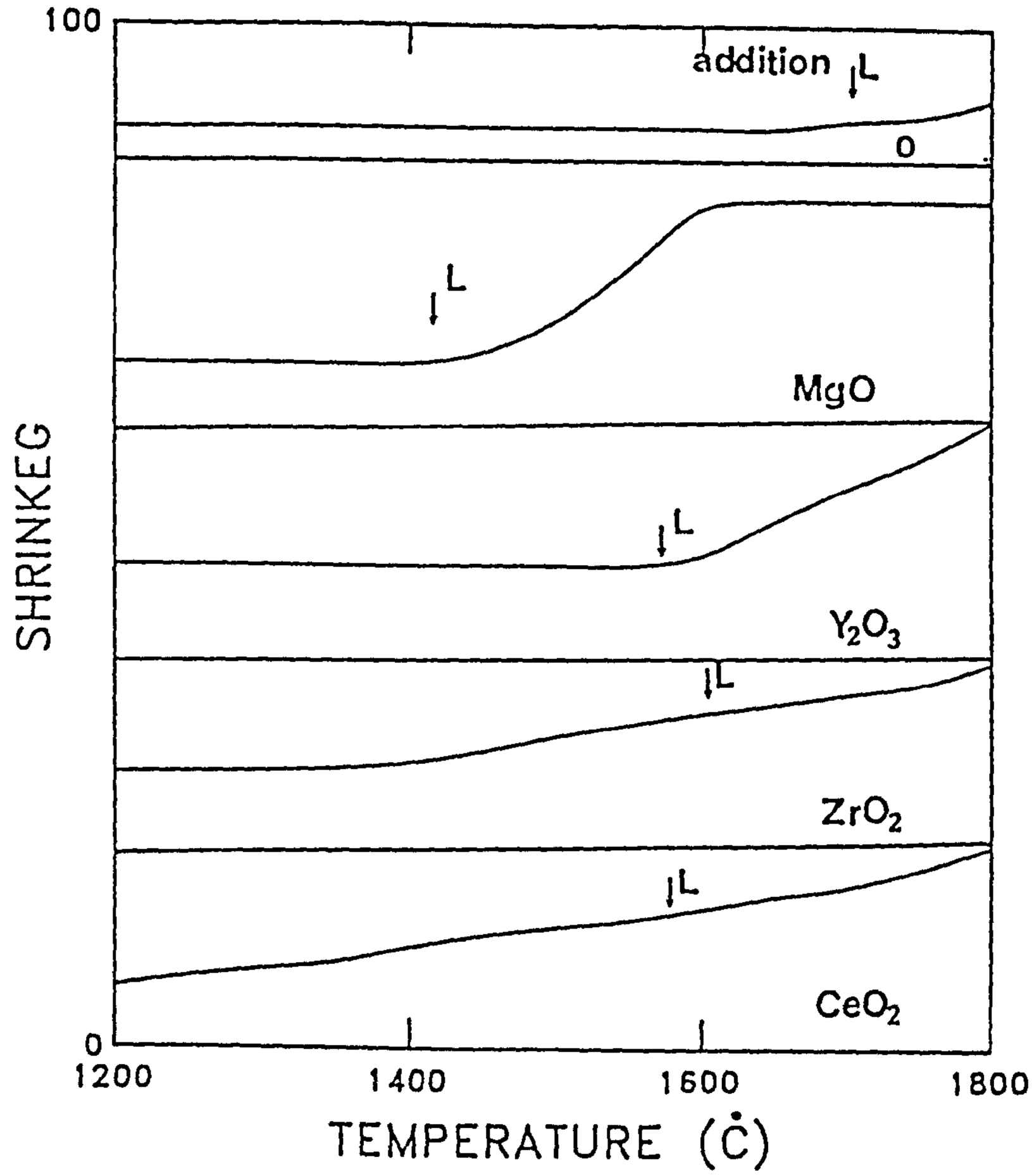

figure 2.3

A schematic plot of the influence of various oxide additives on densification behaviour [Jack 1977]

SiO_2 systems is higher than the liquid formation temperature as can be noticed in the results presented in figure (2.3). The difference in viscosity between Y_2O_3 and MgO–SiO_2 systems at any temperature (figure (2.2)) explains the higher rate of densification for MgO additive in figure.(2.3). In recent studies of pressureless sintering of β'–sialon, however, different rates of densification are obtained by using various types of additive. Sialon with 5%MgO has a higher densification rate than that containing 5%CaO, as can be seen in figure (2.4).[Edrees & Hendry 1989].

Table 2.1.

Liquid formation temperature for silicon nitride powder with 5wt% addition of metal oxide

Oxide	Li_2O_3	MgO	Y_2O_3	CeO_2	ZrO_2
Liquid formation temperature °C	1050	1390	1440	1470	1590
Oxide-SiO_2Liquidus temperature °C	1030	1543	1660	1560	1640

It was found that softening temperature, viscosity and consequently the beginning of sintering, rate of densification and shrinkage can be changed by the addition of a second metal oxide such as Y_2O_3–Al_2O_3 [Quackenbush et al 1983]. Larger amounts of liquid phase at lower temperature and hence lower viscosity was found to be formed when 5%Y_2O_3 plus 5%Al_2O_3 were added to silicon nitride rather than only 5%Y_2O_3 [Jack 1977]. Addition of a small percentage of MgO to the Y_2O_3–Si_3N_4 system results in a significant reduction in the sintering temperature, as shown in table(2.2) [Patel & Thompson 1987].

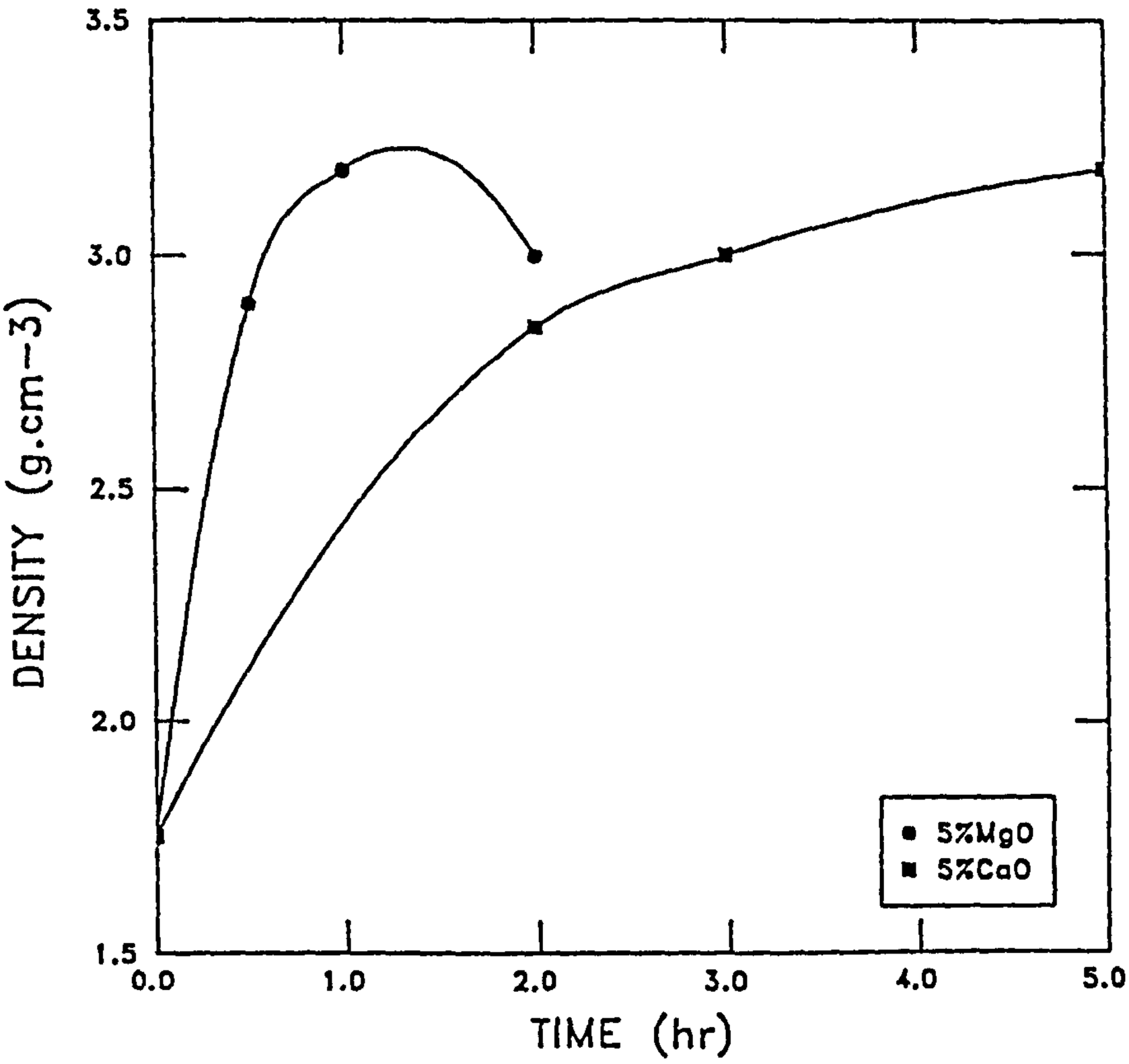

figure 2.4

The influence of different oxide additives on the rate of densification. [Edrees & Hendry 1989]

Table .2.2

Temperature at which densification starts for silicon nitride hot-pressed with yttria /magnesia additions at 1700°C for 1hr.

MgO	Y_2O_3			
	6	8	10	12
0	1570	1570	1580	1568
1	1410	------	1320	1340
2	1350	1350	-----	-----

Additionally the amount and type of additives seems to have a great effect on the grain morphology. For example, the average grain size of hot-pressed silicon nitride increases from 0.8μm to 1.7μm as the additive (MgO) content increases from 0.1wt% to 0.8wt% [Grathwoll et al 1982]. Moreover the addition of 7wt% yttria to Si_3N_4, Al_2O_3 and AlN mixture was found to be more than enough to allow a considerable grain growth of sialon with a typical elongated shape, whilst the addition of only 1wt% Y_2O_3 to the same mixture resulted in small and more or less equiaxed grains.[Ekstrom and Ingelstrom 1986]. Direct observation on the micrograph of pressureless sintered β'-sialon samples fired under identical conditions with either MgO or CaO additives shows that the amount of grain bondary glass is greater and the grains are bigger in the case of using a CaO additive.[Edrees & Hendry 1989]. These differences, however, can be attributed to the viscosity and the volume fraction of the liquid phase present at the sintering temperature. Generally, materials processed with additives which form a high viscosity liquid phase consist of large elongated grains. For certain additives however, the larger the amount of liquid phase, the greater the grain growth.

The work concerned with the effect of the amount of additives on densification rate reveals that the larger the amount of additive (more liquid phase) the faster the materials densify. For example figure (2.5) exhibits the effect of MgO on the rate of densification [Bowen et al 1978] and Boskovic [1988] experiments show that the starting mixture attained higher densification rate as the amount of Y_2O_3 increased. Usually larger percentages of sintering aids are not favorable because of their influence on properties, particularly at high temperature. The amount of sintering aids necessary to achieve high density can be reduced by applying external pressure (hot pressing).

It has been already pointed out that liquid phase works as a medium for the starting materials to dissolve into and precipitate as a more stable phase. In some cases, however, and depending on the starting compositions and additive type, the precipitated phase may remove elements from the liquid to give a modified structure based on the starting materials; such as the β'–sialon containing Mg (β''–sialon).[Gauckler et al 1978]. Depending on the starting composition, the β"-sialon is found to exist (with only MgO additive) with a wide range of hexagonal cell dimensions and fully crystalline β"-magnesium sialon may be produced by careful control of composition, impurity levels and heat treatment.[Wild & Leng-ward 1981]. Additionally CaO or Y_2O_3 additives are found to be incorporated (by the metals cations Ca or Y) into α– Si_3N_4 to form α'–sialon which has an identical structure to α– Si_3N_4 . [Hampshire et al 1978].

The presence of intergranular glassy phase (liquid at sintering temperature) in silicon nitride based materials has a strong influence on their mechanical properties and oxidation behaviour [Lewis & Barnard 1980]. For example, softening of the intergranular glass phase at elevated temperature can promote grain boundary sliding, creep and crack growth. Thus creep deformation and strength of these materials is strongly dependent on the composition of the grain boundary phase. Impurities and

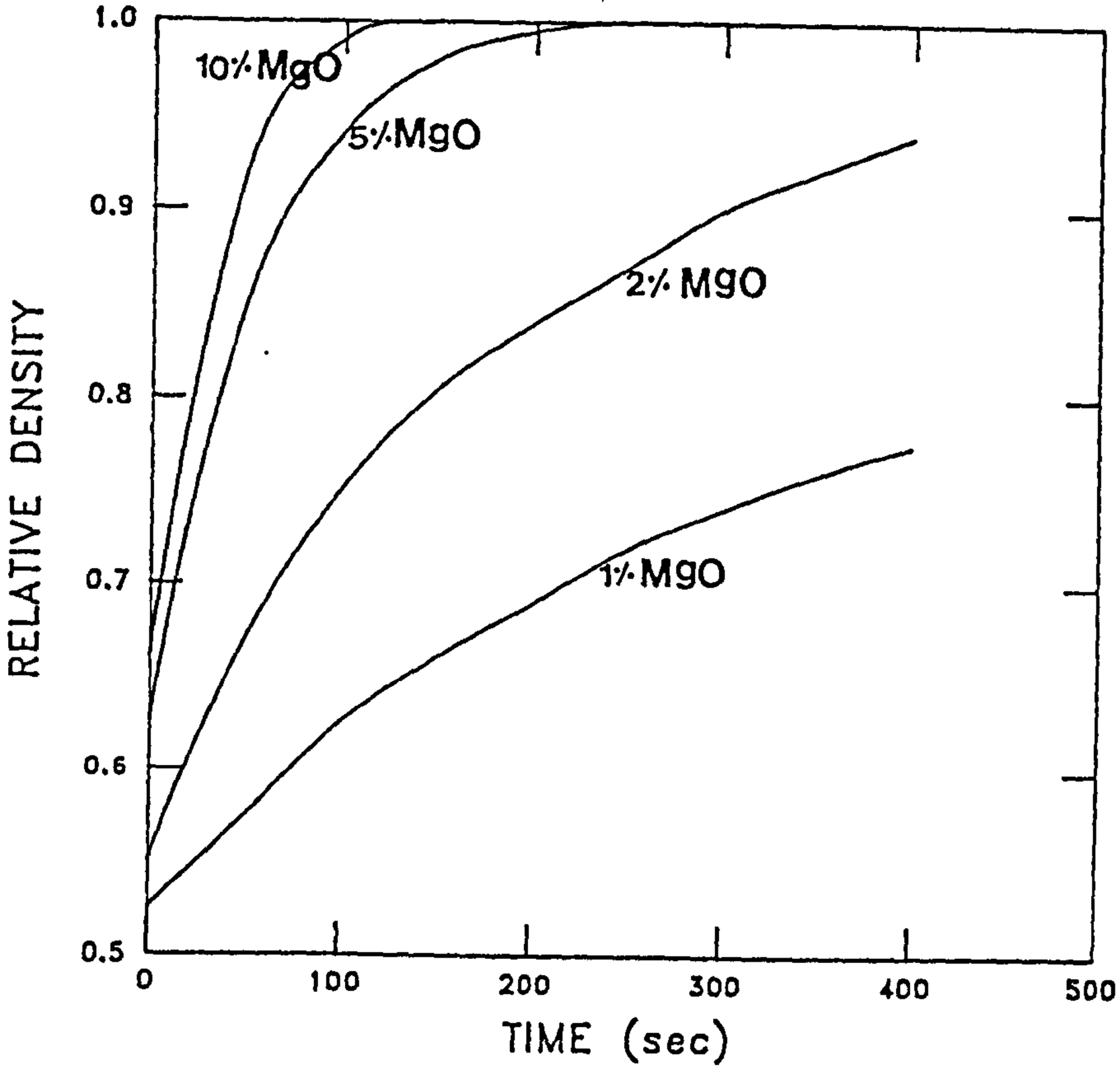

figure 2.5

The effect of MgO additive on the rate of densification of hot pressed silicon nitride. [Bowen et al 1978]

sintering additives are usually concentrated in the grain boundary and it has been demonstrated that impurities such as calcium significantly impair strength and creep performance of silicon nitride materials densified with MgO and the influence of MgO content on creep was very pronounced with high MgO [Isoke et al 1976]. The viscosity and the ability of the intergranular phase to crystallize are important factors in controlling high temperature properties. Using Y_2O_3 as an additive offers the two conditions of higher viscosity, and production of a more refractory intergranular phase. It is also stronger than MgO based grain boundary phase. Additionally, by post sintering heat treatment at about 1400°C the glass phase can react to give crystalline Yttrium-Aluminum Garnet (YAG) which has better mechanical properties. [Jack 1986]. Tsuge & Nishida[1978] found that YAG is only obtained as a grain boundary crystalline phase when Y_2O_3: $Al_2O_3 \geq 2$. Post sintering heat treatment helps to reduce the amount of glassy phase as this precipitates a refractory phase at grain boundaries and hence improves the high temperature properties. For example, a 44% strength enhancement is obtained after heat treatment of Si_3N_4 containing 8%$Y_2O_3$and 1%MgO [Giachello et al 1980]. Additionally, improvement in strength and fracture toughness of pressureless sintered silicon nitride containing Y_2O_3, AlN and SiO_2 was obtained after heat treatment [Das & Mukerji 1988]. Also by using MgO and SiO_2 additive to silicon nitride Das & Mukerji [1989] found that refractory phase $MgAl_2O_4$ could be crystallized and 33% improvement in strength at 1100°C is achieved. As with high temperature properties, oxidation resistance is found to be dependent on the amount and type of the grain boundary phase (amount and type of additive). In hot pressed silicon nitride materials, it was found that oxidation increases with increasing amount of MgO [Grathwohl et al 1982].

2.4 Influence Of Processing Conditions.

The important process parameters are temperature, time, atmosphere, powder characteristics and pressure; each of which is discussed in detail below:

2.4.1 Pressure.

Usually silicon nitride based materials are densified by a liquid phase sintering process in which the liquid forms above the relevant solidus temperature through reaction between the oxide sintering aid and the surface silica on the starting material particles. This liquid promotes densification by serving as a mass transport medium during sintering.[Hampshire & Jack 1981]. As discussed above, the presence of this intergranular glassy phase in the structure has a strong influence on properties. The amount of sintering additive (required liquid phase at sintering temperature), however, can be reduced by applying pressure during the course of sintering [Tsuge & Nishida 1978]. This reduction in the grain boundary phase is found to promote high aspect ratio in the final structure [Wotting & Ziegler 1983] and hence provide good mechanical properties. The applied pressure enhances the densification rate, higher pressure giving faster densification rates [Rahaman et al 1980] by promoting both rearrangement and solution-reprecipitation processes (the first and second stages in Kingery's model). This enhancement helps to complete densification at short times. For example density remains constant at pressing times longer than 10 mins and gives structures with a small grain size in Ziegler & Knoch [1981]. Pressure may also help to give some degree of orientation in the microstructure if there is enough low viscosity liquid [Bahini et al 1980]. However, Kingery et al [1963], in his model of liquid phase sintering ,included the effect of external stress on densification, as the

applied stress can make a significant increase in the capillary force to enhance densification, as will be discussed later.

2.4.2 Time and temperature.

In general the primary requirement with respect to the temperature is the formation of the liquid. Excess temperature over the liquid formation temperature increase the diffusion rates, the solubility of the solid particles, wetting of solid by liquid , the amount of liquid and decreases the liquid viscosity.

However in both hot press and pressureless sintering, temperature and time are equally important factors affecting the sintering process. Upper temperature, however, is limited by the decomposition of the starting materials and the vaporization of the liquid phase. The influence of temperature and time on the densification rate of hot pressed Si_3N_4/MgO is well characterised by Bowen et al in [1978] as shown in figure (2.6) and of pressureless sintering of β'–sialon/ MgO by Edrees & Hendry [1989] figure (2.7). From these figures it can be seen that for a given temperature and sintering additive, the densification process is time dependent and for specified time and sintering aid it is temperature dependent. This is found to be true for both hot press and pressureless sintering except that for the latter case the time for sintering is extended (as seen in figure 2.7) with volatilization from the sample continuing, causing density reduction. This may also be the case in hot press sintering carried out for long periods of time but no information is available concerning this technique. High temperature, however, causes the same effect as time on decomposition. [Futaki et al 1987].

From the above discussion it can be concluded that, as the temperature increases the liquid phase viscosity will decrease and this reduction promotes grain

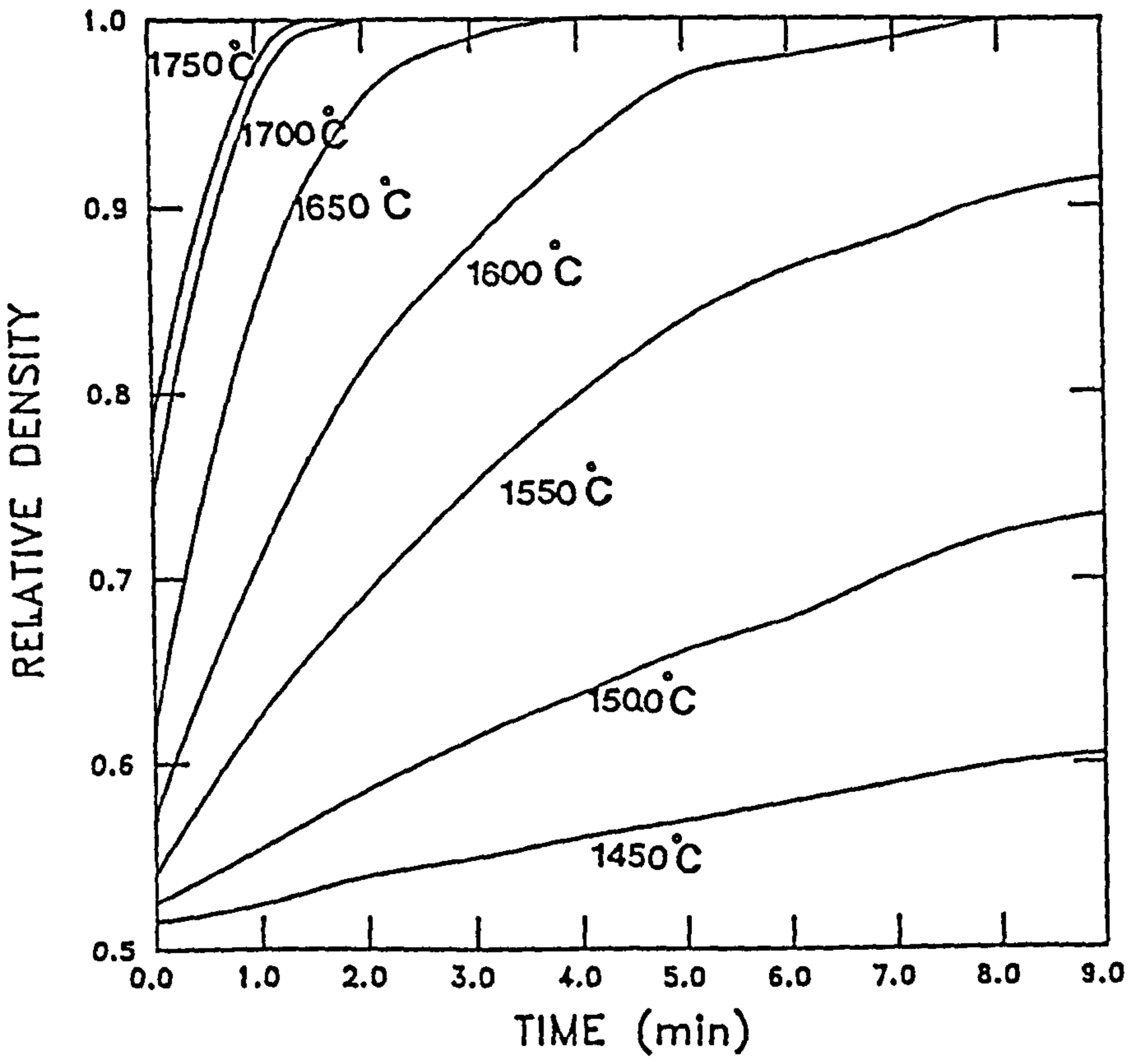

figure 2.6

The influence of temperature and time on the densification rate of hot pressed Si_3N_4/MgO. [Bowen et al 1978]

growth and so reduces aspect ratio. Long sintering time, however, also results in grain growth.

Both temperature and time have influence on the α to β phase transformation. Transformation increases with both temperature and time above a certain temperature. The α / β ratio is noticed to have an effect on the product's mechanical properties. For example, the strength of HPSN is increased with transformed β fraction and the maximum strength value coincides with the time needed for complete phase transformation [Knoch & Ziegler 1977]. The optimum time and temperature for hot press sintering to produce high strength materials of silicon nitride is found to be that for which the α to β transformation and accompanying densification are near to completion whilst still maintaining the small grain size of β crystal, required for high strength. [Drew & Lewis 1974].

2.4.3 Powder characterisation.

It is known that the powder condition has a great effect on the sintering behaviour of silicon nitride based materials especially for pressureless sintering. Wotting & Ziegler [1983] pointed out that the degree of densification in pressureless sintering depends largely on the particle size, and oxygen and carbon content of the starting materials. If the densification rate is determined by solution of the powder in the liquid, acceleration of this rate can be achieved by decreasing the particle size. Since the solution rate is dependent on the particle size, increasing the specific surface area of the powder leads to an improvement of densification by a solution–reprecipitation process. This has been proved in using Y_2O_3 and Al_2O_3 addition to Si_3N_4 which shows that increasing the surface area of the starting composition enhances the densification rate [Wotting & Ziegler 1983]. The presence of carbon in

the starting materials is found to decrease the amount of liquid phase by reaction with surface silica resulting in both CO and SiO gas formation [Miller et al 1979]. In terms of microstructure, however, Mitomo et al [1988] stated that the presence of impurities (metallic and non metallic) lowers the melting temperature of the liquid phase, which increases grain growth. Differences in sinterability of silicon nitride powder are noticed to be related to the average particle size, the smaller the particles the more sinterable the powder [Futaki et al 1987].

2.4.4 Atmosphere.

The sintering atmosphere is a final and very important processing factor of liquid phase sintering.The atmosphere protects the specimen against oxidation, decomposition and reactions during sintering. Due to the oxidation and decomposition of silicon nitride based ceramics ;

$$Si_3N_4 + 1.5O_2 = 3SiO + 2N_2 \quad \text{(oxidation)}$$

$$Si_3N_4 = 3Si + 2N_2 \quad \text{(decomposition)}$$

sintering must be carried out in a nitrogen atmosphere in order to inhibit both oxidation by the absence of oxygen and decomposition at high sintering temperature by increasing the nitrogen partial pressure in the atmosphere. High nitrogen atmosphere pressure, however, has enabled sintering to be carried out at high temperature by stabilizing the silicon nitride , therefore the amount of additives could be reduced to a small level [Mitomo 1976]. During the course of sintering, however, the equilibrium partial pressure of the various silicon compounds (the most important one is SiO gas)

must be established and overcome. High densification rate, as in hot press sintering, represents another way to inhibit SiO gas volatilization. Using the powder bed technique, however, is the optimum solution in pressureless sintering. Generating SiO gas, with partial pressure higher than that generated from the sample, is an effective technique used to densify β'-sialon containing 5%MgO in nitrogen at atmospheric pressure [Edrees & Hendry 1989]. In ceramic–matrix composites the problem of chemical incompatibility between the reinforcing phase and the matrix also appears and represents a major obstacle in addition to the volatilization problem. Control of the interfacial reaction of β'–sialon/carbon fiber composite is achieved through understanding of thermodynamics and rate of reaction ; a 40%CO/60%N_2 gas mixture is claimed to be sufficient to inhibit the reaction [Bower et al (1989)].

2.5 Formation Mechanisms.

The above discussion reveals that the requirements for complete densification are, fine particle powders, applying external pressure (hot pressing), increased sintering time and temperature (within certain limits), controlling the firing atmosphere, using powder bed technique, and addition of a suitable amount of oxide additive. If the addition of oxide provides a liquid with suitable viscosity and of good wetting to the matrix powder particles, densification can be described according to mechanisms of liquid phase sintering formulated by Kingery [1959]. Densification is the change in porosity from the green condition to sintering divided by the initial porosity. Because densification is dimensionless it is often expressed as a percentage; for example a densification of 100% corresponds to a compact which has been sintered to theoretical density. Densification is usually determined by shrinkage which refers to

a decrease in linear or volumetric dimensions of the sample during sintering. The sintering density is related to the green density through the linear shrinkage as follows;

$$\rho_s = \rho_g/(1-\Delta L/Lo)^3 \ldots\ldots\ldots\ldots\ldots\ldots (2.1)$$

where ρ_s is the sintered sample density, ρ_g is the green sample density and $\Delta L/Lo$ is the linear shrinkage.

Kingery [1959] proposed that densification in the presence of liquid occurs by a mechanism in which the overall change is believed to take place by three consecutive process. The initial stage is often referred to as rearrangement. The liquid formation during the course of sintering, associated with capillary force, causes rearrangement between solid particles to a higher coordination. The density increases during this stage. Rearrangement process occurs in a very short time to make such a model very difficult to test accurately. Kingery [1959] give a shrinkage dependence on time to the $(1+y)$ power;

$$\Delta L/Lo = R^{-1}t^{1+y} \ldots\ldots\ldots\ldots\ldots (2.2)$$

where R is the solid particle radius, and $1+y$ is slightly larger than unity.

The volume fraction of the liquid phase is important to the rearrangement stage. At a high volume fraction of liquid, densification is possible by rearrangement and pores will be filled by liquid especially if the liquid has low viscosity. As the amount of liquid in ceramics should be minimized (for good properties at high temperature), then other processes must be active for full densification. This process is solution precipitation and represents the second stage of Kingery's model.

After rearrangement, pores remain in the sample if the volume fraction of the liquid is not high enough. Although the solution and precipitation process might occur at the same time as rearrangement, it is not dominant in the first stage. During the second stage of liquid phase sintering, rearrangement ends and solution of the solid into the liquid and then precipitation processes becomes dominant. The rate of densification in this stage depends on the rate of mass transfer through the liquid. The principle materials transport mechanisms are understood in a very general way. Kingery [1959] ,however, in his model proposed that densification occurred by particle contacts flattening in which the stress at the particle contact point due to the capillary force from the wetting liquid cause the dissolution of the solid at the contact points and then reprecipitation at areas away from the contact. The flattening of the particle interfaces is accomplished by transport of the materials leading to "center to center approach" (shrinkage). The rate of materials transport determines the densification rate. As the size of the contact area increases with time, the stress along the interface is decreased and densification slows. Solution-reprecipitation occurs either by dissolution or diffusion. If transport is limited by the rate of mass transfer from the source (the contact) to the sink through the liquid then the process is diffusion limited. If the transport of matter is controlled by interface dissolution then the process is reaction limited. For diffusion control, Kingery expressed the shrinkage ($\Delta L/Lo$) as;

$$(\Delta L/Lo)^3 = 12\,\delta\,\gamma\,\Omega\,C\,D\,t\,/\,R^4\,K\,T \quad \text{.....(2.3)}$$

and for reaction control as;

$$(\Delta L/Lo)^2 = 4\,Kr\,\Omega\,C\,\gamma\,t\,/\,R^2\,k\,T \quad \text{.....(2.4)}$$

where;

δ = is the thickness of the liquid layer between the grains

γ = is the liquid-vapor surface energy

Ω= is the atomic volume

D= is the diffusivity of the solid in the liquid

C= is the solid concentration in the liquid

t= is the time

k= is the Boltzmans' constant

T= is the absolute temperature

R= is the grain radius

Kr= is the reaction constant

These equations demonstrate the effect of the main process variables on shrinkage. The difference in time dependence on shrinkage is the basis for analysizing the behaviour of several systems. The shrinkage exponents will depend on the grain shape. For grains which are not regular the exponents become **5** and **3** for diffusion and reaction control respectively. For liquid phase sintering with pressure Kingery et al [1963] expressed the effect of the external stress on the shrinkage as follows

$$(\Delta L/Lo)^3 = [g\ \delta\ D\ C\ \Omega\ t / G^3\ K\ T]\ [\sigma+2g/r] \ldots\ldots (2.5)$$

where

g = is geometric constant

G = is grain size

r = is the pore size

σ = is the applied stress

In silicon nitride ceramic systems and according to Hampshire & Jack [1981] interpretation of Kingery's model, there is always some α to β phase transformation in order to complete densification. Brook et al [1977], however, did not consider transformation to be a necessary factor for densification which is supported by several investigators; for example Mitchell & Hendry [1986] and Edrees & Hendry [1989].

As an alternative approach to Kingery's model the hot pressing model proposed by Coble [1970], which describes the densification rate for control by grain boundary diffusion, was used to interpret the densification mechanism in liquid phase sintering. The Coble model has been applied to liquid phase sintering by assuming that the boundary thickness in the model is the thickness of the liquid phase boundary film [Brook 1977]. The intermediate stage of the Coble hot–pressing model applied for liquid phase sintering by Brook is in the form;

$$d\rho/dt = 47.5\ P\ D_b\ a^3\ w\ /\ G^3\ \ k\ \ T \qquad \text{.....(2.6)}$$

where ;

P = is the applied pressure

$\mathbf{D_b}$ = is the boundary diffusion coefficient

$\mathbf{a^3}$ = is the volume of material transported for each atom of the rate controlling species.

w = is the boundary thickness

G = is the grain size

Applying this model, Bowen et al [1978] found that diffusion of Si/N through the liquid phase away from the region of high stress between particles is proportional to the amount of the liquid phase. They also attributed the slow densification rate below 1550°C to the process of diffusion through the solid grain boundary phase. In

general the intermediate stage of liquid phase sintering is characterized by densification and grain shape change to attain minimum surface energy and grain growth.

The third and final stage in liquid phase sintering is microstructure coarsening through which the maximum density is attained and rigidity of the compact is provided in this stage.

CHAPTER THREE

EXPERIMENTAL TECHNIQUE

3.1 Raw Materials.

3.1.1 Matrix material.

Syalon 201 (Cookson Ceramics & Antimony Ltd, Wallsend, England) is used as the matrix phase in the present investigations. It is a mixture of α-Si_3N_4 , Al_2O_3, AlN polytype and 8wt% Y_2O_3 designed to give β'-sialon of Z= 0.75 after sintering.

3.1.2 Reinforcement phases.

(i) Carbon fiber was supplied by the Osaka Gas Company, Japan. The specifications are given in the table in appendix (1).

(ii) Stainless steel AISI 316. Commercial powder of AISI 316 stainless steel (18%Cr, 10%Ni, 3%Mo) with mesh size less than 300 (<47μm).

(iii) TiN powder supplied by Goodfellow Metals (England) with a maximum particle size of 45μm and of 99% purity.

3.2 Green Sample Preperation.

3.2.1 Carbon fiber reinforced sialon.

The addition of carbon fiber to ceramics in order to improve the properties results in difficulties in distributing the fiber in the matrix. Different methods were tried to disperse the chopped fiber and produce green pellets as discussed below.

(i) Wet mixing, drying and uniaxial pressing.

The matrix and relevant amount of carbon fiber were wet mixed using propan 2-ol and alumina balls as a mixing media. The plastic bottle containing the mixture was placed on a Turbula mixer for 100hr. The mixture was then dried under a heating lamp and remixed in the dry condition. The pellets were made by uniaxially pressing the required quantities of the mixture (depending on the pellet size needed) in a steel die. The pressure required for compaction was applied and removed slowly to reduce the incidence of cracking and lamination during the pelletization process.

(ii) Slip casting.

In wet mixing long times are necessary for uniform distribution of the fiber in the matrix. However, long mixing times result in the length of fibers being broken. Slip casting offers the advantage of overcoming this problem and near net shape consolidation is achievable. The green compact can be prepared directly from wet mixtures without the necessity of the dry processing step and the fiber is distributed uniformly during casting.

In the present study a slip of chopped fiber and sialon powder was prepared by mixing in distilled water. The pH of the solution was then adjusted by the addition of NH_4OH in order to prepare a homogeneous slip. After 5 to 10 hours of mixing, as discussed above in (3.2.1 i) the slip was poured into a calcium sulphate (plaster of paris) mould and dried naturally in the mould.

(iii) Uniaxially pressing of dry slip cast product.

The sample prepared by slip casting may be further consolidated by uniaxial pressing of dry pieces. The aim of this method is to increase the green density but keep the fiber distribution as even as the slip cast product.

(iv) Uniaxially pressing and heating of the wet slip cast product.

A schematic representation for this technique is shown in figure (3.1) in which a wet specimen of slip cast material or any wet powder mix is placed into a preheated steel die at a temperature high enough to evaporate the liquid from the sample. Pressure is then applied to the wet sample and held until it dries and then cooled down to room temperature.

(v) Atmospheric drying of the slip

Green compacts with a near net shape can be formed easily by leaving the slip, prepared as in (3.2.1 ii), drying in the atmosphere at room temperature in a glass dish.

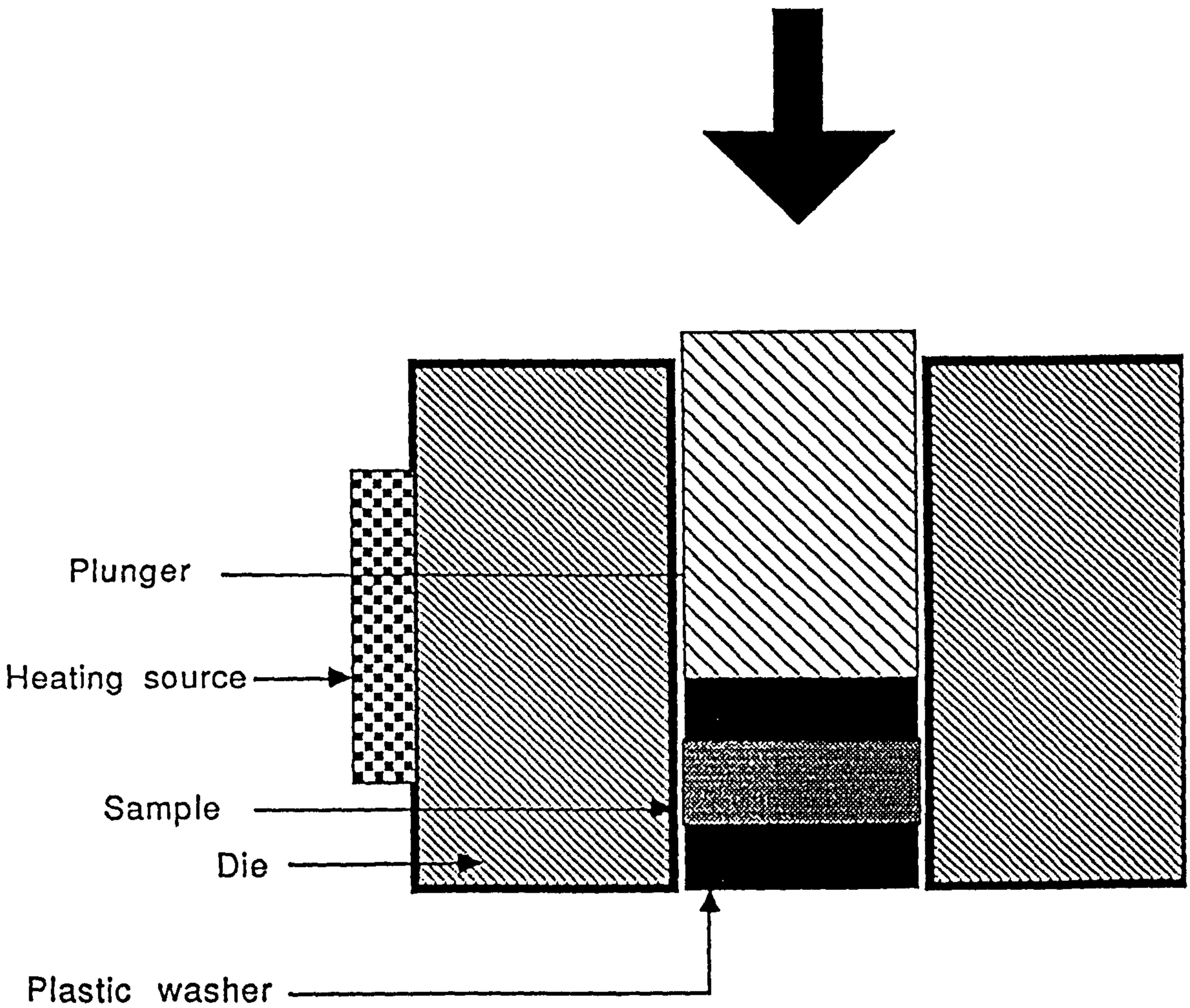

figure 3.1

Schematic representation of compact formation technique.

3.2.2 Stainless steel or TiN reinforced sialon.

Pellets of these mixture are prepared as in the method discussed in 3.2.1 a.

3.3 Density Measurement.

The density of the samples was evaluated using a mercury balance displacement method using the following equation;

$$\rho_{bulk} = M\,\rho_{Hg} / M+m$$

where;

M = mass of sample in air

m = mass required to immerse the sample into mercury

ρ_{Hg} = density of mercury (13.56 $gm.cm^{-3}$)

3.4 Pressureless Sintering.

Sintering in atmospheric pressure was carried out in different types of furnaces as discussed below;

3.4.1 Horizontal tube furnace

A horizontal alumina tube furnace with internal diameter of 39 mm was used for sintering at temperature up to 1550°C. Heating was accomplished by electrical resistance. Green samples embedded in sialon 401 set on an alumina boat were

introduced to the hot zone. The tube ends were closed and nitrogen gas switched. Sintering temperature was then selected with the monitor. The heating rate is automatically controlled by a built–in thermocouple.

3.4.2 Graphite element furnace.

A Balzer's carbon element sintering furnace with capacity of 2100°C was used for pressureless sintering . In this furnace the samples were embedded in sialon 401 ($Si_3Al_3O_3N_5$) in order to reduce the volatilization of the specimen. The furnace was first evacuated, flushed with nitrogen and evacuated again. The furnace chamber was then filled with nitrogen or a nitrogen/carbon monoxide gas mixture (in the case of carbon fiber /sialon composite sintering). The gas mixing is controlled by using two flowmeters on the inlet of the furnace chamber. Temperature measurement was carried out with a Pt/Rh thermocouple inserted through the cover of the furnace. After sintering the furnace was left to cool down to room temperature and the sample was removed for examination.

3.5 Hot Pressing

The arrangement for hot–pressing is shown in figure (3.2). The cold compacted powder is embedded in boron nitride (in order to prevent reaction between the die and the sample) and placed in the graphite die with a lower silicon nitride plunger already inserted. The upper plunger is then put in place. Pressures 20MN/m^2 are transmitted to the sample inside the die from the hydraulic press via the silicon nitride plungers. The samples were fired under this pressure at different temperatures. Heat was supplied by an induction coil, and the temperature was monitored by a

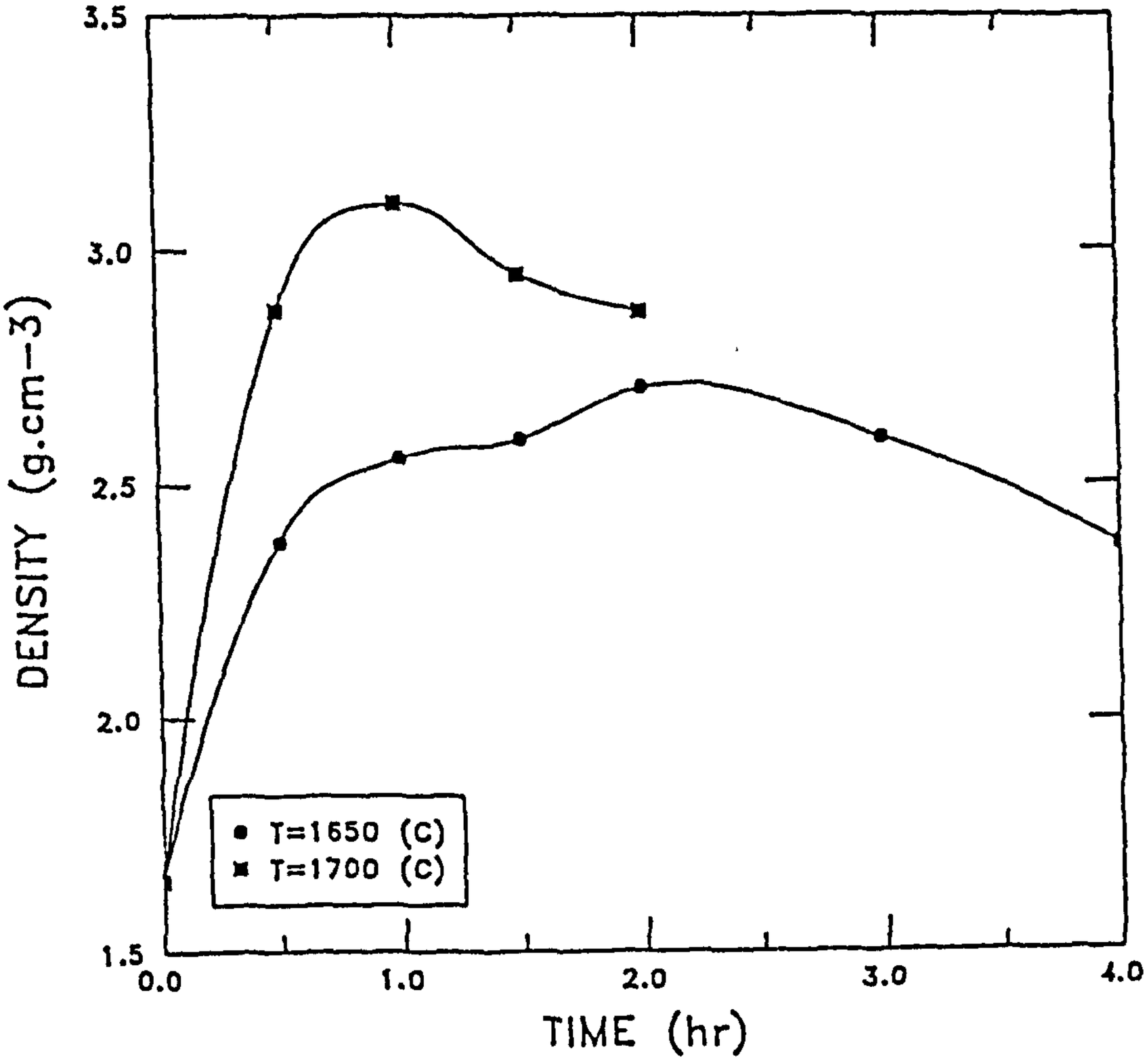

figure 2.7

The influence of temperature and time on pressureless sintered β'–sialon with 5wt% MgO additive.[Edrees & Hendry 1989]

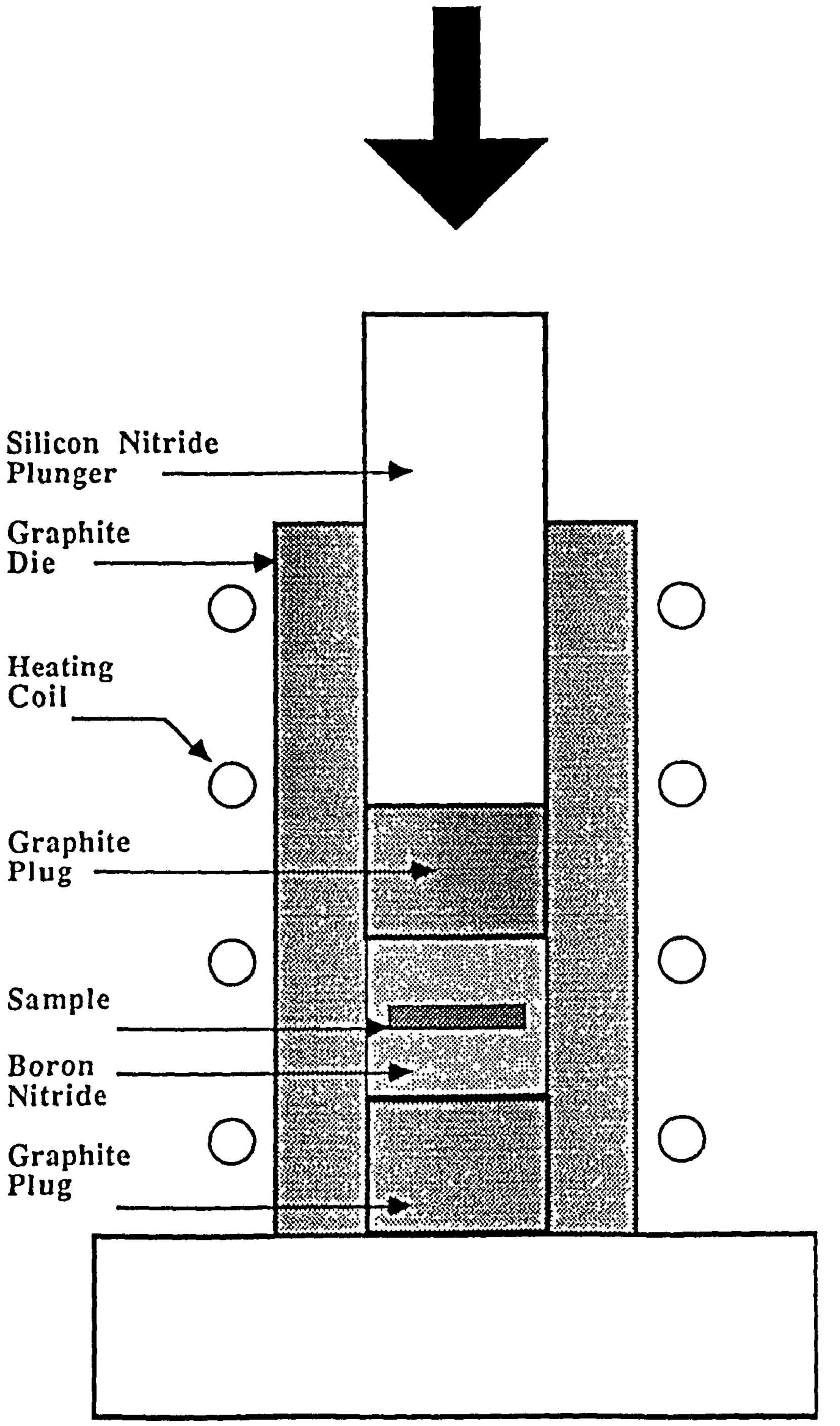

figure 3.2

Schematic representation of the hot pressing die

disappearing filament pyrometer. A transducer was attached to the system to monitor the shrinkage of the specimen during the course of sintering.

3.6 Preparation For Optical & Electron Microscopy.

For optical microscopy the samples were set either into cold setting resin, (8 : 1 epoxy resin to hardener volume ratio) under vacuum to produce good cross sections in porous samples, or hot mounting bakelite for the high density samples.

The specimens were then polished with different grades of silicon carbide paper (starting with low grade 320 and finishing with grade 1200). Dp cloth with 3μm diamond spray is the next polishing step performed on a Struers Automatic Pedimin Machine for 30 minutes. Spray (every ten minutes) and blue lubricant is used. The samples were cleaned after each step of the process by either methanol or acetone to prevent any contamination. For SEM, the samples were coated with gold alloy under vaccum to aid surface conductivity and thus to minimise the effect of charging. Agar quick drying silver paint was used to fix the specimens onto aluminium stubs. Specimens were studied using a Nikon reflecting light optical microscope and a Philips PSEM 500 scanning electron microscope with a link System EDAX analyser. For transmission studies a Philips EM400T analytical STEM with EDAX windowless EDS analyser was used. The TEM samples were polished down to a thickness of less than 30μm and subsequently thinned using an Ion Tech ion beam thinner. The specimens were then carbon coated to prevent charging before examination was performed.

3.7 Phase Identification.

The identification of phases was carried out by X–ray diffraction using Hagg–Guinier focussing cameras with copper radiation. Cell dimensions of the sialon were determined using a computer program [Carr 1988]. The Z values of the sialon were calculated by the following formulae [Liddell 1986]

$$Z = (a - 7.6023)/ 0.030$$

$$Z = (c - 2.9060)/ 0.027$$

$$Z = (c/a - 0.38226)/ 0.002$$

3.8 Hardness & Fracture Toughness Measurements.

Hardness and fracture toughness values were measured by using a Vickers diamond pyramid indenter and evaluated using the Lawn & Fuller [1975] method by measuring the crack length induced for median crack type;

$$Kc_{Idt} = \psi_b \ (P/c^{3/2})$$

where;

$$\psi_b = 1/ ((3/2) \pi \ \tan \psi),$$

and ψ is the half angle of the vickers indenter (68°), **P** is the indentation load in **MN** and **c** is the radial crack length in **m.**

However, Shetty et al [1985] method was used to evaluate the toughness of palmqvist type crack;

$$Kc = 0.0319\ P/a\ (l)^{1/2}$$

where **P** and **c**, are as above and **a** is half of the sum of the two indent diagonals.

3.9 Differential Thermal Analysis.

STA 1640 apparatus has been used to evaluate the reactions that might occur during the course of sintering. A small piece of the sample (maximum of 200 mg) is placed in an alumina crucible (of 6mm diameter) and heated under a controlled heating rate in one atmosphere of nitrogen gas. The reactions results are analysised by a computer software written by PL Thermal Science Ltd. The sample weight change during the experiments has been recorded. Temperature has been measured by using a Pt/Pt.13Rh thermocouple.

3.10 Conductivity Measurements.

Samples resistivity was measured using a digital multimeter (Schlumberger). A small pieces of the sample with flat parallel surfaces and known area and thickness were placed in a rig designed for this purpose. The contact areas of the sample with the rig were coated with a silver paint to make sure that there was a good contact. The power was then switched on and time of five minutes was given for the system to stablise. After that the resistance of the sample was taken. The resistivity was then evaluated by measuring the area and the thickness of the sample as follows;

$$\rho = R\ A/h$$

where ;

ρ is the resistivity

R is the resistance

A is the sectional area of the sample

h is the thickness of the sample

CHAPTER FOUR

CARBON FIBER/SIALON COMPOSITES

4.1 Introduction.

For many years, researchers have sought to develop tough ceramics with performance characteristics which will retain high strength at elevated temperatures. The addition of whiskers or fibers to ceramics has been known for many years to be one approach to achieving this goal. Recently, fiber-reinforced ceramic matrix composites have received a great deal of attention for use in high temperature structural applications. The primary reason for these efforts lies in the assumption that strong fiber, or whiskers, can prevent brittle failure in ceramics and density reduction may be achieved by using lower density fiber. A range of different fiber materials potentially suitable for ceramic matrix reinforcement are commercially available and are also under development. These include whiskers as well as continuous fibers.

Depending upon the applications required for the fiber reinforced ceramic matrix composites, nearly all ceramic materials are potential matrix materials (these include glass and glass ceramic, crystalline oxides, carbides, and nitrides). Glass and glass ceramics have been widely used owing to their relative ease of composite fabrication by hot pressing and the principle of fiber reinforcement, however, has been successfully applied in developing composites with glass and glass ceramic. Here

it has been indicated that there exists a series of promising carbon fiber reinforced glass materials which not only have higher strength but also higher fracture toughness. They also exhibit excellent thermal and mechanical impact resistant behaviour [Sambell et al 1972]

Only very limited work has been performed on fiber reinforcement to silicon nitride matrices. Early work, however, showed that the addition of ZrO_2 to carbon fiber reinforced silicon nitride and low temperature hot pressing enables the problems of physical (thermal expansion mismatch) and chemical incompatibility (reaction between the fiber and the matrix) to be overcome [Guo et al 1982]. Also by employing hot isostatic pressing (200 Mpa at 1650°C) as a sintering method for slip cast carbon fiber reinforced silicon nitride, it was noticed that there is no evidence of any reaction at the fiber matrix interface. However, when pressureless sintering was used the reaction was severe.[Lundberg et al 1985].

Problems with oxidation during fabrication of carbon fiber reinforced matrix composites led researchers to use alternative fibers ,such as SiC, instead of graphite. It was demonstrated that the SiC fiber reinforced glass matrix composite system was capable of achieving excellent mechanical properties (fracture toughness and fracture strength) up to 600°C [Prewo & Brennan 1980]. A more recent investigation of SiC fiber reinforced glass and glass ceramic matrix composites, shows that they can be fabricated with high strength and excellent toughness properties from room temperature to over 1000°C. In addition, low density and low thermal expansion were achieved [Brennan & Prewo 1982]. Development of oxidation-resistant SiC fibers and their successful application to glass-ceramic matrix composites has been a major factor in the increased research on fiber reinforced silicon nitride matrix composites. The fracture toughness of SiC fiber reinforced Si_3N_4 matrix consolidated via hot pressing

has been reported to be significantly higher than that of hot pressed Si_3N_4 [Rice et al 1980].

Improvements in both the strength and fracture toughness of SiC whisker reinforced silicon nitride matrices has also been recorded by several workers. For example, Sergej et al [1987] claimed a 40% increase in fracture toughness and a 25% enhancement in strength when 30% SiC whisker was used to reinforce a silicon nitride matrix. Silicon carbide whiskers have been extensively used to reinforce alumina matrices to produce, as is reported by many researchers such as Becher & Wei [1984] and Homeny et al [1987], materials with attractive mechanical properties.

In both systems, however, (carbon or SiC fibers reinforced composites) chemical incompatibility between the reinforced phase and the matrix is expected during the course of sintering at certain temperatures; resulting in fiber degradation and poor product density. Kyotoku et al [1987], however, suggested a method to adjust the chemical compatibility. The principle of the reaction at one atmosphere total pressure has been elucidated, but attention must always be directed to potential problems of alternative reactions when change in the thermodynamic variables (p , T) occur.

Graphite particles have a different application to those discussed above. It is found that a dispersion of over 2V% of these powders in an aluminum alloy matrix markedly improves the wear resistance [Gibson et al 1984]. The addition of carbon or graphite to ceramics is not recorded in the literature.

The poor oxidation resistance of carbon fibers in composites need not stand as an obstacle to applications since this material could be used in low temperature applications, or in non oxidizing environments. The present study investigates carbon fiber reinforced β'-sialon composites from the green sample preparation stage (using different fabrication techniques) to the evaluation of properties.

4.2 Thermodynamic Aspects Of Carbon /β'-Sialon System.

Ceramic matrix composites are prepared by sintering using high temperature powder technology and in general are used for high temperature applications. Chemical reactions between the matrix and the reinforcing phase might occur, especially during the course of sintering (which represents the most important stage in ceramic component fabrication). This chemical incompatibility leads to inhibition of the densification process. Minimization of the interfacial reaction between the composite components is considered to be the most essential factor for densification optimization. A prediction of the reactions which may occur at sintering temperature is required in order to control them and hence promote densification. Kyotoku et al [1987], has described the principles of control of the interfacial reaction in ceramic matrix composites.

To apply these principles to the present system (carbon fiber/sialon) it is first necessary to predict the reactions which might occur. The sialon being used in this study is β'-sialon with low Z value (0.75). The general equation governing this system is;

$$Si_{6-Z}Al_ZO_ZN_{8-Z}+ZC+(Z/3)N_2 = (6-Z/3)Si_3N_4+ZAlN+ZCO \quad ...(4.1)$$

The free energy for reaction (4.1) assuming total pressure of 1 atm and an activity of unity for all solid components is;

$$\Delta G_{R4.1} = -R\ T\ \ln\ K(T)$$

with the equilibrium constant;

$$K(T) = (P_{CO})^Z / (P_{N_2})^{Z/3}$$

The Gibbs free energies of formation for reaction (4.1) are taken from Hendry (1976) for Si_3N_4 , Kubaschewski & Alcock (1983) for Al_2O_3, AlN and CO and Kaufman (1979) for β'-sialon. However, according to chemical principles, increasing (P_{CO}) in the sintering atmosphere will drive the reaction back towards the left-hand side in other words it will prevent reaction (4.1) from occurring. The partial pressure (P_{CO}) is calculated for different Z values and plotted against temperature in figure (4.1). For Z= 0.7 it can be seen in figure (4.1) that (P_{CO}) required to inhibit reaction (4.1) ranges from 0.01 to 0.06 atm., as the temperature increases from 1500°C to 1750°C. This means that by controlling the sintering atmosphere with the calculated amount of carbon monoxide gas for each sintering temperature, reaction (4.1) should stop unless there is some other reason for the reaction to continue. It can also be seen in figure (4.1) that increasing Z value (which means replacing more nitrogen by oxygen) leads to an increase in (P_{CO}). This figure shows that, (in spite of the fact that the stability of β'-sialon increases with Z value,) at any temperature, the partial pressure of carbon monoxide gas is higher for the higher Z value sialon.

The sialon being used in the present study is Cookson 201 which is an unreacted β'-composition to give Z=0.75 upon sintering. The components are α-Si_3N_4 , Al_2O_3 , AlN–polytypes and 8wt% Y_2O_3. Furthermore, the Si_3N_4 usually contains a surface layer of SiO_2. This means that the carbon fiber could react with any one of these components leading to a low density product. All of these possibilities are investigated below;

$$Si_3N_4 + 3C = 3SiC + 2N_2 \quad \ldots\ldots(4.2)$$

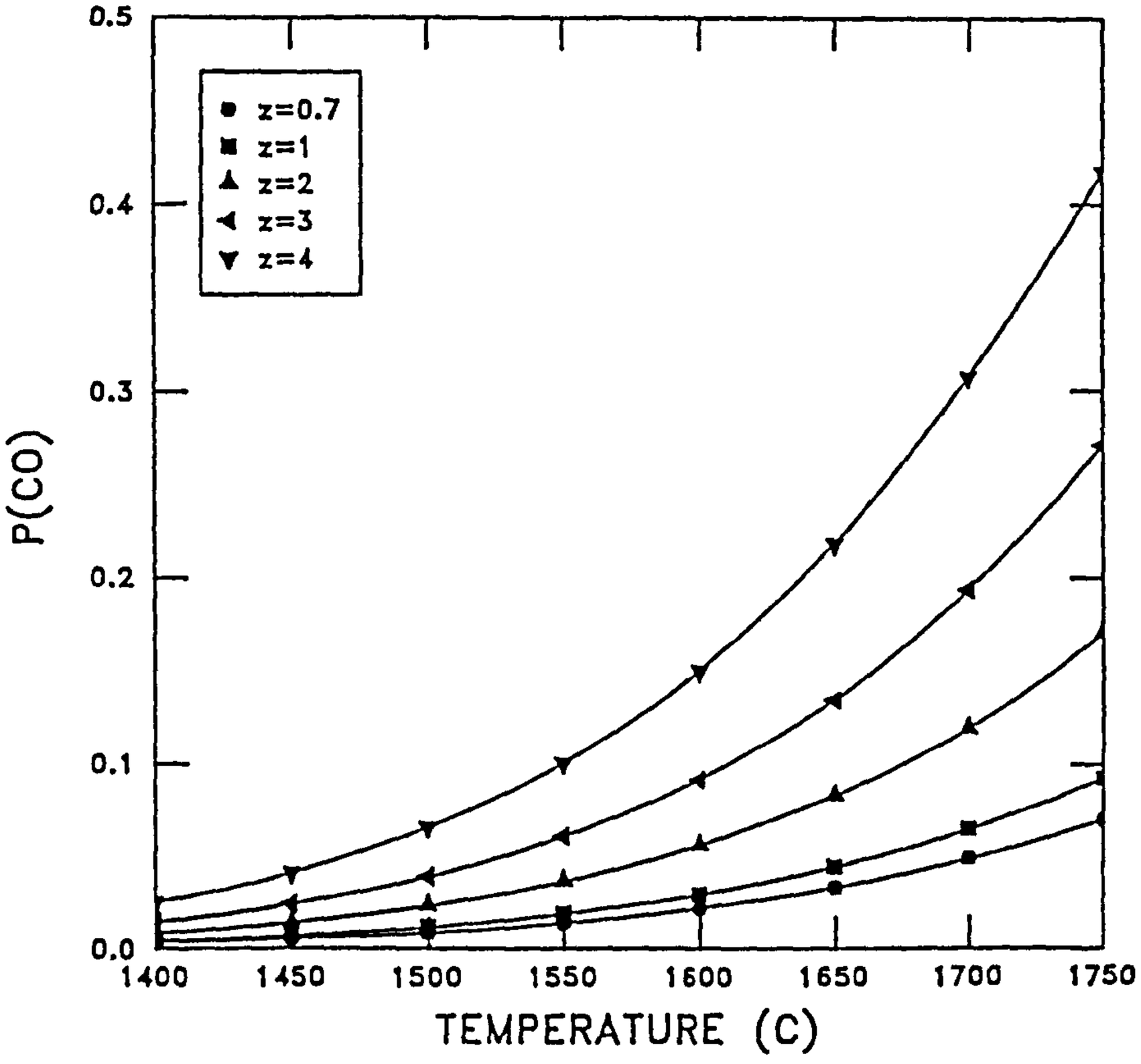

figure 4.1

Variation of carbon monoxide partial pressure in carbon/sialon system with temperature and sialon Z value.

$$\Delta G_{R4.2} = - R\ T\ \ln\ K(T)$$

$$= 197960 - 8.19\ T - 87.8\ T \quad \text{(cal)}$$

with equilibrium constant ;

$$K(T) = (P_{N_2})^2$$

Another reaction which might occur is;

$$Al_2O_3 + 3C + N_2 = 2AlN + 3CO \text{.....(4.3)}$$

$$\Delta G_{R4.3} = - R\ T\ \ln\ K(T)$$

$$= 1166820 - 85.74\ T \quad \text{(cal)}$$

with equilibrium constant;

$$K(T) = (P_{CO})^3 / P_{N_2}$$

The surface silica could also react with the fiber as follows;

$$3SiO_2 + 6C + 2N_2 = Si_3N_4 + 6CO \text{.....(4.4)}$$

$$\Delta G_{R4.4} = - R\ T\ \ln\ K(T)$$

$$= 281200 - 154.9\ T \quad \text{(cal)}$$

with equilibrium constant;

$$K(T) = (P_{CO})^6 / (P_{N_2})^2$$

This assumes that only gases and pure solids are present.

The problem, however, is not as simple as that described above in reactions (4.2), (4.3), and (4.4) because the simultaneous presence of Al_2O_3, SiO_2 , Y_2O_3 and nitrogen gas at a certain temperature lead to the formation of liquid phase Y-Si-Al-O-N [Jack 1977]. This means that reactions between solids and liquids could also occur but there is no information concerning these reactions. Reaction (4.2) is a solid/ solid reaction and the rate may be assumed to be low compared to the gas/solid reactions. Additionally, the nitrogen partial pressure generated from reaction (4.2) is always lower than the partial pressure of the sintering gas atmosphere. Reaction (4.3) and (4.4) have therefore to be considered. The partial pressures of CO gas evolved from these reactions are plotted against temperature as shown in figure (4.2). This figure indicates at a sintering temperature of approximately 1542°C and in nitrogen at atmospheric pressure, reaction (4.4) can not be controlled (ie $P_{CO} > 1$). Similarly reaction (4.3), which is slightly more stable, will produce CO gas with a pressure of over one atmosphere at sintering temperature above 1670°C. Both reactions, however, will inhibit densification and especially in reaction (4.4) where removal of the SiO_2 layer on the silicon nitride particles means that the possibility of liquid phase formation (required for densification) will be very low at sintering temperature. Reaction (4.3) does not affect liquid formation because there is still the possibility of formation in the Y-Si-O-N system as well as in the Y–Al–Si–O–N system, but at higher temperature.

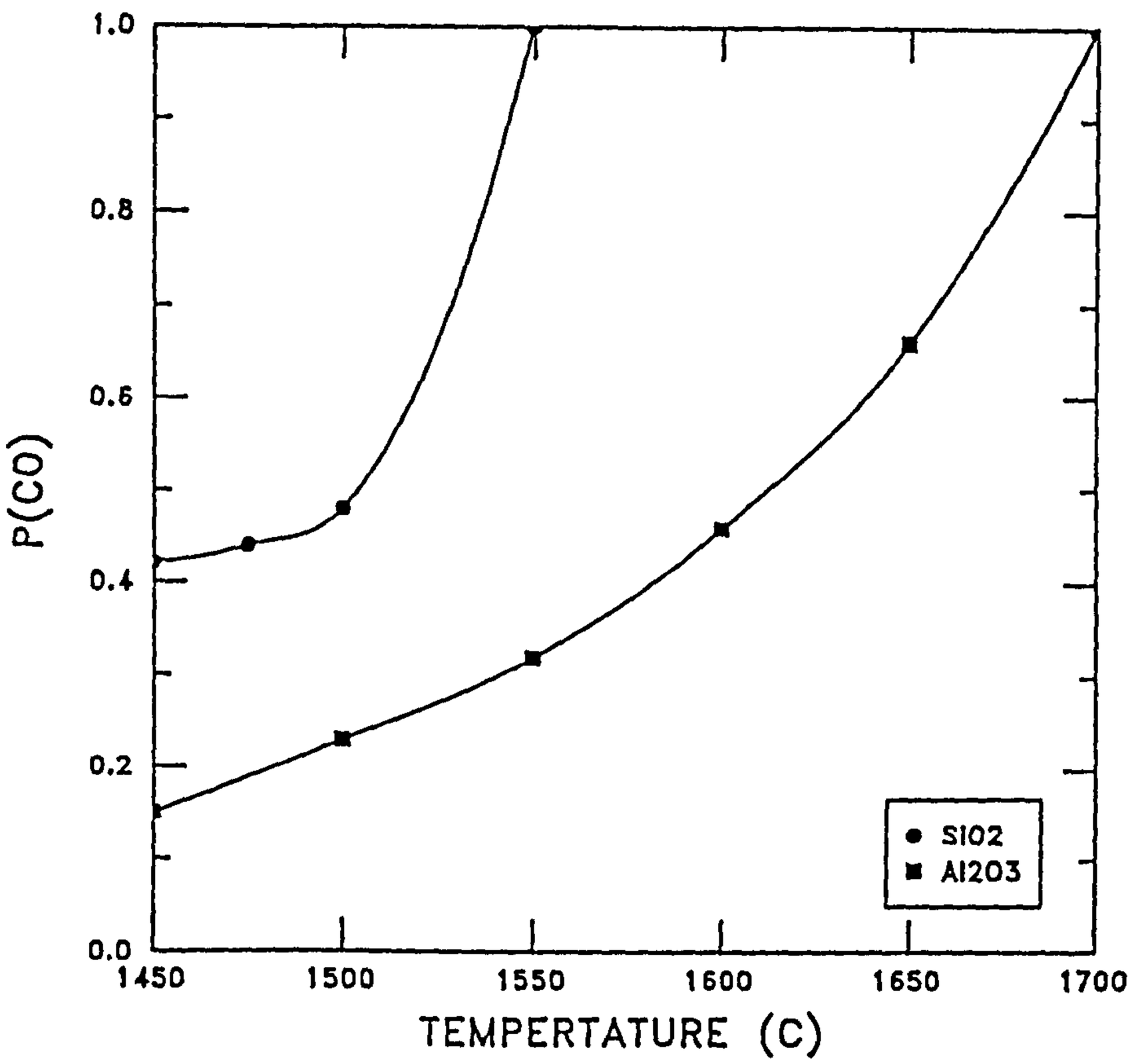

figure 4.2

Variation of carbon monoxide partial pressure in carbon/Al_2O_3 and SiO_2 systems with temperature.

However, in the all the above cases the value of P_{CO} stated represents the maximum since the activity of all the solid were taken to be unity.

4.3 Results and Discussion.

4.3.1 Slip preparations.

Difficulties in producing a homogeneous slip of carbon fiber–sialon mixtures was noticed during the slip preparation. The fiber always floats on the surface of the solution, even in a pH controlled solution. However, the addition of a few drops of propan–2–ol to the carbon fiber/sialon mixture (in water) was found to be very effective in removing the carbon fibers from the surface and dispersing them into the slip to make a homogeneous suspension.

4.3.2 Green sample density results.

The success of ceramic fabrication is highly dependent on the green density of ceramic, or ceramic composite samples. The higher the green density the faster the densification rate and a larger particle to particle contact provides more sites for the the densification process to start. The green density of 10V% carbon fiber sialon composite was investigated by using different processing techniques based on uniaxial pressing and slip casting. The results are listed in table (4.1).

Table (4.1)

Green sample density achieved from different fabrication techniques.

Technique	Theoretical %
A- Slip casting	48
B-Uniaxial pressing of dry slip casting material	56.5
C-Uniaxial pressing and heating of wet mixture	62
D-Atmospheric drying of slip	47

The results above reveal that the most effective technique for producing samples with high green density is by simultaneously pressing and heating a relatively wet mixture. The SEM micrograph in figure (4.3) shows the distribution of the fibers in the matrix and the powder particles around the fiber.

The reason for using the slip cast product in methods (B) and (C) is to retain the advantage of good fiber distribution which was obtained by the casting process.The density enhancement in this technique (C) could be attributed to the presence of liquid films on the surface of the ceramic powder particles which under pressure allow the particles to slide and rearrange to form a high coordination number and remain in this position as the liquid evaporates on heating. It was also noticed that the strength of the samples prepared by this method is adequate for handling and shaping the samples.

figure 4.3

SEM photograph for green sialon sample containing10V% carbon fiber grade (A) perpared as in method (C) table (4.1)

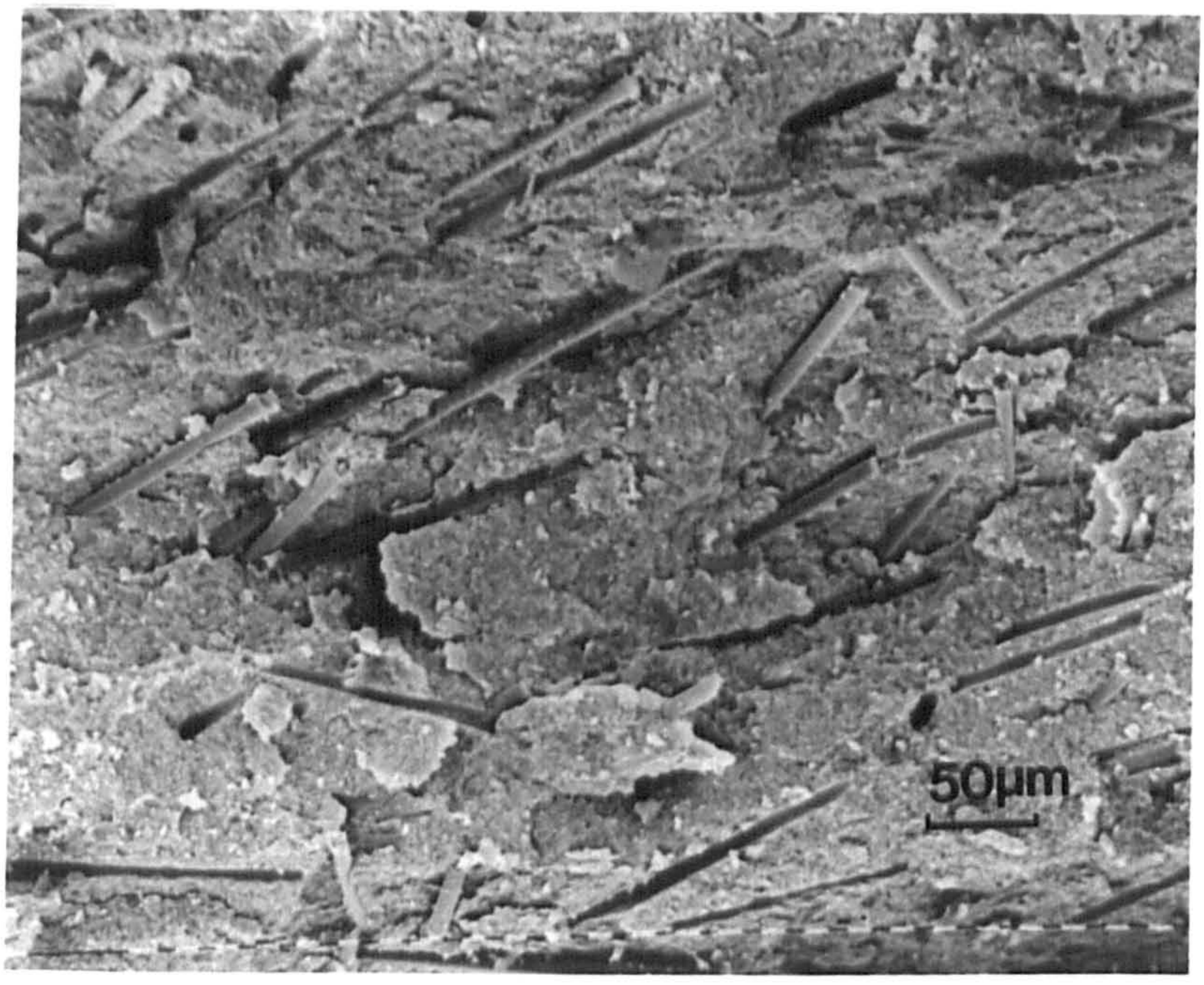
50μm

4.3.3 Pressureless Sintering of carbon fiber/sialon composites.

In order to fabricate carbon fiber/sialon composites it is necessary first to investigate the corresponding reaction properties (which eventually effect the densification), such as the temperature at which reaction starts and the rate of reaction. For this purpose green samples of 5-10V% carbon fiber/sialon composite were prepared either by dry or wet unaixial pressing, packed into sialon powder (Z=3) in an alumina crucible and fired for long times in an alumina tube furnace; or for shorter times in a graphite element sintering furnace using different sintering gas atmospheres.

4.3.3.1 Sintering in nitrogen for 15hr.

Long sintering times should be sufficient to show any reactions that might occur during the densification process. Sintering of 5V% carbon fiber grade C (prepared at 1600°C) or 10V% carbon fiber grade A (prepared at 2600°C)/sialon composites at different temperatures was performed and the results are discussed below (Fiber grades are given in Appendix 1).

At 1400°C

The results from the optical microscope analysis presented in the photograph figure (4.4) for the specimen with 10V% fiber gread (A) show no reaction between the fibre and the matrix. Densification is not good, however, as the temperature is too low to start densification even in pure sialon samples.

figure 4.4

Optical photograph for 10V% carbon fiber grade (A)/sialon composite sintered at 1400°C for 15 hr in nitrogen.

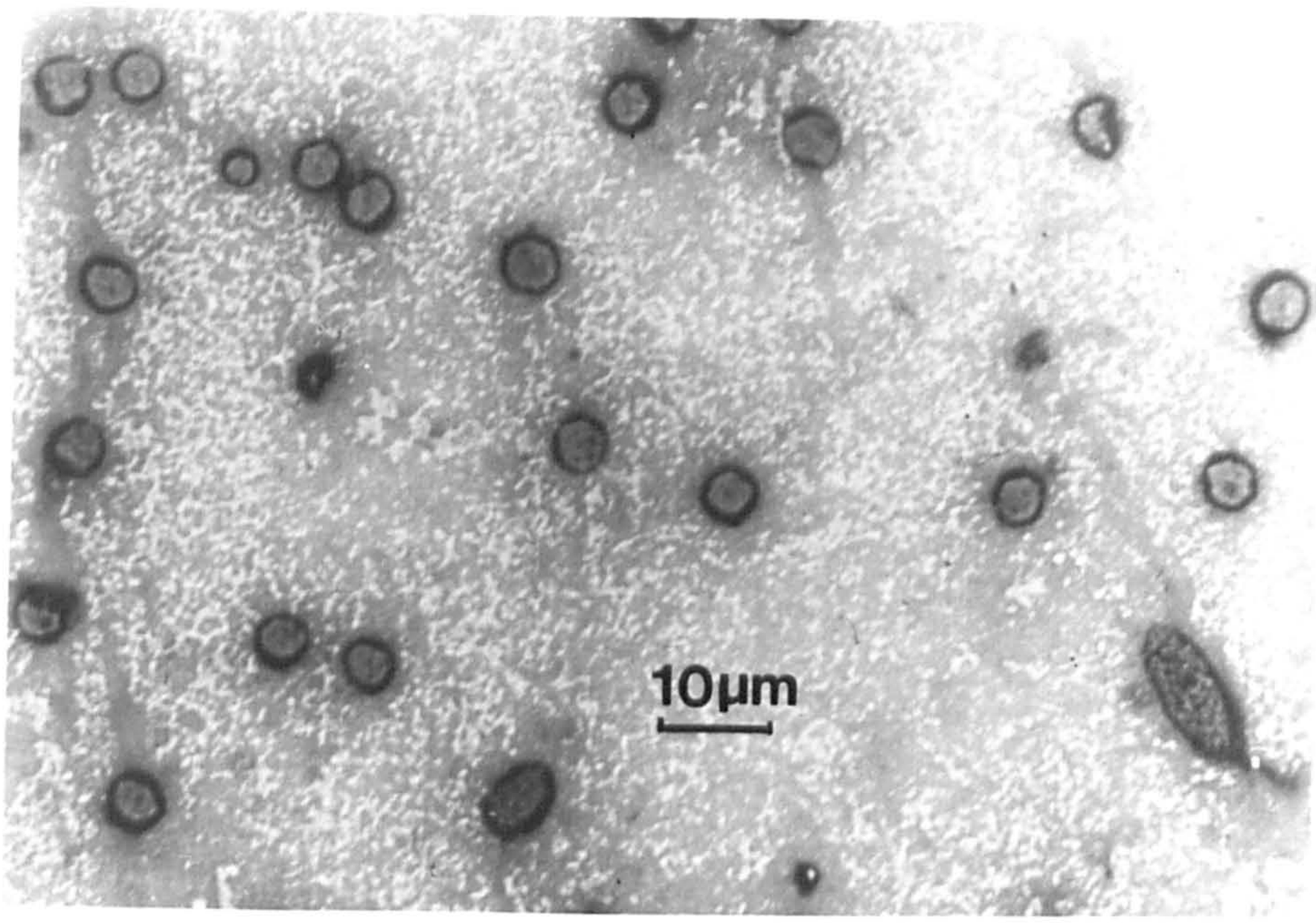
10µm

At 1500°C

Better densification is achieved, as can be seen in the SEM photograph for carbon fiber (grade A)/sialon composites in figure (4.5). The general SEM examination of this sample reveals that there is no reaction observed at this sintering temperature. However, the density of a sintered sample prepared by the technique presented in method (D) in table (4.1) but containing no fibre and fired under the same conditions (1500°C & 15hr) has more than 90% theoretical density whilst the density of the specimen containing 10V% fiber has not improved above the green density. This experiment represents a good example of the effect of carbon fiber on densification and will be discussed further later.

At 1530°C

An interfacial reaction has started and it is quite obvious at the surface of the sample as shown in the SEM photograph, figure (4.6.a). This figure shows that the fibre at the surface has been volatilized leaving large pores behind but the matrix at the surface has higher densification than that of the center of the sample. This is illustrated in figure (4.6.b) in which it is clear that the fiber surface has been attacked, but has not completely vanished. General microscopic observation, however, shows that the surface does not lose all the fiber and the center of the sample still retains fibers which have not been badly attacked. This may be an indication that the reaction is not vigourous at this temperature. Thus if densification can be promoted by external pressures (hot-pressing) and over short times, no interfacial reaction is expected.

figure 4.5

SEM photograph for10V% carbon fiber grade (A)/sialon composite sintered at 1500°C for 15 hr in nitrogen atmosphere.

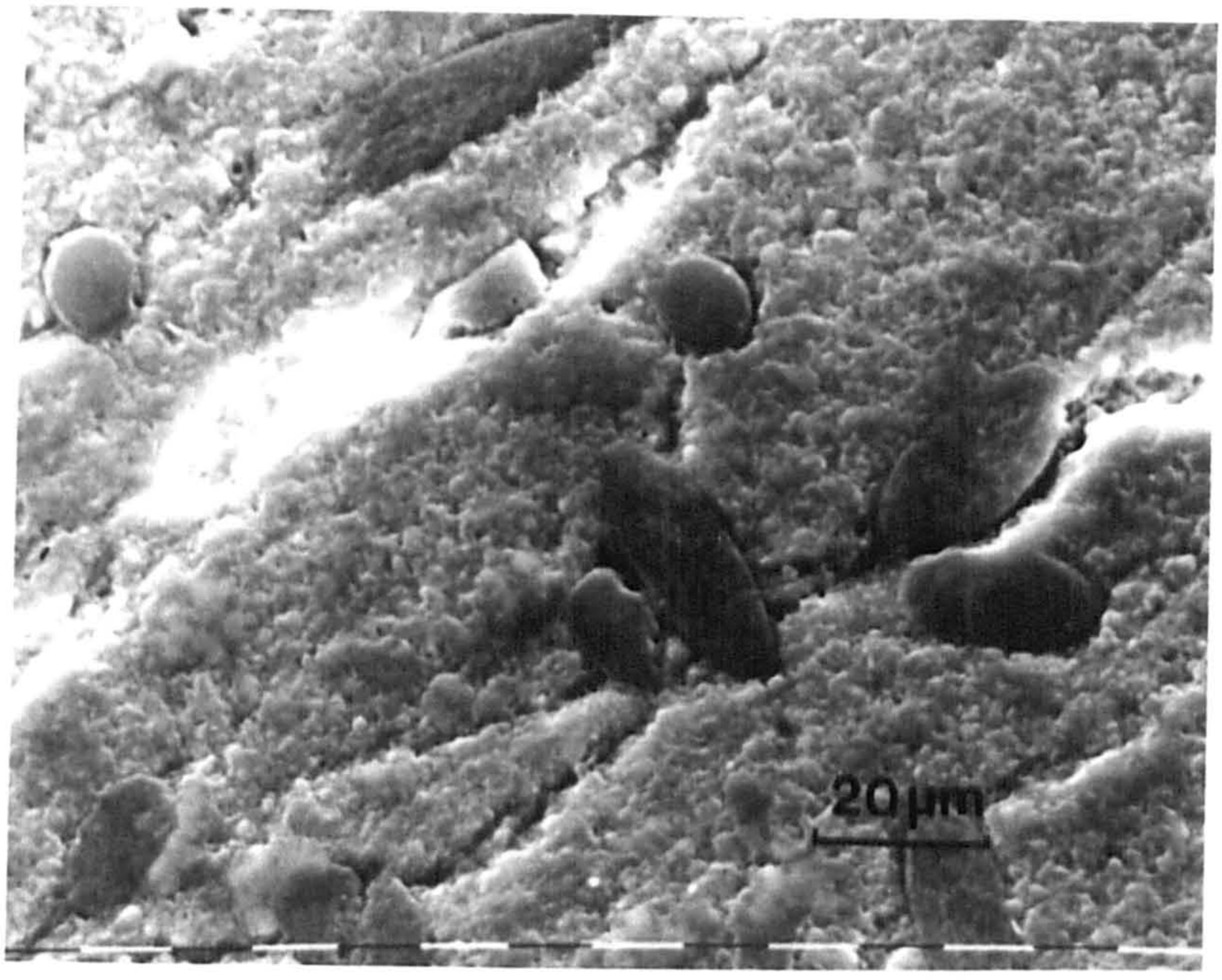
20 µm

figure 4.6.a

SEM photograph for the surface of sialon sample containing 10V% carbon fiber grade (A) sintered at 1530°C for 15 hr in nitrogen.

figure 4.6.b

As in 4.6.a (the centre of the sample).

a

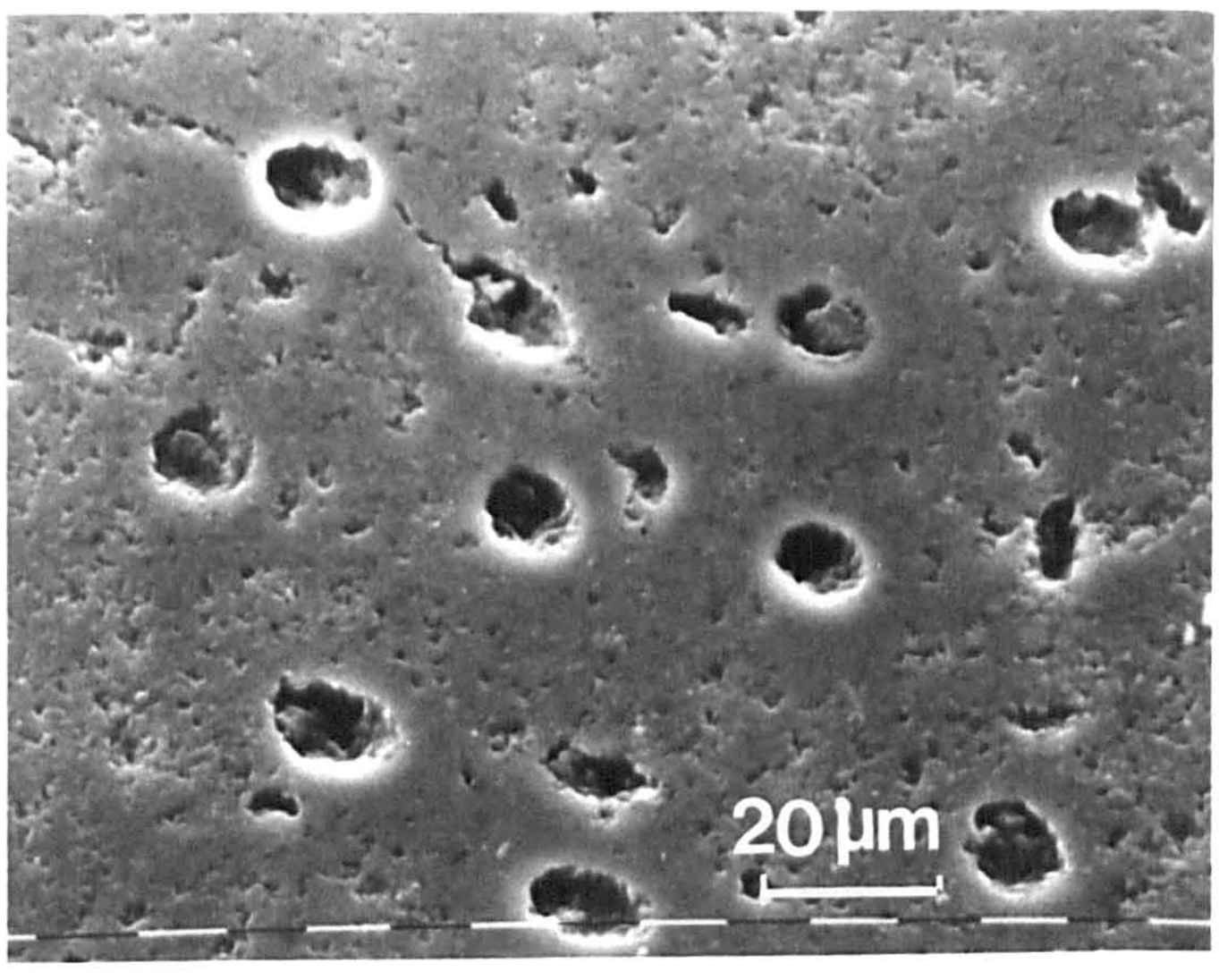

b

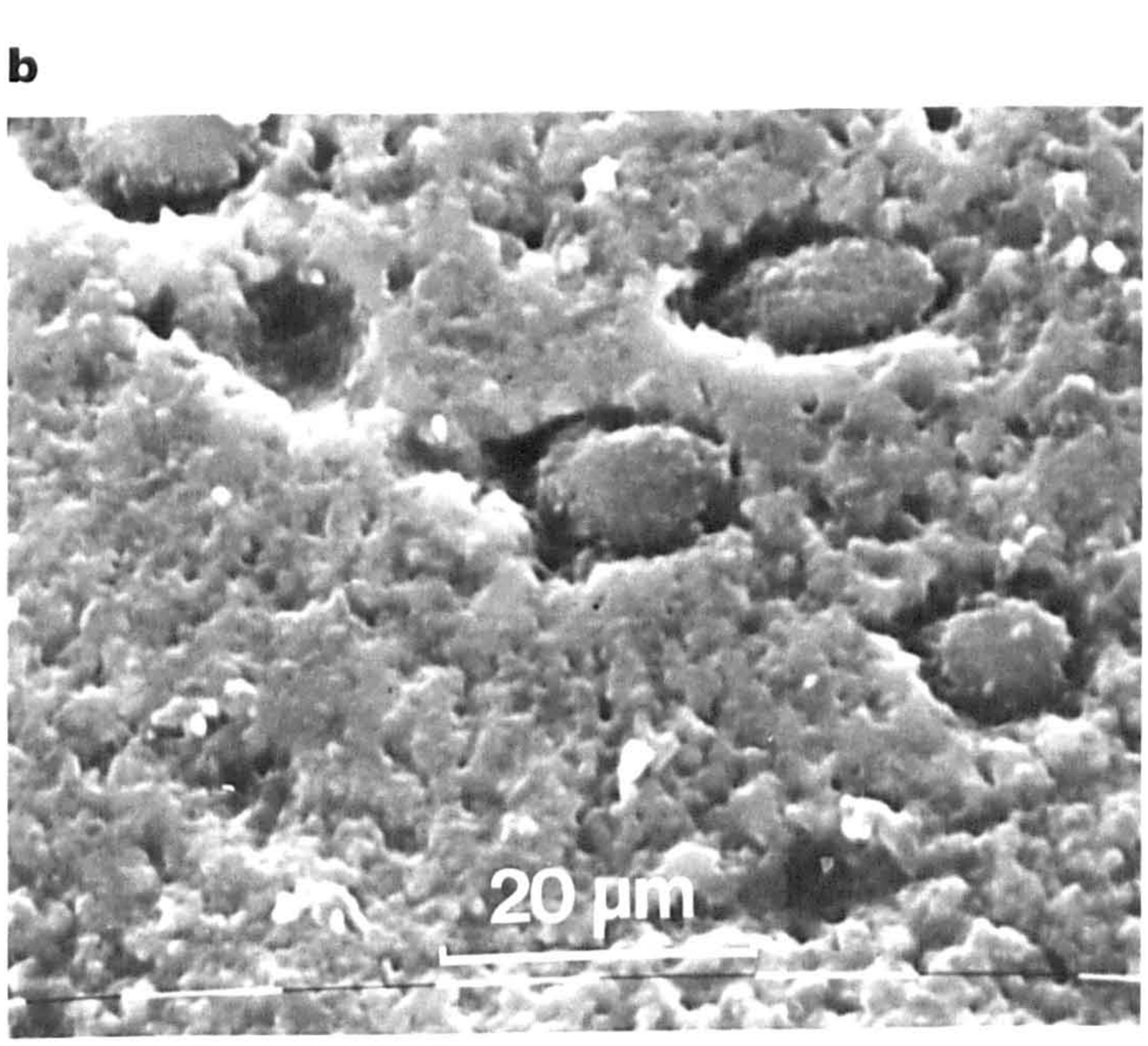

At 1600°C

Three carbon fiber/sialon samples were sintered at this temperature, one of them containing 10V% carbon fiber (grade A) and the other two with 5V% carbon fiber (grade C). One of these two was prepared as in method (A) and the other as in (C), (table 4.1). After sintering, all samples were found to be covered with a metallic phase. The specimens were sectioned and exposed to both SEM and optical microscope examination.

The sample reinforced with 10V% fiber has no sialon phase remaining. The EDAX analysis, however, shows that the general residual material is silicon in which the aluminum and yttrium metals are concentrated in some areas. Additionally, the X-ray analysis confirms no indication of any sialon left in the specimen and the phases present are mainly silicon metal and small amount of aluminium nitride.

The percentage of the metallic phase in the specimen containing 5V% fiber grade (C) (as prepared in method A) is high, as can be seen in the optical photograph given in figure (4.7). The EDAX analysis for this white phase is presented in figure (4.8). It is clear from this figure that it is not pure silicon metal, but is either a metallic phase of an Al–Si–Y compound or an α'-sialon. However, X-ray investigations clarify that the phases present in this specimen are β'-sialon with aluminium nitride and silicon metal similar to those noticed in the sample contaning 10V% carbon fiber but in lower concentrations. The presence of carbon causes the sialon to decompose to the bottom line of the sialon phase diagram (figure 2.1) which are AlN and Si_3N_4. Consequently the silicon nitride over such a long sintering time and at 1600°C decomposes into silicon and nitrogen. However, the yittria seems to form an amorphous phase containing silicon and aluminium ,as the EDAX analysis shows, which is concentrated on some areas.

figure 4.7

Optical micrograph for sample containing 5V% carbon fiber grade (C) prepared as in method (A), table (4.1), sintered at 1600°C for 15 hr in nitrogen gas atmosphere.

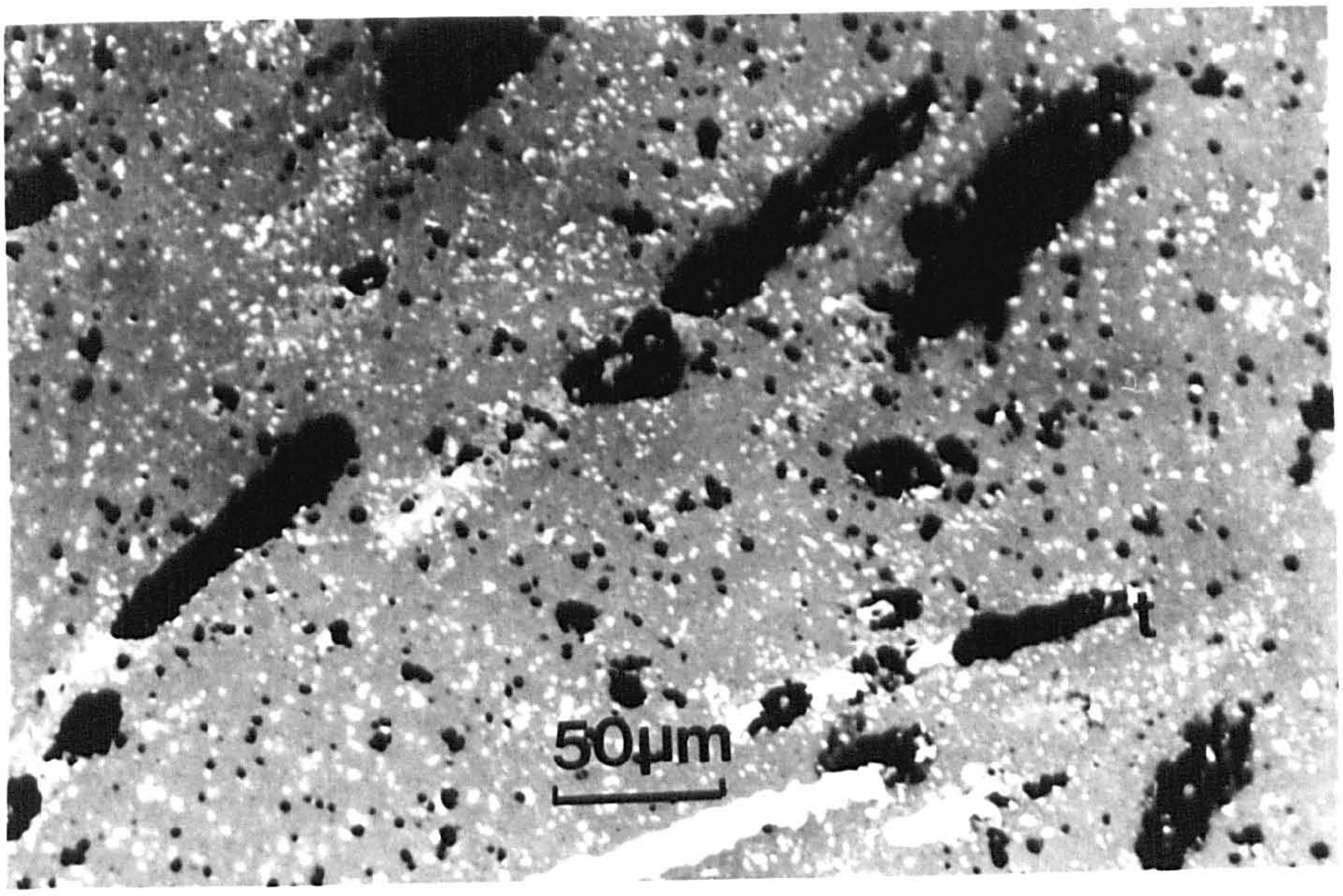
50µm

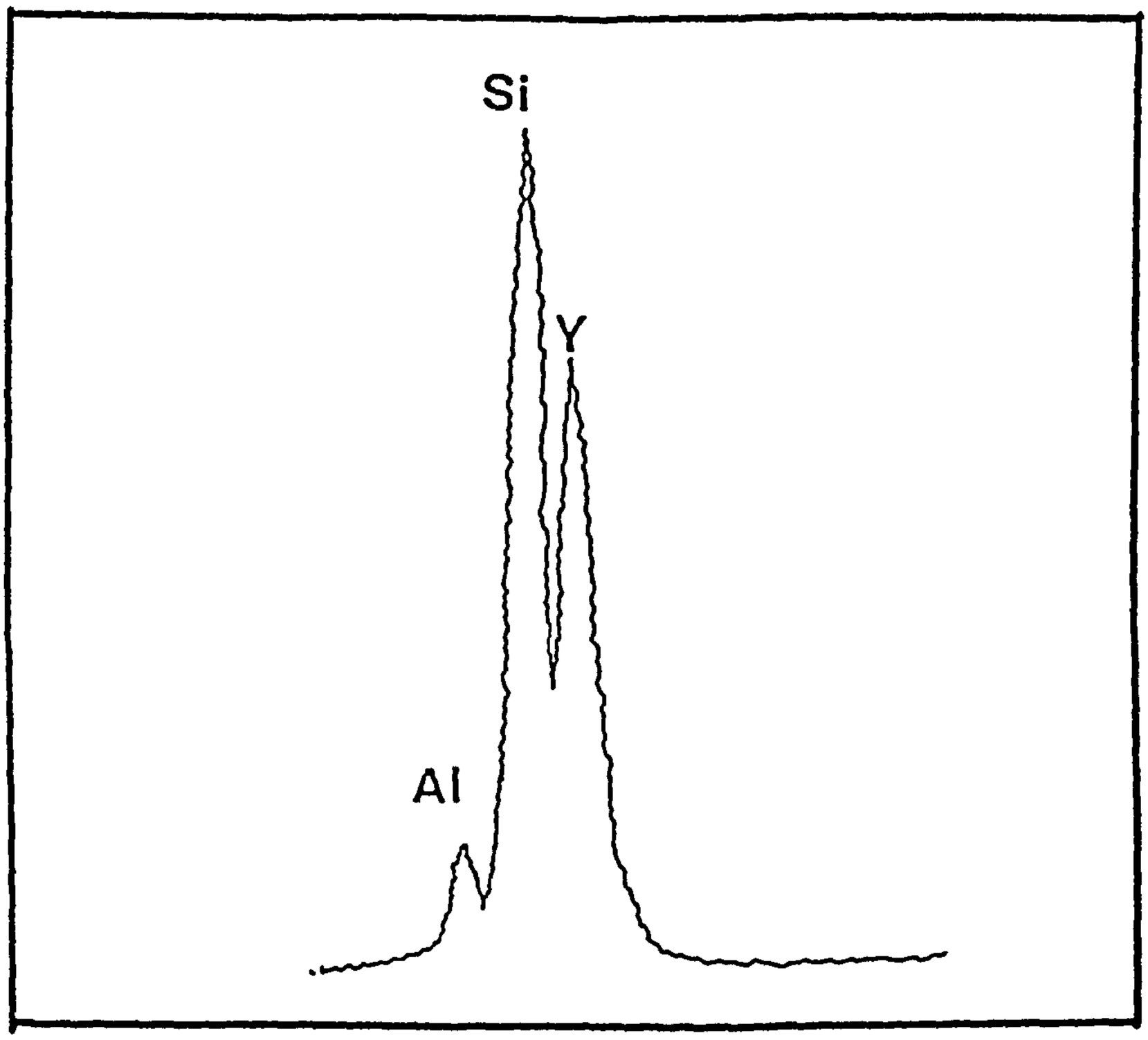

figure 4.8

Schematic representation of the EDAX spectrum for the large white particle shown on figure (4.7).

The last sample in this experiment contains 5V% fiber (C) and was prepared by method (B). The optical examination of this specimen shows that the amount of the white metallic phase is very limited at the surface of the sample (figure (4.9.a)). Here the black areas represent the places where the fiber was present, but where no fiber now remains. The center of this sample, however, reveals no metallic-like phase and the fiber seems to have reacted with the matrix in a different way from that of the reaction at the surface of the specimen, as shown in figure (4.9.b). It can be seen from figure (4.9.b) that there is a reaction product around the fiber which is different to the matrix and the fiber. Furthermore, in some fiber pieces, the core still retains some unreacted carbon phase. The EDAX analysis of the reaction product is given in figure (4.10) in which it is clear that this material is of a slightly different composition to the matrix. It contains a slightly higher yttrium concentration whilst the silicon to aluminum ratio has been almost unaffected and the sialon Z value remains at 0.75.

From this experiment it may be considered that there are two factors which could influence the densification processes of these composites. The first of these is the carbon volume fraction. The experiment shows that with 10V% fiber there must be an extensive reaction within the composite matrix leading, over such a long sintering time, to complete decomposition of the specimen. If the reaction between the carbon fibre and sialon could begin before, or at the onset of the densification process, a large-scale reaction (resulting from the presence of a large carbon volume fraction) will inhibit densification due to the large quantities of gas evolving as a reaction product. This inhibition will make the decomposition easier at higher sintering temperatures.

The second factor is the green sample density. The experiment on the two samples containing 5V% fiber and prepared by different methods resulted in unlike sintering behaviour. The one having green density of 48% of the theoretical density (prepared as in method A (table 4.1)) exhibits more white metallic phase throughout

figure 4.9.a

Optical micrograph for the surface of sialon sample containing 5V% carbon fiber grade (C) prepared as in method (C), table (4.1), sintered at 1600°C for 15 hr in nitrogen gas atmosphere.

figure 4.9.b

As in 4.9.a (the centre of the sample).

a

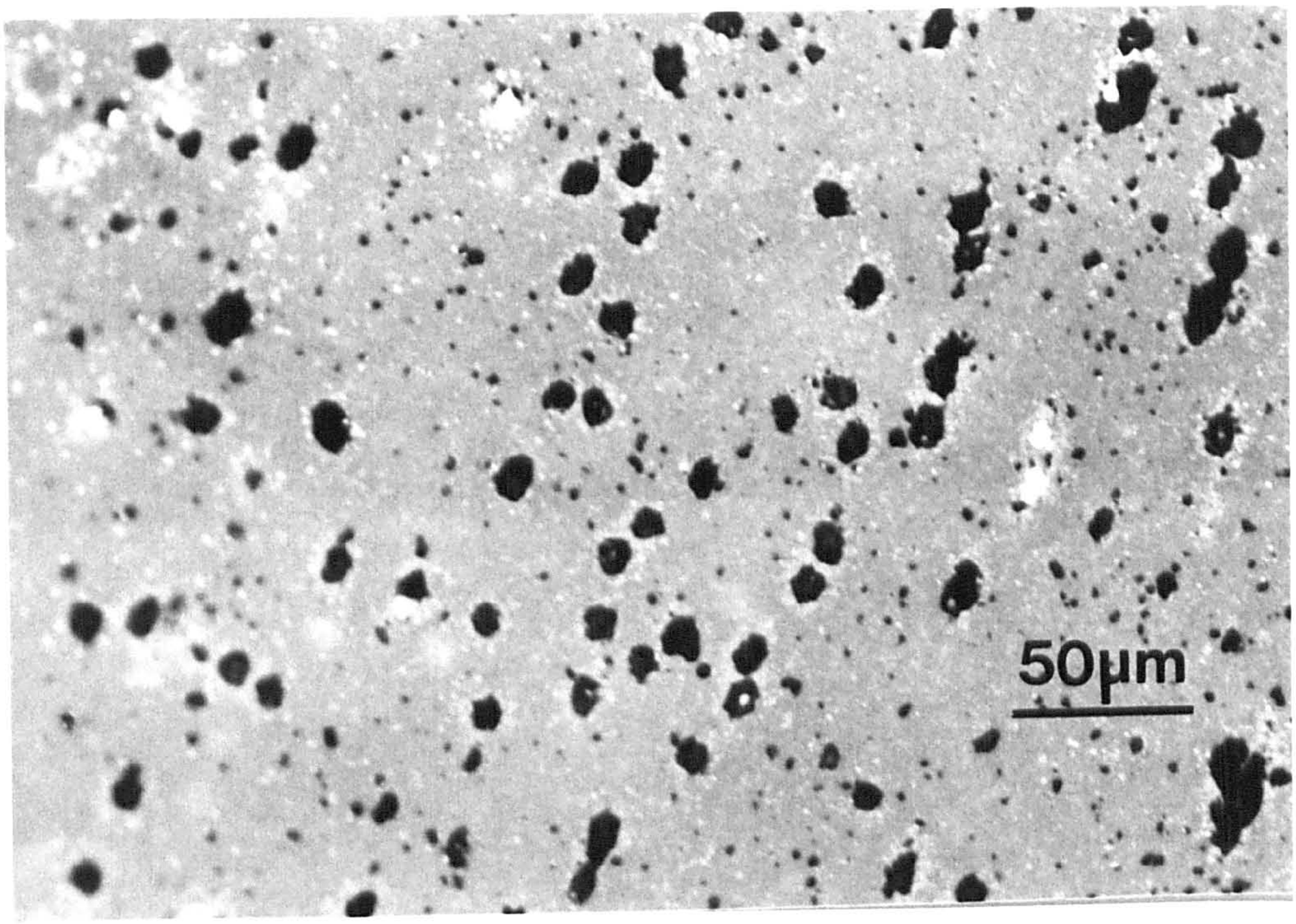

b

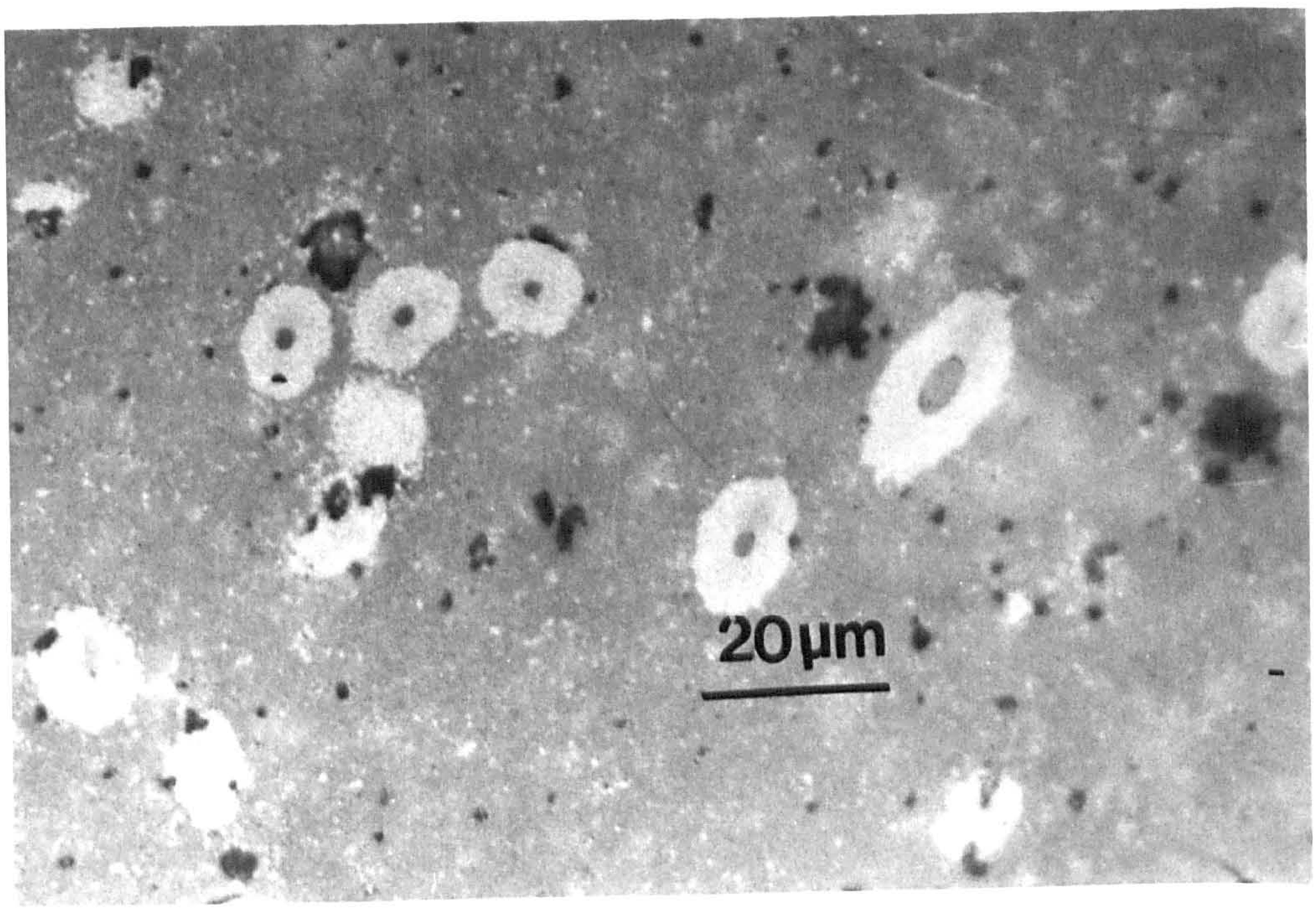

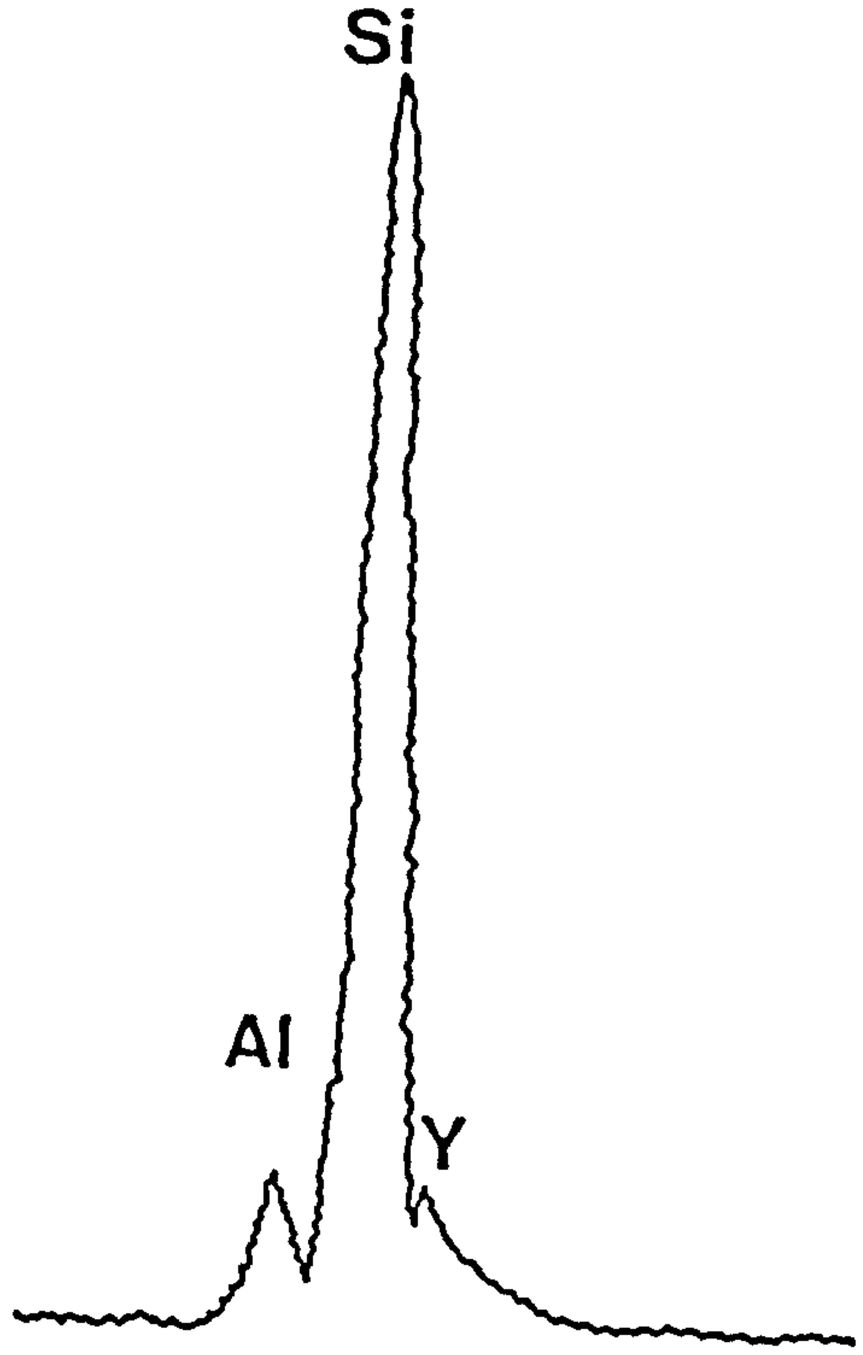

Figure 4.10

Schematic representation of the EDAX spectreum for the reaction product arround the carbon fiber in figure (4.9.b)

the sample. The higher starting density of almost 62% theoretical density in the second sample helps to give a significant inhibitition in the decomposition process. Additionally the fiber has not reacted completely in the centre of the specimen. This again could be related to the higher rate of densification in the sample having greater starting density. The higher rate of sintering appears to make the reaction self–protective by preventing the evolution of volatilizing gas.

It can be concluded from this set of experiments that the reaction between the carbon and the syalon (201) is more likely to be due to interfacial reaction (4.4). The reason for such suggestion is (referring to figures 4.1 an 4.2) the coincidence of the predicted and experimental temperatures at which this reaction becomes effective. The experimental results show that the first observed reaction in such a system occurs at 1530°C and figure (4.2) shows that at such temperatures this reaction is extremely favourable . Furthermore figure (4.2) show that the interfacial reaction (4.2) increases very rapidly as the temperature increases. However, sintering temperatures lower than 1530°C are still considered high to perform reaction (4.4) compared to those obtained from other suggested interfacial reactions. This is because of the carbon monoxide partial pressure generated from reaction (4.4) at temperatures lower than 1530°C is higher than that generated from any other reactions. Additionally, the decomposition of the specimen sintered at 1600°C for 15 hrs could only be related to the absence of liquid phase required to perform densification. Liquid formation at such sintering temperatures is not possible unless there are Al_2O_3–SiO_2–Y_2O_3 components with the right proportions present simultaneously as can be seen on figure (4.11). In this figure it is clear that the minimum liquidus temperature with only two components of Al_2O_3–Y_2O_3 system is 1900°C and it is lower in the case of SiO_2–Y_2O_3.or Al_2O_3–SiO_2 systems. The absence of the SiO_2 component makes the liquid formation impossible in the range of the present experiments conditions. Increasing the carbon volume fraction

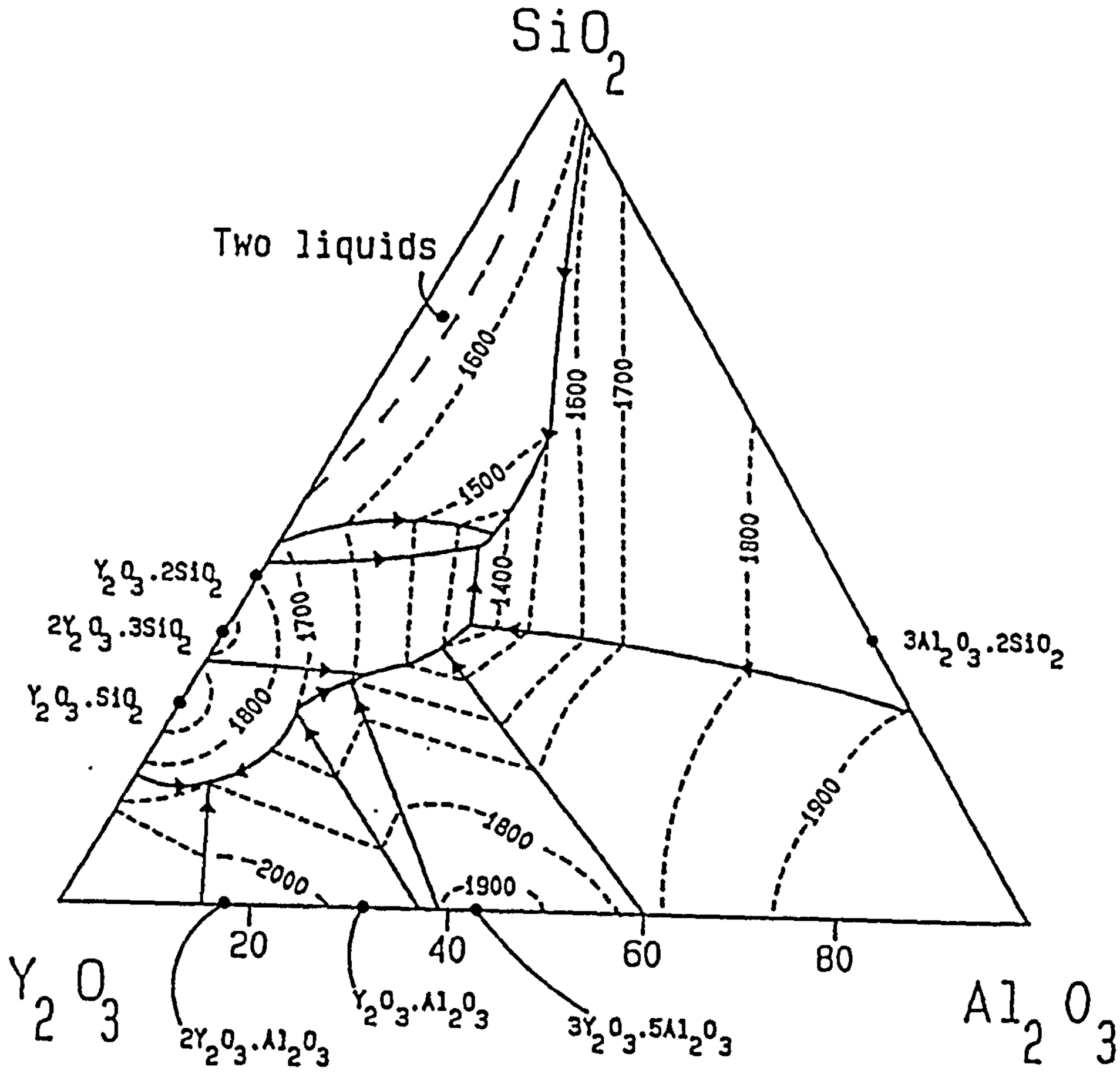

figure 4.11

Al_2O_3-Y_2O_3- SiO_2 phase diagram.

in the matrix means removing more SiO_2, which results in no densification and subsequently increases the decomposition rate.

4.3.3.2 Sintering in $CO+N_2$ gas atmospheres for one hour at 1600°C

4.3.3.2.1 The influence of carbon and carbon monoxide on sintered density and weight loss.

Sintering experiments performed on carbon fiber/β'-sialon composites shows that both the percentage of carbon fiber in the sample and the amount of carbon monoxide gas in the sintering atmosphere have an influence on the final density and weight loss from the samples. Specimens containing 5V% fiber (C) and 10V% fiber (A) were prepared as in method (B), embedded into sialon with Z=3 in an alumina crucible and fired at 1600°C for one hour in a graphite element furnace with different percentages of carbon monoxide gas in the sintering atmosphere. The influence of both the carbon volume fraction and the percentages of carbon monoxide gas in the sintering atmosphere on the sintering behaviour are shown in figures (4.12) and (4.13). It can be noticed in these figures that the weight loss from the sample upon sintering increases with increasing percentage of CO gas in the sintering atmosphere, particularly in the samples containing 10V% carbon fiber. The weight loss in the specimen containing 5V% fiber has also been affected by the addition of carbon monoxide gas to the sintering atmosphere, but to a lesser in extent than in the higher volume fraction carbon fiber composites. As a result of the weight loss from the sample during firing, there is a decrease in the final density. This is illustrated in figure (4.13) in which it can be seen that the density inhibition is very pronounced in the

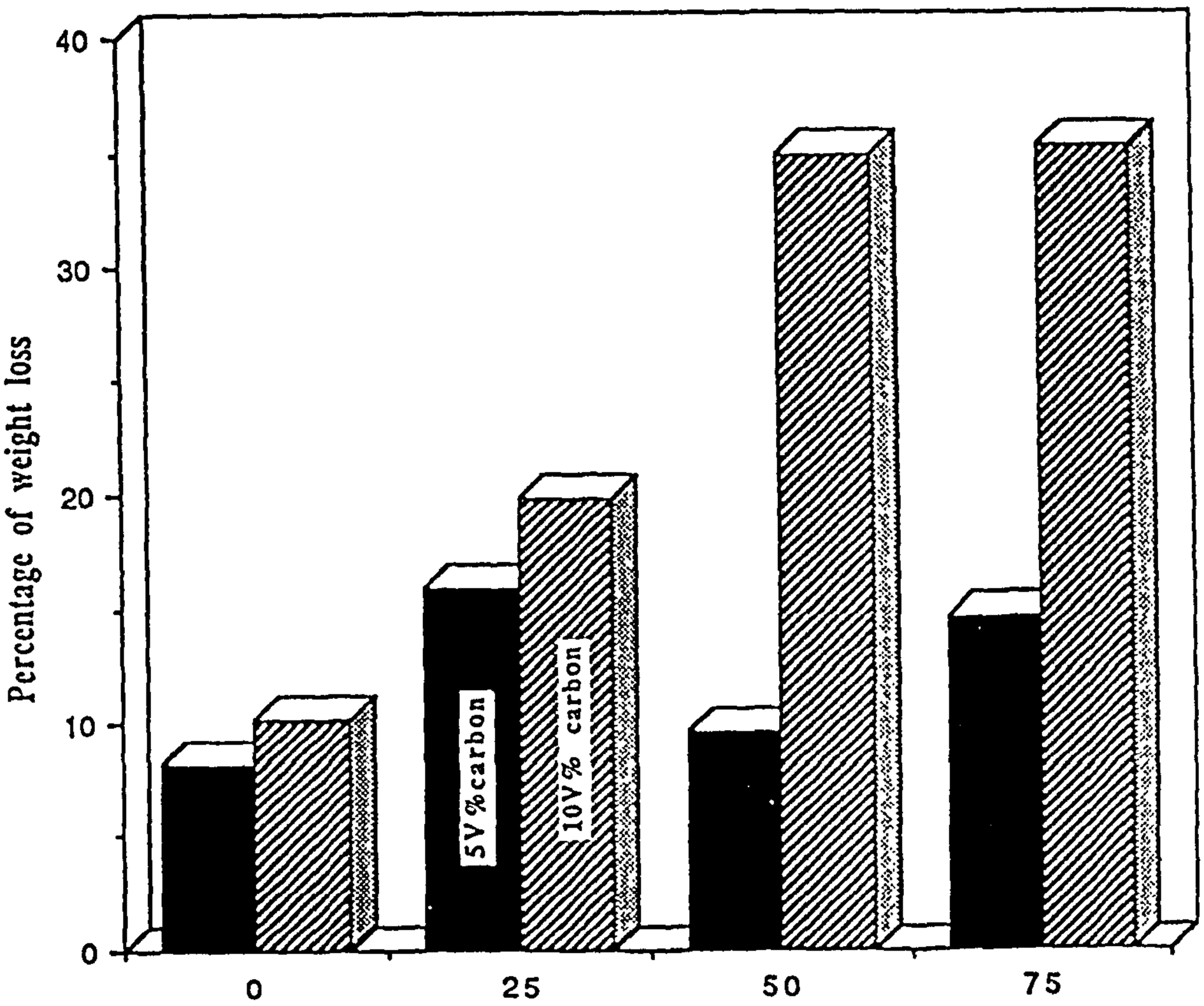

figure 4.12

The influence of carbon monoxide gas present in the sintering atmosphere on the weight loss from the sample

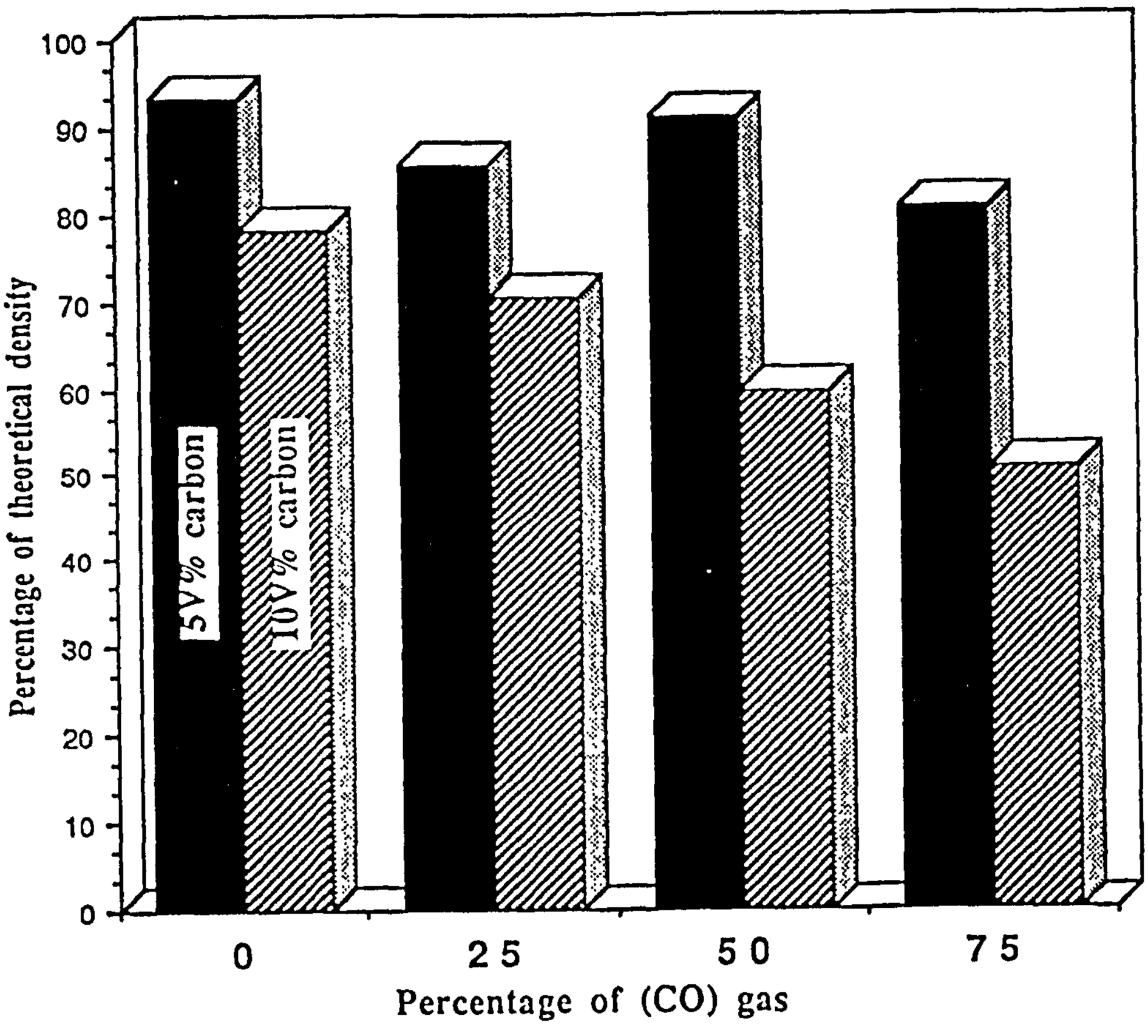

figure 4.13

The influence of carbon monoxide gas present in the sintering atmosphere on the sintered specimen density.

10V% carbon fiber sample but density reduction with increasing CO is less effective in the materials reinforced with 5V% carbon fiber. These observations will be discussed further later.

4.3.3.2.2.The influence of carbon monoxide on carbon fiber/sialon reaction.

The predicted reaction between carbon fiber and sialon given in reaction (4.1) shows that there is always a liberation of carbon monoxide gas. Experiments were carried out following the suggestion of Kyotoku et al [1987] to sinter these composites in environments containing the required quantities of carbon monoxide gas (calculated from the free energy of formation of reactants and product equation (4.1)). From figure (4.1) the equivalent partial pressure of CO for this reaction at temperatures between 1500°C and 2000°C is in a range not exceeding 0.1 atm. Reactions were therefore performed at different values of P_{CO} taking into account the values of P_{CO} generated from other reactions. It can be seen in figure (4.2) that the partial pressure of carbon monoxide evolved from reaction (4.3) at 1600°C is almost 0.4 atm and at this temperature reaction (4.4) becomes out of control at atmospheric pressure.

However, the experimental results on both 5V% fiber (grade C) and 10V% fiber (grade A) reinforced sialon shows that sintering in pure nitrogen at 1600°C for one hour did not lead to complete loss of the fiber. Some reaction appears to have taken place; as the optical photographs for the samples contain 5V% fiber (C) and 10V% fiber (A) in figures (4.14) and (4.15.a) reveal respectively. However, referring to appendix (1), the main difference between the two grades of fibres is actually the fiber formation temperature. It appears that the higher the fiber formation temperature the more stable the fiber becomes.

figure 4.14

Optical micrograph for sample containing 5V% carbon fiber grade (C) sintered in nitrogen at 1600°C for one hour.

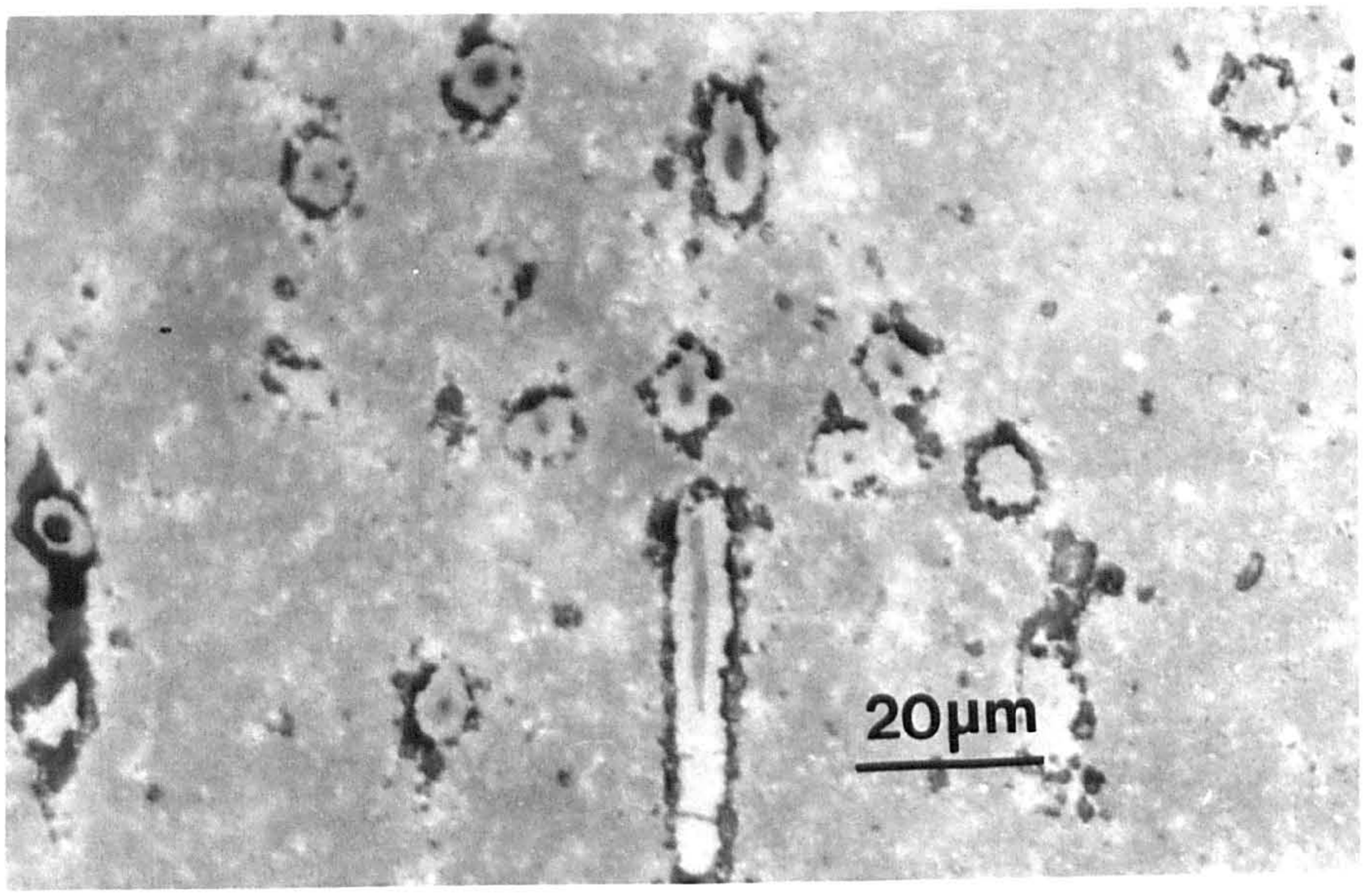
20μm

figure 4.15.a

As in figure (4.14) sample containing 10V% carbon fiber grade (A) .

figure 4.15.b

As in figure (4.15.a) sample sintered in 75%CO + 25% N_2

a

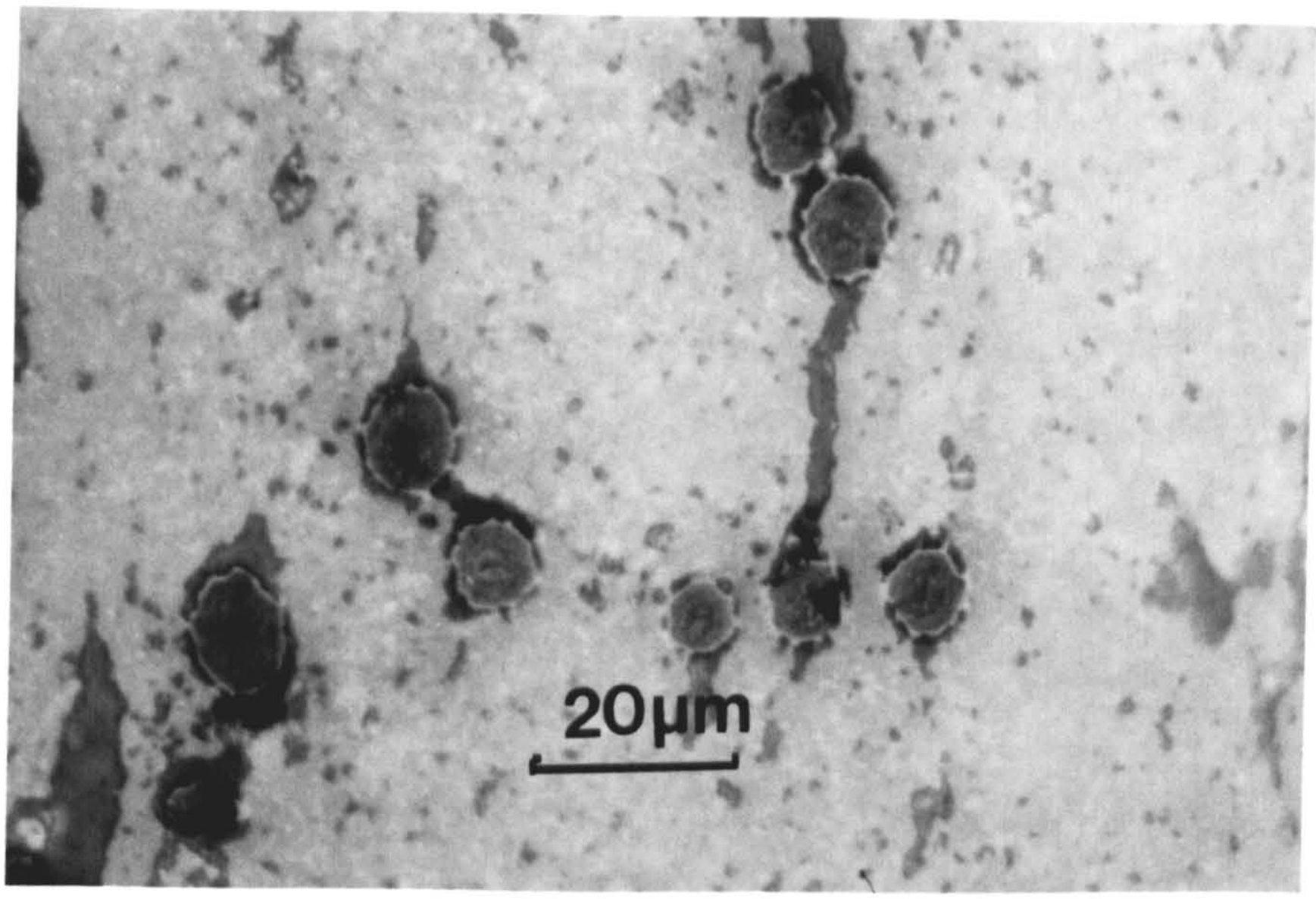

b

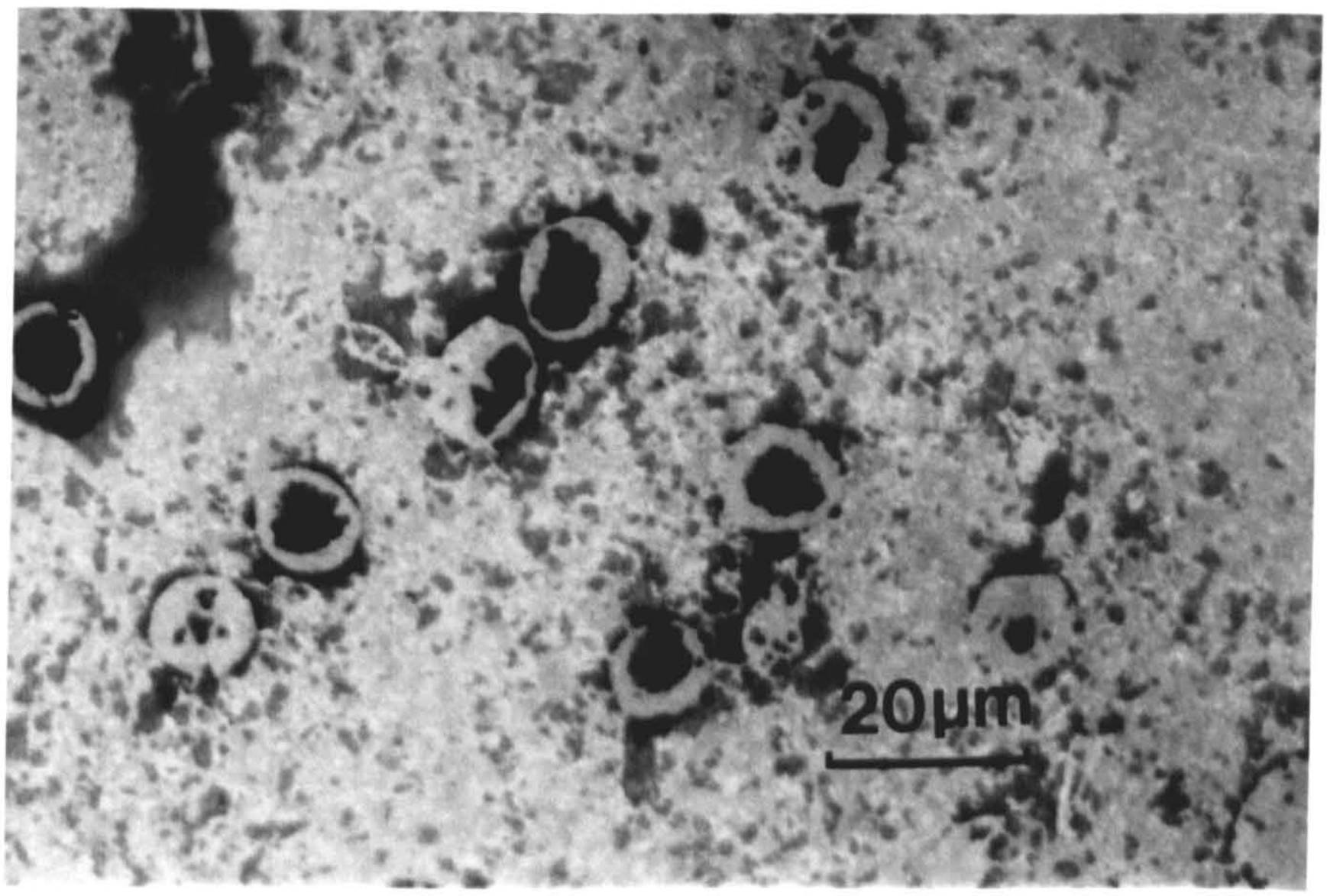

The reaction between the fiber and the sialon looks to be more extensive in the case of sintering in atmospheres containing 75% carbon monoxide than of those sintered in pure nitrogen gas as shown in figure (4.15.b). It is noticed that almost all of the fiber (grade A) has reacted to form a relatively white material around the original fiber. The influence of the fiber volume fraction on the density is represented and discussed in figure (4.13) and figures (4.14) and (4.15.a) exhibit consequently the microstructures of the samples containing 5V% fiber grade (C) and 10V% grade (A) sintered under the same conditions. The matrix containing 5V% fiber looks more dense than that reinforced by 10V% fiber. In all of the photographs presented above, fiber grade (A) always appears to be less reactive than the grade C fiber for the reason mentioned above.

Side reactions resulting from controlling the sintering atmosphere with CO gas seem to occur; these will be discussed later.

Investigations of reactions (4.1), (4.3) or (4.4) using the EDAX on the SEM are difficult. It is not possible to show whether those reactions take place since there is no change in the overall Si/Al ratio (as was seen in the suggested formulas of those reactions). Referring to figures (4.1) and (4.2) and at a sintering temperature of 1600°C, reaction (4.1) (according to Le Chatelier's principle) will not occur in a CO gas controlled atmosphere as the experimental conditions of P_{CO} are always higher than the calculated values. Additionally the formation of β'–sialon, which is inhibited by the addition of carbon fiber, at the beginning of the carbon fiber/sialon proposed reaction is not complete (as the starting material is a composition of $Z = 0.75$ sialon). These reasons make the possibility of interfacial reaction (4.1) very limited. Reaction (4.2) has been eliminated since there is no silicon carbide phase formed in the case of sintering the composite in a nitrogen atmosphere. Reaction (4.3) will be favourable, but if there are no other reasons for this reaction to continue it should be inhibited by

sintering in a 75% CO gas atmosphere. Further, alumina is more stable, at all experimental temperatures, than the other components in the carbon/sialon systems and therefore, reaction (4.3) is inhibited.

These experiments indicate that the sintering conditions given by Kyotoku et al (1987) to control the interfacial reaction in composite materials are not as simple as presented. In the carbon fiber/sialon system, as discussed above, the reaction between the fiber and the matrix materials are not simply controlled by the addition of carbon monoxide gas. Chemical compatibility in the carbon/sialon system then should be promoted by another means, rather than by controlling the sintering atmosphere. Interfacial reaction, as a general conclusion from what the previous experiments shows, could be controlled by either low temperature sintering (in which there will be no significant densification) or high rates of densification at relatively high temperature. The volume fraction of carbon in the matrix (which influences the densification rate) also appears to have some influence on the carbon/sialon compatibility as will be discussed later in the hot–press sintering.

Increasing the P_{CO} in the sintering atmosphere is accompanied by a reduction in nitrogen partial pressure (P_{N_2}) since $P_{CO} + P_{N_2} = 1$. Changing the potential of the nitrogen gas in the environment could promote decomposition of the sialon which in turn causes large weight loss. Also, by considering that the starting material is a composition of sialon containing almost 80wt% silicon nitride, the following reactions could occur which would explain the large weight reduction resulting from high partial pressures of carbon monoxide gas in the sintering atmosphere. However, none of the reactions discussed above could cause the weight loss values represented in figure (4.13). The alternative reactions in the presence of carbon monoxide in the sintering atmosphere are discussed as follows:

$$Si_3N_4 + 3CO = 3SiO + 2N_2 + 3C.....(4.5)$$

Simple calculations concerning reaction (4.5) reveals that there is maximum loss of 75wt% if this reaction is completed. The partial pressures of silicon monoxide (P_{SIO}) were obtained from reaction (4.5) at a sintering temperature of 1600°C in different P_{CO}/P_{N_2} ratio, where $P_{CO} + P_{N_2} = 1$ atm. Gas atmospheres are calculated according to the free energy of formation of reaction (4.5) as follows;

$$P_{SIO}^3 = (P_{CO}^3/P_{N_2}^2) \ (K(T))$$

As the P_{CO} increases, the corresponding value for P_{N_2} decreases and the P_{SIO} will rise. However, upon sintering the sample was embedded into sialon of Z = 3. This sialon (401) will decompose at high temperature and supply a silicon monoxide gas atmosphere around the sample during sintering to suppress sample decomposition. Calculations show that at a sintering temperature of 1600°C the (P_{SIO}) generated from the powder bed decomposition is equal to 0.048 atm. At a given temperature this figure will be constant for certain time and the (P_{SIO}) values from reaction (4.5) corresponding to the sintering condition are given in table (4.2).

Table (4.2)

Relation between CO, N_2 and SiO gases in carbon fiber/sialon system according to reaction (4.5).

P_{CO}	P_{N_2}	P_{SIO}
0.00	1.00	0.00
0.25	0.75	1.3 x10-3
0.50	0.50	3.4 x 10-3
0.75	0.25	8.1x 10-3

These calculations show that ;

$$P_{SIO}\ (75\%CO)/P_{SIO}\ (25\%CO) = 6.2$$

This means that the generation of SiO gas becomes greater with higher P_{CO} and the effect of the powder bed become less. Additionally reaction between the carbon monoxide gas and the powder bed could make the bed less effective in preventing reactions involving the generation of silicon monoxide gas from the sample. However, high P_{SIO} generated from the powder bed should inhibit the decomposition reaction since calculations show that $(P_{SIO})_{bed}/(P_{SIO})_{sample}$ ranges from **36 to 6** as the (P_{CO}) in the atmosphere increases from 25% to 75%.

The other possible reaction which could take place and cause large weight loss in the sample is ;

$$Si_3N_4 + 1.5CO = 1.5SiC + 1.5SiO + 2N_2 \ldots\ldots (4.6)$$

therefore;

$$P_{SiO}^{1.5}=(P_{CO}^{1.5}/P_{N_2}^{2}) \ (K(T))$$

Reaction (4.6) can be easily confirmed by the X-ray diffraction technique which will be discussed later. The silicon carbide phase is expected to be one of the matrix phases after sintering in a controlled atmosphere. Similar to that which has been discussed in reaction (4.5) a maximum of 57.1% reduction in weight of the sample is expected if this reaction is completed. The partial pressure of silicon monoxide gas generated from reaction (4.6) is also calculated with respect to the atmosphere. The results are given in table (4.3)

Table (4.3)

Relation between CO, N_2 and SiO gases in carbon fiber/sialon system according to reaction (4.6).

P_{CO}	P_{N_2}	P_{SiO}
0.00	1.00	0.00
0.25	0.75	4.00 x10-3
0.50	0.50	0.0137
0.75	0.25	0.052

It can be seen from these calculations that;

$$P_{SiO} \ (75\%CO)/P_{SiO}(25\%CO) \ = \ 13$$

This reaction appears to be more effective than reaction (4.5) and the value of (P_{SiO}) generated from the sample is even greater than that from the bed when controlling the atmosphere with 75% carbon monoxide. The ratio of $(P_{SiO})_{bed}/(P_{SiO})_{sample}$ are varying between **12 to 0.93** as the (P_{CO}) in the atmosphere increases from 25% to 75%. According to these calculated and experimental results this reaction is more likely to be the one responsible for the large weight loss from the specimens sintered in CO/N_2 gas atmosphere Decomposition of the sialon, however, represents another factor which contributes to specimen weight reduction upon sintering.

.

4.3.3.3 The influence of C% and CO% on the phases.

X-ray analysis demonstrates that both carbon in the matrix and carbon monoxide gas in the sintering atmosphere have an influence on the type and percentage of phases present in the final structure of the sintered material. The results of these examinations are displayed in table (4.4).

Table (4.4)

Relation between CO gas content in the sintering atmosphere and phases present in the sintered carbon fiber/sialon composite (at 1600°C for one hour)..

%CO gas	%β'-sialon	%α'-sialon	%α-Si_3N_4	%β-SiC
10V% fiber				
0.00	50.00	25.00	25.00	0.00
25.00	90.00	0.00	0.00	10.00
50.00	50.00	0.00	0.00	50.00
75.00	50.00	0.00	0.00	50.00
5V% fiber				
0.00	80.00	10.00	10.00	0.00
25.00	80.00	0.00	0.00	20.00
75.00	80.00	0.00	0.00	20.00
0V% fiber				
0.00	100.00	0.00	0.00	0.00

The sample containing 10V% fiber sintered in pure nitrogen is found to have a considerable amount of α'-sialon and an equal proportion of unreacted α–Si_3N_4 . When the sintering environment is controlled with carbon monoxide gas the phases existing in the structure, as illustrated in table (4.4), change. Both α'-sialon and α–Si_3N_4 phases disappear and an β–SiC phase emerges in the sintered structure. The amount of β–SiC increases with increased partial pressure of carbon monoxide gas in

the sintering atmosphere. Almost 50% β–SiC phase is present in the sample sintered in atmospheres containing more than 50%CO gas.

The phases produced in the sample containing 5V% fiber and sintered in pure nitrogen are similar to the corresponding samples reinforced with 10V% fiber but the amounts of both α'–sialon and unreacted α–Si_3N_4 are less. This leads to the conclusion that the amount of fiber has two effects. One; as the carbon works as a reducing agent for β'–sialon to α'–sialon, the percentage of α'–sialon produced would be expected to be lower with less carbon present. Secondly, the reduction in the amount of unreacted α–Si_3N_4 with decreasing carbon volume fraction explains how the amount of fiber in the matrix influences the α to β' phase transformation. With higher amounts of carbon, there is a lower extent of transformation. This could be due to the reduction in the amount of surface silica by increased carbon content and subsequently less liquid phase (at sintering temperature) this liquid phase being required for transformations to occur. table (4.4) reveals that with pure sialon, sintered in the same conditions, the only phase formed is β'-sialon with almost the expected Z value (0.75).

The amount of silicon carbide phase formed in the samples reinforced with 5V% carbon is lower than that in the specimens containing 10V% carbon. This gives rise to the question is the amount of carbon in the matrix responsible for β–SiC formation (as in reaction (4.2))?. This is unlikely because in this case there should be silicon carbide detected in the samples sintered in nitrogen. The X-ray analysis has not clarified this. Additionally, aluminum and yttrium present in the EDAX analysis of the area next to the fiber in figure (4.10) dismiss the formation of SiC phase. The only reason for low amounts of silicon carbide formation in the samples reinforced with lower volume fraction of carbon is the higher rate of densification obtained in them and

hence less possibility for reaction (4.6), which is responsible for SiC formation, to proceed.

It should be noticed from the X-ray investigations that α'–sialon has only formed when the atmosphere contains no carbon monoxide gas. This occurs because the reduction process from β'–sialon to α'-sialon is accompanied by evolution of CO gas and the partial pressure of this gas at the sintering temperature is low enough to be controlled by the CO gas added to the atmosphere. It is not clear however, whether the α'–sialon is formed from the reduction of β'-sialon, or in a carbothermal reduction process accompanying the densification process.

4.4 Hot-pressing Of Carbon Fiber/Sialon Composites.

Hot–pressing was also applied to the sintering of carbon fiber/sialon composites. This method provided a high densification rate, which is believed to be the optimum condition to overcome the chemical incompatibility in the carbon/sialon system. Different kinds of carbon with a variable volume fraction have been used to reinforce the sialon matrix and then been hot pressed in a temperature range of 1450°C–1550°C. Results are presented according to the physical nature of the reinforcement (chopped, continuous, or particles).

4.4.1 Chopped fiber/sialon composite.

Different types of fiber have been used to reinforce sialon 201. The mean fibre diameter used is 10μm. The fibers were prepared at different temperatures as can be seen in appendix (1). Variable volume fractions of certain fibers was also tried. The results are presented according to the fiber type (i.e. fiber formation temperature).

(i) General purpose carbon fiber.

The physical properties of the G.P fiber were not supplied by the makers, but the formation temperature is known to be 1600°C. Two batches of syalon 201 were prepared one containing 10V% G.P fiber and the other with 20V%. The samples were hot–pressed for one hour at different temperatures at a pressure of 20 MN/m^2 and the experimental results are given in table (4.5).

Table (4.5)

Variation of density with carbon volume fraction and temperature in hot pressed carbon fiber/sialon composites.

fiber grade	volume fraction %	sintering temp. (°C)	sintered density ($g.cm^{-3}$)	Theoretica -l density %
G.P	10	1550	3.13	99
	20	1550	2.955	98
	20	1450	2.64	88
grade (C)				
	15	1550	3.004	98
	15	1450	2.83	92
grade (B)				
	15	1550	3.02	98

It can be seen from this table that almost theoretical densities were achieved using the hot pressing technique. The experimental observations (confirmed by the transducer connected to the press) reveals that densification begins at temperatures as low as 1250°C.

Optical and SEM examination of these samples shows that a very good and clear interface between the fiber and the matrix is obtained in the specimens containing 10V% fiber as shown in the optical photograph in figure (4.16.a). It can be noticed on this figure that the sialon matrix densified very well. The absence of reaction was also confirmed by TEM examination as shown in figure (4.16.b) in which the interface is

figure 4.16.a

Optical photograph for specimen containing 10V% fiber grade (G.P) hot–pressed at 1550°C for one hour.

figure 4.16.b

As in figure (4.16.a) a TEM photograph.

a

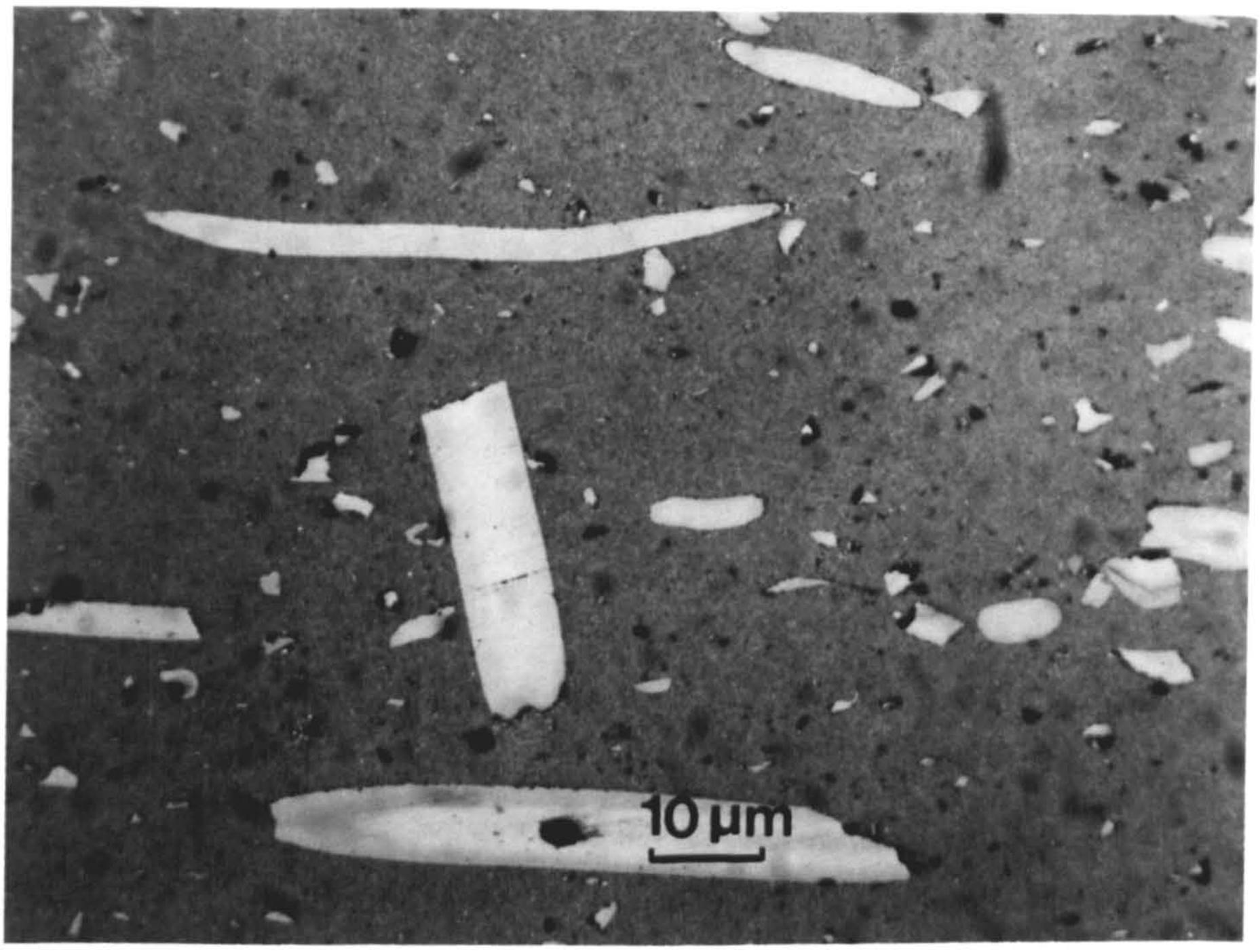

b

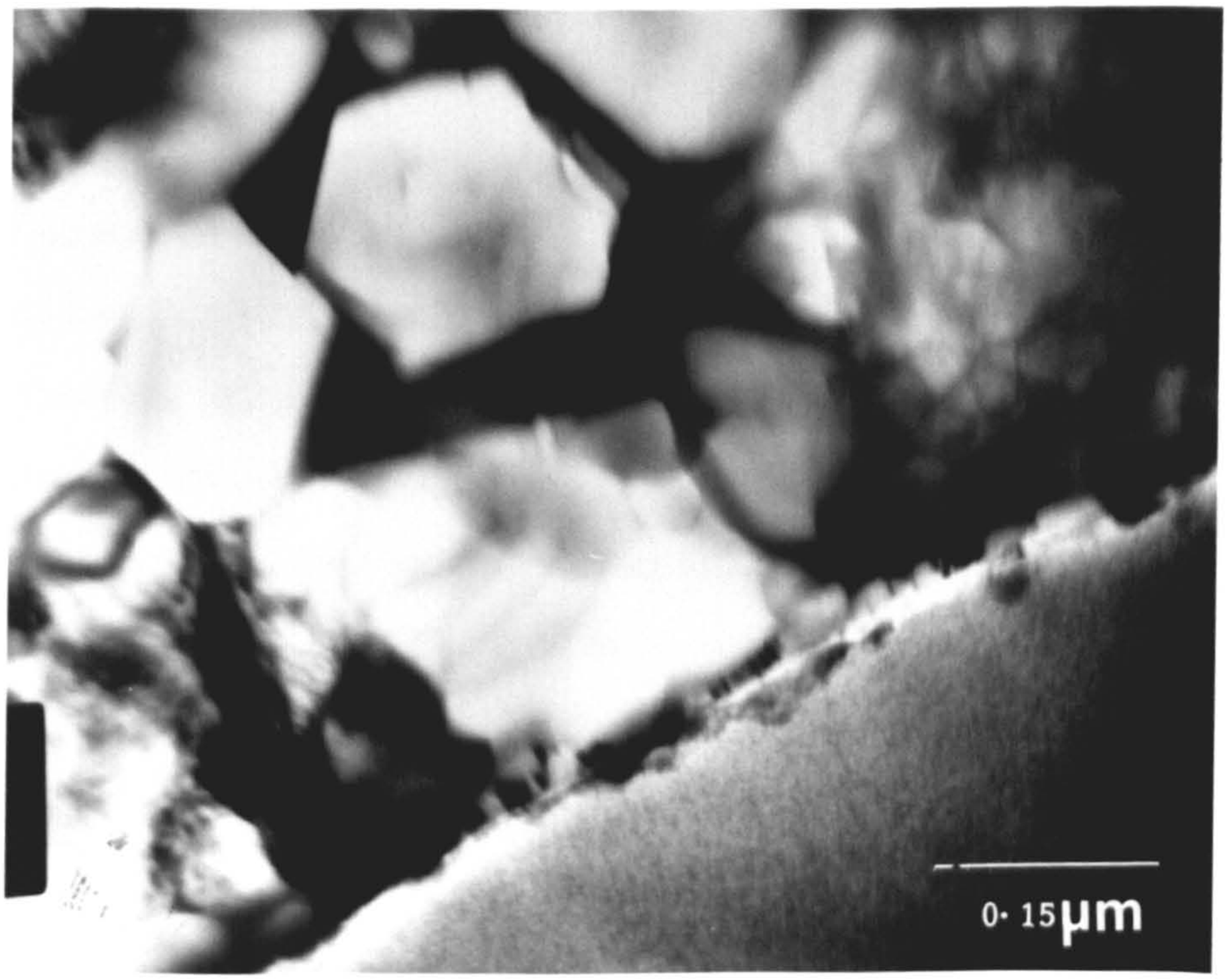

obviously clean and the carbon area is surrounded by a black region which was liquid phase at sintering temperature. However, when the volume fraction of fiber increases to 20V%, reaction in the samples sintered at the same temperature (1550°C) occurs. Initial optical observations on this specimen indicated that almost all of the fiber appeared to have been volatilized, but density measurements show that almost theoretical density is achieved. However, in the case where all of the fiber phase is volatilized, the density of the remaining matrix should not be more than 2.633 $g.cm^{-3}$, which represents 80% of the fully dense syalon 201 (density = 3.296 $g.cm^{-3}$). SEM observations of the fracture surface of this sample show that the general shape of the fiber is still retained but it looks as if it has reacted in some way. EDAX analysis of the reaction product ,using TEM, show Al , Si, Y and carbon peaks as in figure (4.17).The diffraction pattern of this phase shows that it is amorphous. The general TEM examination show that the sample still retain some unreacted silicon nitride. Additionally the general Al/Si ratio on the β'-sialon grains given in figure (4.18) are slightly higher than what it should be for Z= 0.75 sialon. Subsequent careful polishing was performed on the specimen and the results are shown in the optical photograph in figure (4.19) in which it is clear that there are materials in place of the original fiber which are not carbon and this will be discussed below. Temperatures as low as 1450 °C were found to be sufficient to sinter samples containing 20V% fiber to almost 88% of the theoretical density. Good interfaces between the fiber and the matrix can be seen in the optical photograph given in figure (4.20.a). SEM micrograph figure (4.20.b) of the fracture surface of this sample shows that there is some reaction at the surface of the fiber, but it is not as extensive as in the sample hot pressed at 1550°C containing 20V% fiber. It appears that the fiber volume fraction present in the matrix has some influence on the reaction because (as discussed above) the specimen containing only 10V% fiber has not reacted even at higher sintering temperature. This reaction occurs

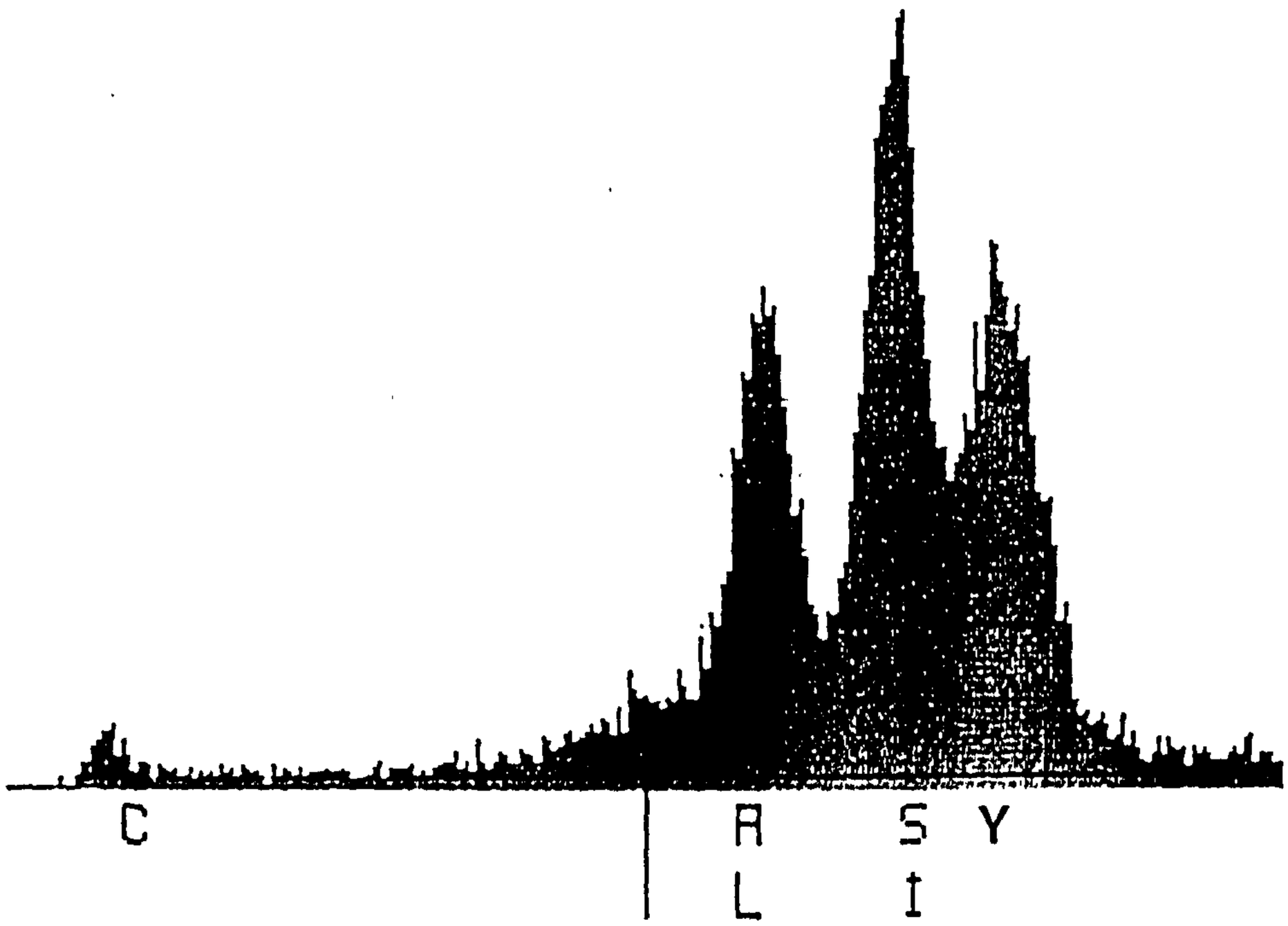

figure 4.17

Schematic representation for the EDAX spectrum for the reaction product arround the hot pressed carbon fiber/sialon composite.

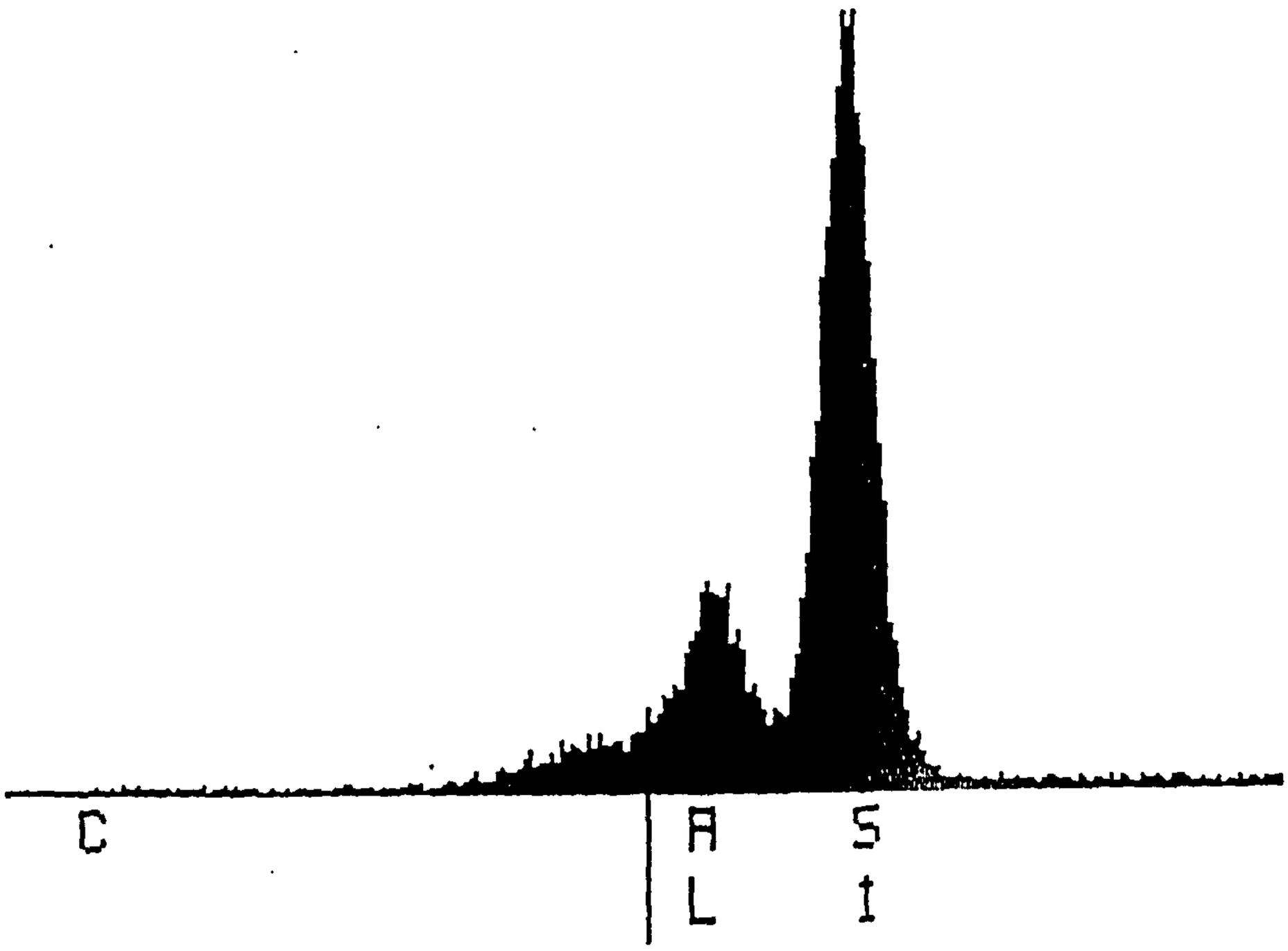

figure (4.18)

Schematic representation for the EDAX spectrum for the β'-sialon grains in carbon fiber/sialon composites.

figure 4.19

Optical photograph for hot-pressed sample containing 20V% fiber grade (G.P) sintered at 1550°C for one hour.

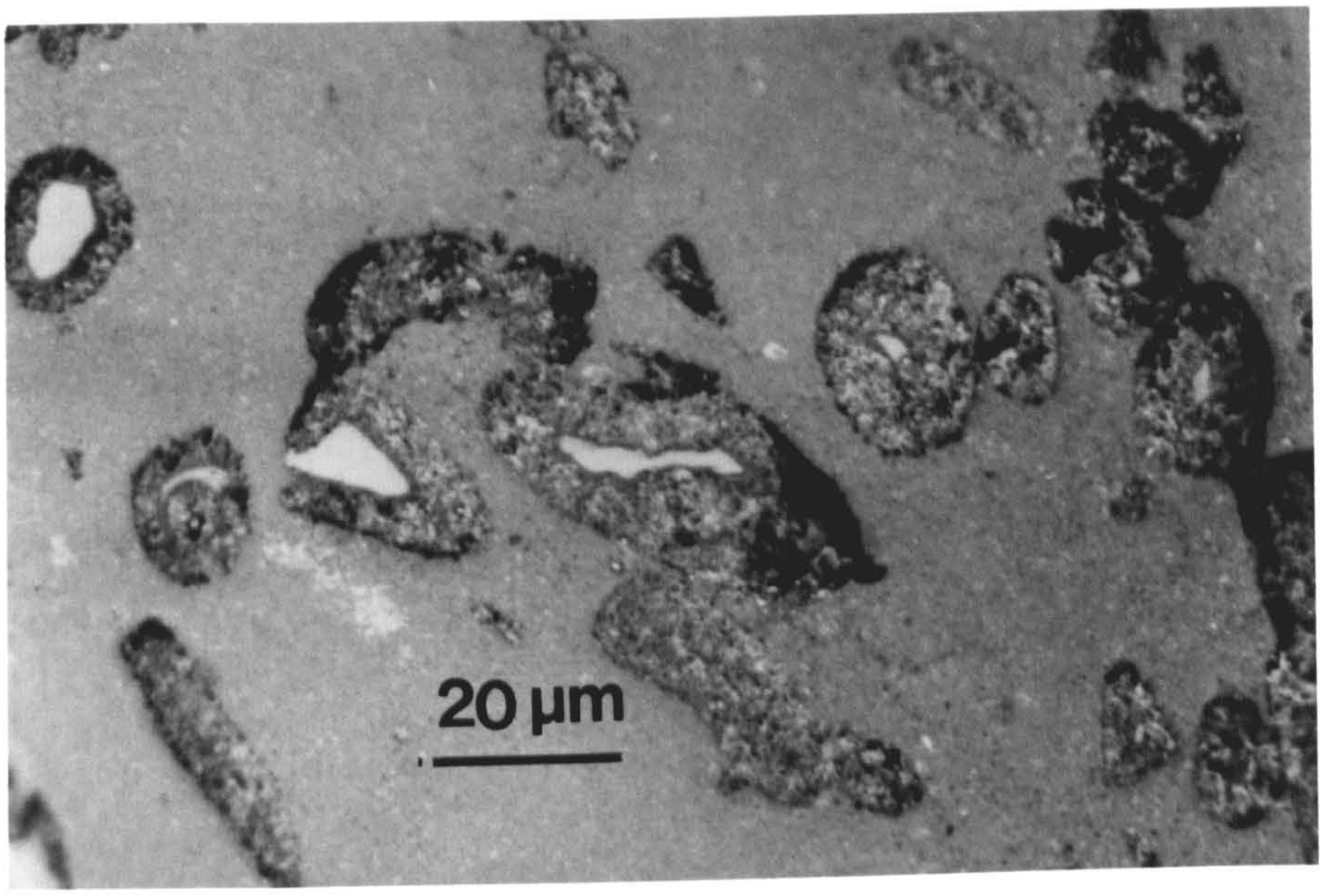
20 µm

figure 4.20.a

As in figure (4.19) hot–pressed at 1450°C

figure 4.20.b

As in figure (4.20.a), an SEM photograph at the fracture surface.

a

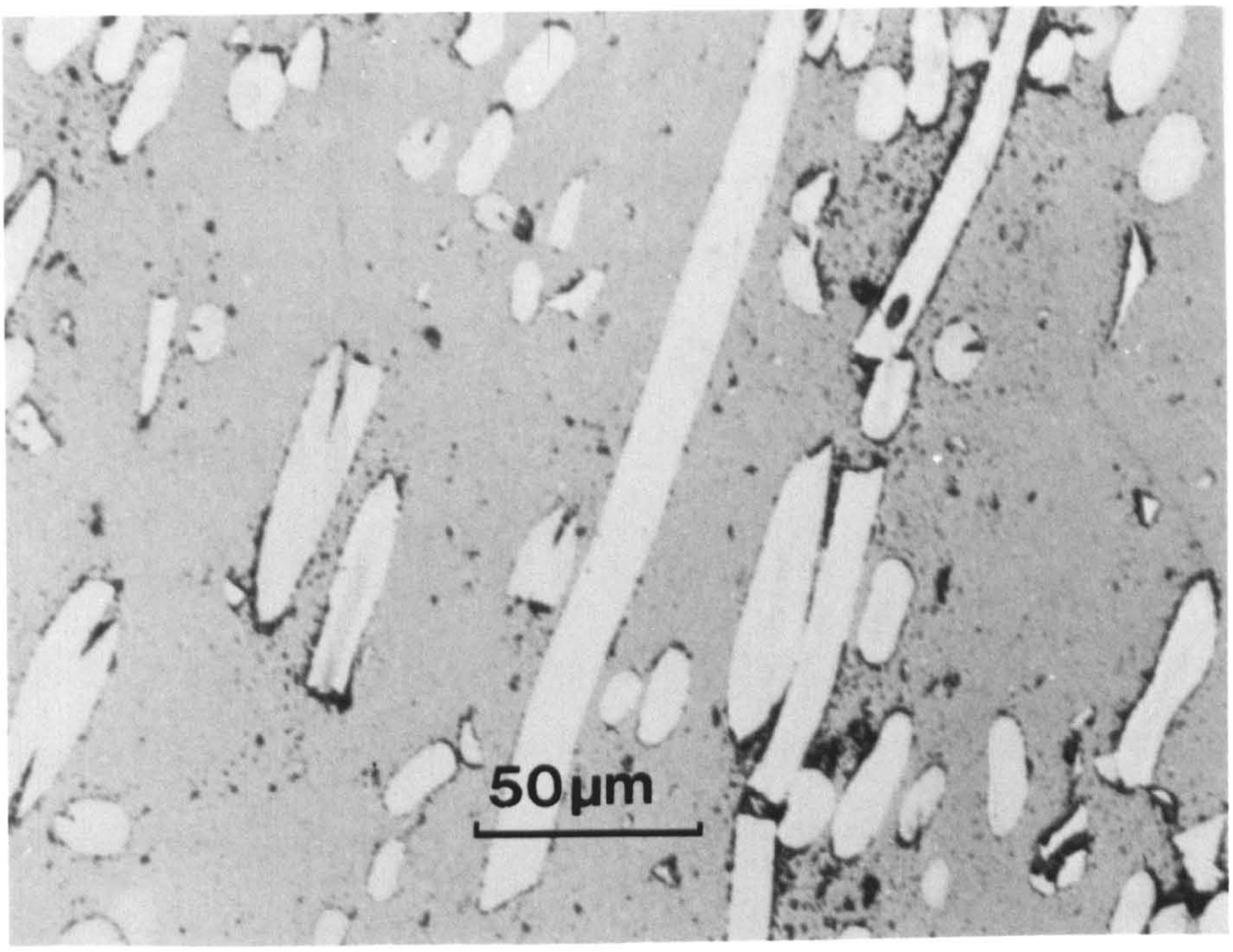

b

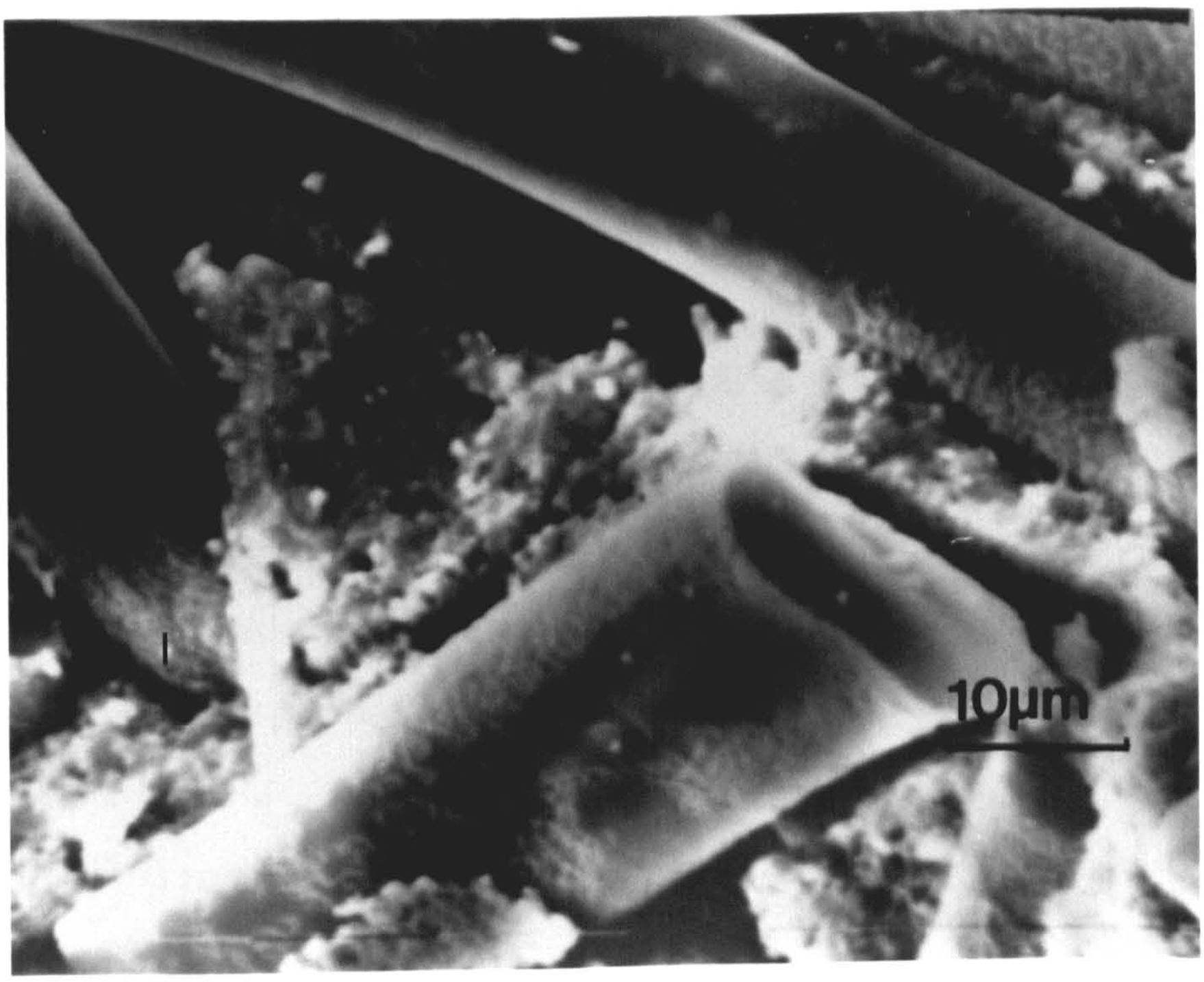

because in a low volume fraction fiber composite, densification is much faster, (as discussed in above under "pressureless sintering") and hence there will be little chance for the fiber to react. The reaction always leads to carbon monoxide gas liberation, so if this gas formation is prevented by a high rate of densification, the reaction will be self limiting.

(ii)Fiber grade (C).

The specifications of this type of fiber are given in appendix (1). The densification behaviour of fiber (C) reinforced syalon 201 was examined by the hot pressing technique. Specimens containing 15V% fiber were hot–pressed at two different temperatures. The results for the sintered density of the samples are given in table (4.5). It can be seen from this table that density of over 90% of the theoretical is achieved, even at temperatures as low as 1450°C. Optical microscopic investigation reveals that sintering at 1550°C causes the fiber at the surface of the sample to react with the matrix in a similar way to that discussed in evaluating the results concerning the densification of 20V%G.P fiber/sialon composites sintered at 1550°C. However, no strong reaction is observed at the center of the sample, as seen in the optical micrograph given in figure (4.21.a). The reason for this difference in behaviour between the surface and the center of the sample is attributed to the influence of densification. High rates of densification help to block the way and it becomes difficult for the gas (as a reaction product) to escape from the inside of the sample.This leads to a pressure build up around the carbon causing the reaction to be inhibited. Therefore, the reaction continous only at the surface.

The fiber volume fraction seems to have an effect on the continuity of the reaction when it starts. The results of hot pressing a 20V% G.P fiber containing sialon

figure 4.21..a

Optical photograph for hot-pressed sample containing 15V% carbon fiber grade (C) sintered at 1550°C for one hour.

figure 4.21.b

As in figure (4.21.a) carbon fiber grade (B).

a

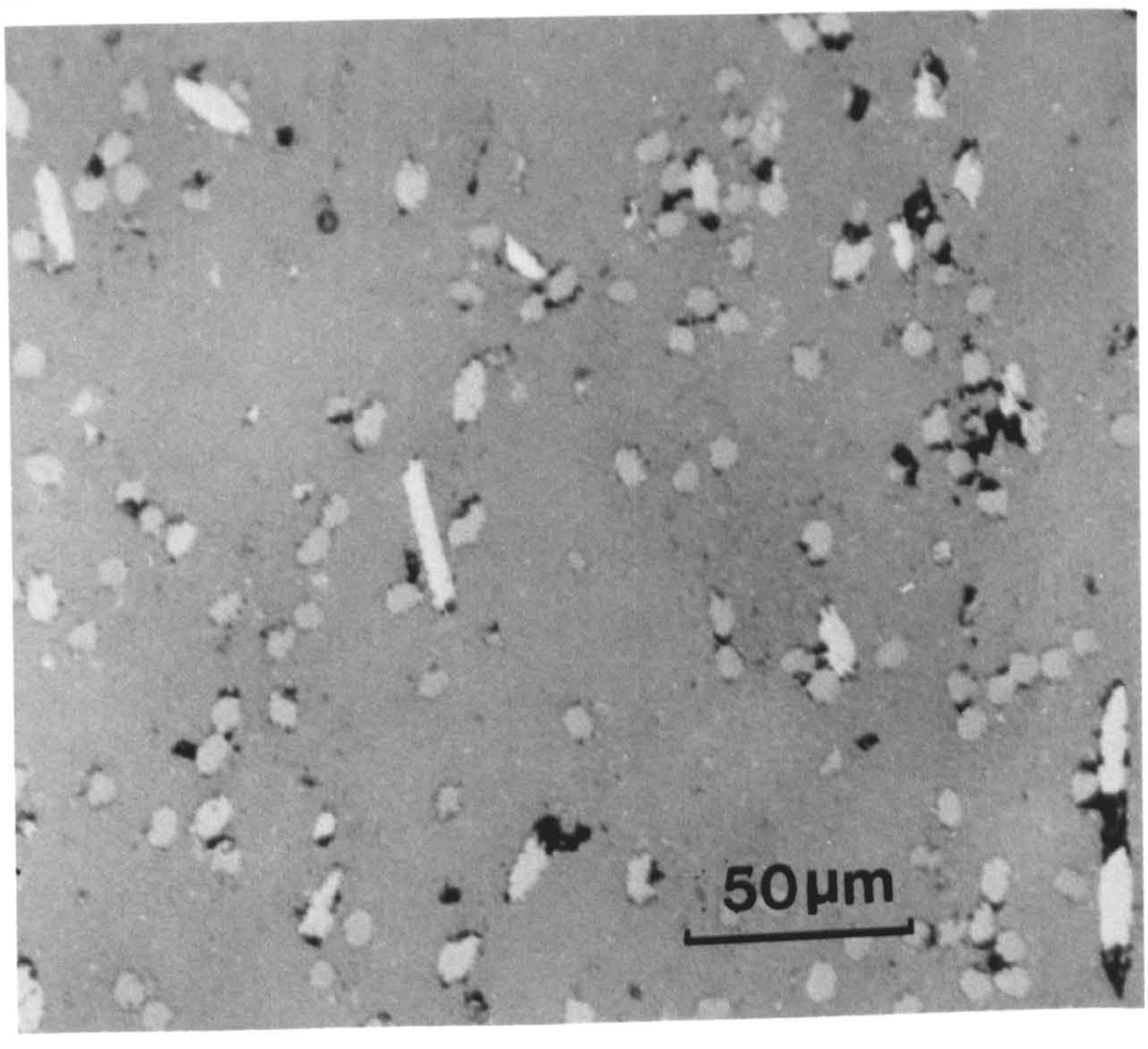

b

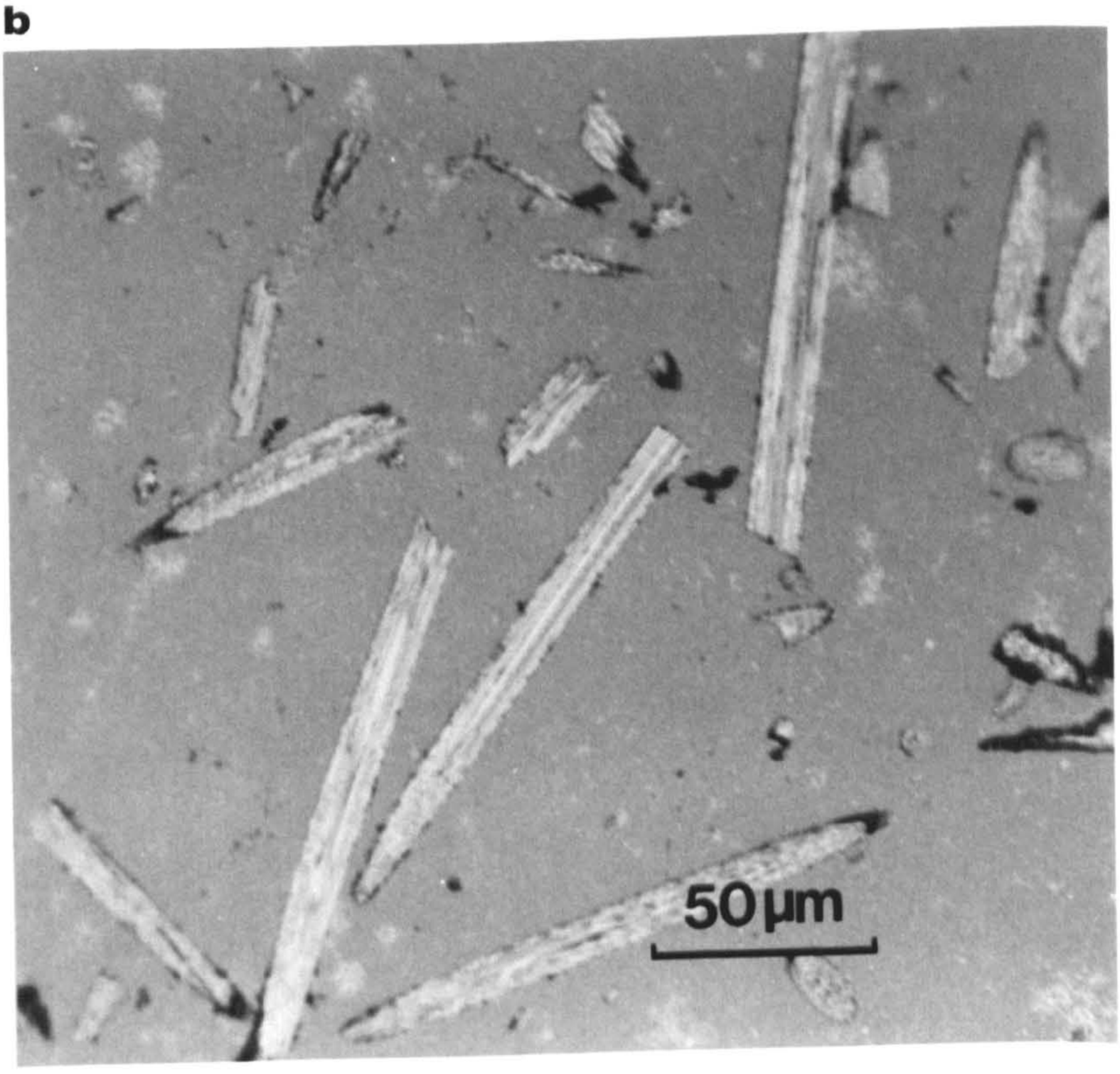

show that both the surface and the center of the sample exhibit similar behaviour. However, the behaviour in a sample containing 15V% fiber (C) is similar to that observed at the surface of the sample only. There is no reaction observed at the center of the sample in the second case. In addition to what has been discussed before about the influence of carbon volume fraction on the amount of liquid phase formed at sintering temperature, there is another reason to explain the effect of the carbon volume fraction on the reaction behaviour. Increasing the amount of carbon means increasing the interconnected channels occuring at the onset of the reaction between the fibre and the matrix. This will enable the continuation of gas evolution and therefore the reaction will proceed.

(iii) Fiber grade (B).

Sialon reinforced with 15V% fiber grade B was hot pressed at 1550°C and the fired sample has almost theoretical density as illustrated in table (4.5). The optical photograph in figure (4.21.b) shows that there is no strong reaction between the fiber and the matrix at either the surface or the center of the sample. It can be seen on figure (4.21.b) that the structure of this type of fiber is different to which has been shown in the other type of fibers. This is due to the different temperature of formation to those fiber discussed before.

4.4.2 Meso–phase carbon/sialon composites.

i-Powder grade (D).

Meso–phase carbon reinforced syalon 201 composites were also investigated in the present study. Two batches of powder (D) reinforced sialon materials were prepared with 10V% and 20V% powder. The samples from these batches were hot pressed at two different temperatures. The density results are given in table (4.6).

Table (4.6)

Variation of density with temperature and carbon volume fraction in the hot pressed meso–phase carbon/sialon system.

fiber grade	volume fraction %	sintering temp. (°C)	sintered density ($g.cm^{-3}$)	Theoretica -l density %
grade (D)	20	1550	2.875	95.7
	10	1550	3.00	95
	20	1450	2.63	87
grade (E)				
	15	1550	3.095	99

The results presented in table 4.6 show that over 95% theoretical density is attainable with the two volume fractions of powder (D) (10V% , 20V%) investigated in the present study. Optical examination of the hot pressed samples at 1550°C shows that it is very well sintered with no reaction between the powder and the matrix–figure

(4.22.a & b). The amount of powder in the sample seems to have no major influence on the reaction starting point . The sample reinforced with 10V% powder was also examined and is comparable with the sample containing 20V% powder. The density of the specimen hot pressed at 1450°C table (4.6) is rather good for such a low sintering temperature and again this sample is comparable with the specimens discussed above.

(ii)Powder grade (E)

15V% of this type of meso–phase carbon was also used to reinforce sialon 201 and the results in table (4.6) reveal that a density approximately equal to the theoretical is obtained. As with the previous samples containing powder (D) it appears that there is no reaction between the powder and the matrix.

4.4.3 Continuous carbon fiber/sialon composites.

Attempts have also been made to produce a continuous reinforced sialon composite, although difficulties were found in producing green samples with continuous fibers. However, samples were produced with either fiber (A) or fiber (C) in 201 sialon and hot pressed. The results reveal that on sintering at 1580°C, fiber (C) has reacted completely at the surface and partially at the center of the specimen. Fiber A at the same temperature is less reactive. At a lower temperature of 1550°C samples containing fiber grade (C) were hot pressed and optical microscopic investigations show a good fiber sialon interface at the center of the sample as can be seen in figure (4.23.a).

figure 4.22.a & b

Optical photograph for a hot-pressed sample containing 20V% carbon powder grade (D) sintered at 1550°C for one hour.

a

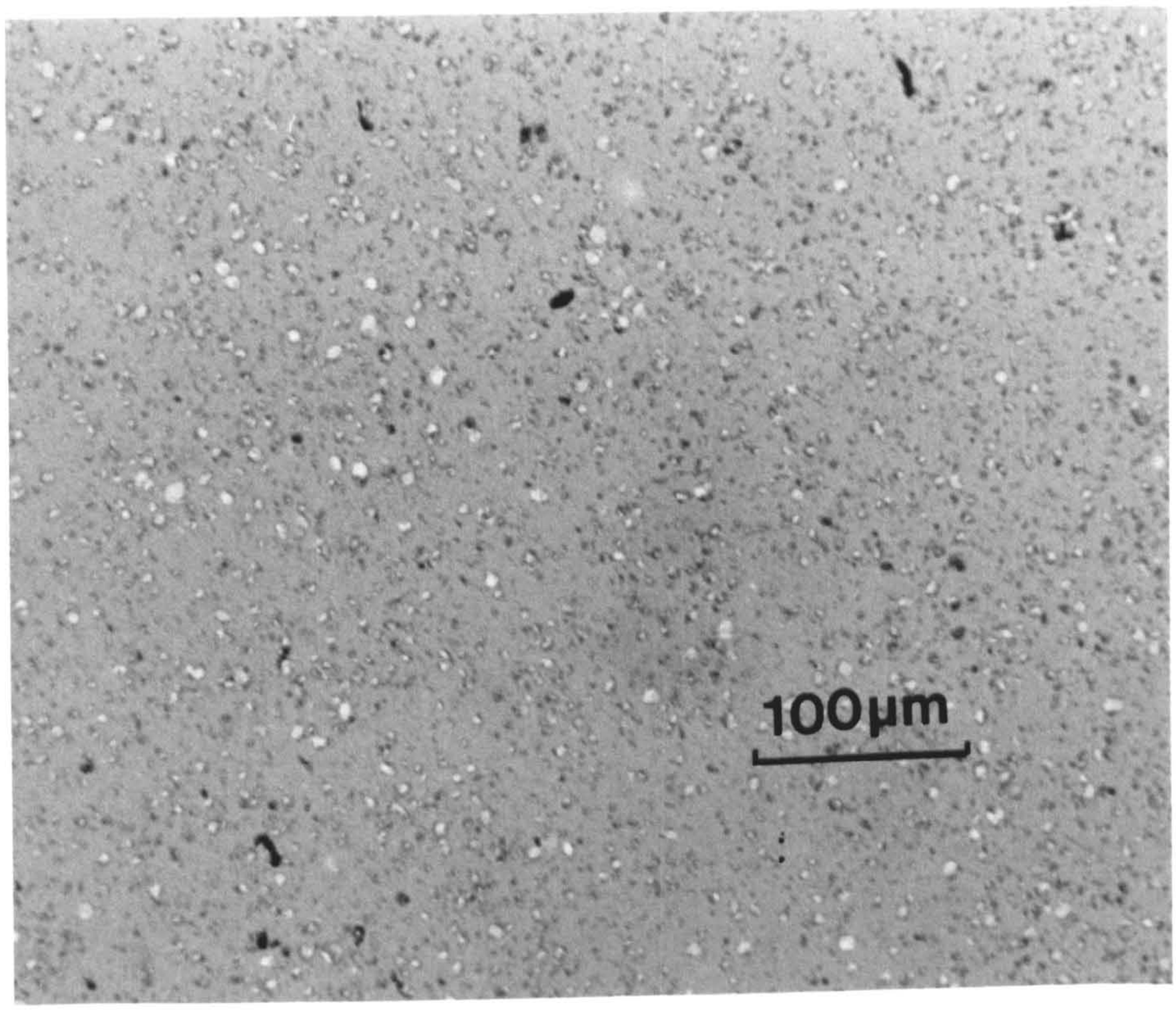

b

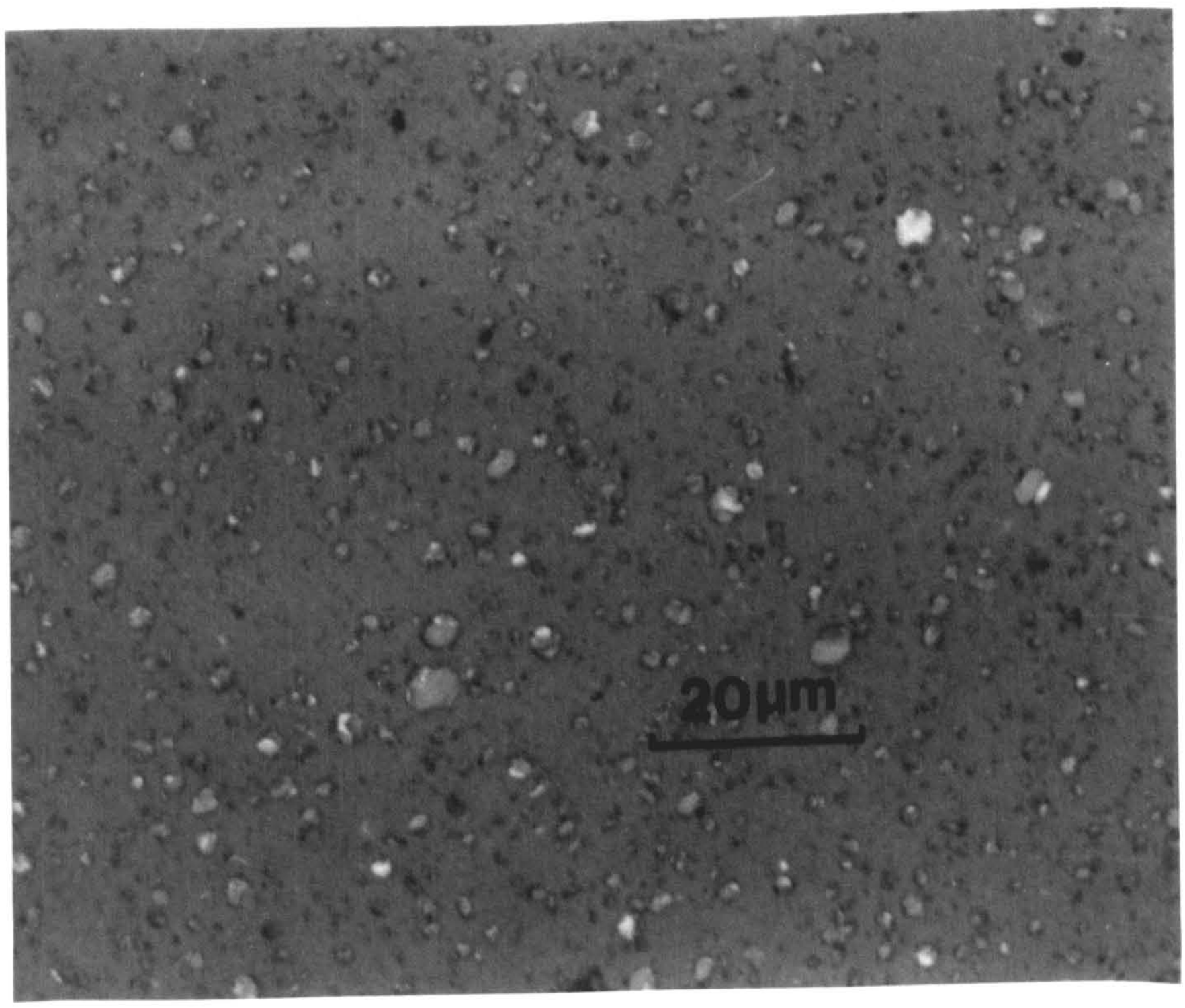

figure 4.23.a

Optical photograph for a hot pressed sample reinforced with a continous fiber grade (C)

figure 4.23.b

TEM photograph for a hot pressed sample containing fiber grade G.P sintered at 1550°C showing the reaction area.

4.5 Phase Identification.

X-ray analysis reveals that there are always two phases present in the structure and these are; unreacted α-Si_3N_4 and β'–sialon. The Z value of β'-sialon and the proportions of these phases are strongly related to the temperature for a fixed sintering time. The higher the temperature the lower the amount of unreacted silicon nitride. More sialon with almost the expected Z value was produced at 1550°C. Samples fired at 1450°C are seen to contain higher quantities of unreacted silicon nitride and smaller amounts of sialon with Z value higher than normal.

The reason that no α'–sialon is formed is related to the presence of carbon monoxide gas formed from the reaction between the die material (graphite) and the oxygen present in the air. The partial pressure of carbon monoxide gas in the sintering atmosphere can be evaluated as follows;

$$2\ C + O_2 = 2\ CO$$

the partial pressure of CO is calculated from the composition of the initial air in the die (79% N_2 + 21% O_2) to give

$$P_{CO} = 0.33 \text{ atm}$$

Since the P_{CO} responsible for preventing α'–sialon formation is less than this value then no α' is formed in the final structure. Also the very high rate of densification may help to inhibit this reaction completely.

The X–ray investigation does not show any other phase apart from sialon and unreacted silicon nitride in the sample reinforced with 20V% G.P fiber grade and

sintered at 1550°C in which ,as the microscopic examination shows, there is a considerable amount of reaction. The question therefore remains as to the nature of this reaction and the phases formed (figures 4.19 and 4.23.b). The answer is not clear although the products are amorphous since they are not identified in the X-ray diffraction pattern.

CHAPTER FIVE

METAL/CERAMIC COMPOSITES

5.1 Introduction.

Significant advances in the technology of engineering ceramics for structural applications have been forecast from developments in the composite behaviour of ceramics. These developments have been directed at increasing the fracture toughness of these brittle materials. The approach which has been almost universally adopted in developing ceramic–matrix composites is that of classical composite behaviour (i.e by control of the matrix–composite interface properties.) An alternative approach for improved matrix properties have been noticed in zirconia composites, where the phase transformation from tetragonal to monoclinic results in a useful increase in the fracture toughness [Stevens 1986]. Phase transformation is not available in the majority of ceramic–matrix systems and so alternative means of absorbing elastic energy and crack arrest must be sought.

The present work on crack arrest was by the incorporation of tough particles dispersed in a brittle matrix. Providing the interface characteristics are suitable then the particles will act as a dispersion of low modulus material, in which crack blunting may occur. The work has been devoted to the study of different metal powders reinforcing a sialon matrix (syalon 201) where the problems of controlling the interfacial

behaviour are considered. Both mechanical and electrical properties of the composite have been evaluated.

5.2 Results and Discussions.

5.2.1 Iron/sialon composite.

Experimental results from 10V% iron powder reinforced syalon (Cookson 201) show that such a material can be sintered to about 85% of the theoretical density and could be increased still further by longer sintering times. The experiments carried out using a horizontal tube furnace (in which the heating rate is low), were not successful. The samples are changed in colour (becoming black) and there was no densification. However, a high heating rate was applied to the specimens (150°C/ min in a tungsten element furnace) and the results are given in table (5.1)

.

Table (5.1)

Pressureless sintering of 10V% Fe reinforced β'-Si-Al-O-N composite

Temperature (°C)	Time (hr)	Density $g.cm^{-3}$	Theoretical %
1450	2	2.44	66
1550	1	3.17	85

From these experiments it can be seen that the heating rate influences the resultant density. The higher the heating rate the faster the material will densify and this in turn helps to inhibit the reactions which occur during the sintering process.

The EDAX analyses of the iron particles shows that silicon is always present with the iron and the amount of silicon increases with increasing sintering temperature.

It can be concluded from these experiments that a reaction between the iron and the sialon matrix occurred and the gaseous reaction product (in the case of low heating rate sintering) caused disintegration of the sample and prevented densification. However, the other reaction product (as the EDAX shows the iron particles contain silicon) is a silicon–iron alloy (silicide) having a different Si/Fe ratio. On the Iron–Silicon phase diagram in figure (5.1) it is clear that several types of iron silicide can be formed depending on the temperature and amount of silicon and iron present. In the present study (the iron/sialon system) the source of silicon is the matrix and the amount of iron is fixed. This make the silicide phase–type dependent on how much silicon could diffuse to the iron particles from the surrounding matrix.

The sialon used in these experiments is a mixture containing more than 80wt% silicon nitride (which represents the source of silicon to form iron silicide). Reactions during sintering of syalon 201 occur to form a liquid phase which is required for densification. This happens at a relatively high temperature (almost 1380°C). This temperature is high enough to form iron-silicide (as can be seen in the iron–silicon phase diagram). This means that silicon nitride is not involve in densification reactions at silicide formation temperatures. This could lead to the conclusion that reactions occurring during the course of sintering are between the silicon nitride and iron as follows;

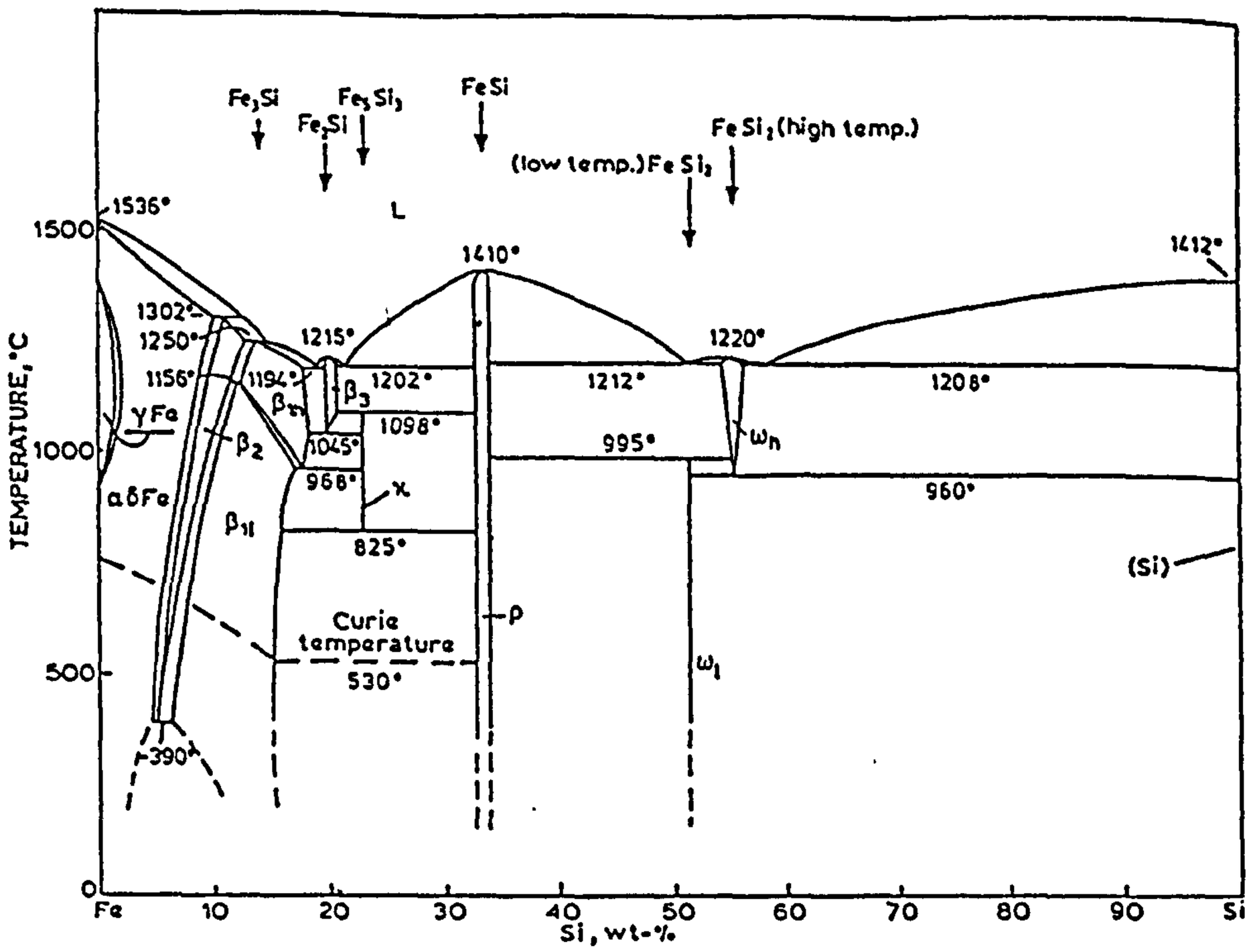

figure 5.1

Iron-Silicon phase diagram.

$$Si_3N_4 + Fe = \text{Iron silicide} + 2N_2 \ldots\ldots\ldots (5.1)$$

However, the different types of iron silicide shown in figure (5.1) have various crystallographic forms given in table (5.2) on which the nitrogen gas partial pressure generated from reaction (5.1) depends. This will be discussed later.

Table (5.2)

Iron Silicide chemical formula and structures

Fe_5Si_3	Hex.
Fe_3Si	Cubic
Fe_2Si	bcc related
FeSi	Cubic

The X-ray analysis of the sintered iron/sialon composite samples, however, eliminated the possibility of formation of any metallic phases structures far from cubic. This means that reaction between iron particles and the matrix could be either;

$$Si_3N_4 + 9Fe = 3Fe_3Si + 2N_2, \ldots\ldots\ldots (5.2)$$

or

$$Si_3N_4 + 6Fe = 3Fe_2Si + 2N_2, \ldots\ldots\ldots\ldots (5.3)$$

or

$$Si_3N_4 + 3Fe = 3FeSi + 2N_2 \ldots\ldots\ldots\ldots\ldots (5.4)$$

Due to the overlapping of the matrix phase and other phase lines, difficulties were encountered when trying to distinguish and precisely identify the silicide phases.

However, β'–sialon with a slightly higher Z value than expected (0.75) and unreacted α-Si_3N_4 constitute the matrix phases. The appearance of α-Si_3N_4 is clearly dependent on the sintering temperature and time. It is noticed that increasing the temperature causes the β'–sialon to dominate the matrix with almost Z = 0.75. (always slightly higher due to the continuous consumption of silicon nitride during the reaction with the iron metal).

The possibility of more than one silicide phase forming seems to exist as the EDAX analysis on the metal particles reveals. Figures (5.2) **a** and **b** respectively are a schematic representation of the EDAX spectrum for the black and white areas shown on the optical photograph for a iron/sialon composite sample sintered at 1550°C for one hour [figure (5.3)]. Alteration in the Si/Fe ratio is clearly noticeable in figures (5.2) **a** and **b.**

In reactions (5.2), (5.3) and (5.4) nitrogen gas evolution always occurs and the pressure of nitrogen gas evolved is strongly dependent on the free energy of formation for the reaction. As the free energy of formation of silicon nitride is unchanged then ΔG(R) 5.2, 5.3 and 5.4 is reliant on the type of iron silicide formed. For the iron silicide phase (and using information in the literature), the nitrogen partial pressure for reaction (5.4) at 1400°C is calculated as below;

ΔG_{FeSi} = -16.644 Kcal/mol [Voitovich (1971)]

$\Delta G_{Si_3N_4}$ = -41.2 Kcal/mol [Hendry (1976)]

$$K(T) = P_{N_2}{}^2 \, a_{FeSi}{}^3 / a_{Si_3N_4} \, a_{Fe}{}^3$$

Assuming that all solids are pure [i.e a=1] then;

$$P_{N_2} = 3.7 \text{ atm}$$

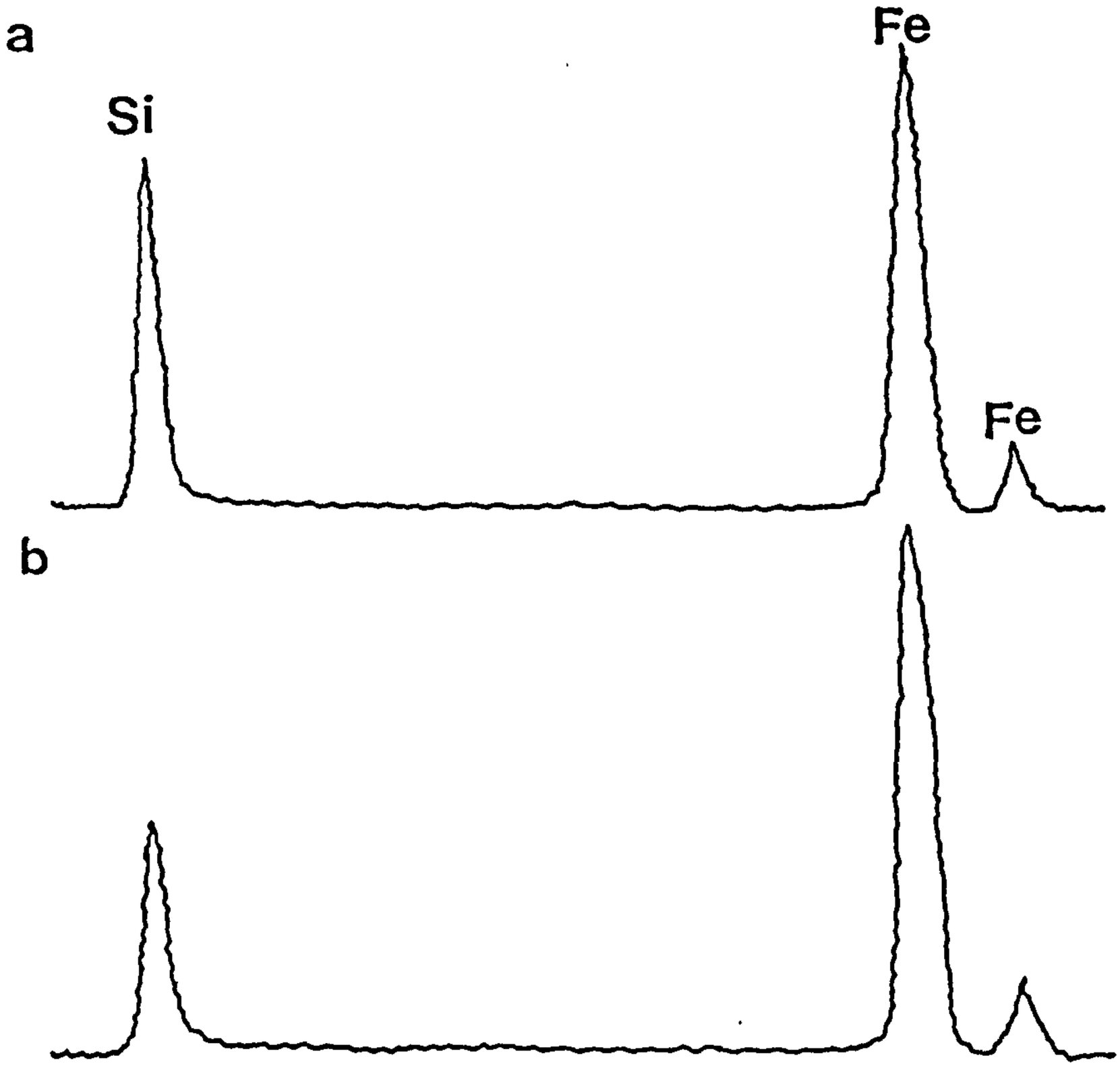

figure 5.2.a & b

Schematic representation of the EDAX spectrium for the black (a) and white (b) phase shown in figure (5.3).

This figure show that in iron/sialon system reaction (5.4) at atmospheric nitrogen pressure can not be prevented. Overpressure sintering with almost 4 atms nitrogen pressure is required to inhibit reaction (5.4), as the above calculations show and by assuming that the free energy of formation of all substance are accurate.

The lack of information on the free energy of formation for other silicide phases prevents the investigation of other reactions. However, the case of more than one silicide phase forming obviously leads to a change in the nitrogen gas pressure derived from any of the above reactions, provided that the two silicide phases are forming during the heating cycle.

The difficulties in sintering such composites may then be related to the high nitrogen gas pressure coming out of the sample during the course of sintering. The high heating rate provided a well sintered composite, but attempts to sinter samples containing 20V% iron failed even at high heating rates.

The general microscopic observations on iron/sialon composites show that the metal particles in the samples fired at low temperature (<1450°C) have some silicon nitride crystals growing in the matrix. The samples fired at slightly higher temperature lose these silicon nitride grains from the center but still retain some at the surface of the sample. These observations will be discussed later in the stainless steel/sialon section. Lastly the poor metal sialon interface noticed on figure (5.3) is believed to be related to the polishing process as the metal particles tends to pull-out from the matrix, which is not very dense.

figure 5.3

Optical micrograph for 10V% iron reinforced sialon composite pressurless sintered at 1550°C for one hour.

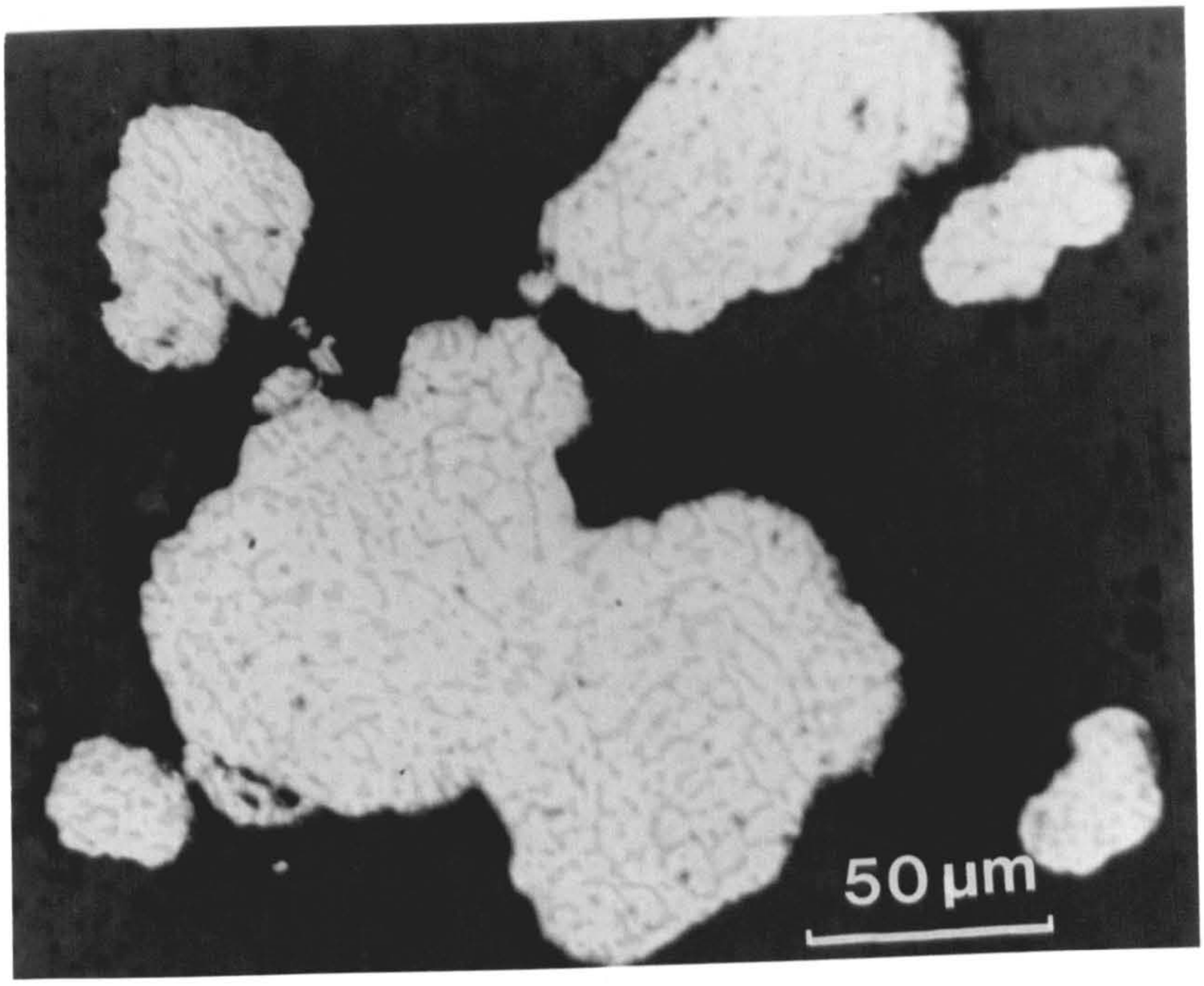
50 µm

5.2.2 Nickel/sialon composites.

Pressureless sintering carried out on nickel reinforced sialon matrix composite indicated that there were no problems such as those faced in the sintering of iron/sialon composites. Densification occurs whether high, or low heating rate is applied. The influence of time and temperature on the pressureless sintered density of 15V% Ni–sialon composites are shown in table (5.3).

Table (5.3)

Pressureless sintering of 15V% Ni reinforced β'–Si–Al–O–N composite

Temperature (°C)	Time (hr)	Density ($g.cm^{-3}$)	Theoretical %
1450	2	3.92	95.5
1500	5	3.95	95.5
1550	2	3.92	96.0
1550	4	4.00	97.0

The first and in some ways, the most remarkable observation on sintering of nickel/sialon composites (table 5.3) was the pronounced decrease in sintering temperature for maximum densification. Syalon 201 as a monolithic ceramic is sintered using 8wt% Y_2O_3 as a densifying aid at 1600°C. However, in the presence of nickel additions this temperature decreases to 1450°C. The reason for this behaviour lies in the formation of liquid phase by reaction between the ceramic and the metal. The DTA analysis of a sample containing 15V% nickel is presented in figure (5.4). On this

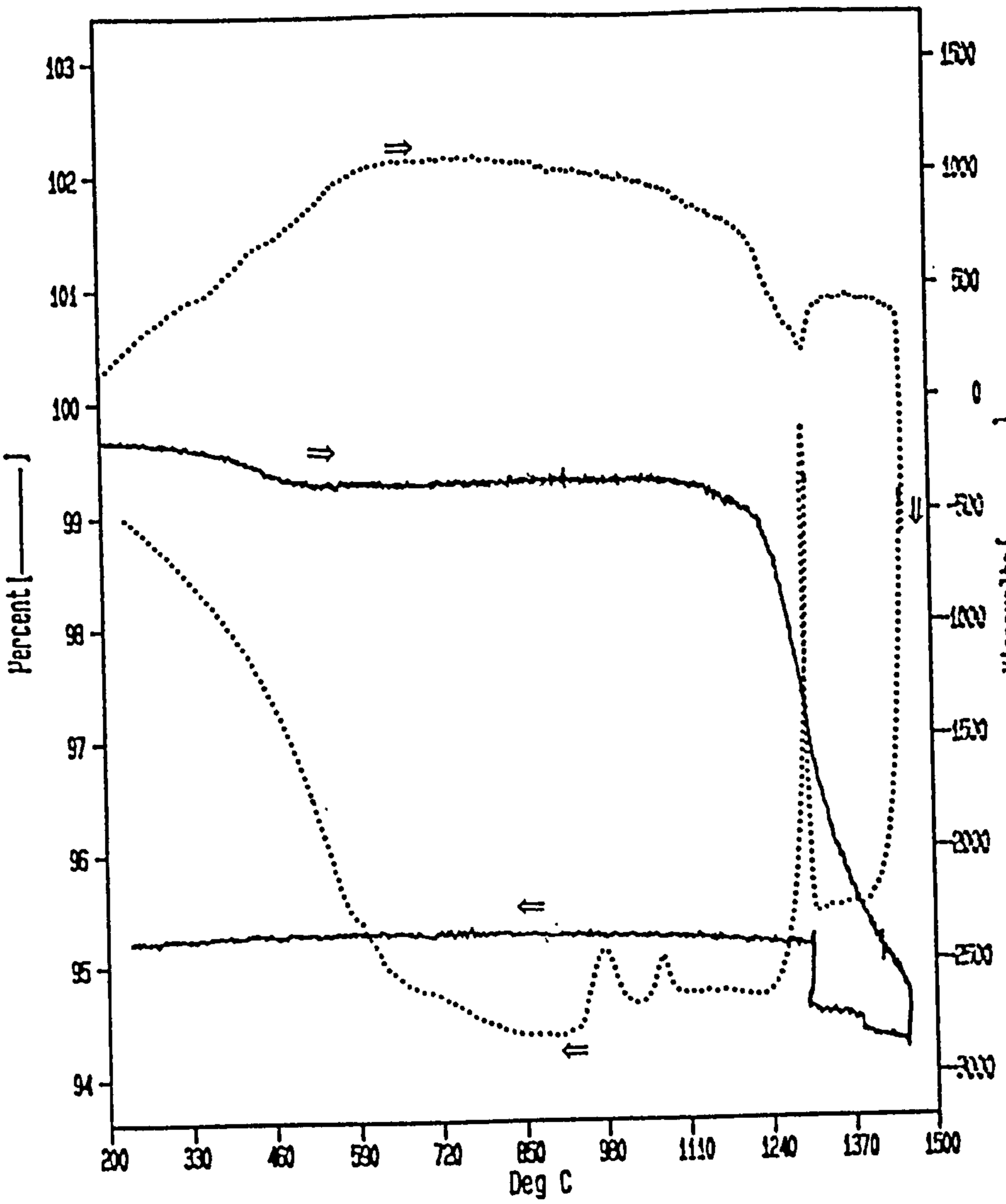

figure 5.4

DTA analysis for 15V%Ni/sialon composite.

figure it can be seen that the first reaction between the sialon and nickel occurs at temperature of almost 1240°C. This reaction is the formation of liquid nickel silicide. Combined with this reaction it can also be noticed on figure (5.4) (solid curve) that there is a continous weight reduction from the sample. Almost 5.5% of the sample weight has been lost over a ten minutes heating from 1240°C (where the reaction started) to 1450°C (the experiment temperature) which is due to the evolution of nitrogen gas from the sample as a reaction product. On cooling the sample to 1300°C and holding it at this temperature for 30 min there is an almost 0.5% increases in the sample weight. This enhancement in weight could be due to the nitrogen absorbed by the sample from the atmosphere. There are two solidification peakes on cooling from 1300°C to room temperature one at 1080°C and the other at 980°C.

The theoretical density of this composite is 4.1 $g.cm^{-3}$ and it can be seen in table 5.3 that values of greater than 95% theoretical can be achieved even at temperature as low as 1450°C. Densification of the ceramic matrix has been promoted at such low temperature by the presence of the metal phase. A detailed discussion of the nickel/sialon interaction requires consideration of the effect of silicon on nickel particles by reference to the nickel–silicon phase diagram given in figure (5.5). The source of silicon is the silicon nitride component in the syalon 201. Consider the Si_3N_4 decomposition reaction in nitrogen gas and elemental silicon involvement in nickel silicide formation;

$$Si_3N_4 \leftrightarrow 3Si + 2N_2 \quad \text{.....(5.5)}$$

where Si_3N_4 is the syalon 201 component, Si is the silicon solubility in nickel and N_2 represents the nitrogen gas pressure therefore;

a

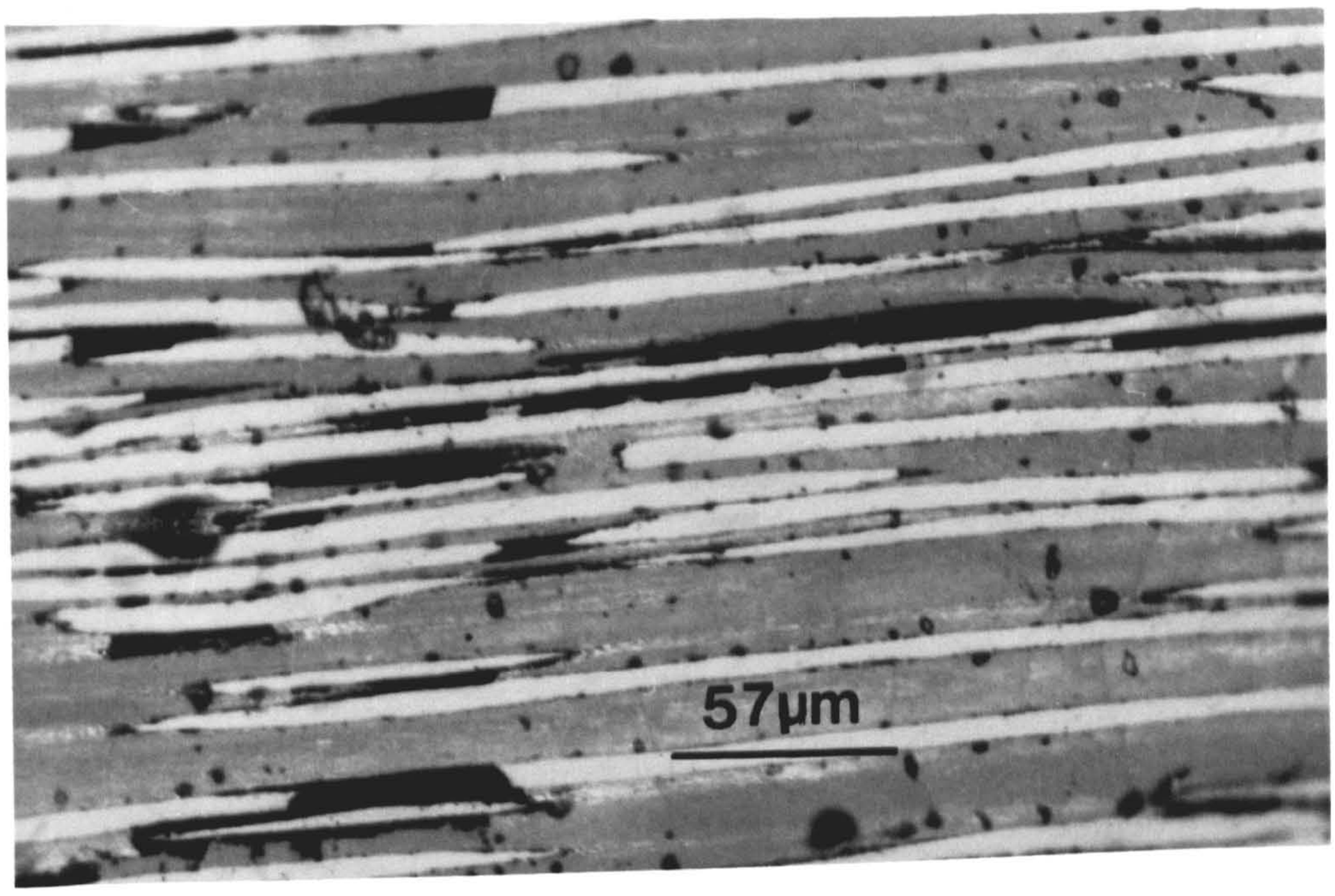

b

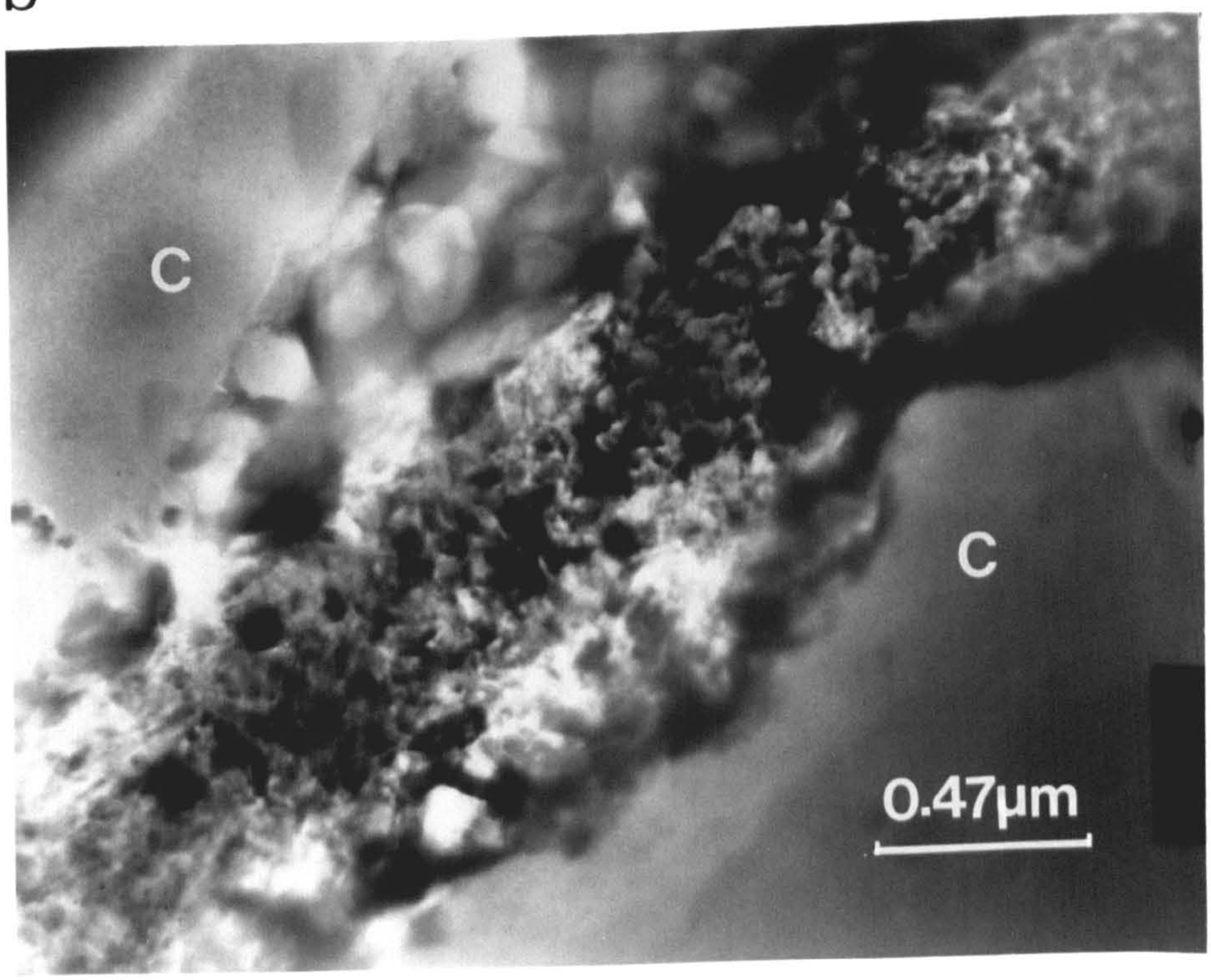

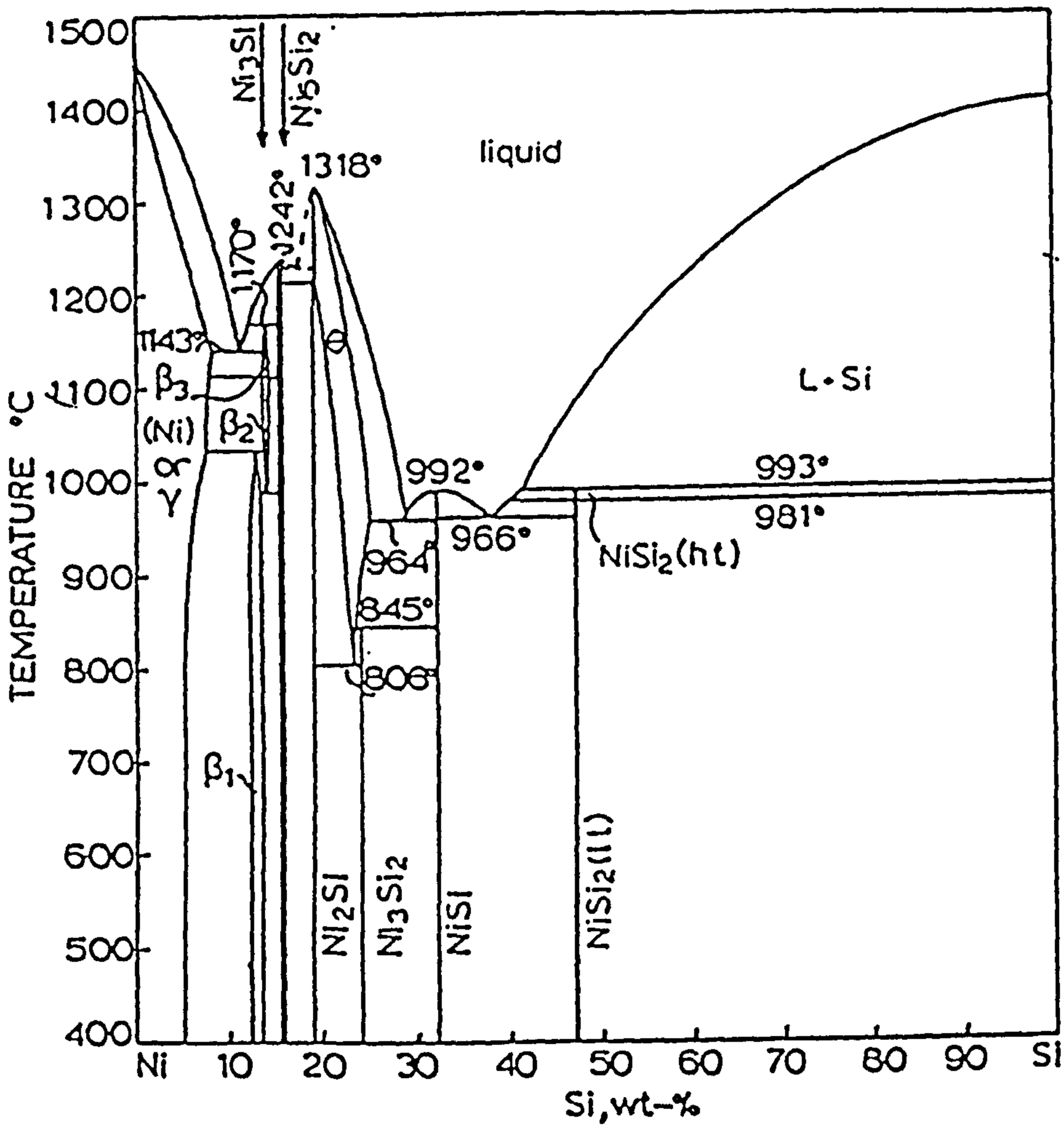

figure 5.5

Nickel-Silicon phase diagram.

$$K(T) = a_{Si}^{3} P_{N_2}^{2} / a_{Si_3N_4} \quad .....(5.6)$$

Where a, represents the activity of the species and P, the partial pressure. For the conditions of pressureless sintering in the present experiment, T=1500°C $P_{N_2} = 1$ atm and the activity of Si_3N_4 equals unity therefore;

$$\Delta G_{5.5} = 30.443 \text{ Kcal}$$

and;

$$a_{Si} = 0.056$$

According to the information given by Chart [1973] for such silicon activity, the approximate weight percent of silicon involved in nickel silicide formation can be calculated. It is found to be almost equal to 24.2wt%, at which (figure (5.5)) silicide liquid is present at even lower temperatures (1150°C) than in the present sintering conditions. Similarly, the calculated silicon weight percent at a sintering temperature of 1450°C is 19.2wt% and liquid silicide is also present.

The sintering process was carried out in a tungsten element furnace and table (5.3) shows that over 95% theoretical density is achieved even at temperatures as low as 1450°C. Thus the densification at these low temperatures is obviously related to the presence of nickel silicide liquid forming at low temperature. The nickel–silicon phase diagram in figure (5.5) shows that liquid phase could be formed at temperatures less than 1000°C and this liquid may serve as a transport medium to promote the densification process. However X-ray diffraction and EDAX analysis confirmed nickel silicide formation and whatever the sintering temperature, there are always two nickel silicide phases formed. These can be distinguished by contrast as white and

dark phases on the SEM micrograph as shown in figure (5.6.a). The Si/Ni ratios of white and dark phases respectively shown in the energy dispersive analysis figures (5.7.a & b) are dis–similar. They are lower in the white than in the dark phase. The general SEM examination indicates that the presence of the white phase (lower Si/Ni ratio) decreases with increasing temperature and time. Additionally it is noticed that as the temperature increases, the nickel particles contain a fine dispersion of darker material which can be seen in the optical micrograph in figure (5.6.b) of a sample sintered at 1550°C for two hour. EDAX analysis shows this dark phase to be in the Si–Al–O–N system. At higher temperatures, it is possible that significant dissolution of sialon can occur in the nickel silicide liquid, reprecipitating crystalline sialon on rapid cooling. In all the previous optical and SEM photographs however, it is clear that the nickel–sialon interface is homogeneous in a very well densified matrix.

The X-ray data files, show that nickel silicide has several type of complex structures. These can be seen in table (5.4).

Table (5.4)

Chemical formula and structures of nickel silicides

Phase	Structure
Ni_2Si	Orthorombic (Hex.)
Ni_3Si_2	Orthorombic
Ni_5Si_2	Hexagonal (trigonal)
NiSi	-------

The X–ray diffraction analysis reveals that Ni_3Si_2 and some other silicide phases represents the metallic phases formed in the composite structure. However, the

figure 5.6.a

SEM photograph for sialon sample containing 15V%Ni sintered at 1500°C for 5 hrs.

figure 5.6.b

As in figure 5.6.a sintered at 1550°C for 4 hrs. (optical photograph)

a

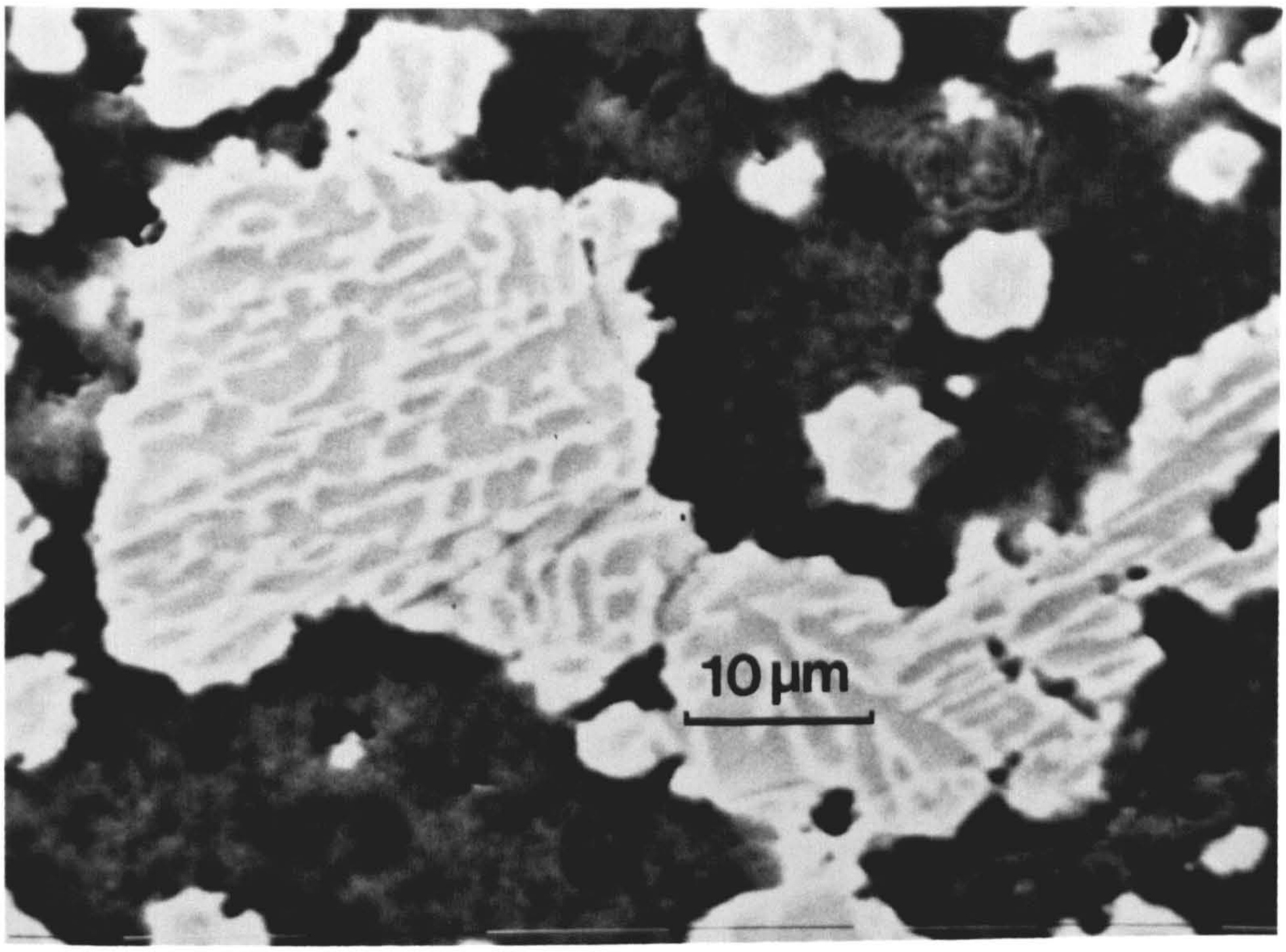

b

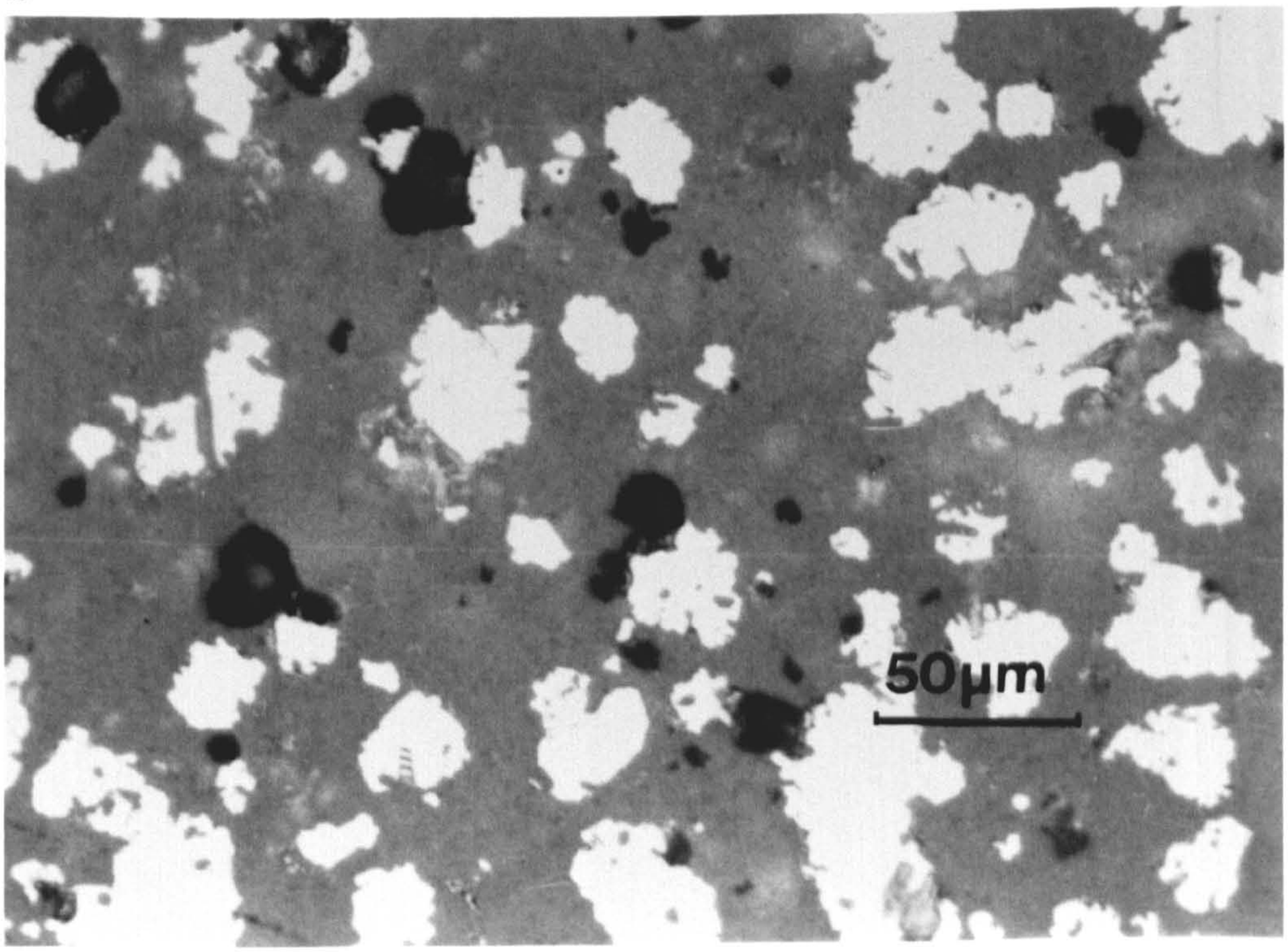

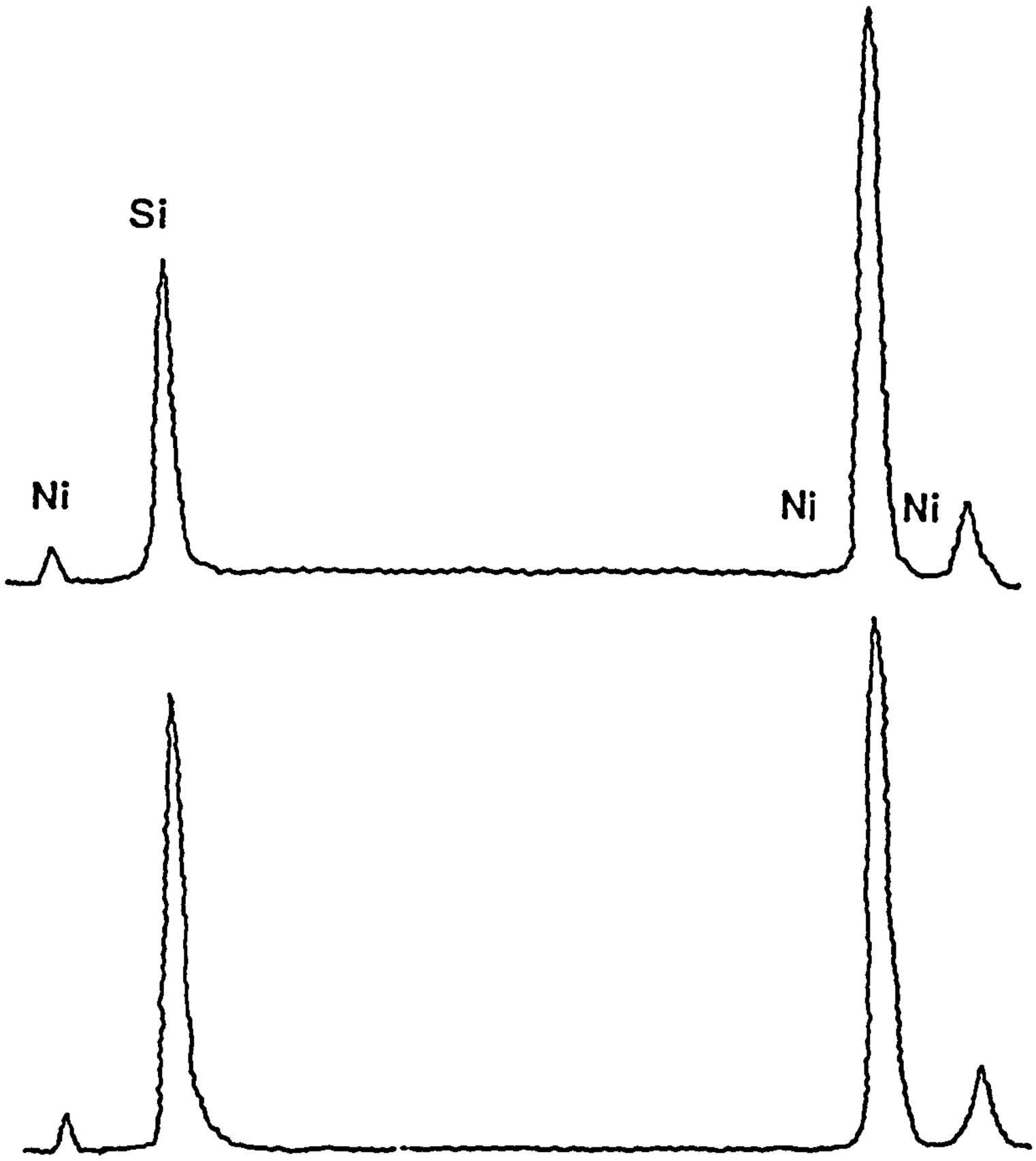

figure 5.7.a & b

Schematic representation of the EDAX spectrum for the white and black phases shown in figure 5.6.a.

ceramic phases are a combination of unreacted α–Si_3N_4 and β'–sialon with different Z values (relying on both temperature and time). In general, and similar to what has been mentioned in the iron/sialon system, the β'–sialon phase (as the X–ray diffraction shows) has a Z value slightly greater than what it was designed for (0.75). This is due to the decomposition of some of the silicon nitride during the reaction with nickel. At low sintering temperatures, the transformation and reaction of α–Si_3N_4 to β'–sialon (over short periods of time) may not be complete, resulting in a considerable amount of residual unreacted α–Si_3N_4 phase in the final structure. For example, the sample sintered at 1450°C for two hours contained almost 30% α–Si_3N_4 and 70% β'–sialon with Z = 1.45. The Z value of the β'–sialon phase in the compact sintered at 1550°C is lower than that in the sample fired at 1450°C and slightly greater than 0.75 (Z=1) combined with a very small amount of unreacted silicon nitride.

Assuming that Ni_3Si_2 is the only nickel silicide phase formed, the theoretical enhancement of the Z value due to nickel silicide formation can be calculated as follows;

Silicon wt% in Ni_3Si_2 = 24

The wt% of Ni in sample containing 15V% Ni = 32.27

The wt% of Si diffused to the Ni particles from the matrix = 7.74

The Si_3N_4 wt% decomposed to supply the 7.74wt% Si = 12.9

The general reaction to form sialon phase is given below;

$$(6\text{-}Z/3)\ Si_3N_4 + (2Z/3)\ Al_2O_3 + (Z/3)\ AlN = Si_{6\text{-}Z}Al_ZO_ZN_{8\text{-}Z}$$

For Z = 0.75 sialon compositions will be;

Si_3N_4 = 80wt%

Al_2O_3 = 16.65wt%

AlN = 4.35wt%

The amount of Si_3N_4 involved in β'–sialon formation will be

= 67.1wt%. which is equal to;

67.1 = [6-Z/3 (140)]/[6-Z/3 (140) + 2Z/3(102) + Z/3 (41)]

from which;

Z = 1.31

Similarly, the formation of lower silicon containing nickel silicide such as Ni_2Si increases the Z value of syalon 201 to 1.2. The formation of two phases of nickel silicide (which is likely to be the case in the present study) such as a combination of Ni_2Si and Ni_3Si_2causes the Z value to increase to 1.23.

These figures of the Z value represents the theoretical lower Z value of the β'–sialon matrix reinforced by 15V% Ni, but the measured values discussed above are 19% lower than the minimum value of 1.23. This may be due either to the difficulties involved in the diffusion process of elemental silicon large distances from the metal particles, or the involvement of silicon nitride in the solution–precipitation process which makes the matrix composition more stable. Measurement and assumption of error also contributed to this difference.

In the nickel/sialon system, the lack of information regarding the free energy of formation of nickel silicide makes the prediction of nitrogen gas pressure required to inhibit the following reaction difficult;

$$Si_3N_4 + Ni = \text{Nickel silicide (s)} + 2N_2 \ldots (5.7)$$

The free energy of formation of nickel silicide phases are required in order to estimate the nitrogen gas partial pressure generated from reaction (5.7). However, in

the literature, ΔG_{NiSi} =-18.62 Kcal at 1400°C [Voitovich 1971] and if this is the only phase formed during the course of the reaction then the partial pressure of nitrogen generated from the following reaction can be calculated;

$$Si_3N_4 + 3Ni = 3NiSi + 2\ N_2 \quad \ldots\ldots\ldots\ldots (5.8)$$

at 1400°C

$$\Delta G_{Si_3N_4} = -41.2 \text{ Kcal/mol}$$

and

$$\Delta G_{NiSi} = -18.62 \text{ Kcal}$$

then;

$$\Delta G_{R5.8} = -R\ T\ \ln\ K(T)$$

$$= -14.663 \text{ Kcal}$$

and;

$$K(T) = (P_{N_2})^2\ (a_{NiSi})^3/(a_{Si_3N_4})\ (a_{Ni})^3$$

Assuming all are pure solids with activity equal to unity then the nitrogen partial pressure can be estimated ;

$$P_{N_2} = 9.1 \text{ atms}$$

This figure indicates that sintering of nickel/sialon composites is very difficult. However, the experimental results reveals that it is much easier to densify these composites than iron/sialon composites in which the nitrogen partial pressure liberated from the iron/sialon reaction is lower than that of this case. This could be attributed to the lower nickel silicide liquid temperature formation, (as in figures (5.1) and (5.5))

which helps the densification to start at lower temperature and block the escape of nitrogen gas at the earlier sintering temperatures. Additionally, the nickel powder has a smaller particle size than iron and stainless steel (to be discussed later) which could cause the reaction to subside at an earlier stage in the sintering. Larger particle sizes required longer times to reach equilibrium with the matrix and this in turn means continuous gas evolution and poor densification.

However, the formation of more than one nickel silicide phase (which is the case in the present situation) has a major influence on the nitrogen partial pressure generated from the reaction. For example the existence of Ni_3Si_2 as well as NiSi in reaction (5.7) will lead to change the stoichometric ratio of the reactant and the product which in turn changes the P_{N_2} to a lower value. This may be calculated as follows;

$$Si_3N_4 + 4Ni = NiSi + Ni_3Si_2 + 2N_2 \ldots\ldots (5.9)$$

At 1400°C

$$\Delta G_{Ni_3Si_2} = -12.2 \text{ Kcal}$$

$$\Delta G_{Si_3N_4} = -41.2 \text{ Kcal/mol}$$

and

$$\Delta G_{NiSi} = -18.62 \text{ Kcal}$$

then;

$$\Delta G_{R9} = -R\ T\ ln\ K(T)$$

$$= 10.38 \text{ Kcal}$$

and then;

$$P_{N_2} = 0.2 \text{ atm}$$

This figure may also explain why it is easy to sinter nickel/sialon composites. The nitrogen gas pressure of the sintering atmosphere is much greater than that

generated from the compacted specimen. Therefore, one could presume that there will be no reaction between nickel and sialon. On the contrary, the experimental results reveal formation of the silicide. Additionally the above calculation assumes that the two silicide phases are formed during the heating cycle which can not be assured.

5.2.3 Stainless steel/sialon composite.

The results obtained from 10V% stainless steel powder reinforced sialon could be divided according to the temperature cycle as follows.

5.2.3.1 Low-temperature sintering.

.

The temperatures for this treatment lie in the range 1350°C–1400°C. Samples containing 10V% stainless steel powder were pressureless sintered using the alumina tube furnace. The densities of fired samples are presented in table (5.5).

Table (5.5)

Pressureless sintering of β'-sialon containing 10V% AISI 316

Temperature (°C)	Time (hr)	Density ($g.cm^{-3}$)	Theoretical %
1375	14	3.04	82
1390	60	3.16	85
1400	60	3.34	89

Regardless of the heating rate, densification occurred without any of the problems encountered in the sintering of the iron/sialon system. However, difficulties did occur in the densification of composites containing 20V% stainless steel, these were partially eliminated by a fast heating rate.

Density measurements presented in table (5.5) show that densities of 80-90% theoretical are achieved and the density increases with both temperature and time. High density is, ,however, required for better mechanical properties. The samples were pressureless sintered at 1375°C where the density achieved was only 81% of the theoretical value (table 5.5), but nevertheless, this figure is remarkably high for such a low sintering temperature.

According to the observations obtained by optical and scanning electron microscopy there are at least three obvious phases in the structure. These can be seen in the optical photograph figure (5.8). These phases are stainless steel, the matrix, and different sizes of prismatic crystals, which have been precipitated in the steel particles during cooling from the sintering temperature of 1390°C. These were identified as silicon nitride crystals by microprobe analysis. The EDAX analysis of the steel particles, however, shows that they all contain silicon. The final silicon content increases with increasing temperature and decreases as the precipitation of silicon nitride crystals increases. Figure (5.9.a) is the X-ray energy dispersive analysis of steel particle in a matrix sintered at 1375°C for fourteen hours in which it can be seen that the height of the silicon peak is smaller than that of the specimen fired at 1500°C figure (5.9.b).

By considering reaction (5.5) and making reference to the Si–Fe binary system shown in figure (5.1) it is apparent that the stainless steel/sialon system exhibits similar behaviour to that in the nickel/sialon system. In the present

figure 5.8

Optical micrograph for sialon containing 10V% stainless steel sintered at 1390°C for 60 hrs.

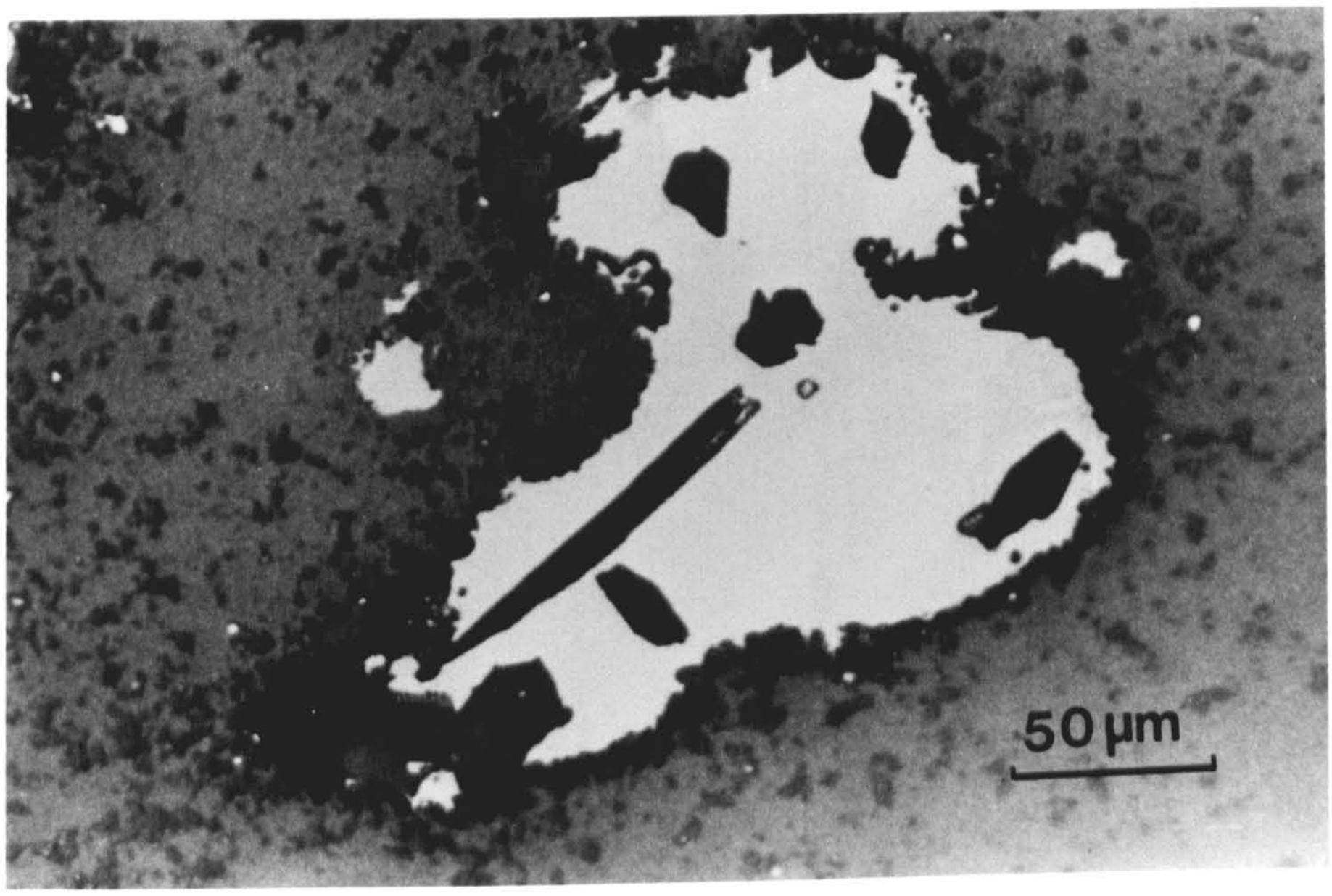
50 µm

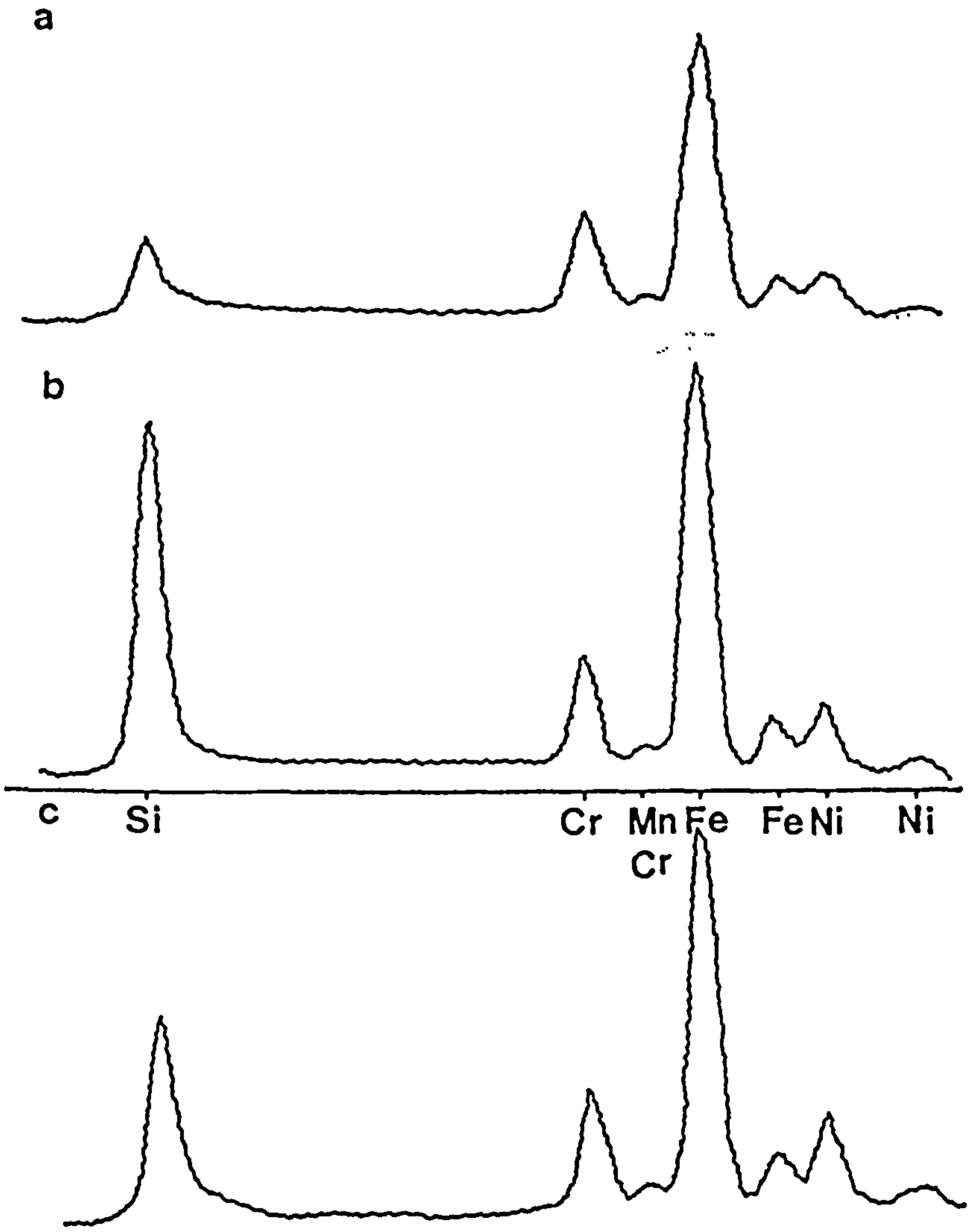

figure 5.9

Schematic representation for the EDAX spectrum for the stainless steel particles in the steel/sialon composite sintered at;

a- At 1380°C for 14 hrs.

b- At 1500°C for 3 hrs.

c- At 1500°C for 3 hrs and at 1380°C for 15 hrs.

experimental conditions, where T= 1400°C and P_{N_2} = 1, the equilibrium solubility of silicon in the stainless steel (represented by pure iron) can be calculated. Since the iron–silicon system has a pronounced negative deviation from ideal solution and using the data given by Chart [1973], the solubility of silicon is found to be high (15wt% Si in iron). It can be seen in the iron–silicon phase diagram therefore that the melting points of such an alloy are low (1250°C) thereby explaining the densification that occurs at such a low temperature. The DTA analysis of 10V% stainless steel reinforced sialon matrix presented in figure (5.10) reveals that first a reaction between the metal particles and sialon occurs at a temperature of 1335°C which is lower than the sintering temperature. The difference between the calculated and experimental liquidus temperature comes from treating the stainless steel as iron. (The stainless steel is more stable than iron so it is must be less reactive toward the silicon). The most remarkable observation in this figure is the weight loss behaviour during both the heating and cooling cycle. It is clear that weight loss from the sample begins when reaction reaches 1335°C. This temperature is too low for considerable weight loss from the sialon by decomposition processes which mainly occur at temperature over 1600°C. This means that the weight loss is attributed to the nitrogen gas evolution as a reaction product between the matrix and the metal. During the cooling cycle and holding time at temperature of 1350°C for 30 min almost 80% of the weight lost is re-gained by disolving nitrogen gas from the atmosphere into the sample to form silicon nitride crystals at the metal particles. This was not been the case in nickel/sialon system as the solubility of nitrogen in Fe-Si melts is considerably greater.

Separation of the stainless steel phase (similar to that discussed in iron/sialon and nickel/sialon systems) occurred due to the reaction with silicon nitride in the matrix but it is not so apparent at low sintering temperatures. This is because at low temperature there is relatively little silicon disolved into the metal particles. (Even if

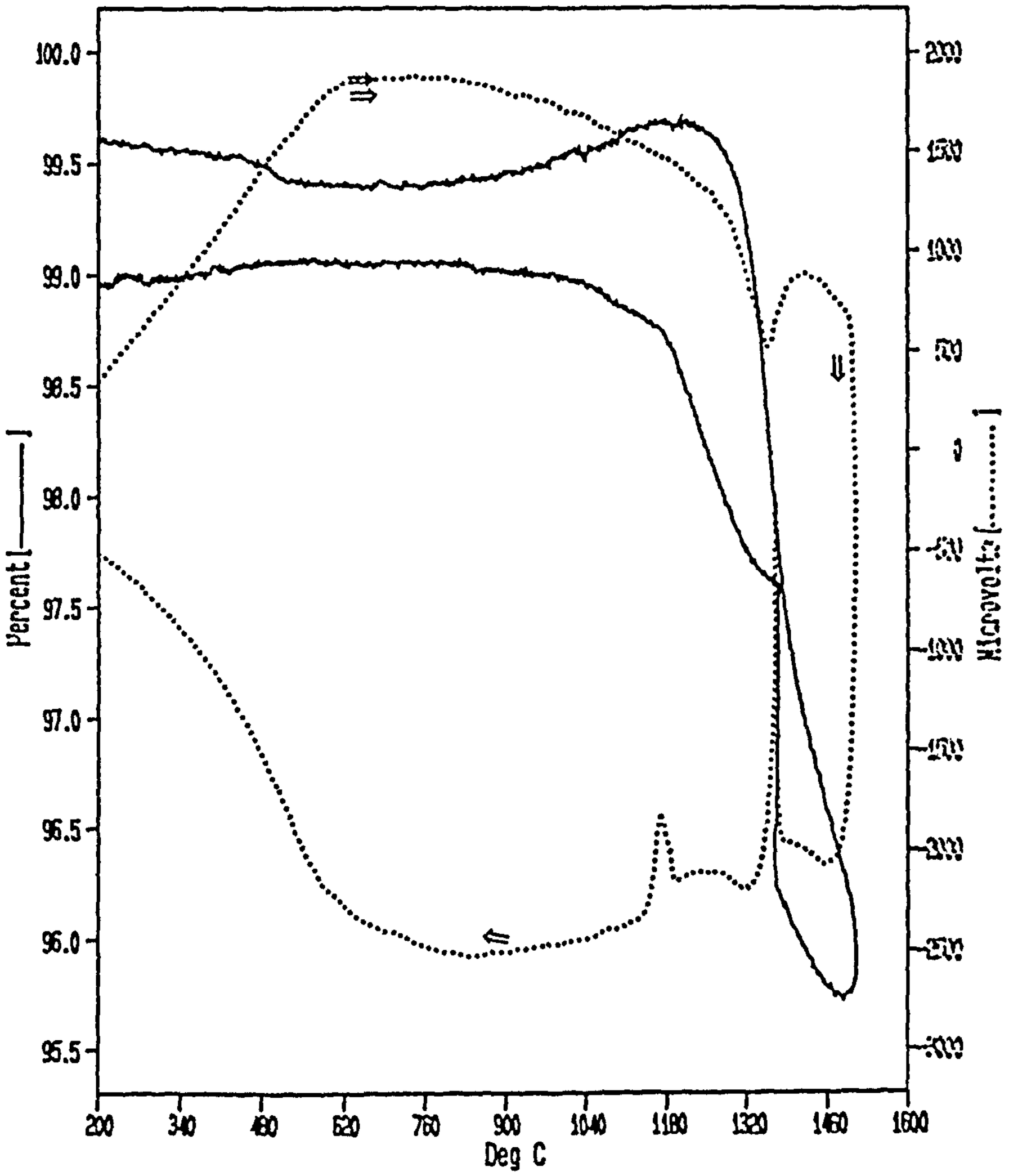

figure 5.10

DTA analysis for 10V% stainless steel/sialon composite.

there is any phase separation it will not be so obvious as one phase will dominate the structure). However, silicon has dissolved in the steel particles forming a silicide phase and this will be discussed later in the two stage sintering cycle.

The X-ray analysis revealed that the matrix behaviour is similar to that discussed in the nickel/sialon system. At this low temperature sintering stage the unreacted silicon nitride phase is dominant in the matrix beside a higher Z value β'-sialon. The Z value,however, depends on the sintering temperature, the higher the temperature the closer the Z value to 0.75. For example the Z value for the sample sintered at 1400°C for 60 hrs is equal to 1.35. Overlapping of the silicide reflecting lines with the matrix lines makes identification of the precise silicide phase impossible. Similar to those formed in the iron/sialon system, these phases are in the cubic system structures.

5.2.3.2 High temperature sintering.

Sintering in which the temperature is equal or greater than 1450°C. High fired density is achieved as can be seen in table (5.6).

Table (5.6)

Pressureless sintering of β'–sialon containing 10V% AISI 316

Temperature (°C)	Time (hr)	Density ($g.cm^{-3}$)	Theoretical %
1450	15	3.54	94.5
1500	3	3.68	98.2

Clearly from this table, density of 95% theoretical has been achieved. The microstructure obtained is shown in figure (5.11) which is an SEM micrograph of a sample sintered at 1500°C for three hours. It can be seen that there are no silicon nitride crystals on steel particles seen in the samples fired at lower temperature and the matrix has densified better than that of examples sintered at lower temperatures.

However, silicon content of the steel particles (shown by the EDAX analysis in figure (5.9.b)) is much greater than that seen in samples sintered at lower temperatures presented in figure (5.9.a). This effect can be explained by calculating the silicon activities using the method shown in equations (5.5) and (5.6) which show that at 1500°C the solubility of silicon in equilibrium with sialon is much higher than that calculated at 1375°C and is equal to 25wt% Si in iron, therefore the corresponding nitrogen solubility is lower. So, there are no silicon nitride crystals in the steel particles.

The X-ray analysis of a drop of liquid metal formed on the surface of the sample shows that the metallic phases present are not related to the unreacted AISI 316 steel reflection and it was not possible to distinguish the reflecting lines of them from those belonging to sialon as they are overlaping. There are at least two silicide phases having cubic structures. However, the matrix phase in samples sintered at 1500°C for three hours is β'-sialon with a Z value (almost = 1) greater than 0.75 and with some residual silicon nitride as the sintering temperature is not high enough to complete the α to β'– phase transformation.

figure 5.11

SEM photograph of a 10V% steel/sialon composite sintered at 1500°C for 3 hrs.

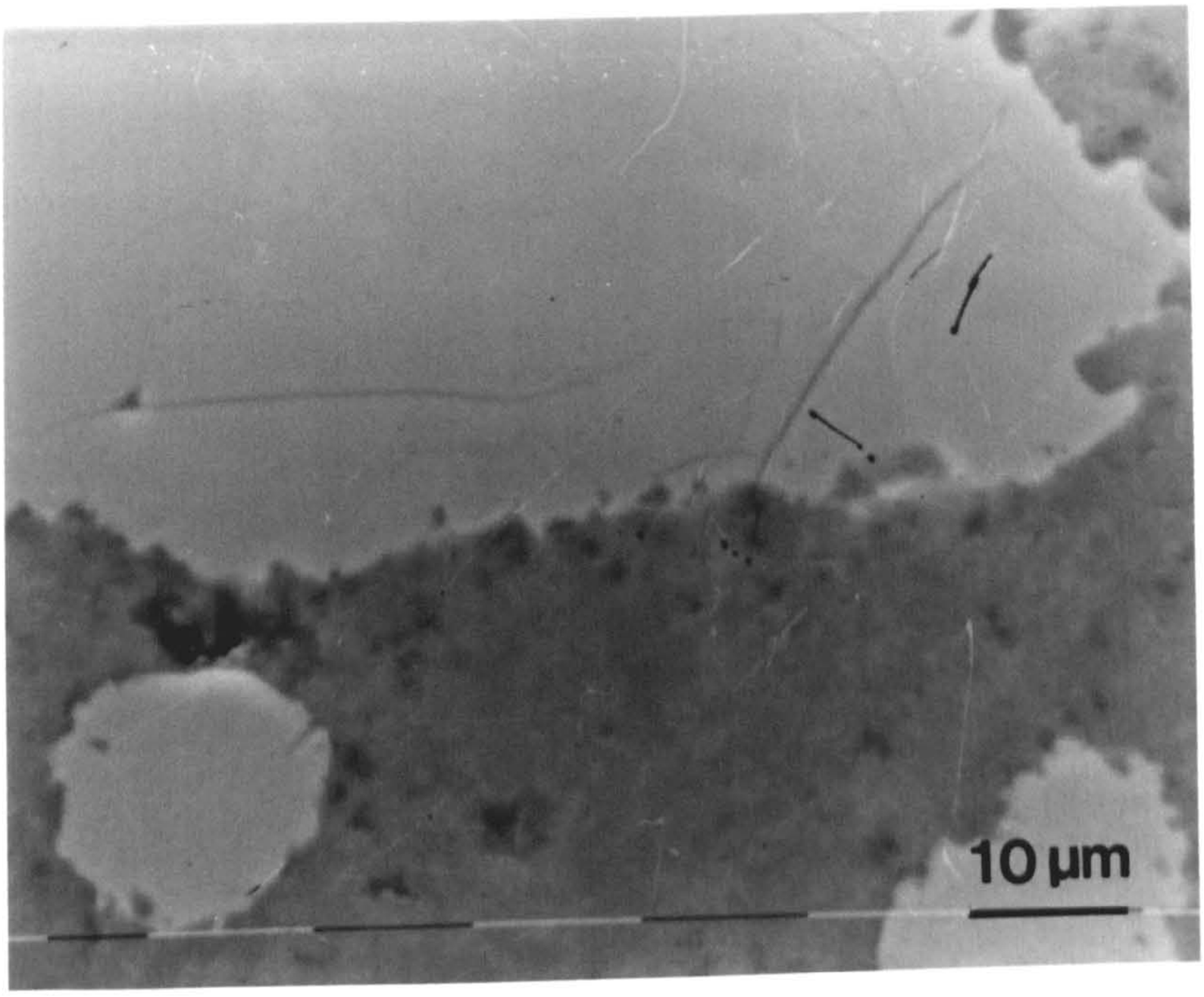
10 µm

5.2.3.3 Two stage sintering.

The silicon content of steel particles, is greater in samples fired at higher temperatures. The silicon content, however, influences the mechanical properties of the composite. Thus, the microstructure produced at low temperature (1375–1400°C) is tougher than that produced at high temperature (1500°C), but the matrix is much less dense in the first case. Combining these observations leads to the conclusion that a two–stage firing cycle would provide the optimum microstructure. The experimental results of the two–stage heat treatment on 10V% stainless steel/sialon composites are given below;

Table (5.7)

Pressureless sintering of β'–sialon containing 10V% AISI 316

Temperature (°C)	Time (hr)	Density ($g.cm^{-3}$)	Theoretical %
1500/1380	3/15	3.68	98.2
1500/1380	1/15	3.54	94.5

In this table it can be seen that density in excess of 98% of the theoretical may be achieved by sintering at 1500°C for a short time this also acts to minimize the decomposition of the sialon through rapid densification of the compacted powder, whilst the lower temperature heat treatment (1380°C) allows precipitation of some of the silicon and nitrogen (dissolved at 1500°C) as silicon nitride. The silicon content in the metal particles is lower than that in those samples fired in one heating cycle as seen in figure (5.9.c)

The microstructure of a specimen sintered in the two–step cycle is shown in the optical photograph, figure (5.12) in which it can be seen that silicon nitride crystals are distributed on the metal/ceramic interface growing on the metal particles. It can be noticed on this photograph that metal/ceramic interface has been affected by the polishing process, as some materials seems to be removed. This frequently occurs around the large particles. This could be due to the stresses created on the interface by the formation of silicon nitride crystals at the second stage of heating , where the rest of the sample is relatively solid. The TEM examination on a pressureless sintered sample via two stage heat treatment shows that the metal particle is surrounded by a layer of silicon nitride grains (figure 5.13.a). Beyond this layer sialon grains can be seen in a very small size. The general TEM examinations shows that some other particles are surrounded by a dark area shown in figure (5.13.b) and having an EDAX analysis presented on figure (5.14). On these figure it can be noticed that the metal/sialon interface is very good and the dark area next to the interface has a composition not related simply to the Si-Al-O-N system. It contains a high concentration of yttrium and is similar to the glass composition. (This could be another reason to explain the removal of the materials from the metal/sialon interface during polishing). Additionally the general EDAX analysis on the matrix shows that the sialon grains have a higher Al/Si ratio than that on the sialon in the carbon fiber/sialon system and for syalon 201 (Z=0.75) as can be seen in figure (5.15). This is due to the decomposition of silicon nitride to react with the metal leaving the matrix relatively richer in aluminium. Moreover the diffraction of the metal particle near to the interface shows that it is an amorphous structure of stainless steel composition containing silicon.

The general optical microscopic examination reveals that the metal particles contain two different colour phases similar to those shown in iron/sialon and

figre 5.12

Optical micrograph of a 10V% steel/sialon composite sintered at 1500°C for 3 hrs and 1380°C for 15 hrs.

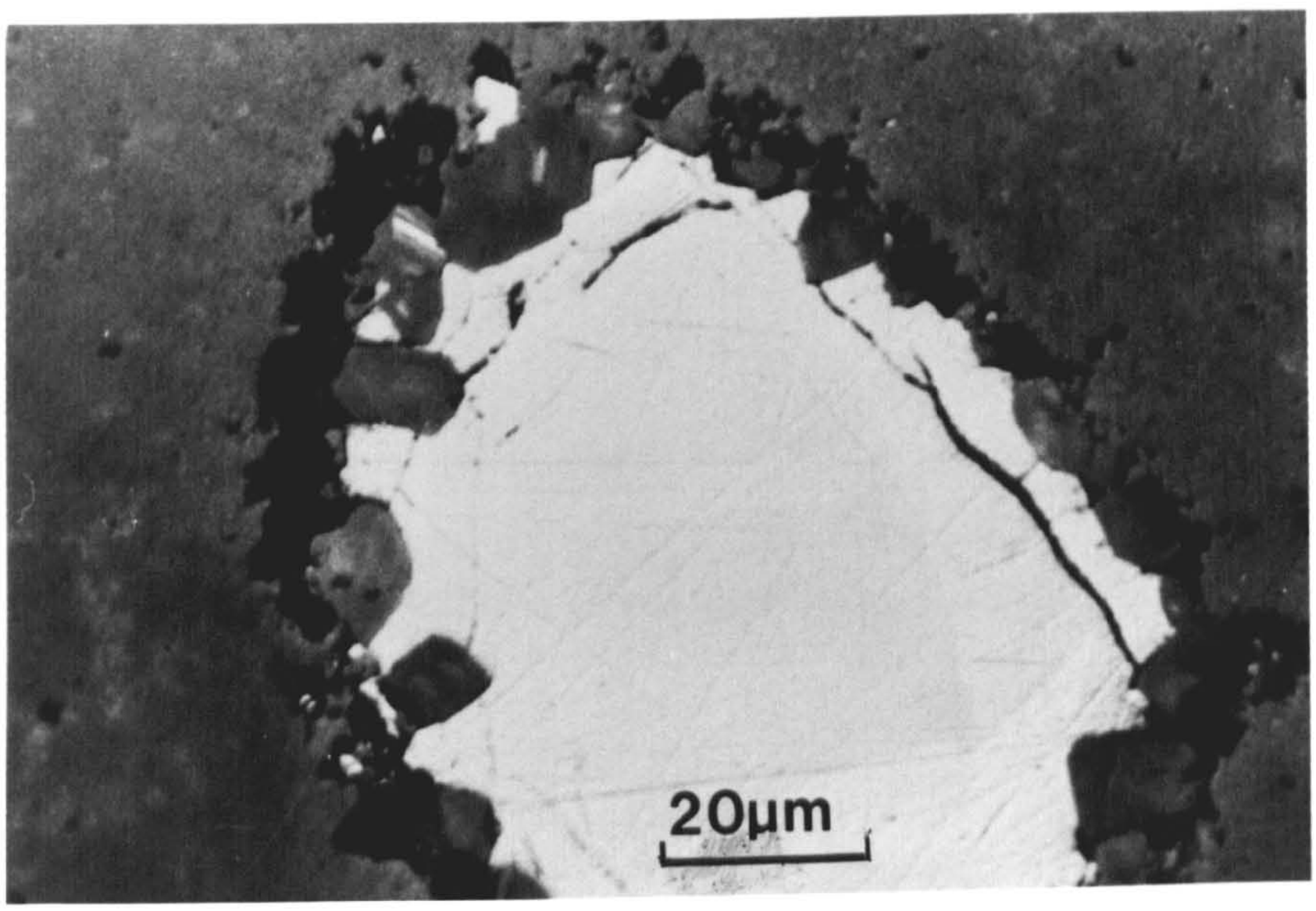
20µm

figure 5.13.a & b

TEM photograph of a 10V% steel/sialon composite sintered by the two-stage heat treatement.

a

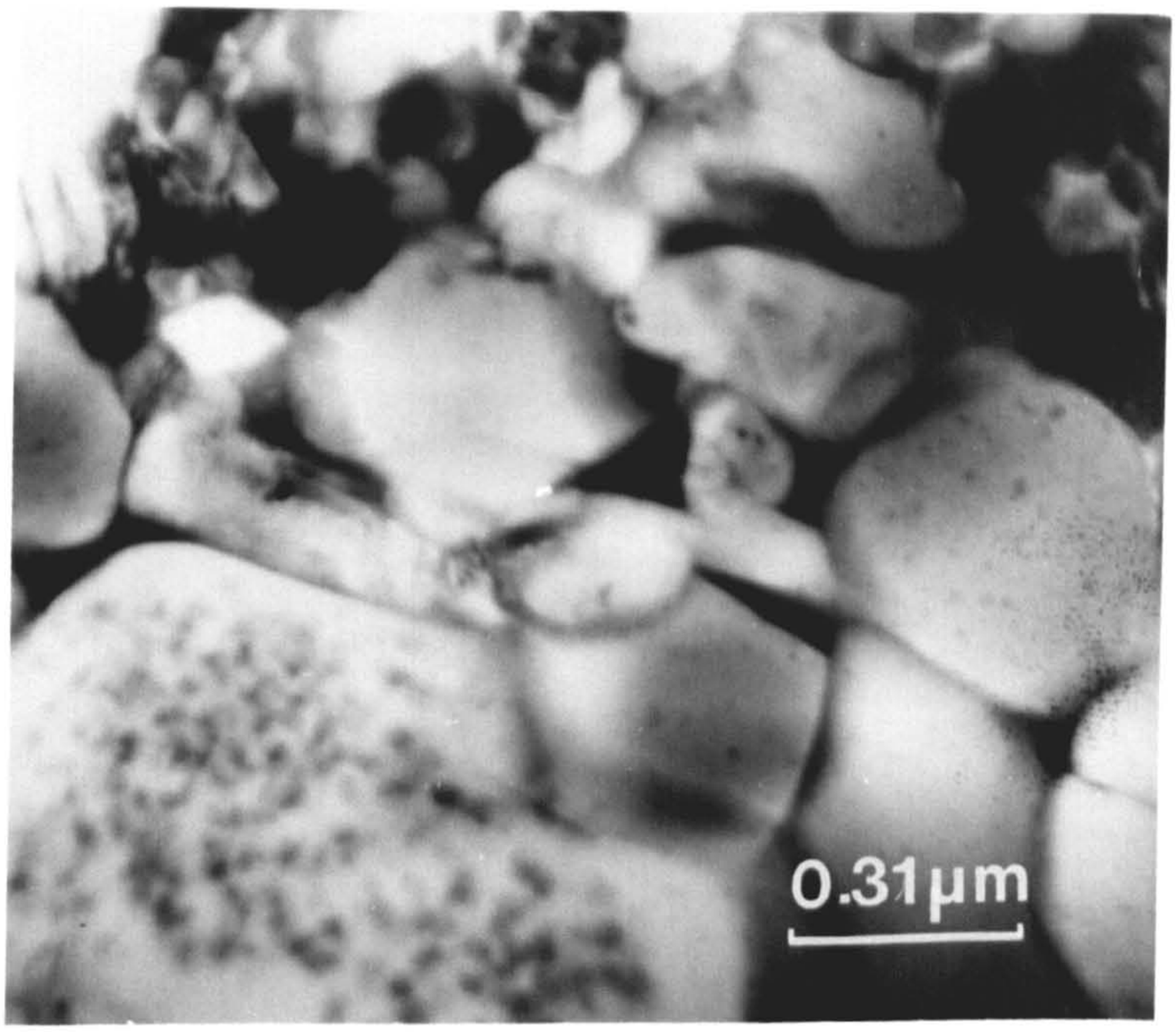

b

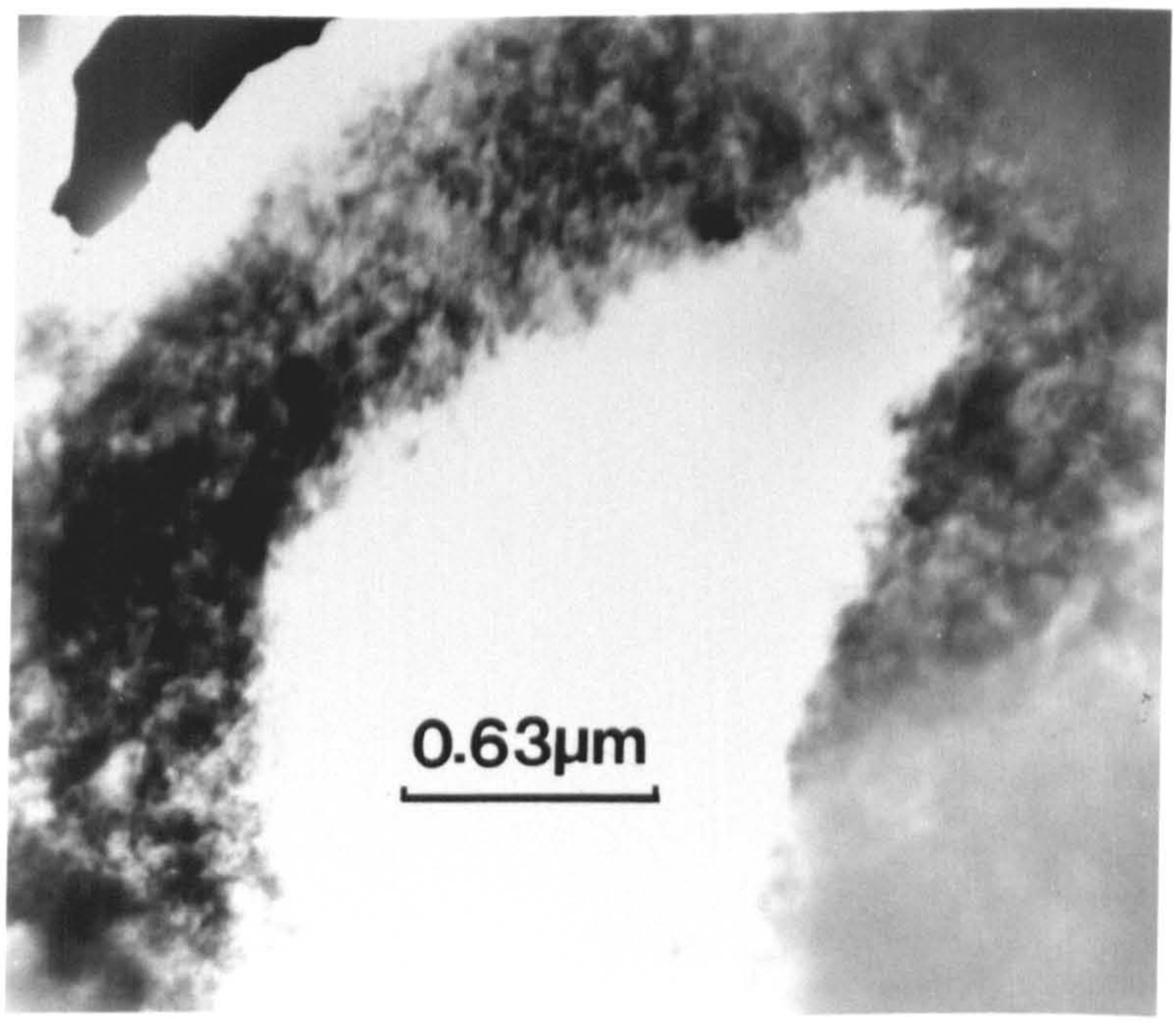

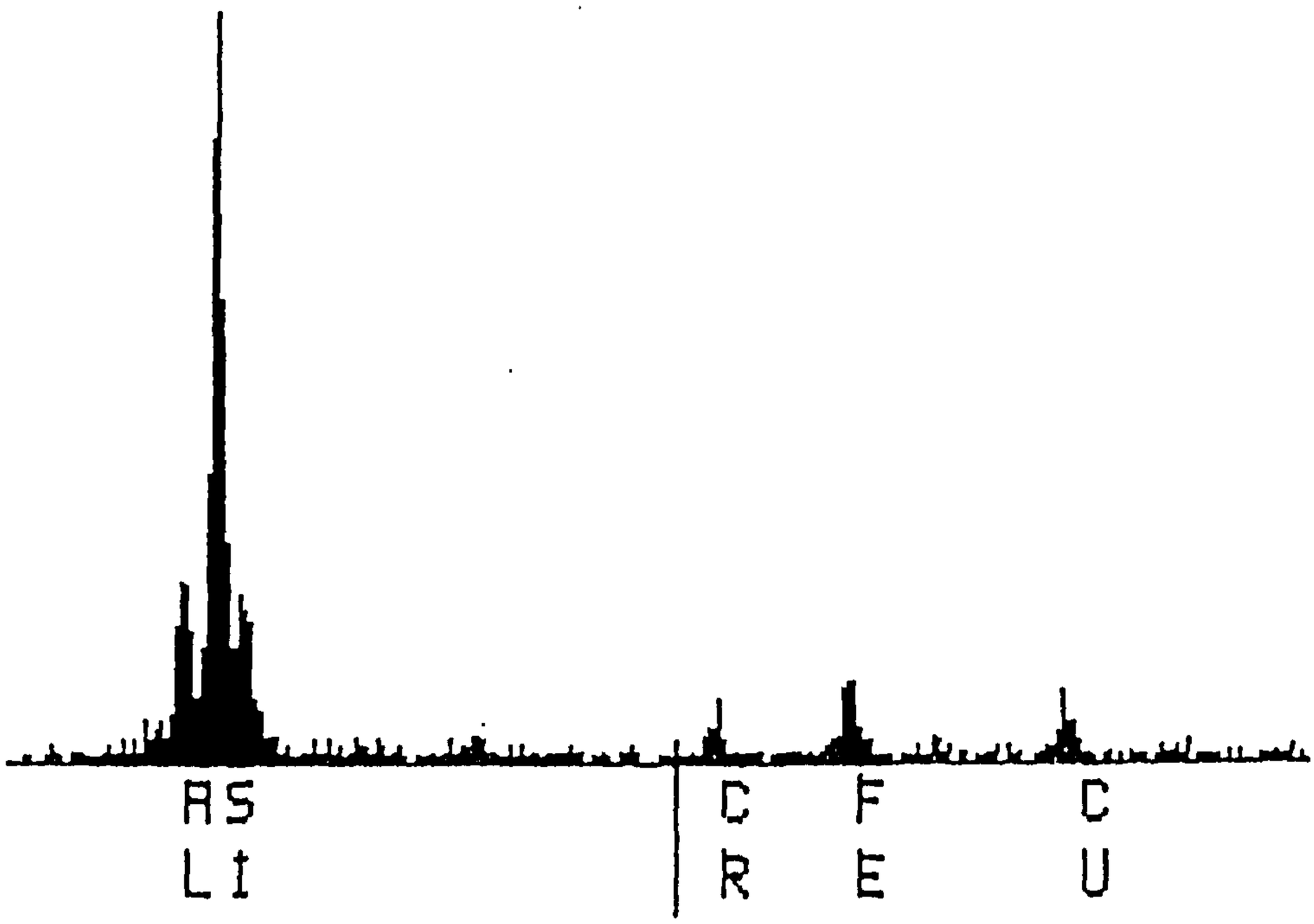

figure 5.14

Schematic representation for the EDAX spectrum for the stainless steel/sialon interface.

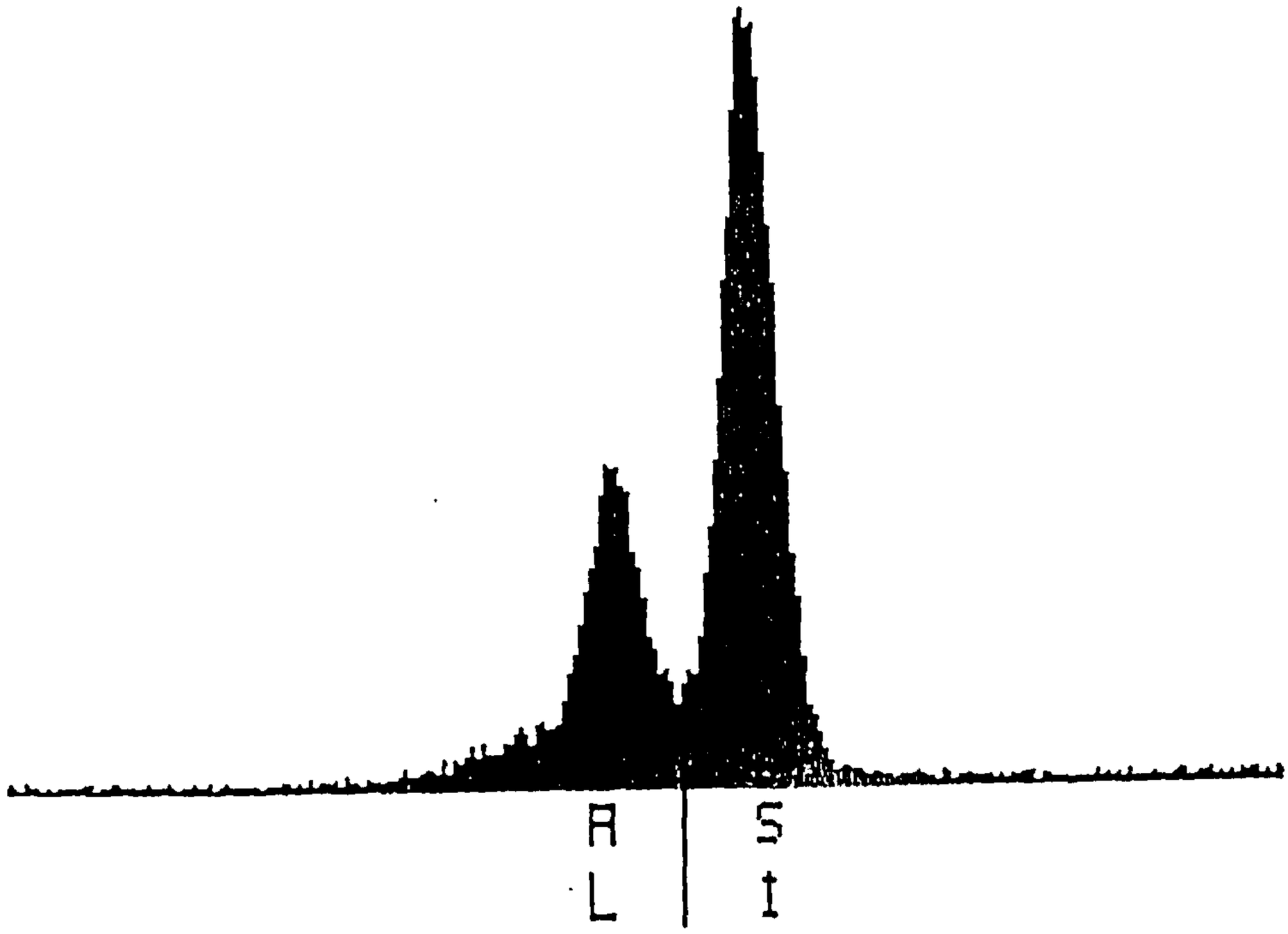

figure 5.15

Schematic representation for the EDAX spectrum for β'-sialon grains.

nickel/sialon systems. The EDAX analysis of these phases are presented in figure (5.16) in which it is clear that the dark phase has higher silicon and chromium and lower nickel than the white phase. However, this phase separation condition is not so dominant in those metal particles containing reprecipitated silicon nitride.

X–ray diffraction studies of samples fired in the two–step cycle show a ceramic microstructure of β'–sialon with Z value slightly greater than that expected (0.75) and some α–Si_3N_4 (which is a combination of unreacted α–Si_3N_4 and the silicon nitride formed on the metal particles). It may therefore be concluded that the reprecipitated silicon nitride in the metal particles is α–Si_3N_4 phase. The formation of silicon nitride crystals, however, is found to be more dominant on the surface of the samples fired via two–stage heat treatment method where there is a sufficient amount of nitrogen available for Si_3N_4 precipitation. At the center of dense samples the Si_3N_4 precipitation is dependent on the amount of nitrogen present within the metal area, whether it is from the matrix, or from the dissolved nitrogen in the metal, during the heating cycle.

5.2.4 Hot pressed stainless steel/sialon composite.

In order to produce specimens of maximum density for microstructural and property evaluation, samples of syalon 201 with 10V% and 20V%AISI 316 powder were hot pressed at a maximum temperature of 1500°C. A uniformly dispersed microstructure was obtained in a theoretically dense sample, as seen in figure (5.17.a) which is an optical micrograph for a hot pressed sample containing 10V% steel sintered at 1500°C. Good adhesion was obtained between the metal and ceramic under the applied pressure of 30 bar on a 20 mm diameter die. The pressure transducer trace for this experiment is shown in figure (5.18) where two important features should be

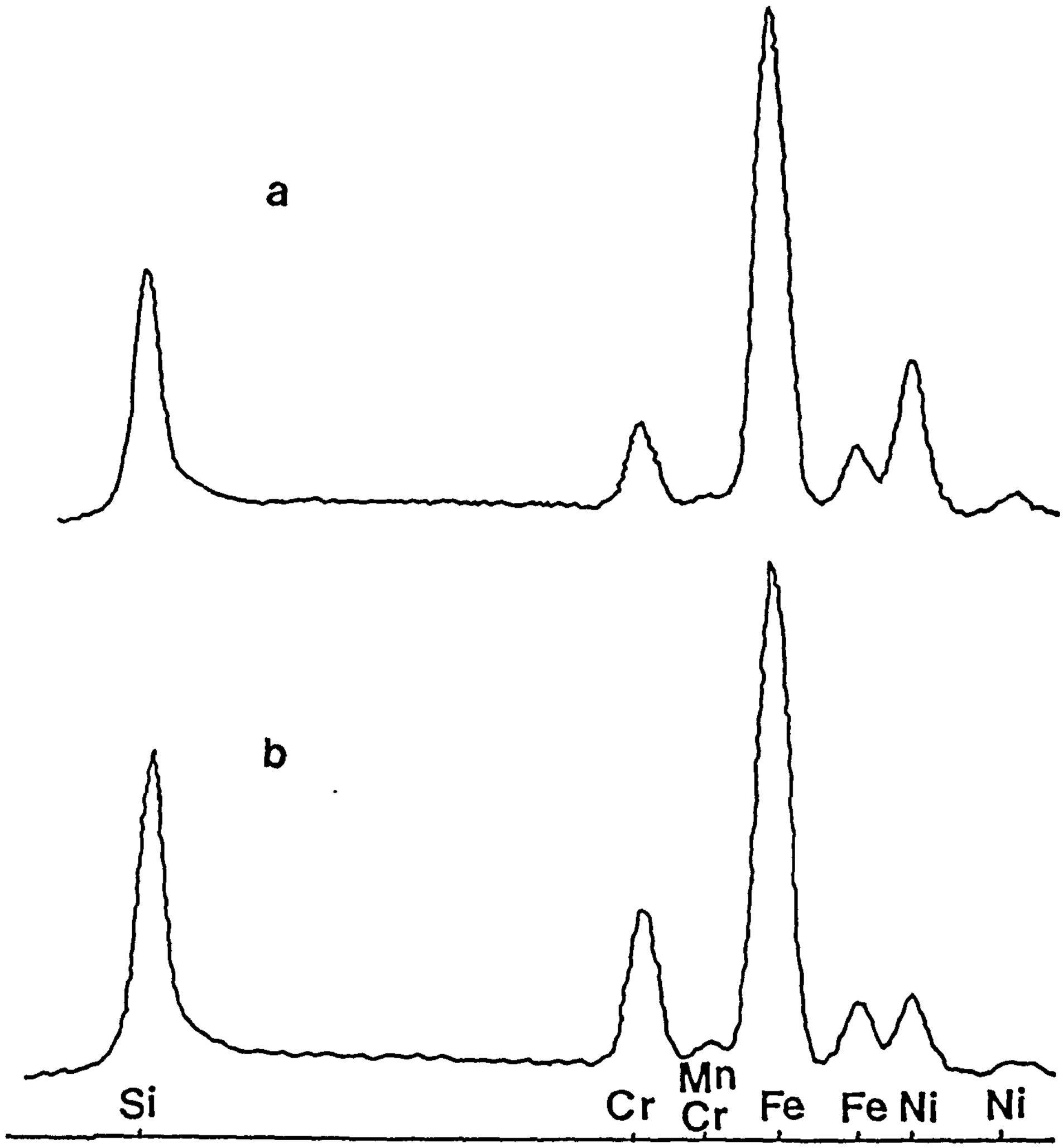

figure 5.16 a & b

Schematic representation for the EDAX spectrum for the white (a) and dark (b) areas in the stainless steel particles.

figure 5.17.a

Optical photograph of 10V% steel/sialon composite hot-pressed at 1500°C for one hour.

figure 5.17.b

As in 5.17.a showing the two phases in the steel particles.

a

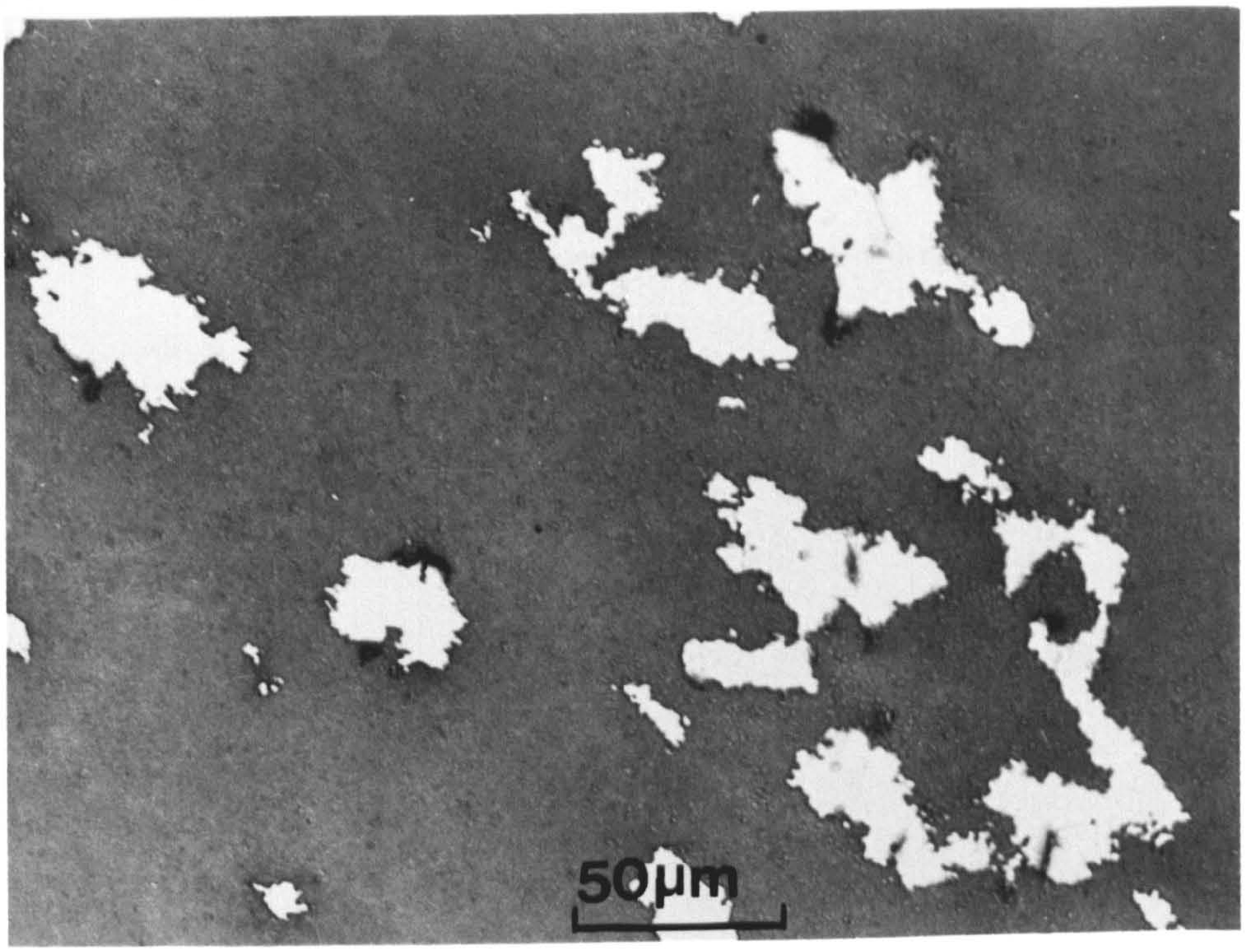

b

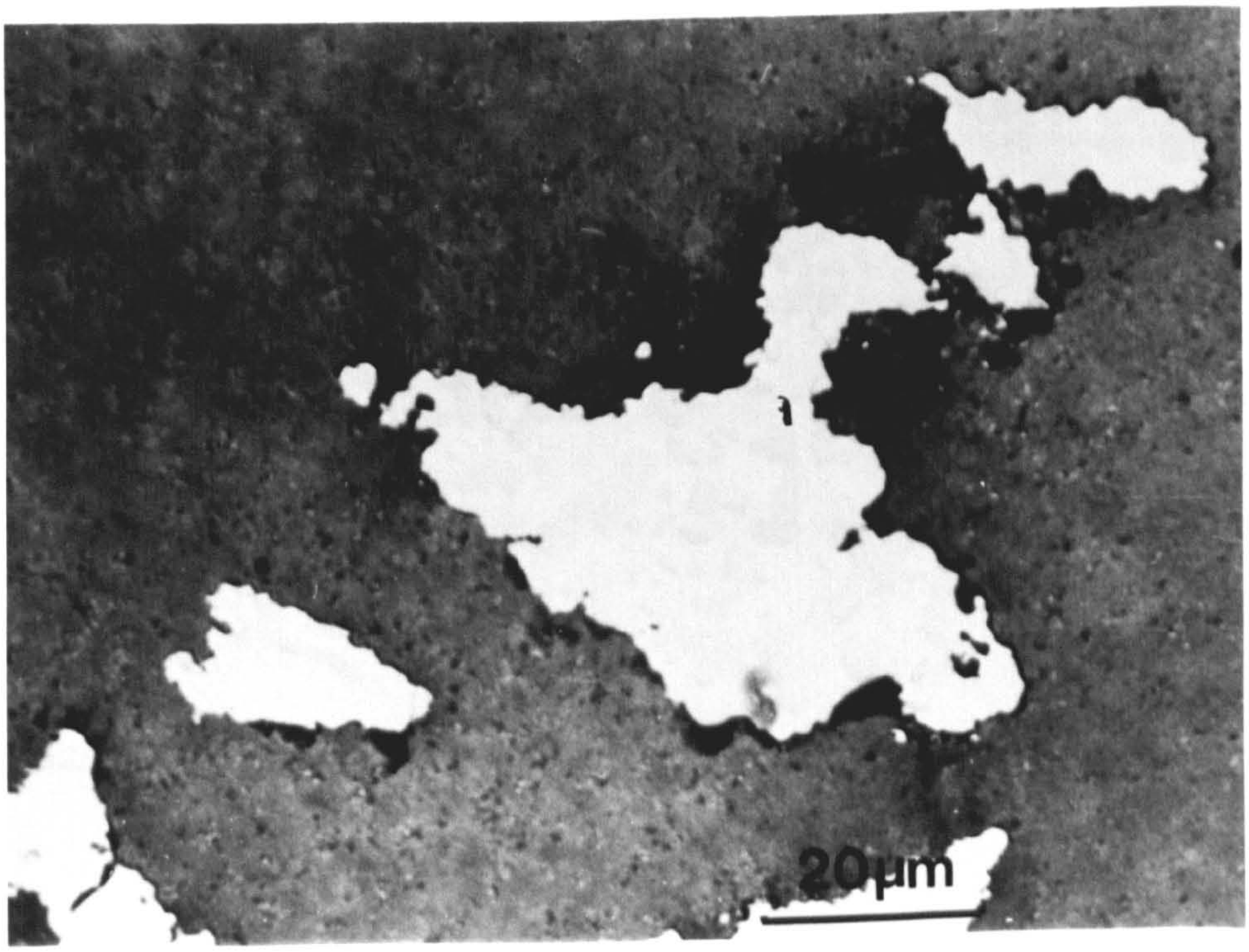

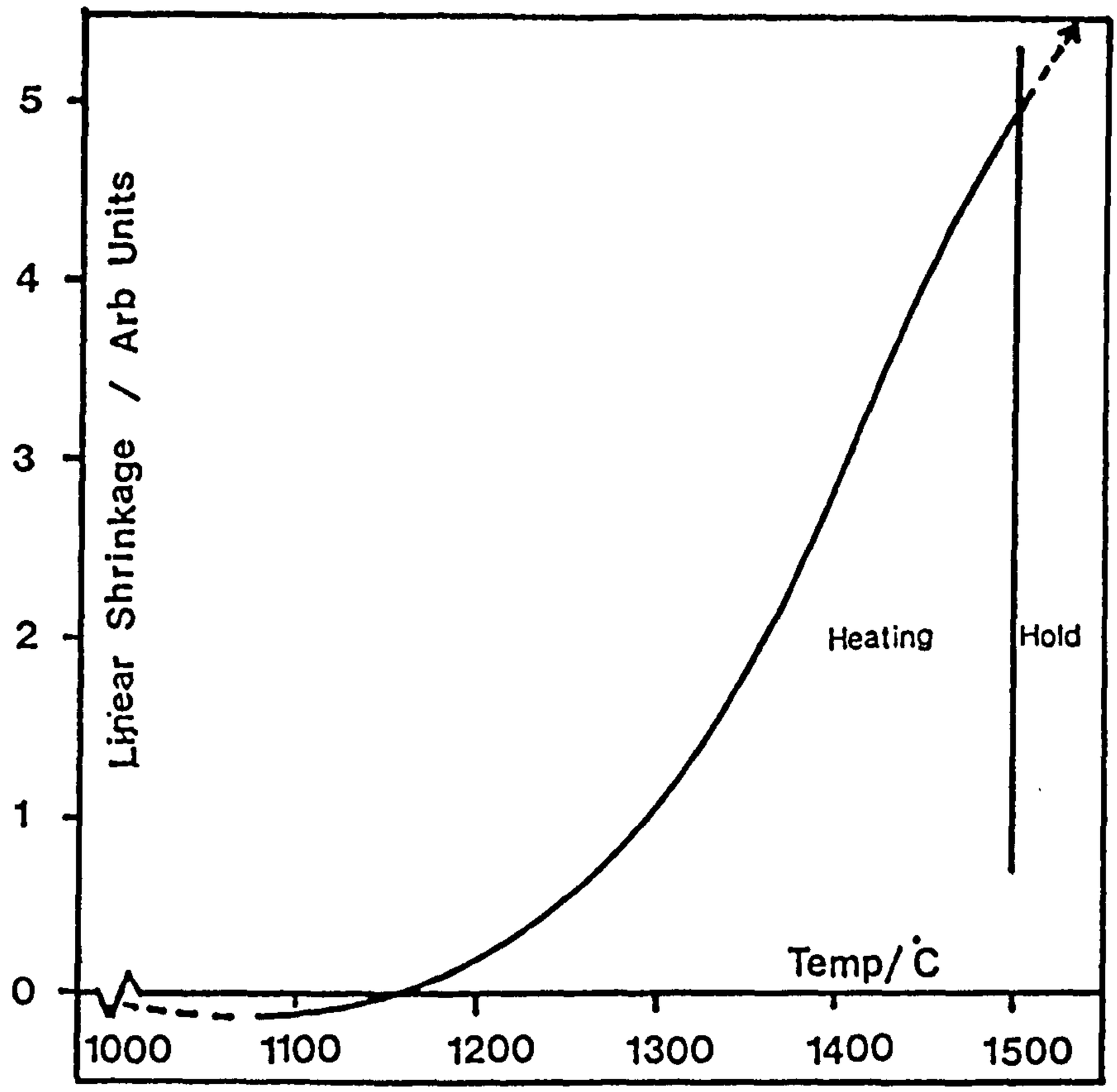

figure 5.18

Pressure transducer trace for hot pressed sialon containing 10V% steel.

noted. Firstly, the onset of densification at below 1200°C and secondly the continued deformation of the specimen at the holding temperature. The lowest liquidus temperature in the syalon 201 system is given as 1350°C [Hampshire & Jack 1981]. However, in the presence of stainless steel particles these temperatures have no significance as shown in figure (5.18). The reason for this low–temperature densification lies in the formation of liquid phase by ceramic/metal reaction as discussed above. Similar to what has been noted in the previous systems, the optical micrograph in figure (5.17.b) indicates that a change in the chemical composition of the metal particles has also occurred and the solidified particles are two–phase whilst AISI 316 is a single–phase austenitic steel. Microprobe analysis confirms that these two phases have a similar element distribution to those shown in figure (5.16).

CHAPTER SIX

CERAMIC/CERAMIC COMPOSITES

6.1 Introduction.

The mechanical properties of monolithic ceramics can be enhanced through the composite approach. One or more component can be added to the matrix to affect the properties thus creating a better material. The most important properties that researchers are seeking to improve is the fracture toughness. Compared with monolithic ceramics, toughened composites exhibit greater fracture toughness and strength. The most important toughening methods are the introduction of platelets, particles, whiskers and fibers to the matrix. Considering the difficulties encountered in its development, the utilization of particles as toughening constituents appears more reliable due to simpler processing. It has been assumed that the crack deflection in particulate composites, which produce tilting and twisting of the advanced crack front, is an effective toughening method. While fracture toughness is an important issue in composite propriety development, others such as hardness, electrical and thermal conductivity ,and wear resistance were given more attention in composite investigations. Development of Al_2O_3–based composites, for example, with addition of TiC particulate , resulted in improved toughness and thermal conductivity [Wahi & Illschner 1980]. Other results on Si_3N_4 /TiC composite indicated that an increase in

fracture toughness can be achieved [Mah et al 1981]. Similar results have been reported in silicon nitride systems using SiC as a disperesd particle. [Buljan et al 1987].

6.2 Results and Discussion.

6.2.1 Weight change on sintering.

Typical weight change behaviour as a function of sintering temperature and time is shown in figure (6.1), where all the experiments were carried out for one or three hours in sialon containing 30V%TiN powder. The weight change, which is due to the volatilization of silicon monoxide gas from the sample, increases slightly with temperature but not to such extent as to affect the final sample density. Sintering time at temperature also influences the weight change. This is presented in figure (6.1) in which it can be seen that a sample sintered at any temperature for three hours has a greater weight loss than that fired for one hour. As the temperature increases, longer sintering time means more weight loss since the powder bed becomes less effective. This is exemplified by a sample densified at 1600°C for three hours and that sintered for one hour..

6.2.2 Density change on sintering.

Density changes on sintering have been investigated on a TiN/sialon composite with different TiN volume fractions. The observed densities are found to vary with sintering temperature. The density increases with increasing temperature up to almost theoretical density at 1600°C for mixtures containing both 10V%TiN and 20V%TiN before decreasing slightly at 1700°C as shown on figure (6.2). This reduction in density at 1700°C is attributed to the continous volatilization of silicon monoxide gas from the surface of the sample especially at high temperature. For the mixture contaning 30V%TiN, the maximum density achieved is 97% of the theoretical when

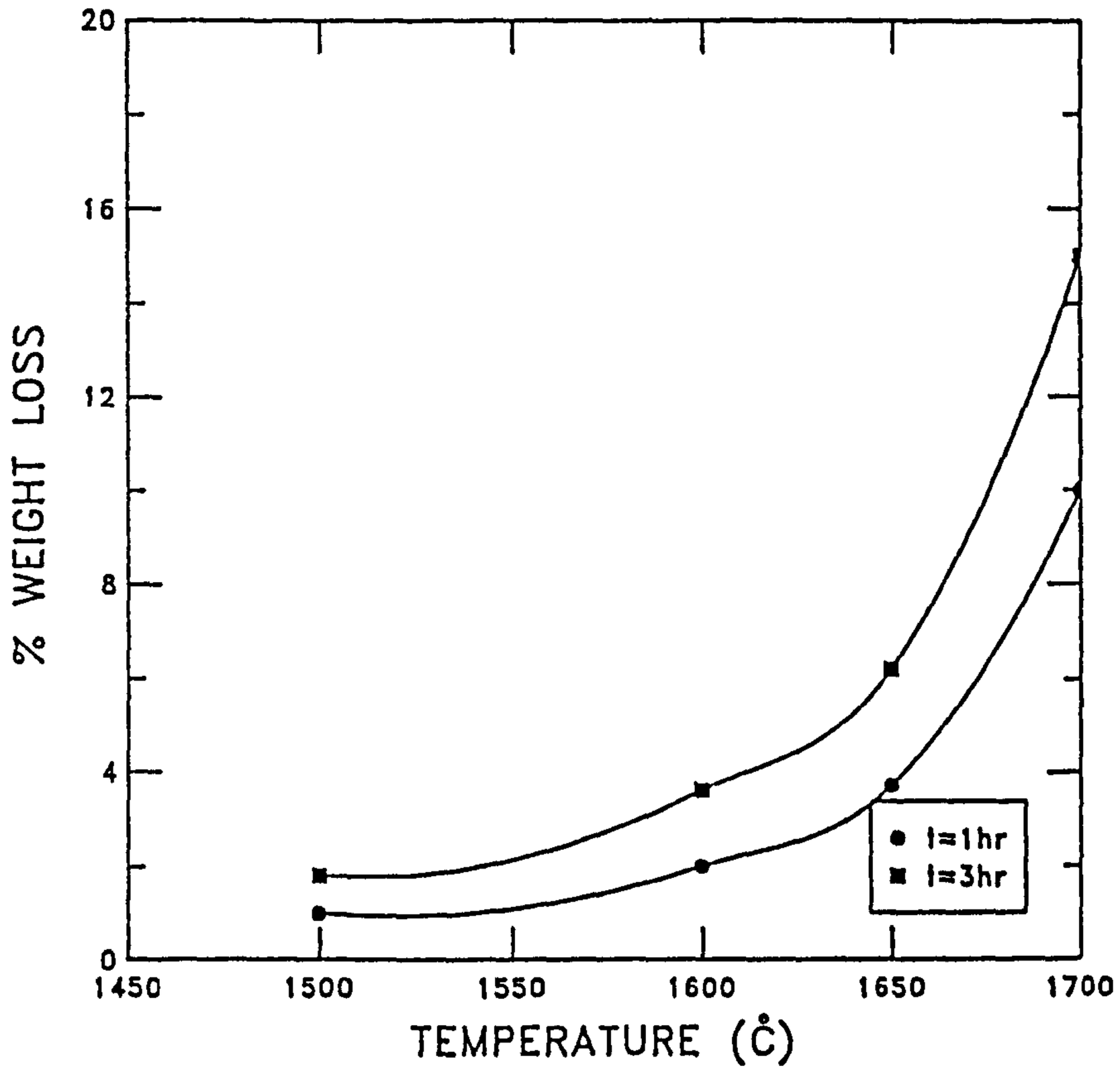

figure 6.1

The influence of sintering time and temperature on the weight loss from pressurless sintered 30V%TiN/sialon composite.

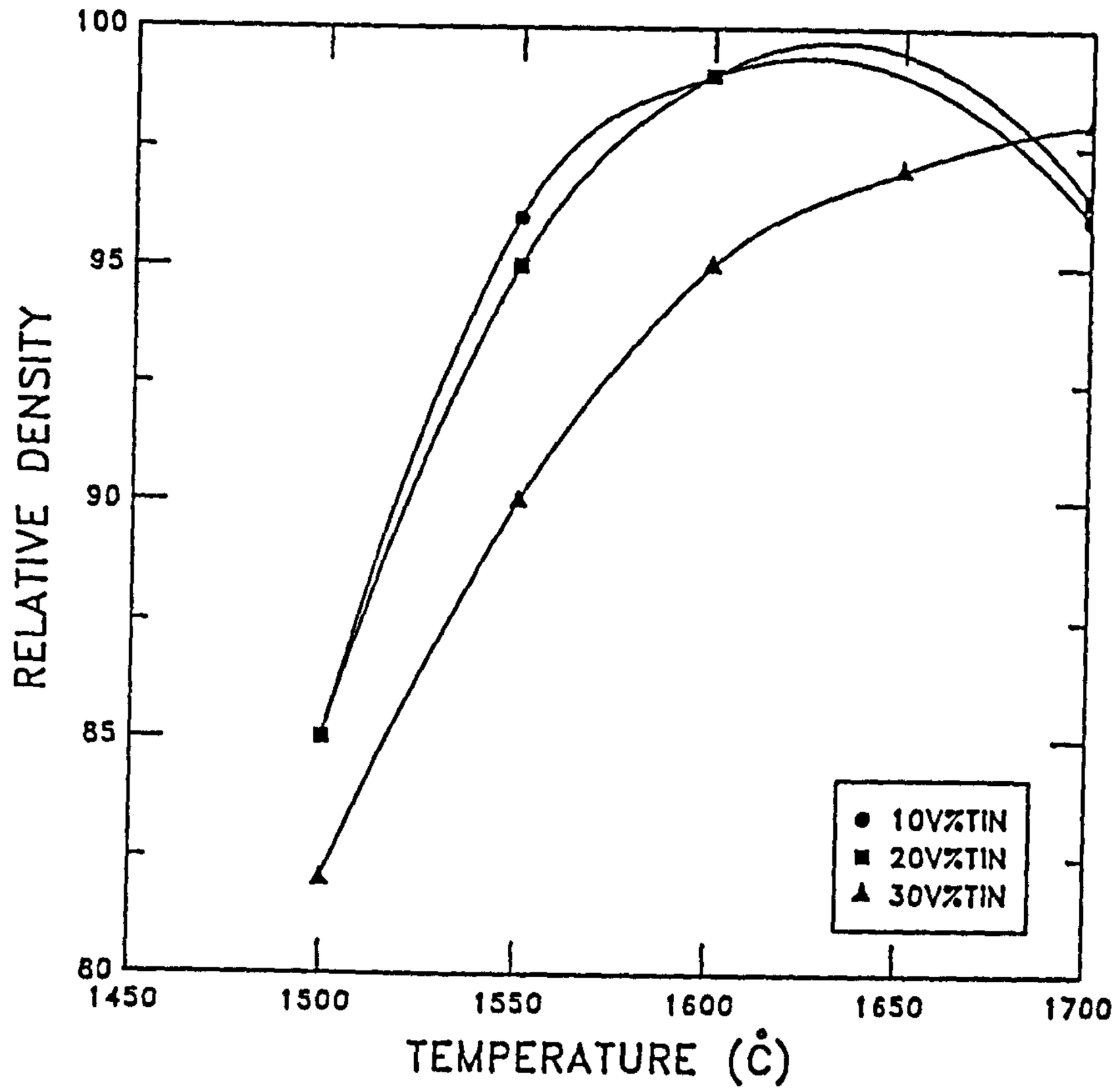

figure 6.2

The influence of temperature and TiN volume fraction on the sintered sample density in TiN/sialon composite.

sintered at 1700°C for one hour, as shown on figure (6.2). In this figure it could also be noticed that the maximum densities and the slope of the temperature–density curve for the mixtures containing 10V%TiN and 20V%TiN are identical. The densification rate of the sialon reinforced with 30V%TiN is slightly lower than the previous two mixtures.

However, there was no observed chemical incompatibility between the TiN and the sialon during pressureless sintering at any compositions or temperature. An optical micrograph of the sample containing 30V%TiN is presented in figure (6.3.a) where a good interface between the matrix and the TiN is observed.

6.2.3 Phases change on sintering.

The X–ray powder diffraction analyses on TiN/sialon composites indicates that there are always two phases present; β'–sialon with a correct Z value and lines for a cubic structure which is close to the published data for TiN. No reaction between the sialon and the TiN is detected and a clean interface can be noticed on the TEM micrograph presented on figure (6.3.b). The general TEM analysis shows that the matrix has a uniform structure of β'–sialon with no residual silicon nitride and the Al/Si ratio on the sialon grains is what it should be for syalon 201 as shown in figure (6.4) which is less than Al/Si ratio in both metal/sialon and carbon fiber/sialon composites.

figure 6.3.a

Optical photograph for a 30V%TiN/sialon sample sintered at 1700°C for one hour.

figure 6.3.b

TEM photograph for 10V%TiN /sialon composite sintered at 1600°C for 3 hrs.

a

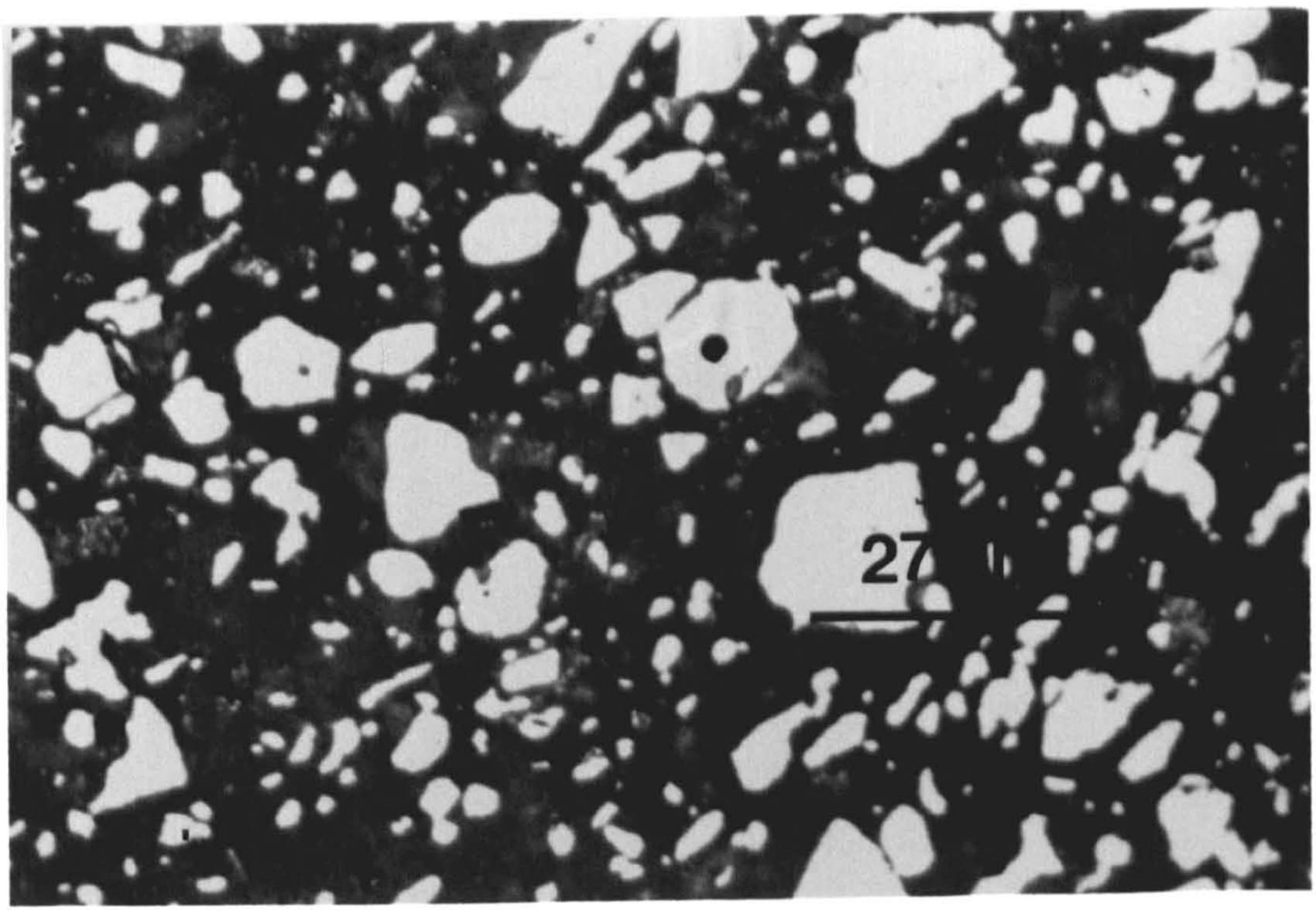

b

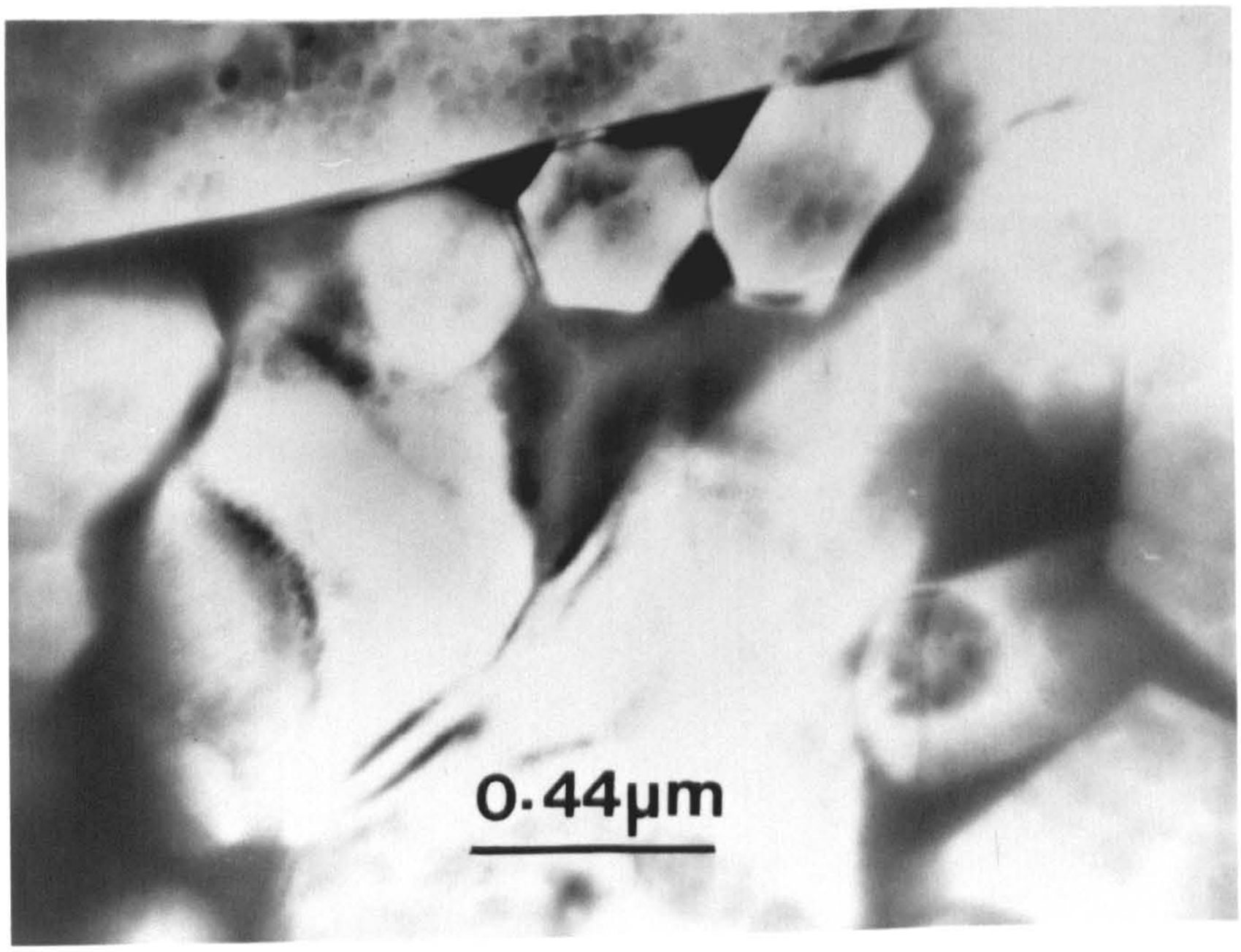

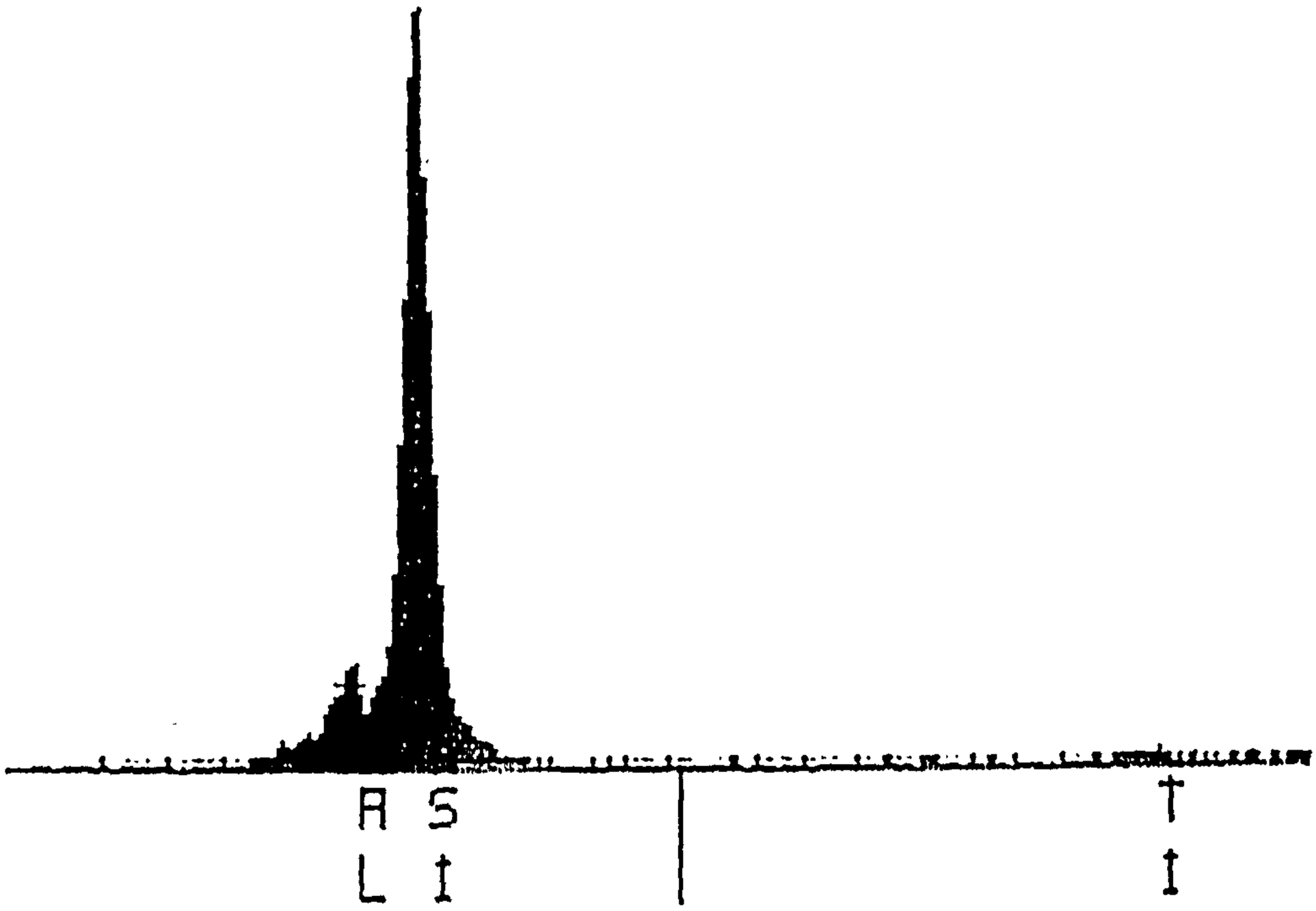

figure 6.4

Schematic representation for the EDAX spectrum for β'-sialon grains in TiN/sialon sample

CHAPTER SEVEN

MECHANICAL PROPERTIES

7.1 Hardness.

The indentation method of hardness measurement, based on point measurement of deformation developed by Vickers, is used to evaluate hardness in the present investigation. The method consist of driving a tetrahedral pyramid with a dihedral angle $2\psi = 136°$ into a flat and smooth sample under a certain pressure perpendicular to the surface and then measuring the diagonal of the indent obtained. Vicker hardness which is the ratio of load to lateral surface of indent is given by ;

$$Hv = 1.8544 \ .P \ /D^2 \quad .....(7.1)$$

where **P** is the load in **Kg** and **D** is the mean indent diameter in **mm.**

7.2.Fracture Toughness.

Fracture toughness has become established as an effective method of evaluating the strain of ceramics materials, by measuring the critical stress intensity factor Kc. There are a number of different fracture toughness test methods which use

different specimen configurations. It is generally accepted that different tests may result in slightly different **Kc** values. The advantage of the indentation fracture toughness method is that it is independent of the specimen geometry and only a small specimen is required to carry out the measurement.

The indentation fracture toughness method was first suggested by the work of Palmqvist who used it to study the fracture of hard–metals and Wiederhorn [1973] later suggested that this method had application to fracture toughness of glass materials. Further development was done by Evans & Charles [1976] and the technique has been subsequently evaluated and a theoretical basis for the procedure established by Lawn & Swain [1975], Anstis et al [1981] and Marshall [1983]

The method involves indentation with a Vickers indenter into a smooth polished surface. A load is selected to cause the indent to occur with readily observable fracture at the four corners of the diamond pyramid indentation.

In principle, the indentation method requires measurement of the size of the crack formed around the indent at loads in excess of the critical load, which is required to initiate the crack around the indent. After measuring the indentation radius, the crack length and the load we can use several expression to obtain the **Kc** value.

Crack profiles formed by indentation were classified into two types MEDIAN and PALMQVIST types according to which different methods for evaluating fracture toughness were suggested.

7.2.1 Median crack type.

On this type, as in figure (7.1), the earlier work of Lawn & Swain [1975] shows that the fracture toughness **Kc** for penny shaped cracks (with **c** the crack radius) in a homogeneous stress field could be derived from the assumption that the

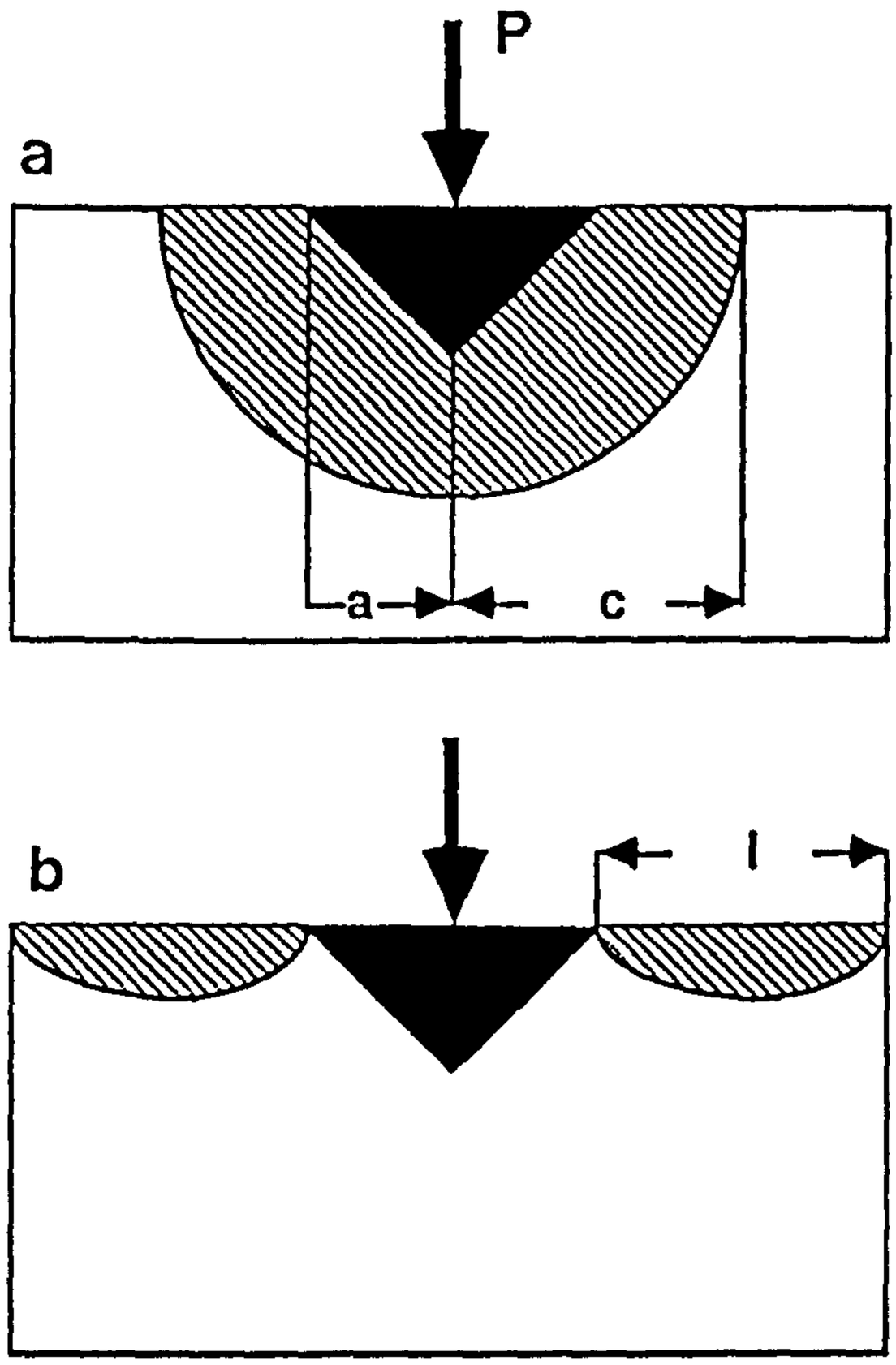

figure 7.1

Schematic representation of the crack types which occur by the indentation technique in brittle materials (a) Median (b) Palmqvist..

(Kc) for a penny–configuration crack is simply ($\sqrt{2}/\pi$) times that for a straight-fronted crack shape (with **c** crack length) which has an identifiable solution. The indentation method to calculate **Kc** is according to the following equation;

$$Kc=[(1-2\ \nu)/2^{1/2}\pi^{5/2}\beta\ ]\ [P/a\ (D)^{1/2}].....(7.2)$$

where;

Kc= the critical stress intensity factor for indentation fracture.

P = the applied load

D = the median crack depth

ν = Poissons' ratio

a = the indentation half diagonal length.

β = is a dimensionless factor determined by zone geometry as

= the ratio of depth / half diagonal of deformation zone. The typical value for β =2.

Equation (7.2) can be rewritten as;

$$Kc=\ 0.0202\ (1-2\ \nu)\ P/a\ c^{1/2}.....(7.3)$$

Equation (7.3) is only valid for $D \geq 2a$ and because for a median crack then **D = c**. However, work continue to establish more applicable formulae to evaluate the Kc and involving more parameters related to crack propagation such as the geometry of the indenter and the friction between the indenter and the material. In 1975 Lawn & Fuller derived an equation to calculate **Kc**. This equation is derived from the treatment of the indentation fracture having basically a single well-defined penny–like crack without involving the lateral crack which forms upon unloading. In this case again the equation below is valid for $D \geq 2a$.

$$Kc = (1/\pi^{3/2} \tan \phi)(P/D^{3/2}) \ldots\ldots\ldots\ldots (7.4)$$

where;

$\phi = \theta + \arctan \mu$

θ = the indenter cone half angle

μ = the coefficient of sliding friction between the indenter and the material

For $\mu = 0$, $\theta = 68°$ (Vickers indenter half angle) and **D=c** equation (7.4) can be rewritten as;

$$Kc = 0.07255\ P\ /\ c^{3/2} \ \ldots\ldots\ldots\ldots (7.5)$$

[Notice that the constant value (0.07255) is not the same as in Lawn & Fuller (0.0515) because the Vicker's indenter half angle is taken 68° rather than 74°]

Based on the analyses of the elastic - plastic zone created by the sharp indenter Evans & Wilshaw [1976] put another equation to find the **Kc** value in a median crack type as;

$$Kc = Sy\ a^{1/2}\ F1(c/a)\ F2(Ry/a)\ F3\ (\nu)\ F4\ (\mu) \ldots (7.6)$$

where;

Sy = the uniaxial yield stress, given by

$$Sy = H\ /\ \phi$$

H = is the mean contact or indentation pressure exerted by the Vicker indenter and given by;

$$H = P/2a^2$$

ϕ = a constraint factor given by

$\phi = f(E/Sy, \nu)$ and taken ≈ 3

Ry = the indentation plastic zone

F1, F2, F3, F4, = are empirical functions and they assumed that F2, F3, F4 are constant.

Then;

$$Kc\ \phi\ /H\ (a^{1/2})\ \alpha\ F1(c/a)$$

By plotting this relation they find that the crack can be described over a range $0.6 \leq (c/a) \leq 5$ according to the following equation;

$$Kc\ \phi\ /H\ (a^{1/2}) = 4.5\ \log(4.5a/c).....(7.7)$$

substituting for H by;

$$H = P/2a^2$$

therefore;

$$Kc = 0.78\ (P/(a^{3/2}))(\log\ (4.5a/c)).....(7.8)$$

Evans & Charles [1976] have examined the previous assumption already made in solution of equation (7.6) about F2, F3 and F4 by using materials with a wide range of hardness (the primary parameter affecting Ry), toughness and value of Poison's ratio. By inspection of the ($Kc\ \phi\ /H\ (a^{1/2})$) and c/a relation they found that F2 in equation (7.6) should have some influence because of the hardness dependence on c/a

which was due to (Ry/a) increasing with decreasing hardness. They characterized F2 in terms of hardness as;

$$F2 = (H/E\phi)^{0.4}$$

then equation (7.6) becomes

$$(Kc\ \phi\ /H\ (a^{1/2}))(H/E\phi)^{0.4} = (c/a)$$

According to this more general approach the slope of the fracture was then corrected for the dependence on (H/E ϕ) and is found to be almost exactly (-3/2) which is the same slope obtained for a penny-shape crack wedged by a force (P) at its center with a general solution of;

$$Kc = 2\ Pp/(\pi c)^{3/2}$$

$$Pp = P/2\ \tan 68$$

taking;

$$Hv = 0.4636\ P/a^2$$

and $\phi = 2.7$

The final equation they find then is;

$$Kc\ \phi\ /Hv\ (a^{1/2}) = 0.211k\ (c/a)^{-3/2} \quad \ldots\ldots\ldots (7.9)$$

where ;

Hv = vicker hardness

and k is the correction factor taken as 3.2.

Then equation (7.7) could be written as;

$$Kc = 0.116\ P/(c)^{3/2} \quad \text{.....(7.10)}$$

[Notice the constant (0.116) is different than that in Evans & Charles (0.0824) as the Vicker's indenter half angle is taken 68° rather than 74°]

The elastic plastic model of indentation fracture produced by a sharp indenter was modified further by Lawn et al [1980] in which they resolved the elastic -plastic stress under the indenter into

A- Residual stress component characterized by a residual stress intensity factor of the form given by Lawn & Fuller [1975] as;

$$K_r = Xr\ P/c^{3/2}$$

where Xr is a constant depending on the ratio of Young's modulus to the hardness (E/H) to the one-half power as;

$$X_r = \$\ (E/H)^{1/2}\ (\cot\psi)$$

$ = is a materials independent constant for production of a radial crack

B- Elastic component characterized by

$$K_e = c_e\ P/c^{3/2}$$

with c_e is a dimensionless indenter/specimen constant

From the condition of equilibrium in which ($Kc = K_e + K_r$) and for c>>a Lawn et al [1980] derived the following crack extension equation;

$$c = \Delta r \ (\cot\psi)^{3/2}[(E/H)^{1/2})/Kc]^{3/2} \ P^{3/2} \ldots\ldots (7.11)$$

where **c** is the equilibrium surface radial crack length after unloading, **Δr** is a dimensionless constant independent of the indenter-specimen and is found to be equal to (0.032), and ψ is the indenter half angle (68°) then equation (7.11) becomes ;

$$Kc = 0.00231 \ (E/H)^{1/2}P/(c)^{3/2} \ldots\ldots\ldots (7.12)$$

Using the expression of Evans & Charles [1976], Liang et al [1990] find that in plotting log-log of $(Kc\ \phi\ /H\ (a^{1/2})(H/E\ \phi\ )^{0.4}$ against (c/a) for all materials they used the slope of these curves are a function of (c/a) fitted with a parameter equal to [(c/18a) - 1.51] which is value close to -3/2 obtained by Evans & Charles . Moreover Liang et al studied the effect of Poisson's ratio and they concluded that it has an effect on calculating the Kc, and F3(ν) in equation (7.6) is given by;

$$F3(\nu) = 1/ \ \{14[1-8(4\ \nu - \ 0.5)/(1+\nu)^4]\}$$

The final equation Liang et al proposed based on Evans & Charles equation is given as;

$$(Kc\ \phi\ /H\ (a^{1/2})(H/E\phi\ )^{0.4}\ \alpha = \ (c/a)^{((c/18a)\ -\ 1.51)} \ \ldots\ldots (7.13)$$

where;

$$\alpha = 14 \{1 - 8[(4\nu - 0.5)/ (1+\nu)]^4\}$$

For a crack system subjected to a mechanical equilibrium and radial crack both during and after the contact event (applied for materials having a broad range of toughness) Anstis et al [1981] obtained basically the same equation given by Lawn et al [1980] with a different calibration constant ;

$$Kc = (0.016 \pm 0.004) (E/H)^{1/2} P/c^{3/2} \ldots\ldots\ldots (7.14)$$

Niihara et al [1982] plotted fracture data for a number of brittle materials (according to the equation given by Evans & Charles) in terms of $[(Kc\ \phi /H (a^{1/2})(H/E\ \phi)^{0.4}]$ against (l/a) or (c/a) from which it appears that the normalizing parameter $(H/E\ \phi)^{0.4}$ proposed by Evans & Charles for a median crack is appropriate for Plamqvist crack as well. For median crack ($c/a \geq 2.5$) the corresponding expression is ;

$$(Kc\ \phi /Hv\ a^{1/2})(Hv/E\ \phi)^{0.4} = 0.129\ (c/a)^{-3/2} \ldots (7.15)$$

Lankford [1982] claimed that using equation (7.13) in predicting Kc would involve an error of no more than 35% . This error can be reduced by using a best fit curve through his results and those results obtained by Evans & Charles. This modified version of Evans & Charles relationship is expressed by;

$$Kc\ \phi /Hv\ a^{1/2})(Hv/E\ \phi)^{0.4} = 0.142\ (c/a)^{-1.56} \ldots (7.16)$$

7.2.2 Plamqvist crack type

Plamqvist [1962] suggested first that the average length of the crack (l) emanating from the corners of the Vickers indent might be a measurement of the relative toughness at low loads. The crack system (,Palmqvist,) however has been found at low **c/a** values to be such that cracks begin only at the end of the diagonals of the indentation as illustrated in figure (7.1) . Niihara et al [1982] found that in WC/Co alloys at lower values of **c/a** the crack has geometry of Palmqvist rather than median. Then they evaluated the fracture by **(l/a)** for Plamqvist crack rather than **(c/a)** for median crack and Niihara et al found that for this type of crack **($0.25 \leq l/a < 2.5$)** the data can be described by the formula proposed by Evans & Charles for median crack with the best fitting given below;

$$Kc\ \phi\ /Hv\ a^{1/2})(Hv/E\phi)^{0.4} = 0.35\ (l/a)^{-1/2} \ldots (7.17)$$

Alternatively Niihara [1983] established another model for evaluating the **(Kc)** value based on fracture mechanics and elastic-plastic theory. The following equation has been derived ;

$$Kc\ \phi\ /Hv\ a^{1/2})(Hv/E\ \phi\ )^{0.4} = k2\ (l/a)^{-1/2} \ldots\ldots (18)$$

where **k2** is constant = **0.1215 ko k1**

(**Notice** the constant **k2=0.085 ko k1** is given in Niihara paper by using the Vicker's diamond half angle as 74° rather than 68°).

ko = is the free surface correction factor and is taken equal to 1.12

k1 = is the crack depth factor and taken equal 0.5

k2 was then estimated = 0.06804

By taking $\phi = 2.7$ the final form of the equation will be;

$$Kc = 0.0375\ (Hv\ a)\ (E/Hv\ )^{0.4}(l)^{-1/2} \quad \ldots\ldots\ldots (7.19)$$

Shetty et al [1985] , however, modified Niihara [1983] into a general form suitable to use easily for determination of the fracture toughness for Plamqvist crack type. This form is given in equation (7.20).

$$Kc = 0.0319\ P/\ a\ (c)^{1/2} \quad \ldots\ldots\ldots\ldots\ldots (7.20)$$

where **P** is the load used for deformation and **a** and **c** are shown on figure (7.1).

Ceramics such as sialon have been recognized for some time as having great potential as material for structural application, but sialon among many other ceramic materials has low fracture toughness which means they have a little resistance to crack propagation. Attempts has been made in the present study to promote the sialon toughness. Toughness, however, is a measure of energy absorption during crack propagation and in normal ductile materials fracture is accompanied by extensive plastic deformation. Since ceramic materials do not deform then other energy absorbing mechanisms must be employed in attempt to achieve increased toughness. Such mechanisms include reinforcement of other phase such as carbon fiber and metal particles. In the present attempts different type of carbon fiber has been used as reinforcement material as well as stainless steel, nickel and TiN powder.

Evaluating the fracture toughness by indentation (as discussed above) has attracted the attention of many researchers and different methods were employed according to the crack type developed by indentation. Thus the way of evaluating the

fracture toughness in sialon and sialon matrix composite has to follow the identification of the crack type formed upon loading; Equation (7.5), which represents a method to evaluate the fracture of median type, and equation (7.20) to calculate the fracture toughness of crack type Palmqvist were used in the present study (since the modulus of elasticity value for the materials is not needed to find the fracture toughness) to estimate the fracture toughness for sialon and sialon matrix composites.

figure 7.2

Optical photograph for a polished surface of pre-indented pressurless sintered syalon 201.

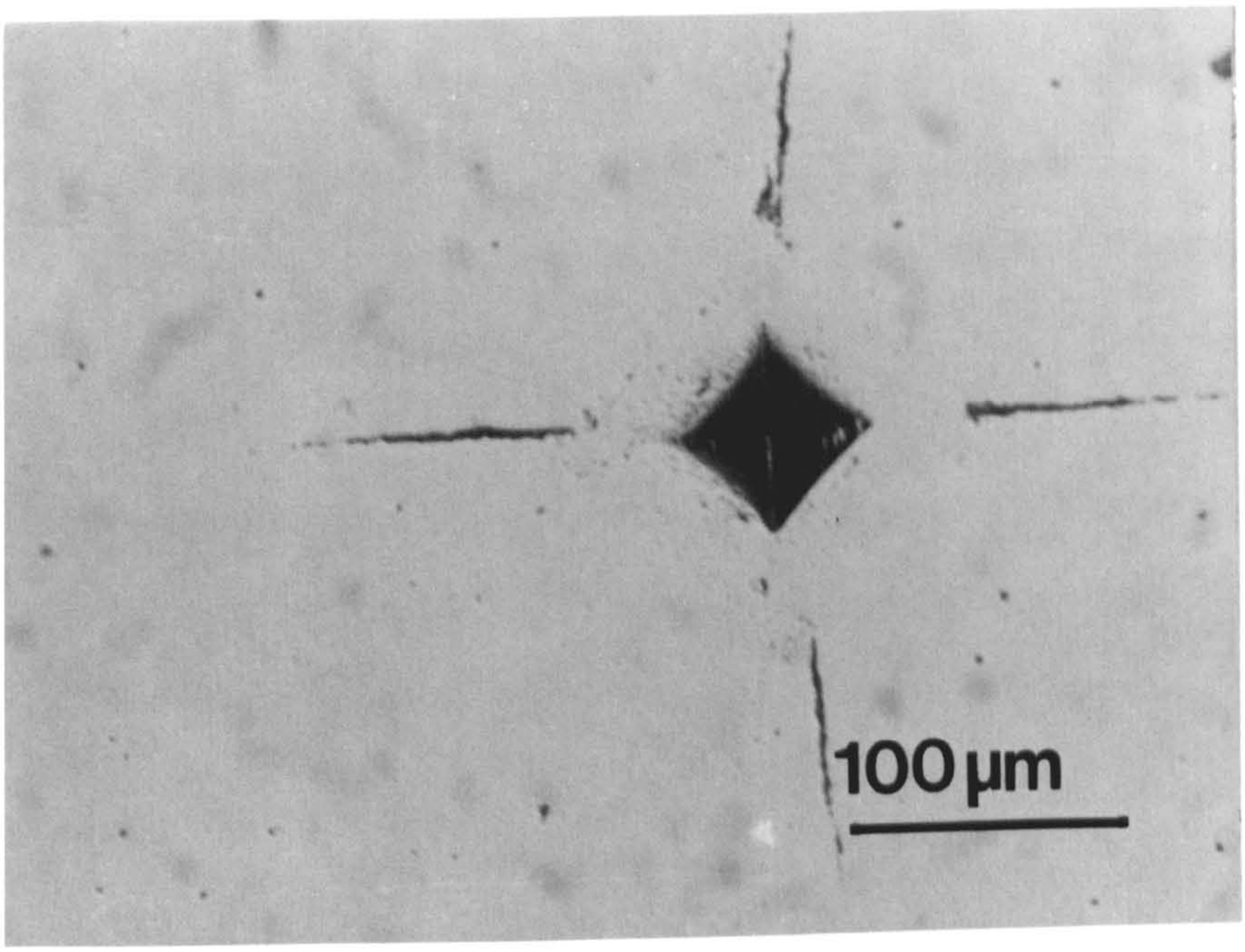
100 µm

7.3 Results and Discussion.

7.3.1 Crack type investigation in sialon systems.

The preliminary objective in order to attain the fracture toughness is to identify the crack type and then choose the right method of evaluation. Indentations with 5 Kg and 10 Kg loads were made on a polished section of a pressureless sintered syalon 201. With continuous polishing and photographing of the indented sample surface, it was noticed that the cracks formed at the indent corners, start to disappear from the indentation ends with increasing polishing time until they completely vanish. However, there is no complete indentation disappearance. Figure (7.2), which is an optical micrograph of a pressureless sintered sialon, shows the indentation–polishing process in the middle where the four cracks are starting to vanish at the indentation ends. This experiment has been repeated several times with the conclusion that the cracks formed by indentation appear to be of a Palmqvist type rather than median; therefore, the fracture toughness evaluating method should be one of that representing the Plamqvist crack type. For materials of unknown modulus of elasticity the Chatty [1985] method is the reliable one for indentation fracture toughness evaluation and the results are presented as **KC2**. In order to compare the fracture toughness of a Palmqvist type crack with the median the Lawn & Fuller [1975] method concerning this type of crack has been used and the results are given below (**KC1**). Hardness and fracture toughness of hot pressed syalon 201 (sialon with Z= 0.75) has been evaluated and the results are presented in table (7.1).

Table (7.1)

Hardness and fracture toughness of hot pressed syalon 201

HV10	KC1	KC2
1589.00	3.45	5.58
1546.56	3.51	5.56
1518.70	3.37	5.41
1546.56	3.41	5.40
1532.50	3.40	5.38
1546.56	3.35	5.37
1546.65 ± 21.5	3.43 ± 0.07	5.45 ± 0.086

These result shows that both hardness and fracture toughness values are reputable. The results reflect how the sample has a homogeneous structure. The influence of the second phase reinforced sialon matrix could then be quite clear by comparing the results achieved from composite materials with this result presented in table (7.1).

7.3.2 Hardness and fracture toughness in carbon fiber/sialon composite.

The general theory of fiber reinforcement suggests that significant strengthing will occur if the elastic modulus of the fiber is greater than that of the matrix and if the tensile stress can be transmitted to the fiber. The strength of the composite is then dependent on the properties of the fiber (strength, volume fraction, orientation and aspect ratio). Depending on the fiber orientation two types of composite may be considered. Firstly, a composite with long continuous fibers, which are generally aligned in a single direction. Green sample preparation and controlling the volume fraction of fibers are both difficult. Secondly, as in the case of the present study, are those composites containing short fibers where the fibers are randomly distributed.

Similar investigations to those discussed in section (7.3.1) were performed on carbon fiber/sialon composites and figure (7.3) illustrates a polished surface of a pre–indent section of a carbon fiber/sialon composite sample hot pressed at 1550°C. It can be seen from this figure that almost all the cracks which radiated from the indent corners have been removed by polishing whilst a large part of the indent is still visible The result concluded from such an experiment is that the crack developed during indentation is a palmqvist type.

Evidence that carbon fiber has an influence on crack propagation has been noticed. SEM and optical microscopy observations of crack propagation inspections on carbon fiber/sialon composites reveals that both deflection and absorption toughening mechanisms are present. The influence of carbon fibers on crack behaviour is illustrated in the SEM micrograph of a sample containing 10V% fiber hot pressed at 1550°C, figure (7.4.a), in which it can be seen that the crack deflected around the fibers. Figure (7.4.b), an optical micrograph of a sample containing 20V% G.P fiber hot pressed at 1450°C, is an example of an absorption toughening mechanism. In

figure 7.3

Optical photograph for a polished surface of pre-indented pressurless sintered carbon fiber/sialon composite hot pressed at 1550°C.

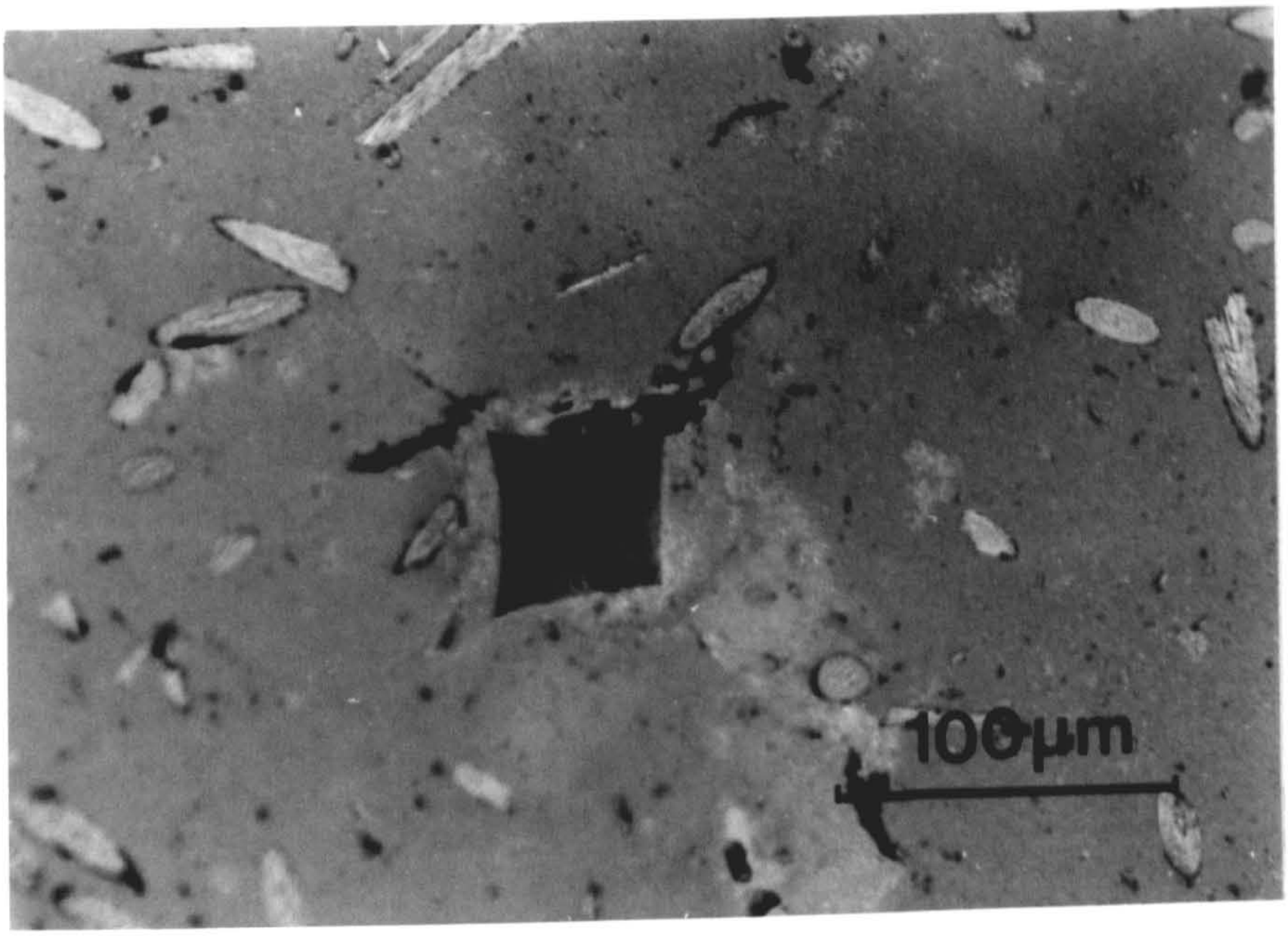
100µm

figure 7.4.a

SEM micrograph for a pre-indent 10V% carbon fiber grade (G.P)/sialon composite hot pressed at 1550°C.

figure 7.4.b

Optical photograph for 20V% carbon fiber grade (G.P)/sialon composite hot pressed at 1450°C.

a

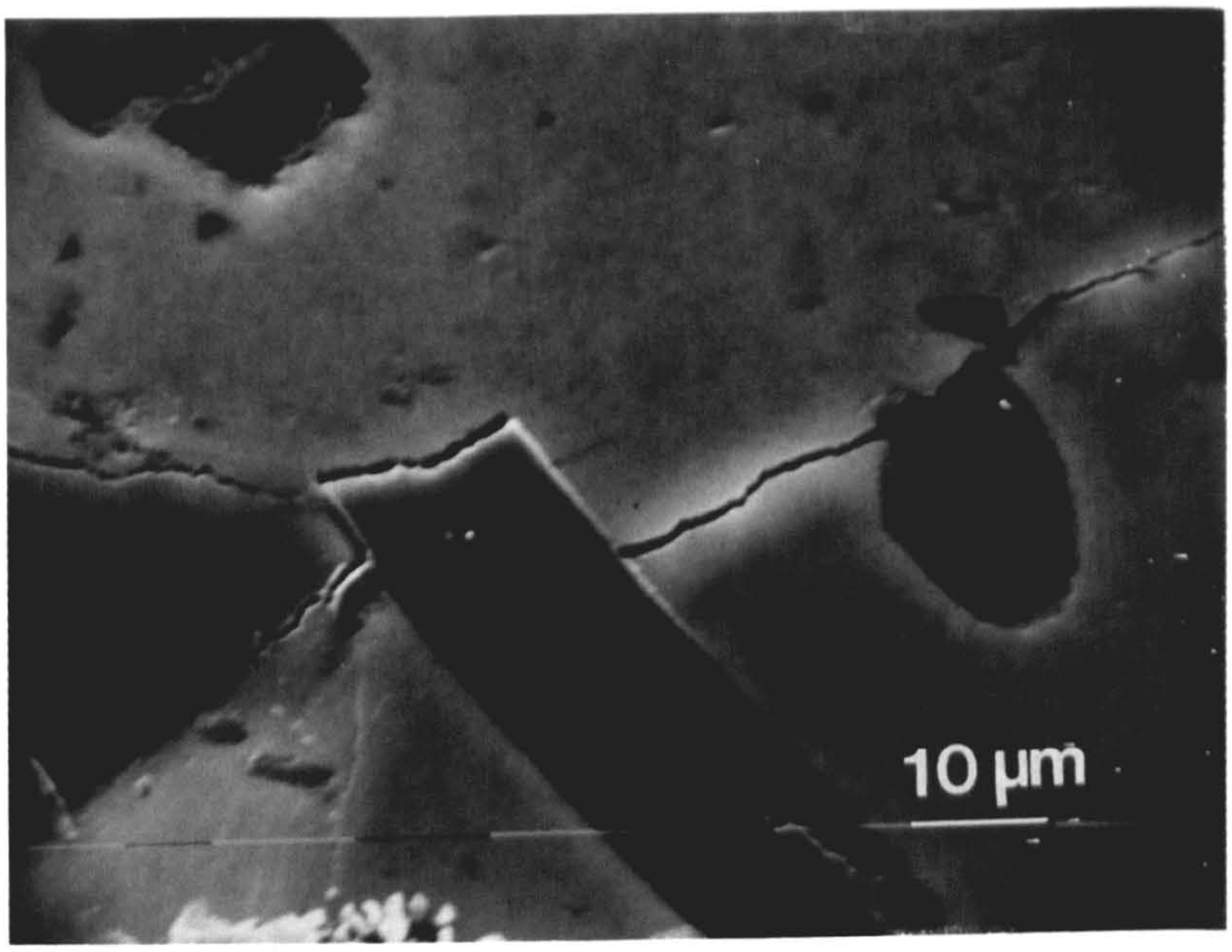

b

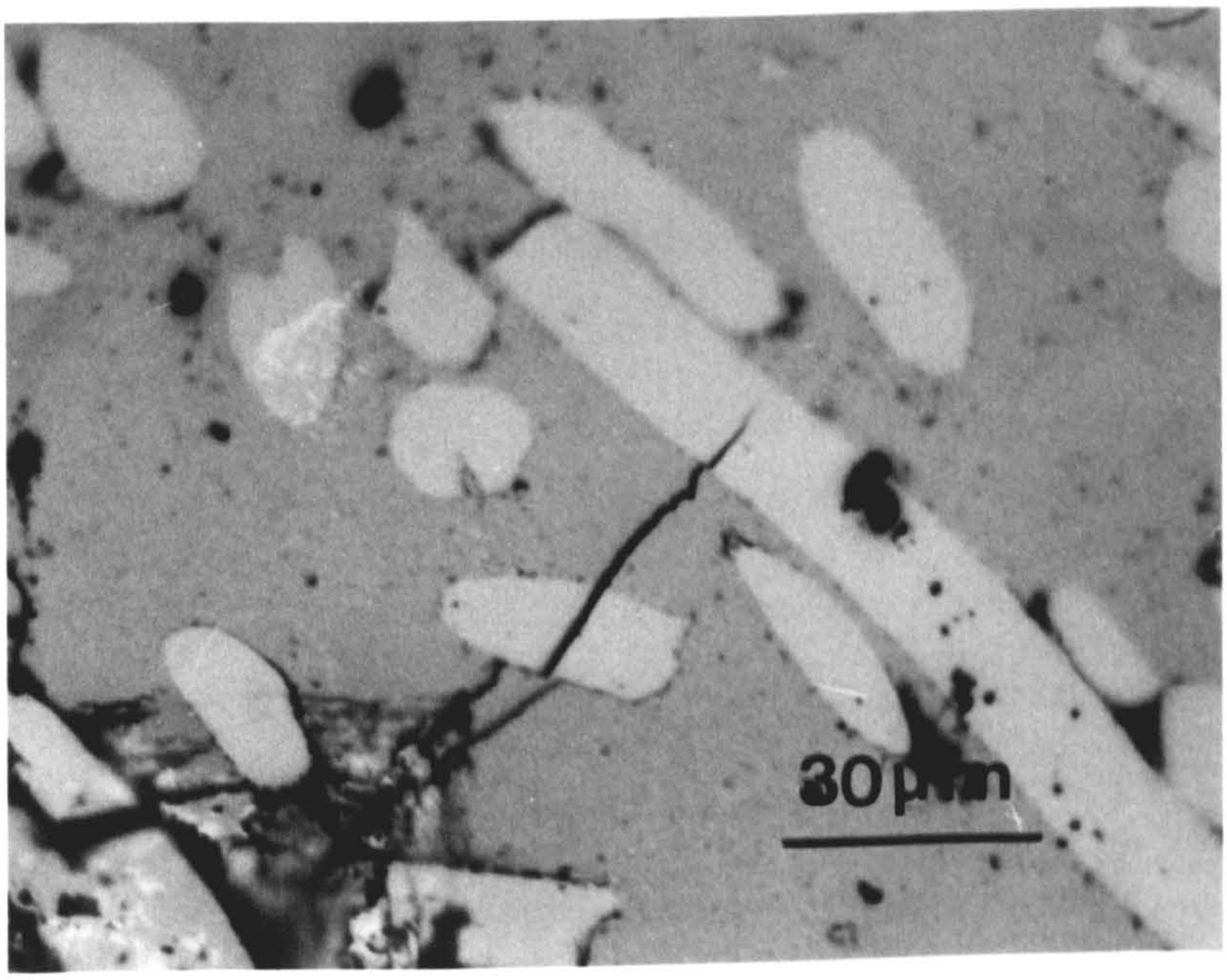

figure (7.4.b) the crack passed through the first piece of fiber and was stopped by the next one.

Difficulties in measuring fracture toughness by indentation methods is unavoidable. Non–uniform impression always occurs, especially when heavy loads such as 10 Kg are used. Cracks radiating from several places along the indent is another common result. Moreover, small fragments are always pulled out from the area around the indent during the measuring process,due to the residual stress on the unloading cycle. These observations are presented on figure (7.5 a & b). It was also noticed that the carbon fiber/sialon composite properties are anisotropic. Both hardness and fracture toughness are different along the fiber direction rather than perpendicular to it. This was observed in figure (7.5 a & b) on which the size of the indent and the crack length for the same sample subjected to the same load are different. A large indent and longer crack formed when the impression was made parallel to the direction along the fiber.

However, results of related hardness and fracture toughness were obtained from an indentation fracture test using a vickers diamond pyramid indenter. A minimum of six good patterns were made for each sample. The tests were performed on a well polished and mounted specimen. The results are presented in table 7.2 to 7.5 according to the sintering temperature, the direction in which the measurement was carried out and the type of fiber reinforced sialon.

Hardness and fracture toughness of meso-phase carbon/sialon composite has also been evaluated and the results are presented in table 7.5 according to the size of the carbon particles. Two different sizes (20μm and 6μm) have been used to reinforce sialon and their properties have been investigated.

The influence of the load, used to create the cracks, on the hardness and fracture toughness was examined by using two different loads (5 and 10 Kg). The

figure 7.5.a

Optical photograph of pre-indent sample (in a direction parallel to the fiber) containing 15V% fiber grade (C).

figure 7.5.b

Às in 7.5.a indented in a direction perpendicular to the fiber.

a

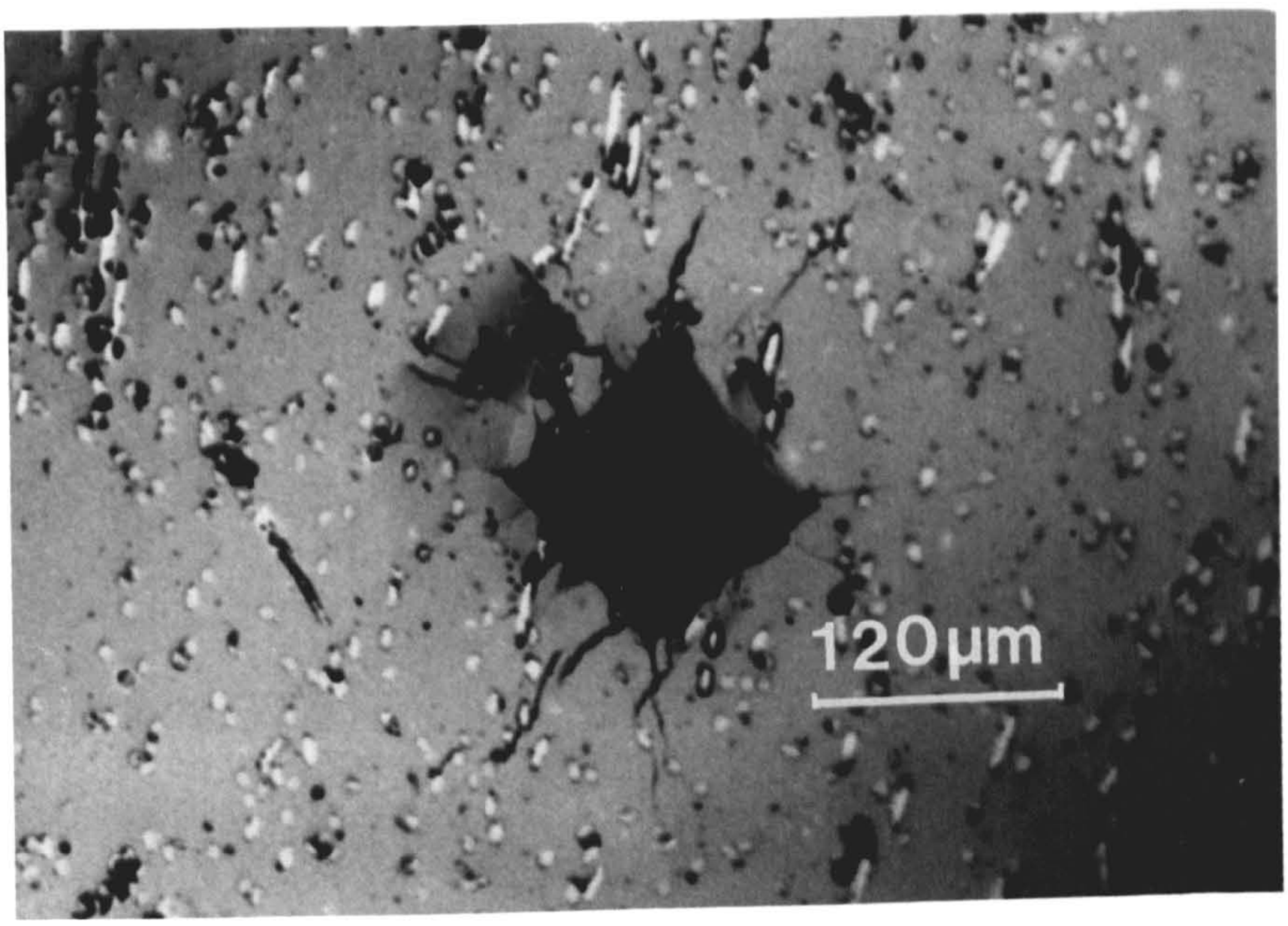

b

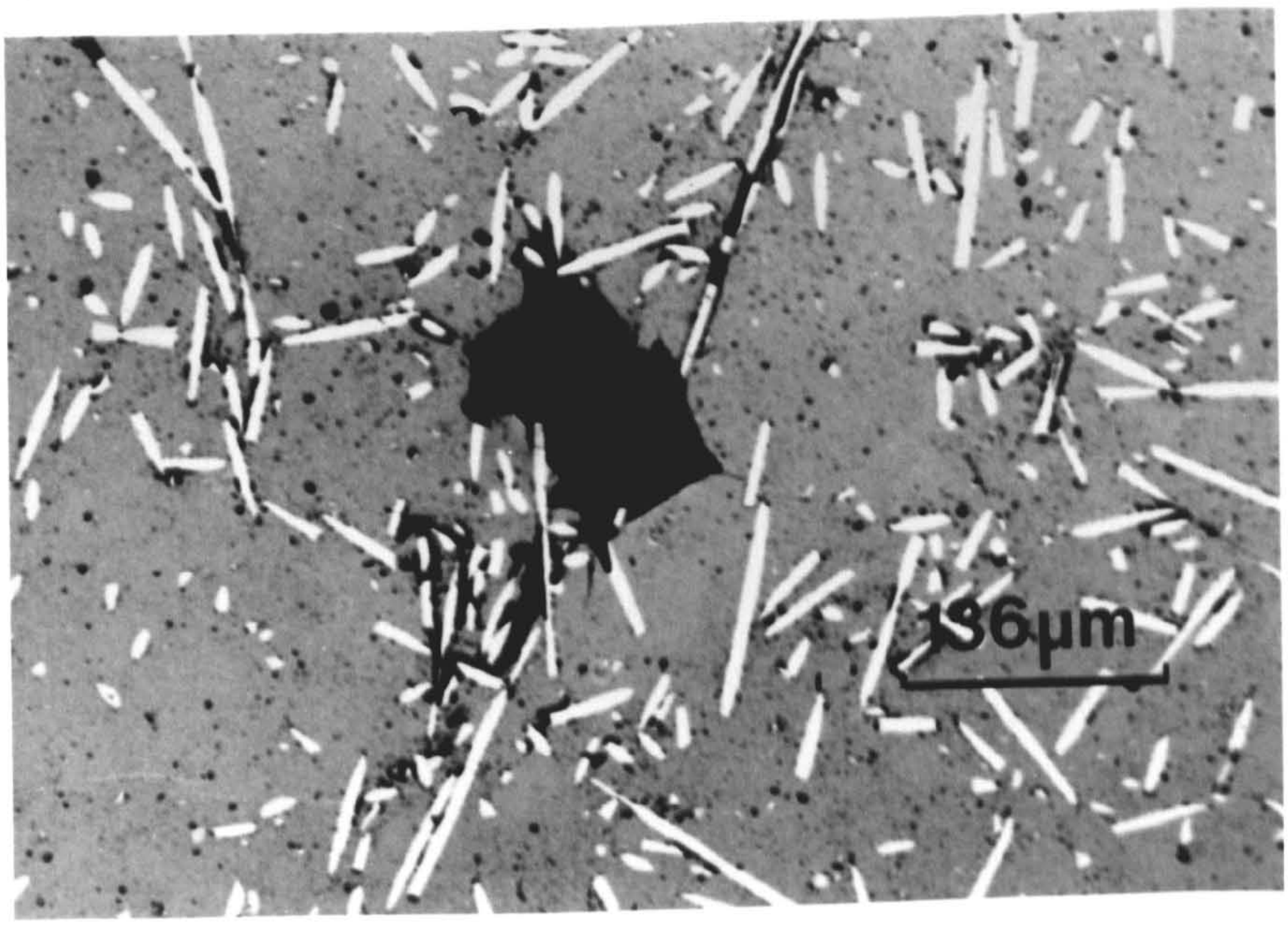

results shows that hardness and fracture toughness are both load independent. Where difficulties were found to produce a uniform indent in using 10Kg load then 5Kg load was used to evaluate the mechanical properties of carbon/sialon composite.

The experimental results are presented as follow;

Table (7.2)

Hardness and fracture toughness of 20V% G.P grade carbon fiber/sialon composite hot pressed at 1450°C

.

HV5	KC1	KC2
766.3	3.71	4.40
773.3	4.71	5.40
780.4	4.41	5.24
1006	5.27	5.40
865.5	4.33	5.93
787.6	3.97	6.30
829.85±85.4	4.4±0.5	5.38±0.61

Table (7.3a)

Hardness and fracture toughness of 15V% carbon fiber grade (C) /sialon composite hot pressed at 1450°C parallel to the fiber orientation.

HV5	KC1	KC2
858.16	3.61	4.47
841.00	3.85	4.60
852.30	3.79	4.26
869.95	3.70	4.70
869.95	3.33	4.80
846.60	4.21	5.14
860.83 ± 18.5	3.67 ±0.29	4.66 ± 0.27

Table (7.3a)

Hardness and fracture toughness of 15V% carbon fiber grade (C) /sialon composite hot pressed at 1450°C perpendicular to the fiber orientation.

HV5	KC1	KC2
1132.10	3.80	4.81
1253.63	3.85	4.74
1049.33	4.30	5.45
1072.00	4.60	5.61
1144.67	3.87	4.86
1059.00	3.78	4.73
1124.45±66.35	4.03±0.3	5.03±0.35

Table (7.3b)

Hardness and fracture toughness of 15V% carbon fiber grade C/sialon composite hot pressed at 1550°C parallel to the fiber orientation.

HV5	KC1	KC2
1095.40	3.20	4.33
1183.80	4.50	4.30
985.40	5.20	5.31
1144.71	3.15	4.20
1119.70	3.00	4.15
1144.67	3.00	5.05
1112.28 ± 63	4.56 ± 0.45	4.65 ± 0.45

Table (7.3b)

Hardness and fracture toughness of 15V% carbon fiber grade (C) /sialon composite hot pressed at 1550°C perpendicular to the fiber orientation

HV5	KC1	KC2
1314.16	5.50	6.50
1298.52	5.85	6.86
1298.52	6.30	7.24
1298.52	7.20	8.24
1298.52	6.70	7.70
1388.34	7.12	8.16
1358.8 ± 38	6.44 ± 0.63	7.44 ± 0.63

Table (7.4)

Hardness and fracture toughness of 15V% carbon fiber grade (B) /sialon composite hot pressed at 1550°C parallel to the fiber orientation.

HV5	KC1	KC2
1123.41	4.31	5.21
1201.61	4.61	5.72
1093.33	4.50	5.12
1198.64	4.00	5.07
1200.83	4.36	5.42
1188.67	4.67	5.80
1188.67 ± 43	4.41 ± 0.22	5.22±0.45

Table (7.4)

Hardness and fracture toughness of 15V% carbon fiber grade (B) /sialon composite hot pressed at 1550°C perpendicular to the fiber orientation

HV5	KC1	KC2
1395.80	7.20	8.24
1379.00	6.53	7.25
1332.30	6.72	7.71
1356.12	7.10	8.11
1330.43	7.00	8.02
1330.75	7.00	8.02
1354.1 ± 25	6.925± 0.23	7.895 ± 0.33

Table (7.5 a)

Hardness and fracture toughness of 20V% powder (D size 6 μm)/sialon composite hot pressed at 1550°C.

HV5	KC1	KC2
852.35	3.11	4.24
858.16	3.46	4.53
852.35	3.75	4.76
840.91	3.35	4.56
852.35	3.75	4.76
851.2 ± 5.62	3.39 ± 0.25	4.46 ± 0.21

Table (7.5 B)

Hardness and fracture toughness of 20V% powder (D) size 20μm /sialon composite hot pressed at 1550°C.

HV5	KC1	KC2
1170.55	7.56	8.80
1157.50	5.20	7.31
975.40	5.00	6.86
1083.64	4.88	6.78
1201.35	4.65	7.01
1117.7 ± 81	5.46 ± 1.066	7.35 ± 0.74

There is no remarkable improvement in fracture toughness in spite of reinforcing the sialon with 20V% G.P fiber. This could be due to low density (88% of

the theoretical) since the sintering temperature is only 1450°C. Hardness, however, is expected to decrease because of the presence of the soft carbon phase. The results given in table (7.3) **a** & **b** reveal the influence of sintering temperature ,and consequently the density, on both the hardness and fracture toughness. Toughness has improved by 45% as the temperature increases from 1450°C to 1550°C in a sample containing 15V% fiber grade (C). In carbon fiber/sialon composites, it was found that both hardness and fracture toughness are greater in the direction perpendicular to the fiber alignment than that parallel to the fiber as shown in tables (7.3) and (7.4). The best properties are obtained by using fiber grade (B) with sialon and the results shown in table (7.4), suggest that there is an impressive improvement (almost 45%) in the fracture toughness compared to those values for syalon 201 presented in table (7.1). In chopped fiber/sialon composites the results presented above show that both hardness and fracture toughness have a lower values in the direction along the fiber. This result reveals that the crack propagation has not been affected by the presence of the fiber when the load is applied in the direction of them. A schematic representation for the fiber distribution into the matrix (figure 7.6) shows the possibility by which the crack could hit the fiber and the crack propagation. Shorter cracks are expected in the case of applying the load perpendicular to the fiber direction. Hardness, however, has lower values in the direction parallel to the fiber because the indent (which is several times bigger than the size of the fiber) upon loading in this direction will always be in contact with a soft phase (carbon fiber), whilst in the other direction the fiber layer will be passed through easily or compressed by the indent and then the indent will be in contact with the matrix materials which exhibit more resistance to the indent movement.

The results in table (7.5 a & b) reveals the influence of carbon particle size on hardness and fracture toughness. Both of them are greater (7.5.b) in the sample

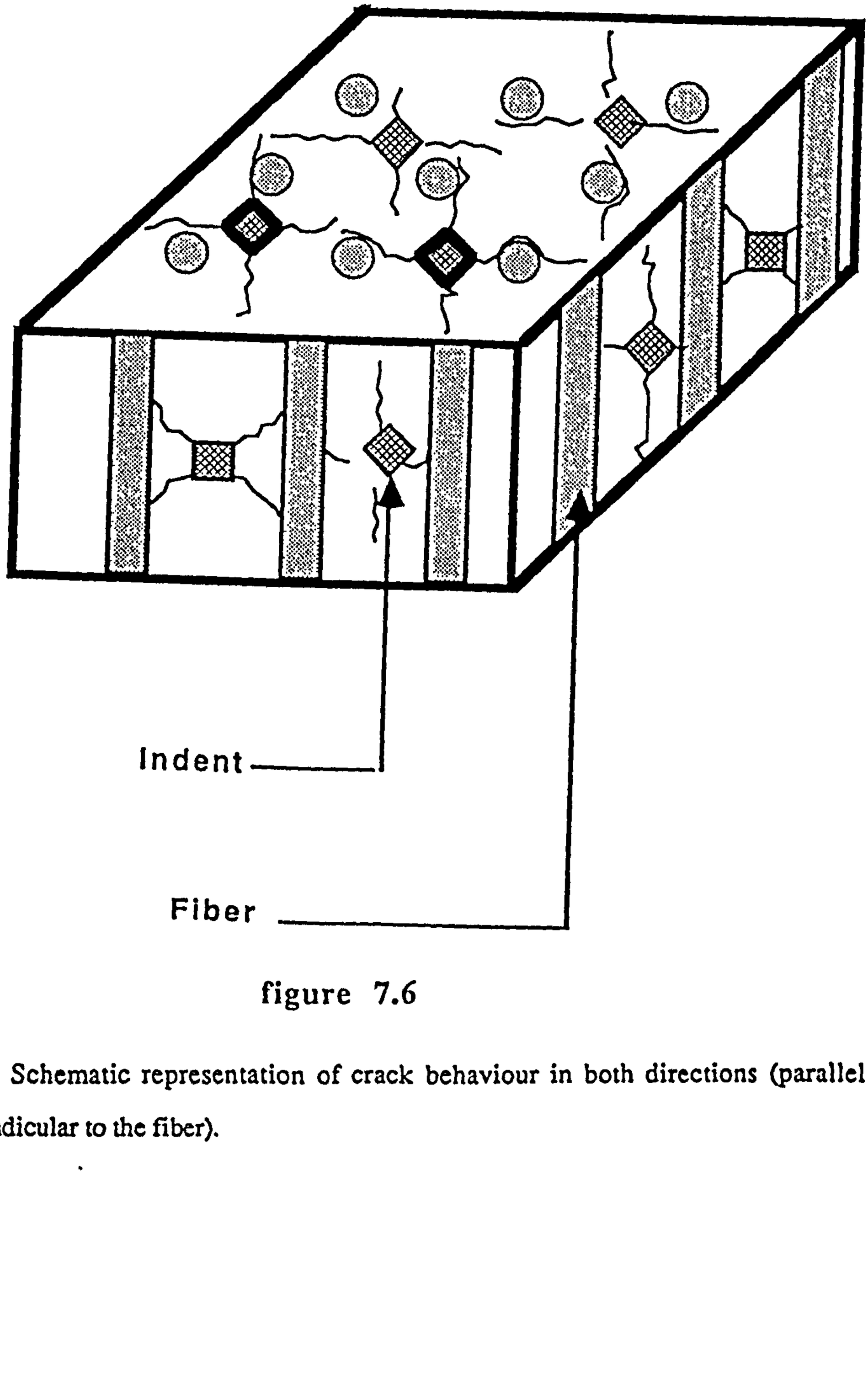

figure 7.6

Schematic representation of crack behaviour in both directions (parallel and perpendicular to the fiber).

containing carbon with particle size diameter of 20μm than that containing carbon with 6μm mean particle diameter.

7.3.3 Hardness and fracture toughness of metal/sialon composites.

(7.3.3.1) Stainless steel/sialon composite.

Hot pressing and two stage sintering cycles provide the best conditions for producing stainless steel/sialon composites. Properties of such composites, however, rely on the metal–matrix interface. Hot press sintering provides a strong interface and precipitation of silicon nitride in the two–stage pressureless sintering process, which nucleates on the ceramic/metal interface, provides a strong graded bond between metal and ceramic Both methods yield good properties.

The indentation technique was performed to evaluate the hardness and fracture toughness. The crack type investigation described in sections (7.3.1) was also been performed on the stainless steel sialon composite. It was found that the crack formed by indentation in this composite is of Palmqvist type. Figure (7.7) is an optical micrograph of a polished preindented sample sintered at 1480°C for two hour and at 1380°C for fifteen hours. The behaviour of the crack propagation is clearly influenced by the presence of the metal particles. The indent corner lying on the steel particle seems to deform the metal, since the load applied to it is absorbed. Therefore, no crack radiated from this end. The cracks developing from the other ends are stopped when they met the steel particles. The disappearance of the cracks originated from the indent corners due to polishing is also apparent.

figure 7.7

Optical micrograph for a polished surface of pre-indented section of 10V% stainless steel/sialon composite sintered at 1480°C for 2 hrs and 1380°C for 15 hrs.

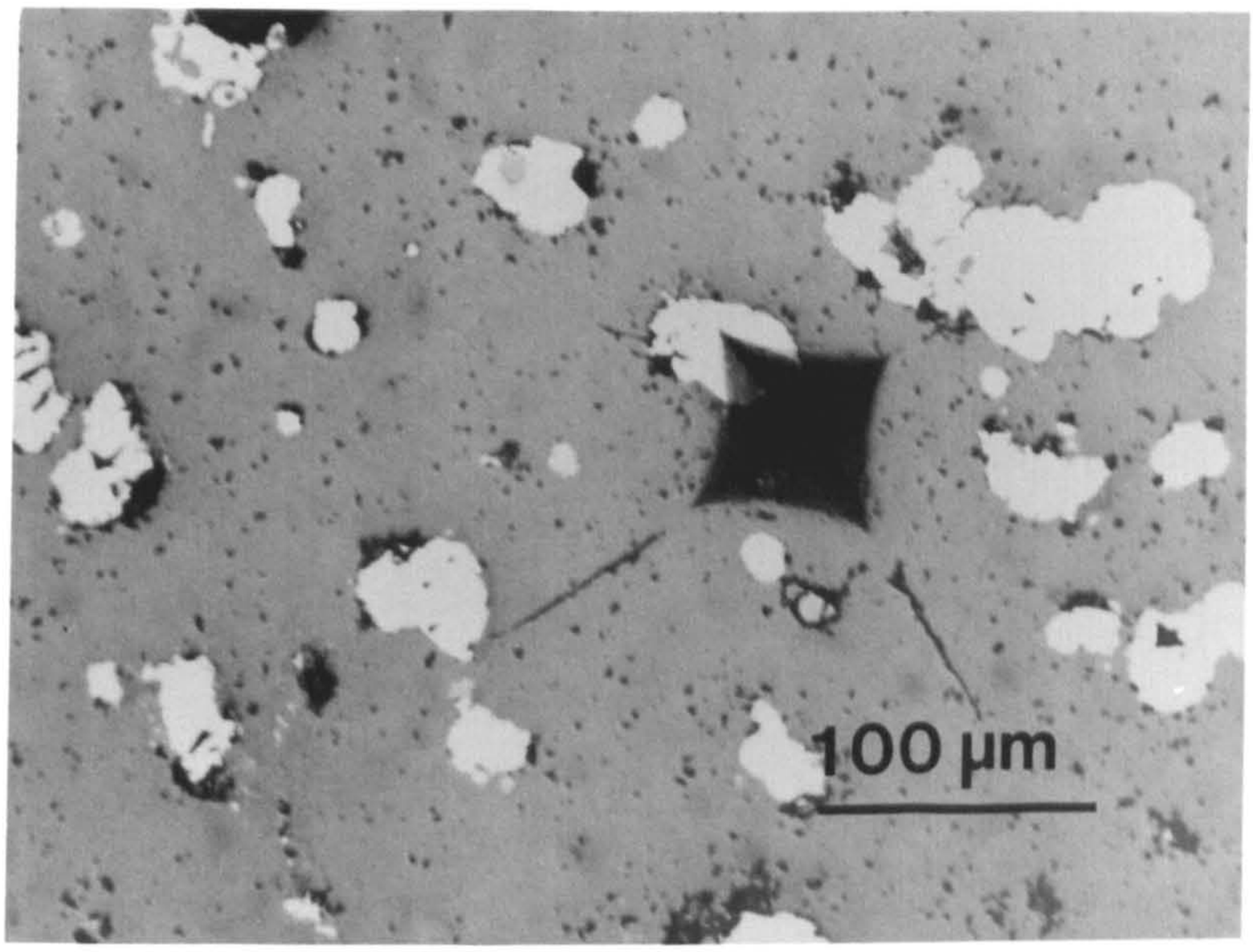
100 µm

Hardness and fracture toughness values for the β'–sialon/AISI 316 containing 10V% and 20V% stainless steel and prepared by pressureless sintering and hot pressing have been evaluated and the data is given in table (7.6) and (7.7 a & b)

Table(7.6)

Hardness and fracture toughness of β'–sialon/ 10V% AISI 316 sintered at 1500 for 1 hr and at 1375 °C for 15 hr

.

HV10	KC1	KC2
1405.63	4.34	6.83
1354.42	4.83	7.05
1391.75	4.54	6.65
1376.28	4.55	7.30
1354.22	5.24	7.36
1375.38	4.67	7.41
1376.37 ± 18	4.7 ± 0.28	7.1 ± 0.28

Table (7.7.a)

Hardness and fracture toughness of β'-sialon/ 10V% AISI 316 hot pressed at 1500°C for one hour.

HV10	KC1	KC2
1491.52	4.11	6.28
1439.73	4.32	6.61
1500.00	4.13	6.53
1485.66	4.34	6.33
1510.81	4.88	6.86
1510.81	4.88	6.86
1488.78± 23	4.57 ± 0.2	6.5 ± 0.2

Table (7.7.b)

Hardness and fracture toughness of β'-sialon/ 20V% AISI 316 hot pressed at 1500°C for one hour.

HV10	KC1	KC2
1293.54	10.96	13.71
1354.63	9.04	10.34
1343.14	7.12	8.35
1378.10	10.91	13.00
1332.00	9.37	10.77
1343.14	8.13	9.31
1340.76	9.25 ± 1.38	10.91 ± 1.9

Although only 10V% of stainless steel has been added to the sialon, significant improvement in the fracture toughness has occurred in both samples hot pressed and pressureless sintered. A two stage heat treatment sintering method seems to be effective in producing tougher samples than that hot pressed and containing the same volume fraction of stainless steel . This could be due to grain boundary recrystallization occuring through time spent in the low temperature treatment. Hardness is greater in the hot pressed specimen as an effect of pressure during sintering. However, increasing the amount of the steel in the sample from 10V% to 20V% and hot pressed under the same condition has led to an increase in the fracture toughness by almost 60%. the results in table (7.7.a & b) shows that hardness decreases with increasing the amount of the steel in the sample. This change in hardness is attributed to the presence of more soft phase (stainless steel).

The optical microscopic examinations on the hot pressed samples containing 20V% steel shows that , in spite of using 10Kg load to make the indent, the cracks radiated from the corners of the indent are very short and some times no cracks are radiated. These observation can be seen in figure (7.8 a & b).

7.3.3.2 Nickel/sialon composite.

In this investigation the experimental results for 15V% Ni powder reinforced syalon 201 show that it provides the best mechanical properties. General optical microscopic observations reveal that nickel particles dispersed into a sialon matrix composite give deformation under loading and some times prevent prevent crack nucleation. This can be seen on the optical micrograph figure (7.9) (sintered at 1450°C for two hours) which was no polishing performed on the sample after indentation and it is clear that there is no obvious crack development at the corner of the indent.

figure 7.8.a & b

Optical micrograph for preindent surface of sialon sample containing 20V% stainless steel powder hot pressed at 1500°C for one hour.

a

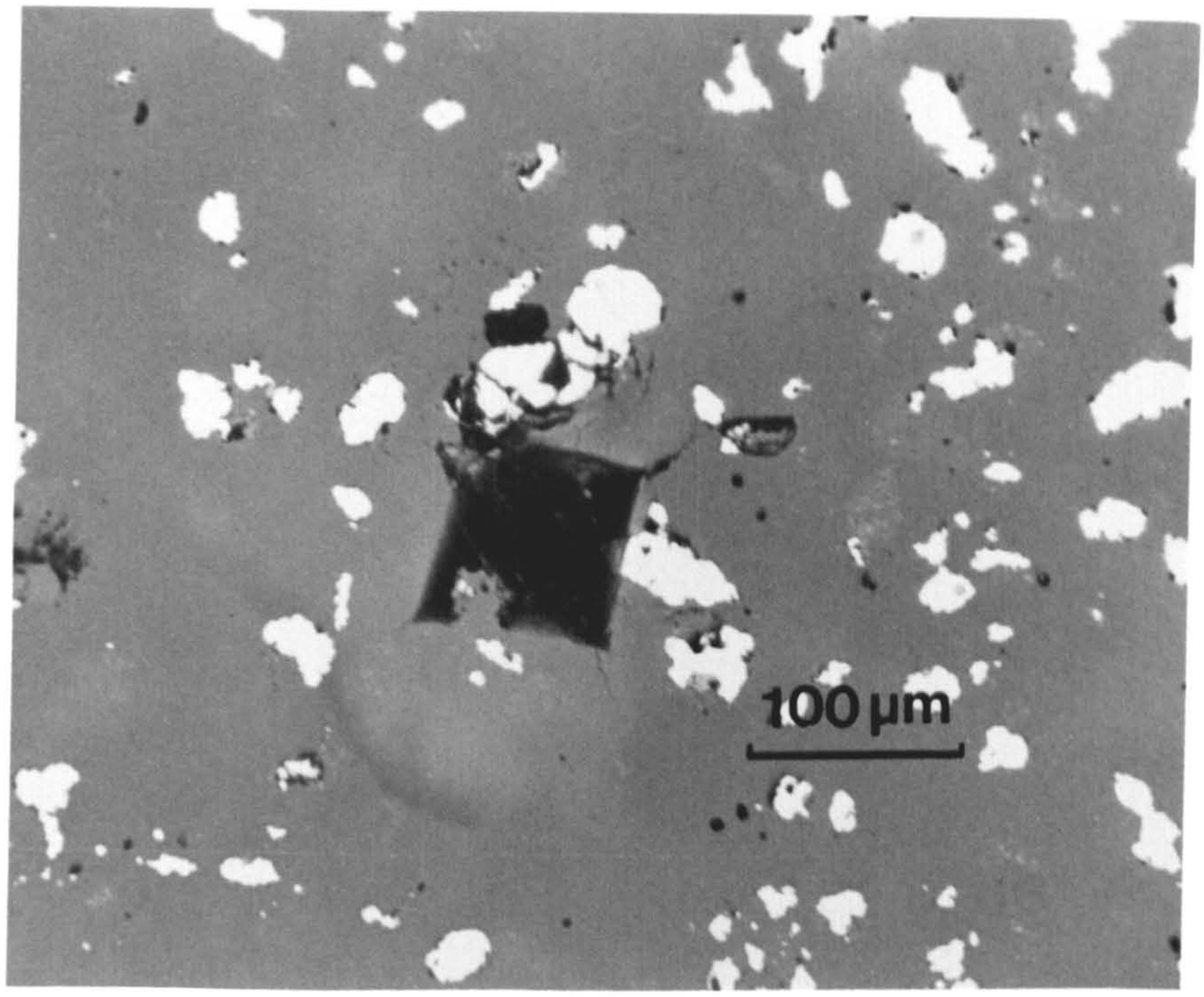

b

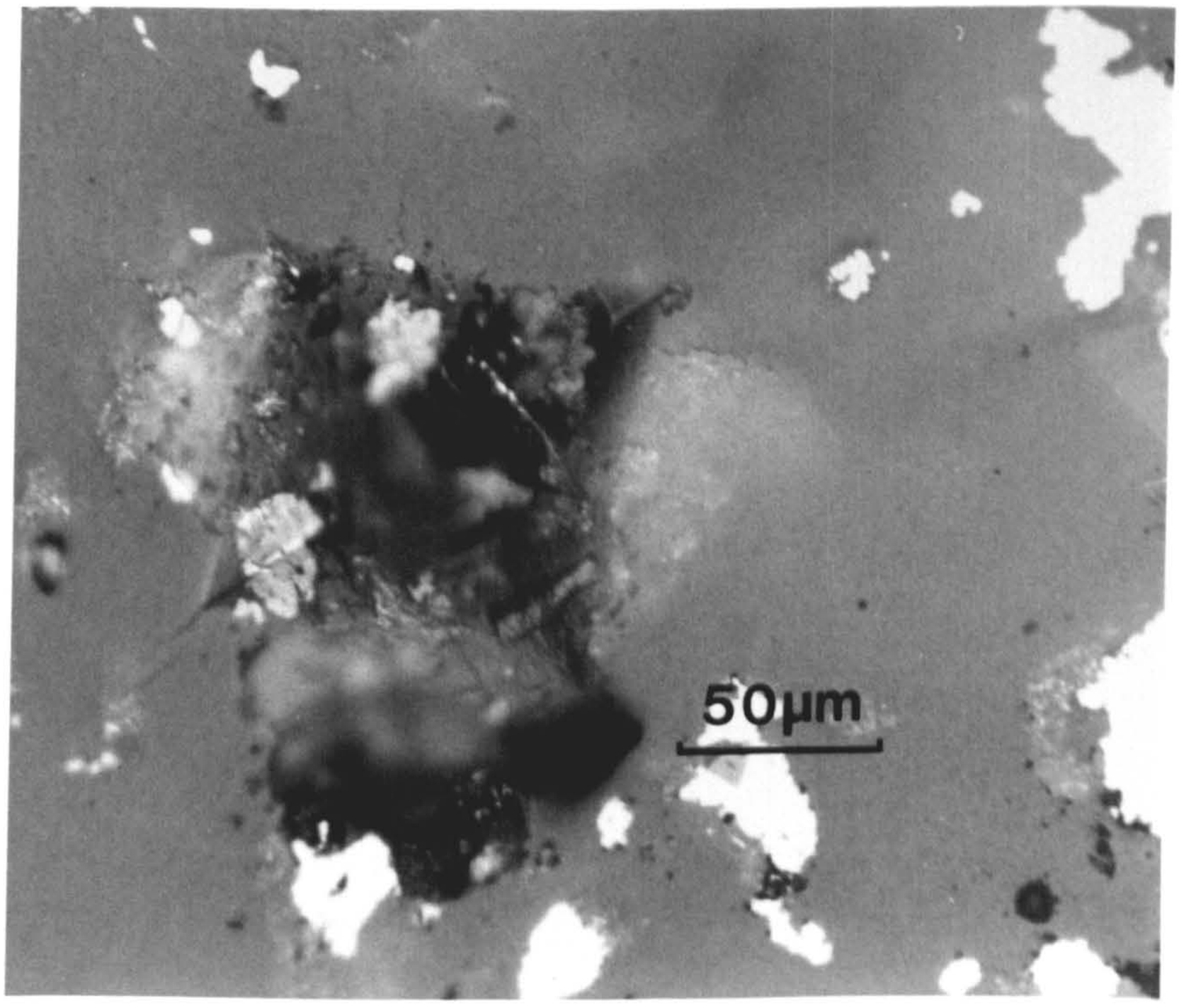

figure 7.9

Optical micrograph for preindent surface of sialon sample containing 15V% nickel powder sintered at 1450°C for two hour.

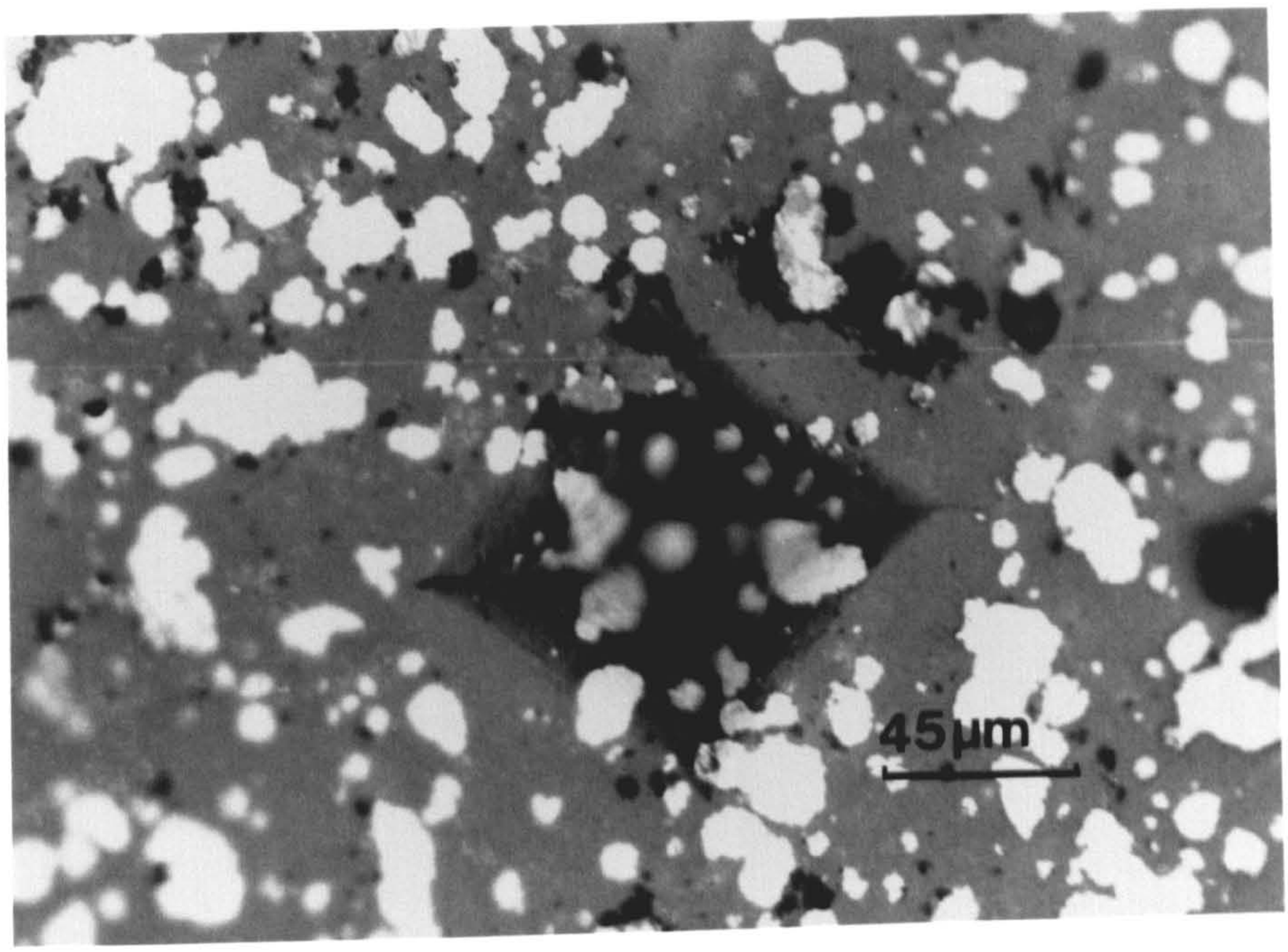
45µm

However, sintering temperature has a major influence on fracture toughness whilst it has no major effect on the hardness.

The hardness and fracture toughness values for the β'–sialon/15%Ni composite have been determined and the data are given below in tables (7.8 a & b) according to the sintering temperature.

Table (7.8.a)

Hardness and fracture toughness for 15V%Ni/sialon composite sintered at 1450°C for two hours.

HV10	KC1	KC2
1320.56	12.63	17.6
1366.30	10.38	12.2
1395.47	11.07	11.2
1410.50	11.41	13.0
1355.80	10.43	13.2
1377.35 ± 33.4	10.9 ± 0.96	13.48 ± 2

Table (7.8.b)

Hardness and fracture toughness for 15V%Ni/sialon composite sintered at 1550°C for two hours.

HV10	KC1	KC2
1320.60	7.06	8.22
1225.70	10.38	12.2
1296.55	5.33	6.61
1298.55	5.33	5.33
1354.60	5.63	7.05
1326.50	9.58	11.07
1315.49 ± 53	5.77 ± 0.62	7.17 ± 0.53

Comparison of the results in tables (7.7.a) and (7.7.b), show that increasing the sintering temperature from 1450°C to 1550°C has caused a drop in the indentation fracture toughness of almost 40%. There was , however, little effect on the hardness and it is greater in the sample sintered at 1450°C. This is due to the presence of almost 30% unreacted α–Si_3N_4 .Reduction in fracture toughness in the sample sintered at higher temperature is related to the formation of nickel silicide containing a high percentage of silicon; therefore, the brittleness of the metal particles increases and leads to no deformation upon loading. It should be noted that samples to which these fracture toughness measurement has been applied are over 95% of the theoretical density.

7.3.4 Hardness and fracture toughness in ceramic/ceramic composite (TiN/sialon composite).

The indentation technique was also been applied to the TiN/sialon composites. The experimental results show that the presence of TiN in sialon matrix helps to improve the fracture toughness and decrease the hardness. The results are presented in tables (7.9) , (7.10) and (7.11). However, the influence of TiN presence is obvious when comparing the two optical micrographs in figure 7.10 **a** & **b** (pressureless sintered at 1600°C containing 10V%TiN and 30V%TiN respectively). It can be seen on this figure that the size of the indent in the specimen reinforced with 30V%TiN in larger and the cracks radiating from the indent corner are shorter than that in the sample containing 10V%TiN. Toughness improvement occured due to deflection, as shown in figure (7.10), and absorption mechanisms as shown in figure (7.11) a & b which are a polished pre–indent surface of sample containing 30V%TiN. It is clear in this figure that the indent impression has formed on the TiN particle without cracking the particle.

figure 7.10.a

Optical micrograph for preindent surface of sialon sample containing 10V%TiN powder sintered at 1600°C.

figure 7.10.b

Optical micrograph for preindent surface of sialon sample containing 30V%TiN powder sintered at 1600°C.

a

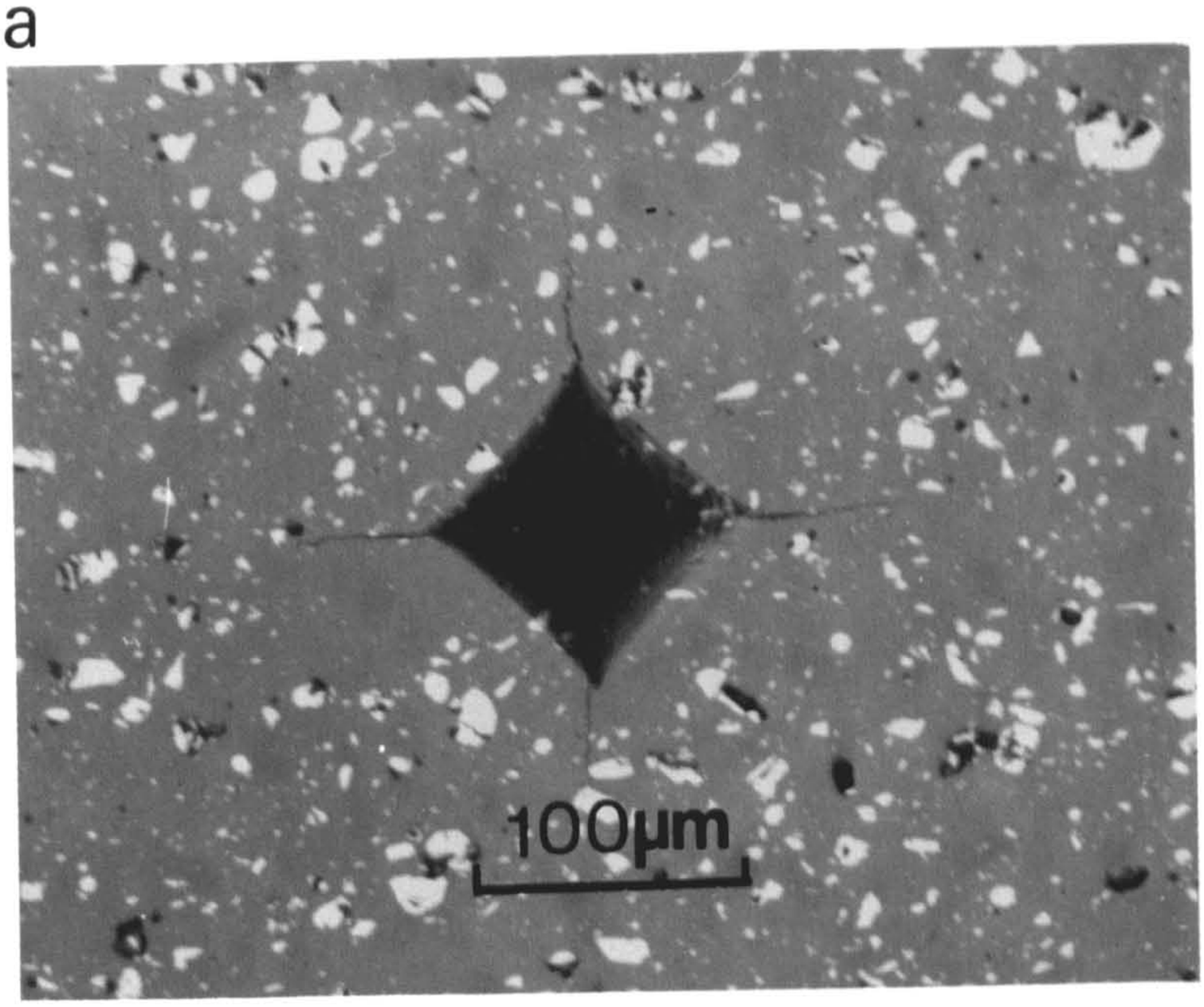

b

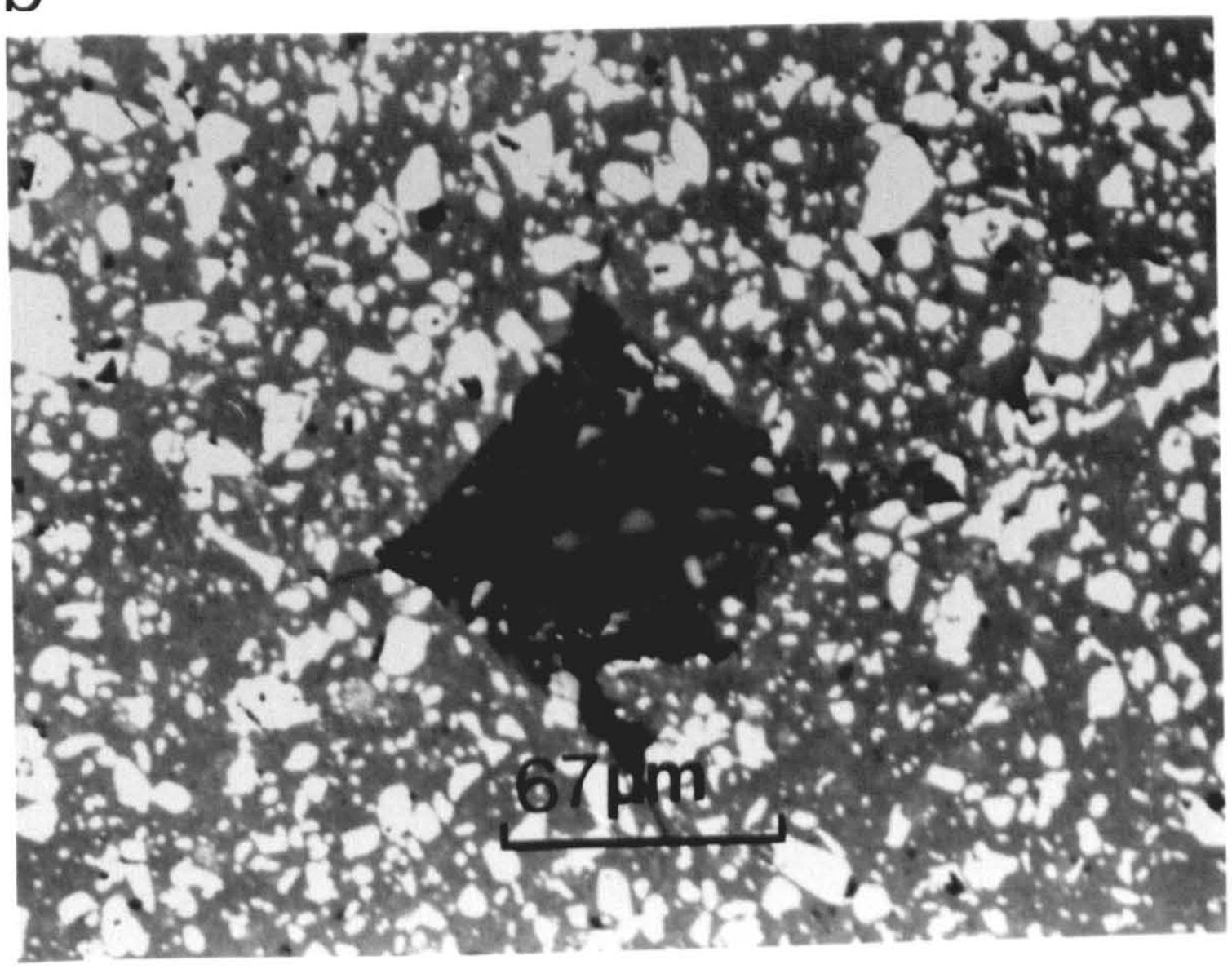

figure 7.11.a & b

As in figure 7.10.b a polished surface

a

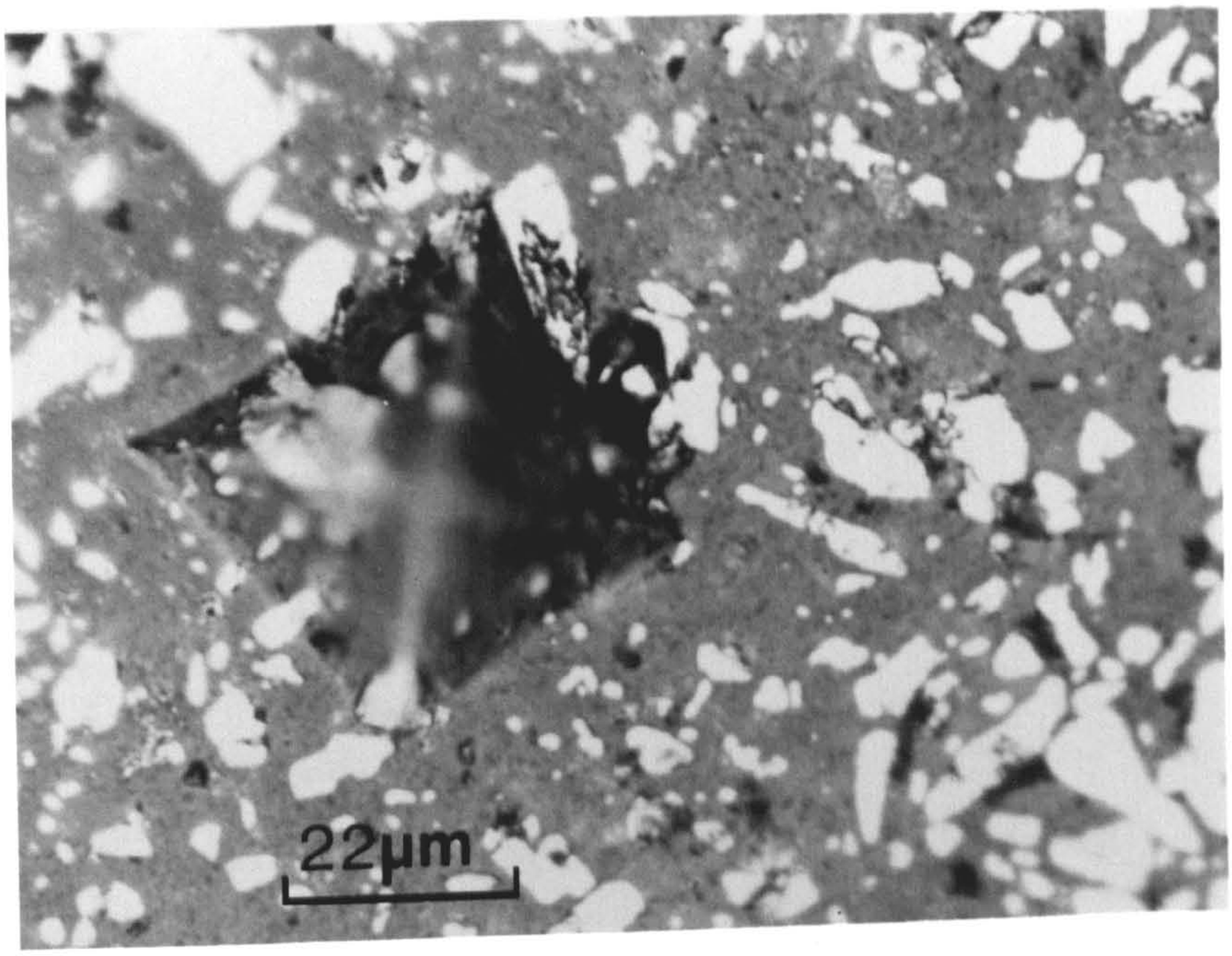

b

Table (7.9)

Hardness and indentation fracture toughness of 10V%TiN/sialon composite pressureless sintered at 1600°C.

HV10	KC1	KC2
1390.00	5.54	6.97
1378.10	5.62	7.03
1390.05	6.05	7.40
1414.44	5.66	7.10
1402.20	5.30	6.79
1402.20	5.64	7.01
1439.50	7.50	8.72
1402.33 ± 18.6	5.90 ± 0.68	7.30 ± 0.61

Table (7.10)

Hardness and indentation fracture toughness of 20V%TiN/sialon composite pressureless sintered at 1600°C.

HV10	KC1	KC2
1309.50	6.03	7.30
1332.00	7.12	8.30
1320.60	7.40	8.54
1298.60	6.44	7.62
1331.70	6.43	7.66
1331.70	7.51	8.66
1309.50	6.76	7.93
1319.8 ± 12.5	6.82 ± 0.51	8.0 ± 0.47

Table (7.11)

Hardness and indentation fracture toughness of 30V%TiN/sialon composite pressureless sintered at 1600°C.

HV10	KC1	KC2
1266.56	7.42	8.54
1206.90	7.91	9.03
1186.80	8.23	9.42
1196.30	7.14	8.2
1235.70	7.68	8.80
1206.00	7.40	8.50
1226.70	8.88	10.23
1235.70	7.54	8.64
1220.1 ± 24.3	7.76 ± 0.49	8.92 ± 0.6

It can be seen from the results given in tables 7.9 –7.11 that increasing the TiN volume fraction in the structure helps to promote the fracture toughness and decreases the hardness .

Discussion.

The density of sintered samples of carbon fiber/sialon composites has a major influence on mechanical properties. The results presented in tables 7.3.a and 7.3.b show that samples having 98% theoretical density (1550°C, table 7.3.b) are harder than samples with 92% theoretical density (1450°C, table 7.3.a) but both are considerably lower than fully dense syalon 201 (1546 HV10, table 7.1). This difference in hardness is independent of testing direction although, as discussed above

(figure 7.6), the orientation of the fiber affects the magnitude of the hardness. In the case of fracture toughness, KC2, the measured value is independent of density when measured parallel to the fiber but is higher in higher density material. When compared to syalon 201 (table 7.1) in the fracture toughness is not improved except in the case of high density (98%) material tested perpendicular to the fiber direction (table 7.3.b). Thus the effect of the composite action on toughness is specific to this orientation in dense samples. The presence of porosity appears to have little effect on KC2 in these composites.

Both hardness and fracture toughness in metal/sialon composites which are all of high density, are mainly dependant on the amount of reinforcing phase and sintering temperature, both of which influence the degree of α to β' transformation. Samples sintered at low temperatures retain a considerable amount of unreacted α-Si_3N_4 due to which these samples are harder than those sintered at higher temperature as can be seen in tables 7.8.a and 7.8.b. The effect of volume fraction is shown by tables 7.7.a and 7.7.b where for hot-pressed samples the hardness decreases and the toughness increases with reinforcement volume fraction. As discussed previously these results are somewhat surprising as the metallic phase is relatively brittle after sintering.

This is also an unexplained facter in the behaviour of TiN/sialon composites where the hardness progressively decreases from that of syalon 201 with increasing volume fraction of TiN while the fracture toughness simultaneously increases. Since TiN is a extremely hard and brittle material, these results can only be interpreted as showing the importance of the matrix/reinforcement interface in governing mechanical behaviour.

In the three systems mentioned above it can be noticed that the best fracture toughness can be achieved by reinforcing the sialon with metal particles. Difficulties in fabrication of such composites can not be avoided as the chemical incompatibility

between the metal and the sialon represents the major obstacle in fabrication of such materials.

The carbon fiber/sialon system has the same problems beside the difficulties in green sample preparations. Moreover, for the same volume fraction of metal/sialon and carbon fiber/sialon, higher fracture toughness can be obtained in the metal/sialon composite.

The TiN/sialon system is the easiest one in fabrication as the system components are chemically compatible. This reason could make such composite very attractive since it also possess a good hardness and fracture toughness. Additionally it can be used for high temperature applications with no problems of softening which could occur in metal/sialon systems, and oxidation in carbon fiber/sialon composites.

CHAPTER EIGHT

ELECTRICAL PROPERTIES

8.1 Introduction.

The electrical and magnetic properties of solids in general are mainly determined by the properties of free electrons (electrons free to move around and conduct electricity) in them. Ceramic materials which are covalently bounded have no free electrons similar to those in metals. Thus ceramics are potentially good insulating materials.

However, the need to improve the mechanical reliability of advanced ceramics has led to developments of high–strength high–toughness ceramic composites such as whisker, fiber and particle–reinforced ceramic matrix composites. These composites are hard and machining using conventional tools (diamond tools) is not convenient and these are also expensive methods for ceramic machining. Electrical discharge machining is an attractive alternative machining technique for forming such materials, but the components to be machined by this technique require to be electrically conductive. Silicon nitride–based materials as attractive ceramics for high temperature application are known to have a high resistivity which enables them to be used for insulating applications. Addition of a chemically compatible and electrically conductive second phase to silicon nitride–based materials could form an electrical discharge

machinable composite. It has been shown that the addition of silicon carbide fibers to silicon nitride–based composites produced highly conductive materials. [Tanari et al 1986]

In the present study different types of carbon fiber, stainless steel, nickel and TiN particles have been added to syalon 201 to study the composite properties and among them the electrical conductivity.

8.2 Results and Discussion.

8.2.1 Conductivity in carbon/sialon composites.

Syalon 201 as sintered materials exhibits excellent insulation properties, but electrical conductivity measurements performed on carbon/sialon composites show that such materials become conductive. However, the variation of electrical conductivity of carbon/sialon composite is found to be related to the volume fraction of the carbon fiber and the size of the carbon particles. The results are presented according to the type of carbon phase used, volume fraction and density as will be discussed below.

8.2.1.1 Conductivity in meso phase carbon/sialon composite.

Conductivity measurements was carried out on a hot pressed carbon powder sialon composite. Different volume fraction and particles size carbon reinforced sialon were examined. The results are presented in table (8.1) in which two important observations can be noticed. Firstly, for a certain type and particle size of fiber, conductivity is found to be volume fraction dependent. Secondly for a specified carbon fraction, conductivity is particle size dependent. The results in table (8.1) show that even with 20V% carbon, when the particle size is 20μm the sialon resistivity reading is out of range whilst the resistivity of the samples containing the same volume fraction of carbon having particles size of 6μm is almost 2.5 Ω.cm.

However, 10V% carbon powder of the small particles size (6μm) seems to be sufficient to create conduction within the composite as can be seen in table (8.1).

Electrical conductivity of a two phase composite has the attention of many researchers. In a system of metal particles dispersed into a matrix of oxide (insulator),

which is similar to the present system (carbon/sialon composite), it was found that composite conductivity can be represented by the following equation. [Wagner 1972]

$$\sigma = 7\ (V)^{1/3}\ \varepsilon\ k\ T\ u/e\ (L)^2$$

where;

L = the average distance between neighbouring conductive particles

V = volume fraction of the conductive particles

ε = is the dielectric constant of the matrix

k = Boltzmann constant

T = temperature

u = electrical mobility of an electron

e = electron charge

σ = electrical conductivity

This equation noted that conductivity is inversely proportional to the square of the distance of neighbouring particles. However, these distances can be related to the size of the dispersed phase and its volume fraction as follows;

Assuming that the dispersed particles are uniformly distributed in the matrix and the particles are having a uniform shape. Referring to figure (8.1);

L = is the distance between neighbouring particles

a = is the cross section area of a particle

A = the total cross section area of the composite.

H = is the distance between the centers of the two neighboring particles.

n = number of particles in the matrix cross section (A).

Therefore for the carbon as a powder, the distance between the neighbouring particles can be found as follows;

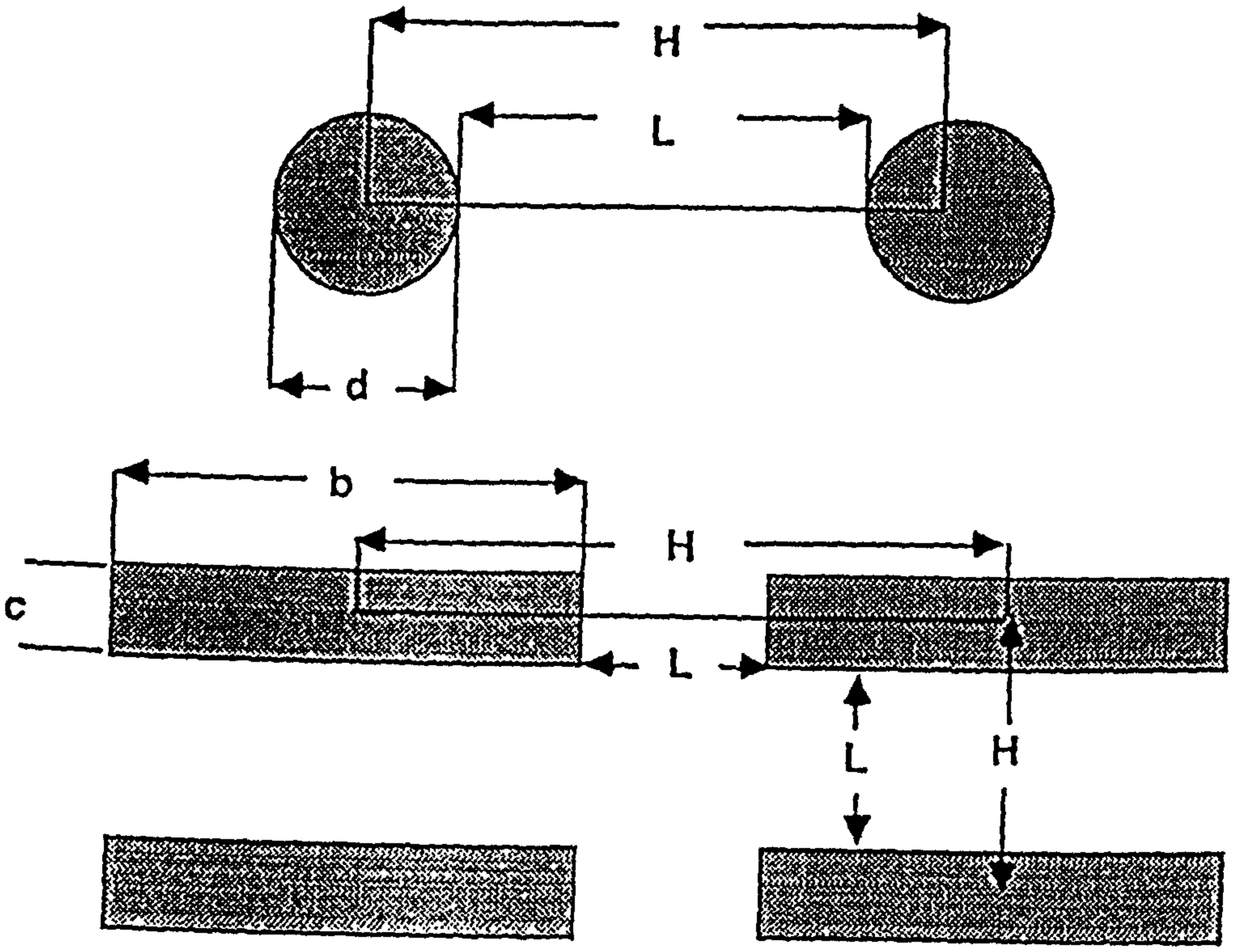

figure 8.1

Schematic representation of the fiber distribution in the sialon matrix.

$$L = H - d$$

$$= (A/n)^{1/2} - d$$

$$= [A/(AV/a)]^{1/2} - d$$

$$= [0.886/(V)^{1/2} - 1]\ d \quad \text{.....(8.2)}$$

This equations is showing that the distance between the carbon particles and consequently the conductivity of such composite is strongly depending on the size of the conductive phase particles. From equation (8.2) the average distance between neighbouring carbon particles in the present system can be calculated. The results are given in table (8.1) in which the distance increases with increasing particle size and therefore the conductivity will decrease.

Table (8.1)

Resistivity measurements in carbon/sialon system

Sample	%T.D	L (μm)	Resistivity (Ω.cm)
Pure β'-sialon	98		∞
β'-sialon/powder(D) composite. (6μm)			
10V% Powder (D)	95.33	10.80	1584 (kΩ.cm)
20V%	65.33	5.88	2.46
20V%	87.25	5.88	0.5
β'-sialon/powder(E) (20μm)			
10V%	98.65	36.00	∞
15V%	97.82	25.75	∞
20V%	86.66	19.62	∞

It can be noticed on table (8.1) that the resistivity values are slightly varied with sample density. This is due to the higher sintering temperature in the sample having high density. The high temperature firing could lead to some reaction around the carbon powder which may change the behaviour of the conductivity in the carbon/sialon system.

8.2.1.2 Conductivity in carbon fibre/sialon composite.

Conductivity measurements has also been performed on sialon reinforced with chopped carbon fiber and similar to what has been discussed in the case of carbon powder, the conductivity of such a composite is strongly influenced by the size of the fiber and its volume fraction. The distance between the fiber has also been estimated by assuming that the fibers are aligned in one direction .Referring to figure (8.1) it can be noticed that there are two possible paths for the electrical charge to follow. The mean distance between the chopped fibers in the direction of the aligned fiber could be presented as ;

$$L = H - b$$

$$L = (bc/V)^{1/2} - b \quad \text{.....(8.3)}$$

and in the direction perpendicular to the fiber as;

$$L = (bc/V)^{1/2} - c \quad \text{.....(8.4)}$$

where; **c** is the mean fiber diameter and **b** is the mean fiber length as shown in figure (8.1).

It can be seen from these equations that the fiber volume fraction required to make the sample conducting through the fiber (i.e $L = 0.00$)is;

$$V = c/b$$

$$V = b/c$$

This means that in order to reduce the fiber volume fraction in the sample and retaining the conductivity properties then fiber aspect ratio should be controlled.

However, the resistivity measurement on carbon fiber/sialon composites are given in table (8.2).

Table 8.2

Resistivity measurements in carbon fiber/sialon composites.

Sample	%T.D	L (μm)	Resistivity (Ω.cm)
Pure β'-sialon	98		∞
β'-sialon/G.P fiber			
20V% G.P	88	10.35	0.95
20V% G.P	98	10.35	1.6
β'-sialon/ fiber (C)			
15V%	92.5	15.82	2.37
15V%	98	15.82	2.89
β'-sialon/15V%fiber (B)	98		4.64
β'-sialon/fiber (A)			
10V%	97	25	∞
15V%	95	15.82	65.34 (KΩ.cm)
20V%	85.5	10.35	12.12

In this table the (L) value was calculated by taking the mean length of the fiber as 25μm and the diameter as 10μm.

Observations similar to those noticed on the previous system can also be seen in table (8.2) and the same explanation should be applied. Different resistivity values can be noticed on table (8.2) when using different fiber grade with the same volume fraction which could be related to the difference in the fiber characteristics.

8.2.2 Conductivity in metal/sialon composite.

Stainless steel and nickel powder reinforced sialon has attractive mechanical properties. Electrical resistivity measurement on these composites show that the particle size of the reinforced phase play an important part in the conductivity measurement. The results presented in table (8.3) show that, in spite of the similarity in the conductivity behaviour of the nickel and steel, 20V% Ni reinforced sialon forms a composite with a resistivity of 3.366 Ω.cm whilst the same fraction of steel fails to make the sialon conductive. The main difference between the two powders is the size which is much smaller in the nickel case. The particle size of nickel powder can be roughly estimated from the photographs presented in figurs (5.6) and (7.9) as in range of 15-20 μm, but with many smaller particles. Therefor the avarage distance between nickel particles is in the range of 20-25 μm in the samples containing 15V% Ni and 15-20 μm in the samples reinforced with 20V% Ni. It should be noted that the sample reinforced with stainless steel 316 is responding very well to the magnetic which is not the case in the nickel sialon composite.

Table (8.3)

Resistivity measurements in metal/sialon system.

Sample	%T.D	Resistivity (Ω.cm)
10V%steel 316/β'-sialon composite	98.54	∞
20V%steel 316/β'-sialon composite	98.78	∞
15V%Nickel/β'-sialon composite	98	23
20V%Nickel/β'-sialon composite	97.14	3.37

8.2.3 Conductivity in TiN/sialon composite.

The maximum particle size of TiN powder is 45μm which means that high volume fraction of TiN is required to get the sialon becomes conductive. The results presented in table (8.4) show that 30V%TiN was needed in order to create conductivity within the composite. Applying the same equation used to evaluate the distance between the neighbouring particles in carbon fiber and assuming that the TiN avarage particle size is 25-30 μm, it can be found that the average distance in 30V%TiN composite is almost 15-20 μm. However, the calculations were based on several assumption and also on the maximum particle size.

Table (8.3)

Resistivity measurements in TiN/sialon system

Sample	%T.D	Resistivity (Ω.cm)
10V%TiN/β'-sialon composite	98.51	∞
20V%TiN/β'-sialon composite	97.8	∞
30%TiN /β'-sialon composite	96.75	443

The production of a conductive ceramic composites seems to be possible with some difficulties in the fabrication stages. The addition of a conductive phase to a ceramic matrix with a certain volume fraction is the way to produce an electromachinable components. The chemical compatibility between the sialon and TiN make such a combination very attractive compared to the metal/sialon and carbon fiber/sialon systems. Conductivity in the three previous systems is dependant on the volume fraction and the particle size of the second phase. The smaller the particle the shorter the distance between the neighbouring particles resulting in a better conductivity.

From the above results for "spherical particles" it can be seen that significant conduction only occurs where L has values less than approximately 15 μm. This figure will however be strongly influenced by other factors such as sintering together and connectivity of the particles. Indeed this effect must have an important influence

on conductivity since a connecting path is necessary for electronic conduction although an insulating matrix. There will be an increased probability of forming an interconnecting network with increasing volume fraction.

CHAPTER NINE

CONCLUSIONS.

(1) The green sample in ceramic matrix composites processing has a great influence on their sintering behaviour. High green density samples can be achieved by applying a uniaxial pressure and heating (at the same time) on a slightly wet powder sample and allowing it to dry under pressure.

(2) Reaction in carbon fiber/sialon composite can not be inhibited by the addition of carbon monoxide gas to the sintering atmosphere as suggested by Koytoku et al (1987). It appears that this technique causes a side effect in which the presence of the carbon monoxide gas carborized the sialon matrix.

(3) The alternative approach to overcome chemical incompatibility in carbon/sialon systems is to apply a high densification rate and low sintering temperature (1500-1550°C).

(4) The higher the carbon fiber formation temperature the more stable the carbon/sialon system becomes.

(5) The carbon volume fraction is found to have an important effect on the stability of the carbon/sialon system at certain sintering temperature. Increasing the carbon volume fraction leads to promotion of the carbon/sialon reaction.

(6) The principle reaction in carbon/sialon composites is between the carbon and the surface silica on the silicon nitride particles.

(7) The presence of the carbon in the sialon matrix inhibits the transformation of α-Si_3N_4 to β'–sialon.

(8) In metal/sialon composite processing there is always a reaction between the silicon nitride component of the sialon and the metal particles to form metal silicide and liberating nitrogen gas. High densification rate which can be achieved in the pressureless sintering technique by increasing the heating rate represents a method to promote densification in such composites.

(9) The reaction in metal/sialon composites forms liquid silicide at relatively low temperature. This silicide liquid seems to promote the densification process. For example the sintering temperature in nickel/sialon composites for maximum densification is 1450°C.

(10) Silicon nitride crystals are found to form on the steel particles at temperatures 1350-1400°C and disappear at temperature over this range.

(11) The solubility of silicon in steel particles (which has a strong influence on the composite mechanical properties) has been adjusted by applying a two stage heat treatment technique.

(12) The Z value of β'–syalon (201) increases with increasing the amount of metal reinforcement in the sialon due to the reaction of the metal with the silicon nitride.

(13) In TiN/sialon composite, no reaction between the sialon and the TiN was detected and the sialon has a uniform structure of β'–sialon with the correct Z value. However, the densification rate decreases with increasing the TiN volume fraction in the matrix.

(14) In sialon and sialon matrix composites the cracks type formed by indentation are of Palmqvist type.

(15) The presence of carbon fiber in the sialon matrix increases the fracture toughness. For example the addition of 15V% carbon fiber grade (B) increases the sialon fracture toughness by 45%.

(16) Hardness and fracture toughness of hot pressed carbon fiber/sialon composites measured by indentation technique were found to be higher in the direction perpendicular to the fiber direction than parallel to the fiber orientation.

(17) The addition of 15V% Ni to syalon 201 and sintering at low temperature(1450°C) increases the fracture toughness by 62%. However, increasing the sintering temperature to 1550°C causes a drop in the resulting fracture toughness. This is because the amount of silicon in the nickel particles increases with increasing the sintering temperature making the nickel particles very brittle.

(18) The stainless steel also helps to increase the composite fracture toughness which increases with increasing steel volume fraction.

(19) Similar results have been obtained by the addition of TiN to the sialon. The hardness decreases with increasing amount of TiN and the fracture toughness increases. For example the addition of 30V%TiN increases the fracture toughness by 64%

(20) Electrical conductivity in the three systems discussed in the present investigation is found to be increased with decreasing the size of the reinforced fibers or particles and increases with increasing the volume fraction of the second phase.

(21)Sialon with a very good conductivity was produced by the addition of 10-20V% carbon, 15-20V%Ni or 30V%TiN.

Appendix (1)

Properties of Carbon fiber

Product No	Tensile strength (Kg/mm^2)	Modulous ton/mm^2	Elongation %	Fired Temp (°C)
(A) F-500	330	55	0.67	2600
(B) F-180	210	19	1.11	1600
(C) T-300	350	23	....	.....

Properties of meso phase carbon

Lot No	Particle Dia μm	Firing Temp (°C)
D-MPA-15-15	6	
E-MPA-17-1	6	2800

REFERENCES

(1) Anstis, G. R., Chantikul, P , Lawn, B. R. & Marshall, D. B. J. Am. Ceram. Soc. **64** [9] (1981) 533

(2) Bahini, G. N., Bellosi, A. & Vincenzini, P. Ceramic International 6 3 (1980) 91

(3) Becher, P. F. & Wei, G. C. J. Am. Cerm. Soc. **67** [12] (1984) C-267

(4) Boskovic, S. "Science of Ceramics **14**" (1988) 455

(5) Bowen, L. J, Weston, R. j., Garruthers, T. G & Brook, R. J. J. Mat. Sci. **13** (1978) 341

(6) Bower, R., Edrees, H. J. & Hendry, A. Brit. Ceram. Pro. "Fabrication Technology" **45** (1990) (Ed)., Davidge R. W & Thompson, D.P.

(7) Brennan, J. J & Prewo, K. M. J Mat. Sci. **17** (1982) 2371

(8) Brook, R. J., Carruthers, T. G. , Bowen, L. J. & Weston, R. J. "Progress in Nitrogen Ceramics" (1977) 383 (Ed) Riley, F. L, Noordhoft, leyden.

(9) Buljan, S. T., Baldoni, J. G. & Huckabee, M. L. Am. Ceram. Soc. Bull **66** [2] (1987) 347.

(10) Carr, A.J. "Privite communication".

(11) Chart, T.G., NPL Report Chem. **18** (1972)

(12) Coble, R. L. J. App. Phys. **41** (1970) 4798

(13) Das, P.k. & Mukerji, P. C. Amer. Ceram. Soc. Bull. **3** [3] (1988) 234

(14) Das, P.k. & Mukerji, P. C. J. Eur. Ceram.Soc. 5 (1989) 105.

(15) Drew, P. & Liwes, M. H. J. Mat. Sci. **9** (1974) 261

(16) Drew, R. A. L. , Hampshire, S. & Jack, K. H. "Special Ceramic **7**" Brit. Ceram. Soc.**31** (1981) 119 (Ed), Taylor, D. & Popper, P.

(17) Edrees, H. J & Hendry, A., "Complex microstructures" , Brit. Ceram. Proc. 42 (1989) 49 [Eds], Stevens, R. & Taylor, D.

(18) Ekstrom, T. & Ingelstrom, N. "Non-oxide technical and engineering ceramics" (1986) 231 (Ed) Hampshire, S..

(19) Evans, A. G. & Charles, E. A. J. Amer. Ceram. Soc. **24** (1976) 939

(20) Evans, A. G. & Wilshaw, T. R. Acta. Metall. **24** (1976) 939

(21) Futaki, S. Shimizg, Y. & Shiralshi, K. J. Mat. Sci. **22** (1987) 4331

(22) Gauckler, L. J. , Weiss, J. & Tien, T. Y. J. Ame. Ceram. Soc. **61** (1978) 397

(23) Giachello, A. , Martinengo, P. C. , Tommasini, G. & Popper, P. Amer Ceram. Soc. Bull. **59** (12) (1980) 1212

(24) Gibson, P. R., Clegg, A. J. & Das, A. A. Wear **95** (1984) 193

(25) Grathwohl, G. , Hanna, S. B. & Thummler, F. Trans. J. Brit. Ceram. Soc. (1982) 193

(26) Grieveson, P. , Jack, K. H & Wild, S. "Spceial Ceramic 4" Brit. Ceram. Res. Assn. (1968) 237

(27) Guo Jing–Kun, Mao Zhi–Qiong, Bao Cue–Di, Wang Rong–Hua and Yan Dong–Sheng J. Mat. Sci. **17** (1982) 3611.

(28) Hampshire, S., Park, H. K., Thompson, D. P. & Jack, K. H. Nature **274** (1978) 880

(29) Hampshire, S. & Jack, K. H. "Special Ceramic 7". Brit. Ceram. Soc. **31** (1981) 37 (Eds), Taylor, D. & Popper, P.

(30) HardY, J. & Jack, K. H. Nature **180** (1957) 332

(31) Hendry, A. "Progress in Nitrogen Ceramics"Proc. NATO (1977) 301 Ed) Riley, F.L.

(32) Iskoe, J. L., Lang, F. F. & Diaz, E. S. J. Mat. Sci. **11** (1976) 908

(33) Jack, K. H. "Non-Oxide Techincal and Engineering Ceramics". (1986) 1 (Ed) Hampshire, S.

(34) Jack, K. H. J. Mat. Sci. Rese. **11** [9-7] (1977) 561 (Eds), Palmour, H. , Davis, R. F. & Have, T. M.

(35) Jack, K. H. "Progress in Nitrogen Ceramic" Proc. NATO (1977) 109 (Ed) Riley, F. L

(36) Homeny, H., Wallace, L. V. & Mattison, K. F. J. Am. Ceram. Soc. **66** 2 (1987) 333

(37) Kingery, W. K. J. Appl. Phys. 30 (1959) 301

(38) Kingery, W. K., Woulbroun, J. M. & Charvat, F. R. J. Amer. Ceram. Soc. **64** (1963) 391

(39) Knoch, H. & G. Ziegler,. "Science of Ceramic " *9* (1977) (Ed) K. J. de Vries.

(40) Kubaschewski, O. & Alcock, C. B. "Metallurgicall Thermochemistry" 5th edtion. pergamon press (1983)

(41) Kaufman, L. **3** [4] (1979) Calphad, pergamon press.

(42) Kyotoku, H., Morrison, F. C. R. & Hendry, A. "Silicate Industriels" **53** (1988) 85 .

(43) Lankford, J. J. Mat. Sci. Lett. **1** (1982) 493

(44) Lawn, B. R. & Fuller, E. R. J. Mat. Sci. **10** (1975) 2016

(45) Lawn, B. R. , Evans, A. G. & Marshall, D. B. J. Am. Ceram. Soc. **63** [9-10] (1980) 574

(46) Lawn, B. R. & Swain, M. Y. J. Mat. Sci. **10** (1975) 113

(47) Lewis, M. H, & Barnard, P. J. Mat. Sci. **15** (1980) 13

(48) Liang, K. M. , Orange, G. & Fantozzi, G. J. Mat. Sci. **25** (1990) 207

(49) Liddell, K. (1984) "privite communication".

(50) Lumby, R. J., North, B. & Taylor, A. J. "Special ceramics 6" Brit. Ceram. Res. Assn. (1975) 283 (Ed) Popper. P.

(51) lundberg, R., Dahlborg, A. Jennfors,P.& Carlsson, R. "First European conference on composite materials" (1985) 469.

(52) Mah, T. Mendiratta, M.G & Lipsitt, H. A Am. Ceram. Soc. Bull. 60 [11] (1981) 1229.

(53) Marshall, D. B. J . Am. Ceram. Soc. 66 [2] (1983) 127

(54) Messier, D. R. & Wong, P. J. Amer. Ceram. Soc. 56 (1973) 480

(55) Messier, D. R. , Riley, F. L. & Brook, R. J. J. Mat. Sci. 13 (1978) 1199

(56) Miller,P. D., Lee, J. G. & Cutter, I. B. J. Am. Ceram. Soc. 62 (1979) 147.

(57) Mitchell, K & Hendry, A "High Tech Ceramics" (1986) 901 (Ed), Vincenzini, P.

(58) Mitomo, M. J. Mat. Sci. 11 (1976) 1103

(59) Mitomo, M.,Vang, N., Kishi, Y. & Bando, V. J. Mat. Sci. 23 (1988) 3413

(60) Moulson, A. J. J. Mat. Sci 14 (1979) 1017

(61) Mulfinger, H. O. , J . Am. Cerm. Soc. 49 (1966) 462

(62) Niihara, K. , Morena, R. & Hasselman, P. H. J. Mat. Sci. Lett. 1 (1982) 13

(63) Niihara, K. J. Mat. Sci. Lett. 2 (1983) 221

(64) Parmqvist, S. Arch. Eisnhuttenwes 33 (1962) 629

(65) Patel, J. K. & Thompson, D. P. Brit. Ceram. Proc. "Engineering with ceramics 2 " 39 (1987) 61

(66) Prewo, K. M. & Brennan, J. J. J. Mat. Sci. 15 (1980) 463

(67) Quackenbush, C., Smith, J. T., Nail, J. T. & French, K. W. "Progress in Nitrogen Ceramics" Proc. NATO. (1983) 669 (Ed), Riley, F. L.

(68) Rahaman, M. N. , Riley, F. L. & Brook, R. J. J. Am. Ceram. Soc. 63 [11-12] (1980) 648

(69) Rice, R. W., Becher, P. F., Freiman, S. W. & MacDonough, W. J. Ceram. Eng. Sci. Proc. 1 [7-8] (1980) 424

(70) Sambell, R.A. J , Bowen, D. H. , & Phillips, D. C. J. Mat. Sci. 7 (1972) 663.

(71) Sergej, T., Buljan, J., Gray, B. & Marvinl, L . H. Am. Cerm. Bull. 66 [2] (1987) 347

(72) Shetty, D. K. , Wright, I. G., Mincer, P. N., & Clauer, A, H., J. Mat. Sci. 20 (1985) 1873.

(73) Shimada, M. , Tanaka,A., Yamada, T. & Koizumi, M. "Ceramic Powder" (1983) 871 [Ed], Vivcenzini, P.

(74) Stevens, R. "Zirconia & Zirconia ceramics", Magnesium Elektron Ltd, London (1986)

(75) Tanari, N., Kondo, I., Keno, K & Toibana, Y. J. Ceram. Soc. Japn. 12 (1986) 1231

(76) Thompson, D. P., Korgul, P. & Hendry, A. "Progress in Nitrogen Ceramics" Proc. NATO (1983) 61 (Ed) Riley F. L.

(78) Tsuge , A. & K. Nishida, Ame. Ceram. Bull. 57 (1978) 424.

(79) Turkdogan,, E. T., Bills, P. M. & Tippett, V. A. J. Appl. Che. 8 (1958) 296

(80) Voitovich, L. F. "Refractory Compounds" (1971) Kiey, Naukova Dumka.

(81) Wagner, C. J Phys. Chem. Solids 33 (1972) 1051

(82) Wahi, R. P. & Illschner, J. Mat. Sci 15 (1980) 875

(83) Wiederhorm, S. M. J. Amr. Cerm. Soc. 56 (1973) 227

(84) Wild, S. & Leng-Ward, G. J. Mat. Sci. 16 (1981) 18152

(85) Wild, S. Grineson, P. & Jack, K. H. "Spceial Ceramic 5" Brit. Ceram. Res. Assn. (1972) 358 (Ed), Popper, P.

(86) Wotting, G. & G. Ziegler,. "Ceramic Powder" (1983) 951 (Ed) Vivcenzini, P.

(87) Ziegler , G. & H. Knoch,. "Special Ceramic 7" Proc. Brit. Ceram. Soc.(1981) 145.(Eds) Taylor, D. & Popper, P.